MCEER

EARTHQUAKE ENGINEERING TO EXTREME EVENTS

ISSN 1520-295X

Fragility Analysis of Water Supply Systems

by
Anita Jacobson and Mircea Grigoriu

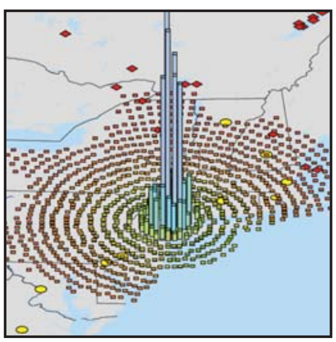

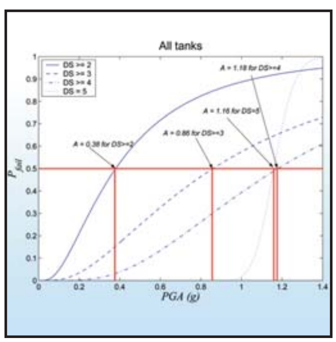

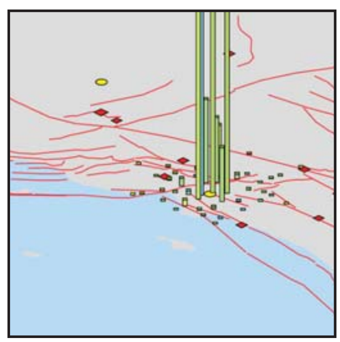

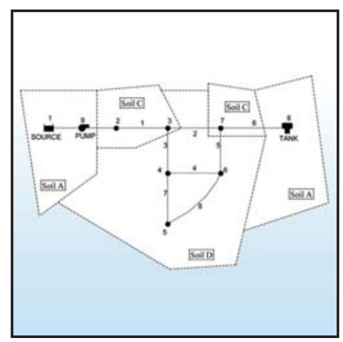

Technical Report MCEER-08-0009

March 10, 2008

This research was conducted at Cornell University and was supported primarily by the Earthquake Engineering Research Centers Program of the National Science Foundation under award number EEC 9701471.

NOTICE

Fragility Analysis of Water Supply Systems

by

Anita Jacobson[1] and Mircea Grigoriu[2]

Publication Date: March 10, 2008
Submittal Date: January 27, 2008

Technical Report MCEER-08-0009

Task Number 10.1.4

NSF Master Contract Number EEC 9701471

1 Graduate Student, School of Civil and Environmental Engineering, Cornell University
2 Professor, School of Civil and Environmental Engineering, Cornell University

MCEER
University at Buffalo, The State University of New York
Red Jacket Quadrangle, Buffalo, NY 14261
Phone: (716) 645-3391; Fax (716) 645-3399
E-mail: *mceer@buffalo.edu*; WWW Site: *http://mceer.buffalo.edu*

Preface

The Multidisciplinary Center for Earthquake Engineering Research (MCEER) is a national center of excellence in advanced technology applications that is dedicated to the reduction of earthquake losses nationwide. Headquartered at the University at Buffalo, State University of New York, the Center was originally established by the National Science Foundation in 1986, as the National Center for Earthquake Engineering Research (NCEER).

Comprising a consortium of researchers from numerous disciplines and institutions throughout the United States, the Center's mission is to reduce earthquake losses through research and the application of advanced technologies that improve engineering, pre-earthquake planning and post-earthquake recovery strategies. Toward this end, the Center coordinates a nationwide program of multidisciplinary team research, education and outreach activities.

MCEER's research is conducted under the sponsorship of two major federal agencies: the National Science Foundation (NSF) and the Federal Highway Administration (FHWA), and the State of New York. Significant support is derived from the Federal Emergency Management Agency (FEMA), other state governments, academic institutions, foreign governments and private industry.

MCEER's NSF-sponsored research objectives are twofold: to increase resilience by developing seismic evaluation and rehabilitation strategies for the post-disaster facilities and systems (hospitals, electrical and water lifelines, and bridges and highways) that society expects to be operational following an earthquake; and to further enhance resilience by developing improved emergency management capabilities to ensure an effective response and recovery following the earthquake (see the figure below).

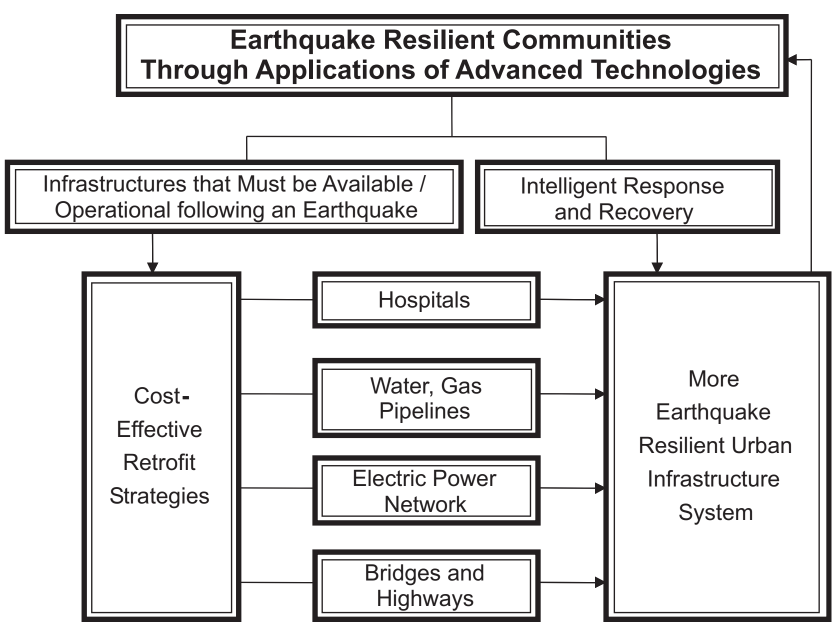

A cross-program activity focuses on the establishment of an effective experimental and analytical network to facilitate the exchange of information between researchers located in various institutions across the country. These are complemented by, and integrated with, other MCEER activities in education, outreach, technology transfer, and industry partnerships.

This report describes a procedure to assess the seismic performance of water supply systems. Seismic hazard models are developed to generate random samples of earthquake activity at both single and multiple sites. Methodologies to obtain the fragility of a given pipeline are developed, including several hazard conditions: continuous and jointed pipelines subjected to seismic waves, pipelines subjected to PGD hazards, and pipelines subjected to fault displacements. Fragility information for other components of the water supply system is obtained from several published sources. These parameters are integrated into an algorithm that uses Monte Carlo simulation to determine the damage states of individual components, and hydraulic analyses to estimate the performance of the damaged water system. The algorithm is applied to a sample water supply system, consisting of a reservoir, pump, water tank and several pipelines, and fragility curves are produced under different limit states. In addition, a procedure to estimate the life cycle damage of a water supply system is presented. Since each type of damage is associated with a cost, the total cost due to seismic hazards during its lifespan can be estimated.

ABSTRACT

Following a seismic event, it is desirable that water supply systems can perform satisfactorily to facilitate the rescue and recovery process. A seismic event can trigger various seismic hazards, such as wave propagations caused by seismic waves, surface faultings, and permanent ground deformation hazards such as landslides and liquefactions. Since the occurrence of these hazards is not deterministic, mathematical models are developed to produce samples of seismic activity at a single site and multiple sites. A sample of seismic activity gives the number of earthquake occurrence during the lifespan of a system and its temporal distribution, along with the moment magnitude and site-to-source distance for each seismic event.

For each seismic event, given its moment magnitude, site-to-source distance, and soil properties at the site, samples of seismic ground acceleration at a single site can be generated by using a ground motion model and Monte Carlo simulation. To generate samples of seismic ground motion at multiple sites, an additional coherence model is needed to capture the spatial variation of motions experienced among different sites. Amount of ground displacement caused by permanent ground deformation hazards can be calculated using empirical models for a given moment magnitude, site-to-source distance, and soil properties.

A water supply system consists of numerous components, such as pipelines, reservoirs, water tanks, and pumps. Since the performance of a water supply system depends on the performance of its individual component, seismic assessment on each component in the system needs to be executed.

A way of assessing seismic performance is by performing fragility analysis, in which failure probability of a system and/or a component is obtain as a function of some earthquake parameters, such as peak ground acceleration, peak ground displacement, and spectral acceleration, for a given limit state.

Several methodologies are developed to perform fragility analysis of pipelines subject to: (1) seismic waves, (2) permanent ground deformations including landslides, lateral spreads and seismic settlements induced by liquefactions, and (3) fault displacements. Fragility information on several components of water supply systems, such as water tanks, water tunnels, pumps, and reservoirs are obtained from published works.

An algorithm for fragility analysis of water supply systems is developed. For a given system, moment magnitude, and fragility information of each component of the system, samples of damaged system can be obtained through Monte Carlo simulation. Performance of the damaged systems can be analyzed using hydraulic analysis to calculate the fragility surfaces of water supply systems for a given system limit state.

A procedure for life cycle damage estimation of water supply systems is presented, which gives the damage sequence of the system during its lifespan. From this, total cost of the system can be estimated.

ACKNOWLEDGEMENTS

This work was supported primarily by the Earthquake Engineering Research Center Program of the National Science Foundation under NSF Award Number EEC-9701471 to the Multidisciplinary Center for Earthquake Engineering Research. This support is also gratefully acknowledged.

TABLE OF CONTENTS

SECTION	TITLE	PAGE
1	**INTRODUCTION**	**1**
2	**SEISMIC HAZARD**	**3**
2.1	Seismic Activity Matrix	6
2.1.1	Calculation from Seismicity Rates	6
2.1.2	Calculation from Deaggregated Seismic Hazard Data	6
2.2	Seismic Activity Model	11
2.3	Ground Motion Model	12
2.4	Ground Motion Generation	13
2.4.1	Ground Motion Generation for a Single Site	13
2.4.2	Ground Motion Generation for Multiple Sites	17
3	**PIPE RESPONSE SUBJECT TO SEISMIC HAZARDS**	**23**
3.1	Seismic Wave Hazard	23
3.2	Pipelines Response to Seismic Waves	23
3.2.1	Continuous Pipelines	23
3.2.2	Jointed Pipelines	26
3.3	PGD Hazard	27
3.3.1	Landslides	27
3.3.2	Lateral Spreadings	30
3.3.3	Seismic Settlements	31
3.3.4	Fault Displacements	33
3.4	Pipelines Response to Permanent Ground Deformations	34
3.4.1	Pipelines Response to Longitudinal PGD	34
3.4.2	Pipelines Response to Transverse PGD	37
3.4.3	Pipelines Response to Fault Displacements	41

TABLE OF CONTENTS (cont'd)

SECTION	TITLE	PAGE
3.5	Summary of Equations	45
4	**FRAGILITY ANALYSIS OF PIPELINES**	**49**
4.1	Fragility of Continuous Pipelines Subject to Seismic Waves	51
4.1.1	Limit State	51
4.1.2	Fragility Analysis	51
4.2	Fragility of Jointed Pipelines Subject to Seismic Waves	54
4.2.1	Limit State	54
4.2.2	Fragility Analysis	54
4.3	Fragility of Pipelines Subject to Landslides, Lateral Spreads, or Seismic Settlements	57
4.3.1	Limit State	57
4.3.2	Fragility Analysis	57
4.4	Fragility of Pipelines Subject to Fault Displacements	63
4.4.1	Limit State	63
4.4.2	Fragility Analysis for Newmark-Hall Model	63
4.4.3	Fragility Analysis for Kennedy, et al. Model	63
5	**FRAGILITY INFORMATION ON SOME COMPONENTS OF WATER SUPPLY SYSTEMS**	**67**
5.1	Fragility Information for Water Tanks	67
5.2	Fragility Information for Water Tunnels	73
5.3	Fragility Information for Other Components	75
6	**FRAGILITY ANALYSIS OF WATER SUPPLY SYSTEMS**	**77**
6.1	Locating the source and the components	77
6.2	Uniformity of Fragility Information	80

TABLE OF CONTENTS (cont'd)

SECTION	TITLE	PAGE
6.3	Hydraulic Analysis	81
6.3.1	Continuity	81
6.3.2	Conservation of Energy	82
6.3.3	Momentum Principal	85
6.4	Application: Numerical Example	86
6.4.1	Example 1	86
6.4.2	Example 2	94
6.5	Life Cycle Damage Estimation	98
7	**SUMMARY AND CONCLUSION**	**101**

LIST OF ILLUSTRATIONS

FIGURE	TITLE	PAGE
1-1	Example of a fragility surface and a fragility curve.	1
2-1	Flowchart of seismic hazard model at a single site.	4
2-2	Flowchart of seismic hazard model for multiple sites.	5
2-3	Discretization of area around a site and range of possible earthquake magnitudes.	7
2-4	Deaggregated seismic hazard of New York City for 0.2 second spectral acceleration, 2% exceedance in 50 years.	8
2-5	Deaggregated seismic hazard of Los Angeles for 0.2 second spectral acceleration, 2% exceedance in 50 years.	10
2-6	Limiting value u for New York City corresponding to 2% probability of exceedance in 50 years.	11
2-7	Seismic activity matrix of New York City.	12
2-8	Power spectral densities for $m_w = 6.5$ and $r = 105$km.	14
2-9	One sided power spectral density of $G_n(t)$.	15
2-10	A sample of acceleration time history $A(t)$.	16
2-11	Separation vector between sites i and j, $\vec{\xi}_{ij}$.	17
2-12	Stationary and non-stationary Gaussian seismic ground accelerations at t=2sec.	19
2-13	Stationary and non-stationary Gaussian seismic ground accelerations at t=10sec.	20
2-14	Stationary and non-stationary Gaussian seismic ground acceleration histories at (250,250).	21
3-1	Seismic wave intersection with buried pipeline.	24
3-2	Cross section for JCCP.	26
3-3	Seismic wave interaction with pipeline.	28
3-4	Types of landslides according to Meyersohn, 1991.	29
3-5	Characteristics of a lateral spread.	30

LIST OF ILLUSTRATIONS (cont'd)

FIGURE	TITLE	PAGE
3-6	Elevation view showing ground slope and free face ratio.	31
3-7	Relation between cyclic stress ratio $(N_1)_{60}$ and volumetric strain for saturated sands.	32
3-8	Fault types.	33
3-9	Five idealized patterns of ground deformation due to longitudinal PGD.	35
3-10	Patterns of transverse PGD.	37
3-11	Horizontal bearing capacity N_{qh} for sand vs. depth to diameter ratio.	39
3-12	Newmark-Hall model of pipe response due to fault displacement.	42
3-13	Kennedy, et al. model of pipe response due to fault displacement.	44
3-14	Equations for pipe responses subject to seismic waves and PGD hazards.	46
3-15	Equations for pipe responses subject to fault displacement hazard.	47
4-1	Typical configuration of fragility curves.	50
4-2	Fragility analysis of continuous pipelines subject to seismic wave hazard.	52
4-3	Fragility surfaces of a continuous pipe for various soil types.	53
4-4	Fragility analysis of jointed pipelines subject to seismic wave hazard.	55
4-5	Fragility surfaces of a JCCP for various soil types.	56
4-6	Seismic input of PGD required to calculate amount of PGD movement δ_{PGD}.	59
4-7	Fragility analysis of pipelines subject to landslides, lateral spreads and seismic settlements induced by liquefactions.	60
4-8	Fragility surfaces of a pipe subject to lateral spreads.	61
4-9	Fragility surfaces of a pipe subject to seismic settlement.	62
4-10	Fragility analysis of pipelines subject to fault displacement hazard using Newmark-Hall or Kennedy et al. procedure.	64

LIST OF ILLUSTRATIONS (cont'd)

FIGURE	TITLE	PAGE
4-11	Comparison of fragilities of a pipe between Newmark-Hall and Kennedy et al. procedure.	65
5-1	The median values, As, for all tanks as a function of fill level.	70
5-2	Fragility curves for tanks as a function of fill level.	71
5-3	Fragility curves for tanks as a function of fill level and anchorage.	72
5-4	Fragility curves for all tunnels, unlined tunnels, timber, masonry, and brick tunnels, and unreinforced concrete tunnels.	74
5-5	Reliability and fragility curves for groundwater system component.	76
6-1	Methodology of fragility analysis of water supply systems.	78
6-2	Locating seismic source and components and measuring site-to-source distance of each component.	79
6-3	Continuity principal shown for a junction in pipelines.	81
6-4	Conservation of energy between two points within a flow.	82
6-5	Example of a water supply system.	86
6-6	Location of the seismic source with respect to the example network.	88
6-7	Fragility surfaces of the sample network for damage states prescribed in option 1 or Table 6-9.	90
6-8	Fragility surfaces of the sample network for damage states prescribed in option 2 or Table 6-10.	91
6-9	Fragility surfaces of the sample network for damage states prescribed in option 3 or Table 6-11.	92
6-10	Fragility surfaces of the sample network for damage states prescribed in option 3 or Table 6-12.	93
6-11	Example of a water supply system (modified).	94
6-12	Fragility surfaces of the modified sample network for damage states prescribed Table 6-16.	97
6-13	Life cycle damage estimation of a system.	99

LIST OF TABLES

TABLE	TITLE	PAGE
2-1	Deaggregated seismic hazard matrix of New York City for 0.2 second spectral acceleration, 2% exceedance in 50 years.	9
2-2	Deaggregated seismic hazard matrix of Los Angeles for 0.2 second spectral acceleration, 2% exceedance in 50 years.	9
2-3	NEHRP Soil Classification.	14
3-1	Pipeline interface angles of friction for contact with granular soil.	25
3-2	Ramberg-Osgood parameters for mild steel and X-grade steel.	36
5-1	Historical tank damaged data provided by ALA.	68
5-2	Tank damage states based on historical data of damaged tanks as provided by ALA.	68
5-3	Fragility curves of tanks as a function of fill level.	69
5-4	Fragility curves of tanks as a function of fill level and anchorage.	69
5-5	Tunnel database for fragility analysis provided by ALA.	73
5-6	Fragility curves of tunnels as a function of liner system.	74
5-7	Reliability information for various components of groundwater systems.	75
6-1	Summary of friction factor formulation for Darcy-Weisbach equation.	83
6-2	Values of equivalent roughness e for some commonly used pipes.	84
6-3	Hazen-Williams coefficient C_{HW} and Manning coefficient n for some common pipe materials.	84
6-4	Minor loss coefficient K_L for valves and other pipe fittings.	85
6-5	Node properties of the example system.	87
6-6	Pipe properties of the example system.	87
6-7	Original states of the nodes and links of the example network.	87
6-8	Capacity of pump, water tank, and reservoir for the sample water supply system at various damage states.	89

LIST OF TABLES (cont'd)

TABLE	TITLE	PAGE
6-9	Damage states of the water supply system for option 1.	89
6-10	Damage states of the water supply system for option 2.	90
6-11	Damage states of the water supply system for option 3.	91
6-12	Damage states of the water supply system for option 4.	93
6-13	Node properties of the example system (modified).	95
6-14	Original states of the nodes and links of the example network (modified).	95
6-15	Capacity of water tank, reservoir and pipelines for the modified water supply system at different damage states.	96
6-16	Damage states of the modified water supply system.	96

SECTION 1
INTRODUCTION

Lifelines play an important role in ensuring the vitality of a community. Disruption of one or more of the lifelines, for example water supply systems and electricity networks, can cause an impairment in the activity and vitality of a community. This disruption can be resulted from either natural or man made hazards. In the even of emergency, such as those following an earthquake, it is even more urgent to ensure that the community has functioning lifelines to speed up the process of rescue and recovery. Thus, existing lifeline systems need to be assessed in order to capture the expected performance if such emergency situations arise.

A way of quantifying the performance is through probabilistic models representing failure probability of a system in the wake of a hazard. For seismic hazards, fragility analysis can be performed to assess the seismic performance of a system for some specified limit states. The outcomes of the analysis are typically presented as either fragility curves or surfaces. Fragility curves provide the failure probability of the analyzed system as a function of a seismic parameter, such as peak ground acceleration (PGA) and spectral acceleration (SA). Fragility surfaces give the failure probability as a function of two seismic parameters, such as moment magnitude m_w and site-to-source distance r. Figure 1-1 (a) and (b) gives an example of a fragility curve and a fragility surface respectively.

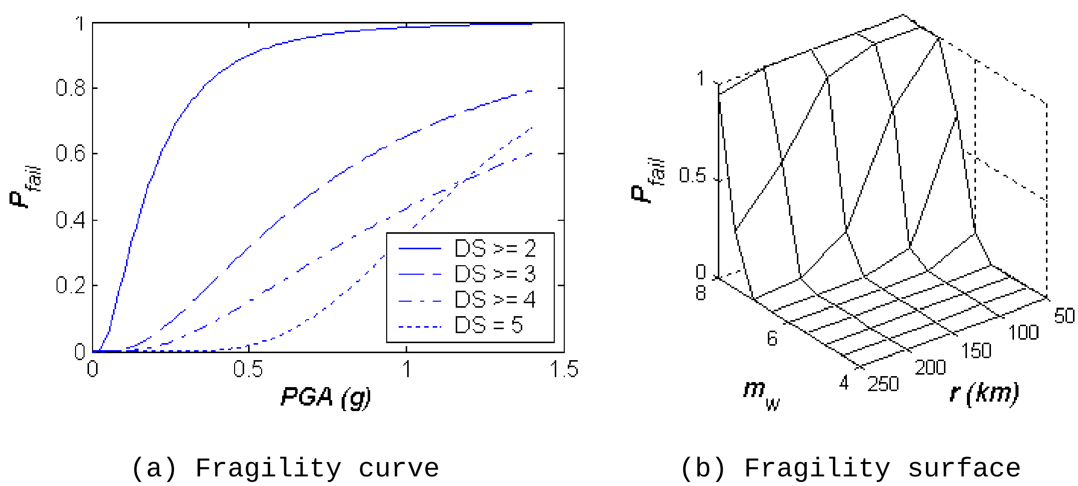

FIGURE 1-1 Example of a fragility surface and a fragility curve.

The thesis focuses on the assessment of seismic performance of water supply systems. Seismic hazard models are developed to generate random samples of seismic activity at a single site and multiple sites. These models give the number of seismic events occurring during a time period of interest, along with the temporal distribution of the events, and the moment magnitude and site-to-source distance of each event.

A ground motion model and Monte Carlo simulation are employed to generate seismic ground motion records for a single site. For multiple sites, an additional coherence model is utilized in conjunction with the ground motion model and the Monte Carlo simulation to produce samples of seismic ground motion records. The coherence model is needed to capture the coherency of ground motions experienced by different sites originating from a same seismic source (i.e., spatial variation).

Permanent ground deformation hazards such as landslides and liquefactions, which may be triggered by seismic events, will cause variable amounts of ground movement. Various empirical models are employed to determine the amount of ground movement related to different hazards, as well as the effects of the movement on pipelines.

A water supply system consists of numerous components, such as pipelines, water tanks, and pumping stations. The overall seismic performance of a water supply system, or any system, depends on the individual performance of its components. Prior to assessing the seismic performance of a water supply system, analysis of individual components in the system must be initiated.

Methodologies for performing fragility analysis are developed for pipelines subject to various seismic hazards. Each of these requires parameters defining: (1) seismic events, (2) pipe and soil characteristics, and (3) limit states to judge the performance of the analyzed pipe under certain circumstances. Numerical examples are presented for each of the methodology developed to better illustrate the analysis procedures. For other components of a water supply system, fragility information is obtained from published works such as those provided by the American Lifelines Alliance.

An algorithm for the determination of the fragility of water supply systems is produced. The algorithm requires parameters defining: (1) seismic events, (2) fragility information of the individual components of the analyzed system, and (3) limit states to judge the performance of the analyzed system. The fragility assessment combines Monte Carlo simulation in determining damage states of individual components and hydraulic analyses to estimate the water delivery performance of the damaged system. A sample water supply system, consisting of a reservoir, pump, water tank, and several pipelines is analyzed. Several fragility curves are produced for the sample system under different imposed limit states. The example serves as an illustration of the procedure prescribed in the developed algorithm.

A procedure for performing life cycle damage estimation of water supply systems is also presented. This procedure yields the damage sequence of the system during its lifespan. Since each damage of the system is associated with an expected cost, the total cost of the system during its lifespan can be estimated.

In Chapter 2, seismic hazard models and generation of seismic ground acceleration algorithms are discussed for a single site and multiple sites. Models for analyzing pipeline response to various seismic hazards are described in Chapter 3, while the fragility analyses of the pipelines are presented in Chapter 4. As mentioned previously, fragility information for other components of a water supply system can be obtained from published works, and are reproduced here in Chapter 5. Finally, Chapter 6 presents the algorithm for performing fragility analysis of water supply systems and the procedure for life cycle damage estimation.

SECTION 2
SEISMIC HAZARD

During an earthquake, a site is likely to experience various seismic hazards, such as transient ground motion (i.e. seismic waves) and permanent ground deformation (PGD) in the form of fault displacements, landslides, and liquefaction. The occurrence of one or more of these hazards during an earthquake is not deterministic. A mathematical model is developed to represent the seismic hazard at a site.

Figure 2-1 shows the flowchart of a seismic hazard model for a site. A seismic activity model can be used to generate random samples of seismic activities at a site for a given time period t, which usually equals the lifespan of the analyzed systems, and the seismic activity matrix of the site. A seismic activity scenario in $[0, t]$ is characterized by the number of earthquakes N, the temporal distribution of earthquakes, and the moment magnitude m_w and site-to-source distance r of each seismic event in $[0, t]$.

Given the soil properties at a particular site, the moment magnitude m_w, and the site-to-source distance r, samples of seismic ground motion at a site can be generated. To generate samples of seismic ground acceleration, a ground motion model is utilized to obtain the spectral density of the seismic ground acceleration at the site. Using a Monte Carlo simulation algorithm, samples of seismic ground acceleration can be generated at an arbitrary site.

Amount of PGD can be determined for a given moment magnitude m_w, site-to-source distance r, and soil properties at a site using empirical models for various types of possible PGD hazards, which include landslides, lateral spreads and seismic settlements induced by liquefactions, and fault displacements. Thus, it should be noted that the amount of PGD is not a random variable for a given moment magnitude m_w, site-to-source distance r, and soil properties. The various empirical models will be described later in Chapter 3 Section 3.3.

Occurrence of an earthquake can affect a large area, for example, the area occupied by a water supply system. The seismic ground accelerations experienced by various components of a water supply system may differ, but are not independent of each other since they are caused by the same event. Thus, a mathematical model is needed to capture the correlation of seismic ground motions among the various sites (i.e. spatial variation).

Figure 2-2 shows the flowchart of a seismic hazard model for multiple sites. The steps are very similar to the model developed for a single site. The differences between the multiple sites model and the single site model are: (1) the incorporation of a coherence model in the multiple sites model to represent the correlation of seismic ground motions among the various sites; and (2) the use of Monte Carlo simulation for vector processes to generate samples of seismic ground acceleration at multiple sites.

Note that spatial variation is not applied in the calculation of the amount of permanent ground deformation. The reason for this limitation is that the only models available are empirical, and these models account only for moment magnitude m_w, site-to-source distance r, and soil properties as described later in Chapter 3, Section 3.3.

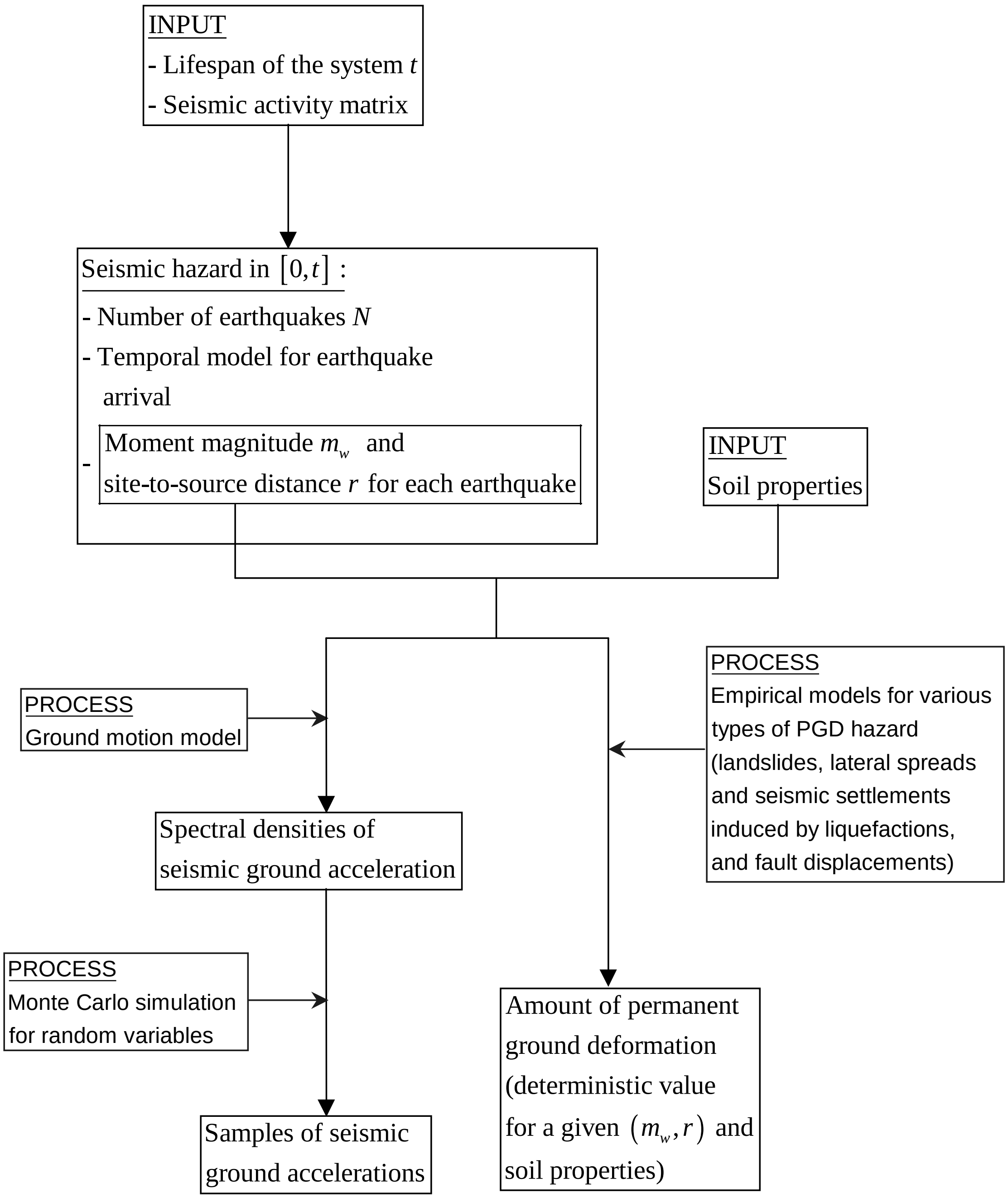

FIGURE 2-1 Flowchart of seismic hazard model at a single site.

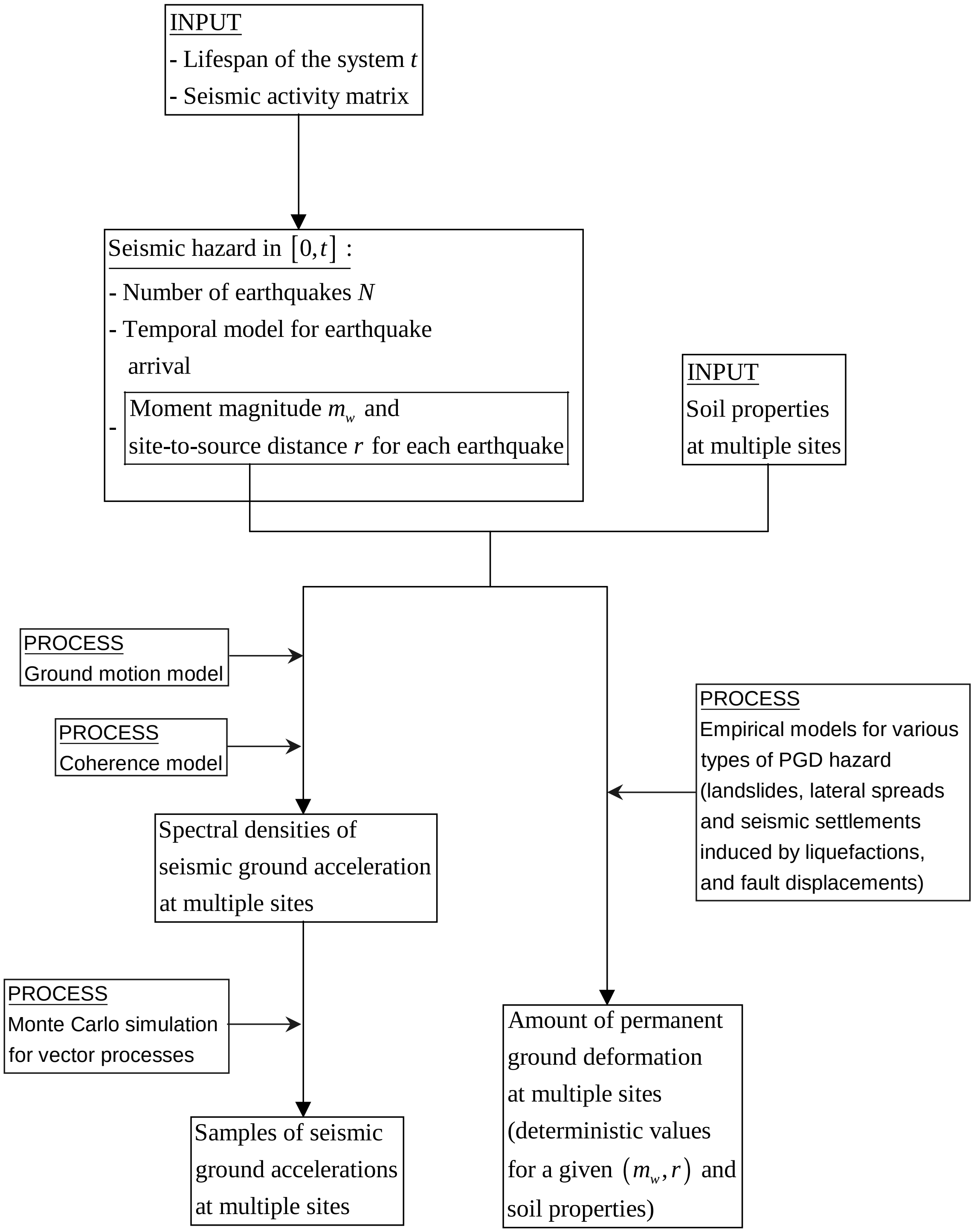

FIGURE 2-2 Flowchart of seismic hazard model for multiple sites.

2.1 Seismic Activity Matrix

Consider a site and a collection of rings centered on the site with radii $r_1 < r_2 < \ldots < r_i < \ldots < r_n$ [Refer to Figure 2-3]. In each of the ring, the occurrence of all possible earthquake moment magnitudes is binned into ranges with mid-points $m_{w1} < m_{w2} < \ldots < m_{wj} < \ldots < m_{wm}$.

Let $N_{ij}(t)$ be the number of the events during a time period t coming from ring i (i.e. $r \in [r_i - \Delta r/2, r_i + \Delta r/2]$) with moment magnitude range j (i.e. $m_w \in [m_{wj} - \Delta m/2, m_{wj} + \Delta m/2]$). The objective is to obtain the mean annual rate ν_{ij} as follow:

$$\nu_{ij} = \frac{N_{ij}(t)}{t}. \tag{2-1}$$

The mean annual rate ν_{ij} is referred as the seismic activity matrix.

Seismic activity matrix can be constructed either from the seismicity rates or from the deaggregated seismic hazard data using back calculation, both are available at the website of the U.S. Geological Survey (USGS) at http://eqhazmaps. usgs.gov/.

2.1.1 Calculation from Seismicity Rates

The values of the mean annual rate $\nu_{ij}, i, j = 1, 2, 3, \ldots$ can be calculated from seismicity rate data that gives the annual rate of occurrence of earthquakes of different magnitudes in each 0.1^o by 0.1^o cell in a grid covering the United States. These data can be obtained at http://eqhazmaps.usgs.gov/html/rategrid.html.

By summing the rates of occurrence of earthquakes in ring i with moment magnitude range j, the mean annual rate ν_{ij} can be obtained. This method involves dealing with a large amount of data. For example, to calculate all of the seismicity rates in a 500 km radius of New York City, approximately 7800 cells must be considered. It is therefore more practical to obtain the mean annual rate ν_{ij} from deaggregated seismic hazard data (Grigoriu and Mostafa, 2002b).

2.1.2 Calculation from Deaggregated Seismic Hazard Data

Deaggregation matrices provide the percent contribution of different pair of rings and moment magnitude ranges to the seismic hazard at the site. Seismic hazard is defined by the event where a specific ground motion parameter, U, at the site exceeds some limiting value, u.

Some of the typical ground motion parameters used are peak ground acceleration (PGA) and spectral acceleration (SA). PGA is the maximum acceleration recorded in an earthquake. SA is the maximum acceleration experienced by a system, as modeled by a particle on a massless vertical rod (i.e. single degree of freedom) having the same natural period of vibration as the system.

The limiting value, u, is chosen as the value of the ground motion parameter that has a specific probability of exceedance, p_e, during a given time period, t_e, expressed mathematically as follow:

$$P(U > u| \text{ all earthquakes in } t_e) = p_e. \tag{2-2}$$

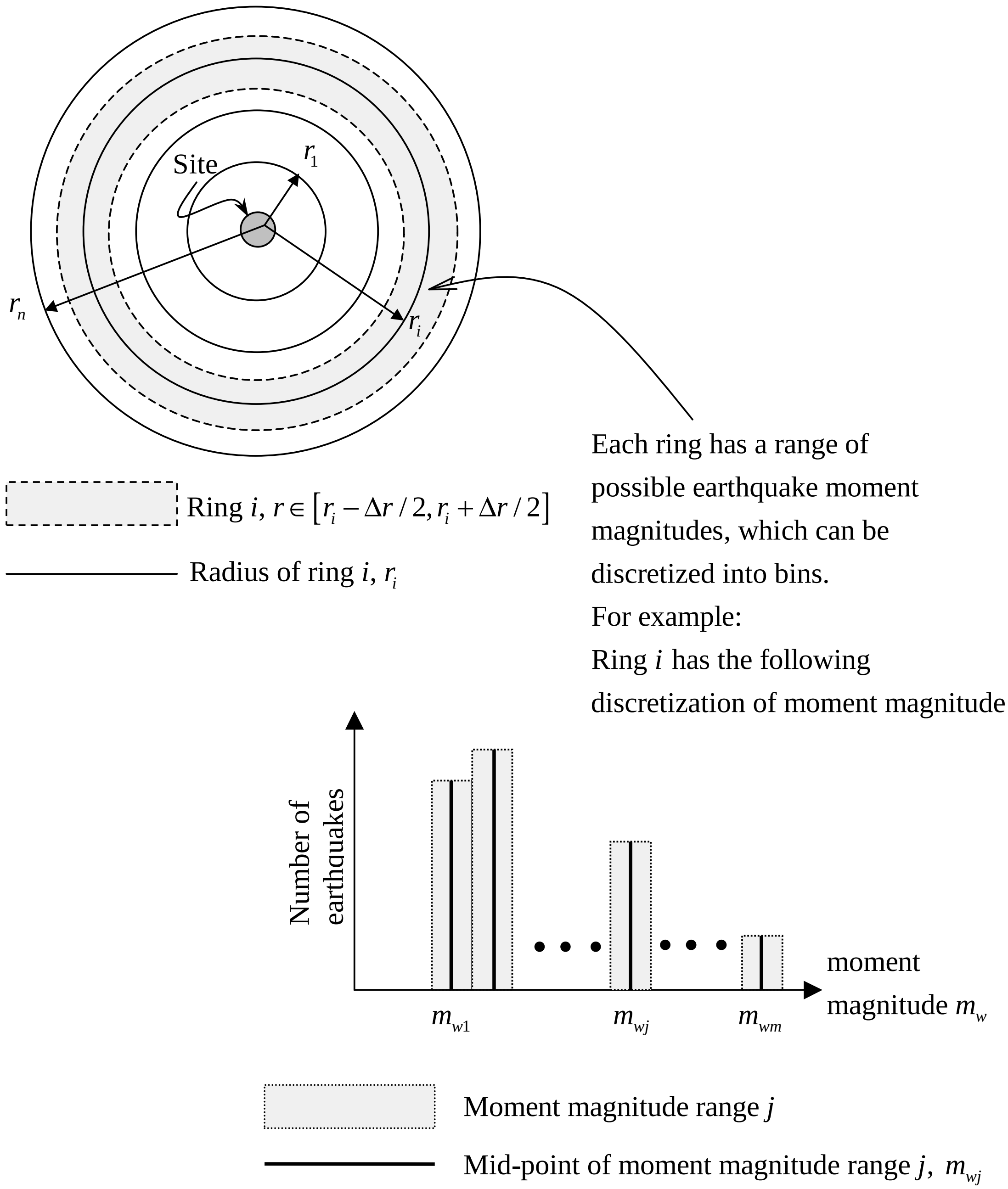

FIGURE 2-3 Discretization of area around a site and range of possible earthquake magnitudes.

USGS has calculated deaggregated seismic hazard data for more than 60 cities in the Central and Eastern United States (CEUS) and more than 50 cities in the Western United States (WUS). The moment magnitude is binned into intervals of 0.5 moment magnitude (i.e. $m_{wj} = m_{w(j-1)} + 0.5$), while the site-to-source distance is binned into intervals of 25 km (i.e. $r_i = r_{i-1} + 25$ km). The limiting value of the ground motion parameter is chosen to have 2% probability of exceedance in 50 years (i.e. $P(U > u|\text{all earthquakes in 50 years}) = 2\%$).

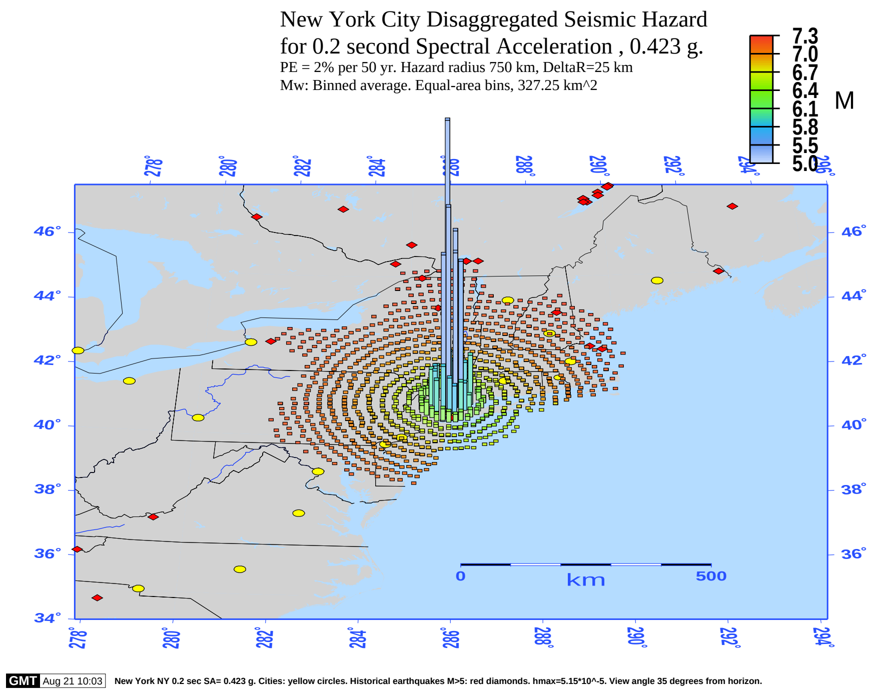

FIGURE 2-4 Deaggregated seismic hazard of New York City for 0.2 second spectral acceleration, 2% exceedance in 50 years.

The hazard probabilities are deaggregated for the ground motion parameters: PGA, SA of 1.0, 0.3, and 0.2 second. All results can be reached at http://eqhazmaps.usgs.gov/html/deagg.html. Examples of deaggregated seismic hazards for 0.2 SA with 2% probability of exceedance in 50 years are shown graphically for New York city in Figure 2-4, and for Los Angeles in Figure 2-5. These data can also be represented with matrices as shown in Tables 2-1 and 2-2 for New York City and Los Angeles respectively.

By considering the methodology used to generate the deaggregated seismic hazard matrices, the value of the mean annual rate ν_{ij} can be back-calculated. To have a good understanding of the mean annual rate, it is useful to review the methodology used by USGS to calculate the deaggregated seismic hazard matrices,as follows:

Assume that the distribution of the ground parameter U at a site caused by earthquakes in ring i with moment magnitude range j is $F_{ij}(u)$, and this distribution is independent of ν_{ij}. The complement of $F_{ij}(u)$ is $\bar{F}_{ij}(u) = 1 - F_{ij}(u)$.

It is assumed that $F_{ij}(u), i, j = 1, 2, \ldots$ follows lognormal distributions. The means of the distributions are given in Tables A1 to A4, for ground motion parameter: PGA, SA of 1.0, 0.3, and 0.2 second, of Frankel et.al. (Frankel *et al.*, 1996), which is available at http://eqhazmaps.usgs.gov/hazmapsdoc/junetab.html for the Central and Eastern United

TABLE 2-1 Deaggregated seismic hazard matrix of New York City for 0.2 second spectral acceleration, 2% exceedance in 50 years.

Deaggregated Seismic Hazard (h_{ij}) PE = 2% in 50 years 5.0 Hz (0.2 s)
New York NY 40.750 deg N 73.980 deg W SA = 0.42260 g

M<=	5.0	5.5	6.0	6.5	7.0	7.5
d<= 25.	15.534	14.515	9.960	5.564	2.193	1.354
50.	3.460	5.838	7.014	6.184	3.319	2.468
75.	0.446	1.197	2.315	3.165	2.370	2.238
100.	0.057	0.227	0.631	1.185	1.143	1.273
125.	0.012	0.067	0.239	0.557	0.635	0.819
150.	0.004	0.027	0.115	0.319	0.424	0.639
175.	0.001	0.010	0.051	0.170	0.266	0.477
200.	0.000	0.003	0.021	0.085	0.155	0.326
225.	0.000	0.001	0.008	0.041	0.085	0.208
250.	0.000	0.000	0.003	0.018	0.044	0.125
275.	0.000	0.000	0.001	0.009	0.026	0.085
300.	0.000	0.000	0.001	0.005	0.016	0.061
325.	0.000	0.000	0.000	0.003	0.011	0.049
350.	0.000	0.000	0.000	0.002	0.007	0.037
375.	0.000	0.000	0.000	0.001	0.005	0.028
400.	0.000	0.000	0.000	0.000	0.003	0.018
425.	0.000	0.000	0.000	0.000	0.001	0.011
450.	0.000	0.000	0.000	0.000	0.001	0.006
475.	0.000	0.000	0.000	0.000	0.000	0.004
500.	0.000	0.000	0.000	0.000	0.000	0.002

TABLE 2-2 Deaggregated seismic hazard matrix of Los Angeles for 0.2 second spectral acceleration, 2% exceedance in 50 years.

Deaggregated Seismic Hazard (h_{ij}) PE = 2% in 50 years 5 Hz
Los Angeles CA 34.000 deg N 118.200 deg W SA = 1.55200 g

M<=	5.0	5.5	6.0	6.5	7.0	7.5	8.0
d<= 25.	0.000	3.493	3.025	12.349	78.304	1.962	0.000
50.	0.000	0.001	0.001	0.007	0.779	0.069	0.000
75.	0.000	0.000	0.000	0.000	0.003	0.001	0.005

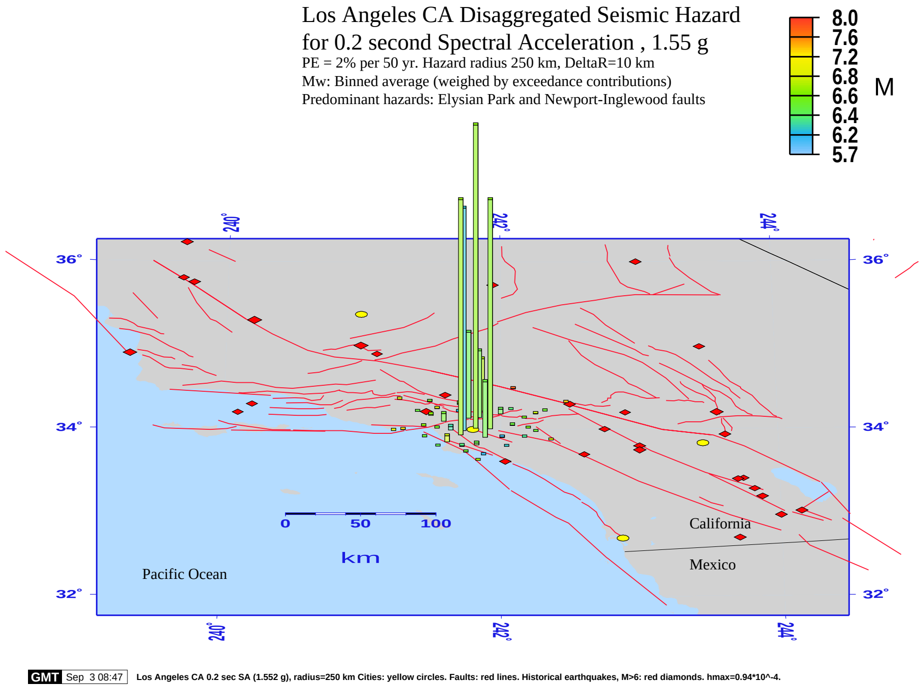

FIGURE 2-5 Deaggregated seismic hazard of Los Angeles for 0.2 second spectral acceleration, 2% exceedance in 50 years.

States (CEUS). The standard deviations are given in Table 5 of Atkinson and Boore (Atkinson and Boore, 1995).

Let $N_{ij}(t_e, u)$ be the number of events in time t_e from sources in ring i with moment magnitude range j where the ground motion parameter U exceeds the limiting value u having a Poisson distribution with mean annual rate $\nu_{ij}\bar{F}_{ij}(u)$.

Let $N(t_e, u)$ be the number of events in time t_e for which the ground motion parameter U exceeds the limiting value u at a site due to earthquakes from all sources with any moment magnitude. Assume that $N(t_e, u)$ has a Poisson distribution with annual rate

$$\lambda(u) = \sum_{i,j} \nu_{ij}\bar{F}_{ij}(u). \tag{2-3}$$

The probability of getting at least one event exceeding u during the time period t_e is

$$P(u) = p_o = 1 - e^{-\lambda(u)t_e}. \tag{2-4}$$

The USGS is interested in the value of u that has a 2% probability of exceedance in 50 years. Using $t_e = 50$ and several different values of u in Equation (2-4), a graph like Figure 2-6 can be drawn and the value of u for which $p_o = 0.02$ determined by interpolation. For New York City, it was found that the value is 0.423 g for a 0.2 second spectral acceleration.

Thus, for the New York City site

$$1 - e^{-50\lambda(0.423)} = 1 - e^{-50\sum_{i,j}\nu_{ij}\bar{F}_{ij}(0.423)} = 0.02, \tag{2-5}$$

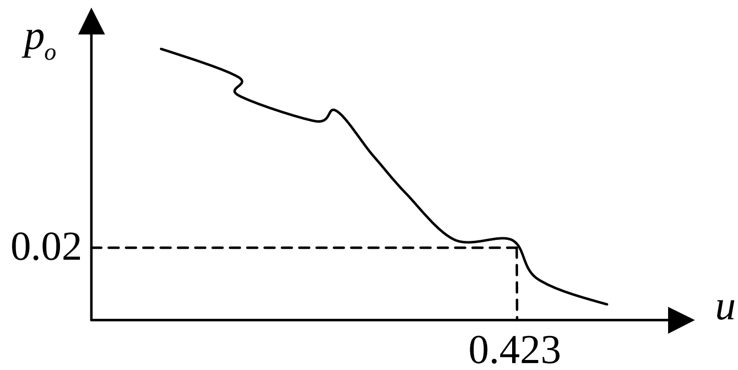

FIGURE 2-6 Limiting value u for New York City corresponding to 2% probability of exceedance in 50 years.

or equivalently

$$\sum_{i,j} \nu_{ij} \bar{F}_{ij}(0.423) = 0.0004. \tag{2-6}$$

The deaggregation matrices [Tables 2-1 and 2-2] gives the percentage contribution of each term, h_{ij}, in the above sum. The number h_{ij} appearing in Tables 2-1 and 2-2 in the position corresponding area in ring i and moment magnitude range j is thus calculated from

$$h_{ij} = 100 \frac{\nu_{ij} \bar{F}_{ij}(u)}{\lambda(u)} = 100 \frac{\nu_{ij} \bar{F}_{ij}(u)}{\ln(1 - p_o)} t_e. \tag{2-7}$$

The number 100 in the Equation (2-7) is simply to convert to a percentage.

Thus, calculating the values of $\nu_{ij}, i, j = 1, 2, \ldots$ is straightforward. From Equation (2-7), we can obtain the seismic activity matrix as follow:

$$\nu_{ij} = -\frac{\ln(1 - p_o) h_{ij}}{100 t_e \bar{F}_{ij}(u)}. \tag{2-8}$$

Figure 2-7 shows an example of a seismic activity matrix for New York City.

Unfortunately, although deaggregation matrices have been produced for sites located at Western United States (WUS), no documentation on the mean and standard deviation of the lognormal distribution F_{ij} for WUS has been published. Instead, the earthquake occurrences have been cataloged by USGS and can be found at http://eqhazmaps.usgs.gov/html/catdoc.html. From these data, the mean and standard deviation can be obtained by histogram analysis.

2.2 Seismic Activity Model

Random samples of seismic activities at a site can be generated given a time period t and the seismic activity matrix of the site. Each sample is defined by the number of earthquakes

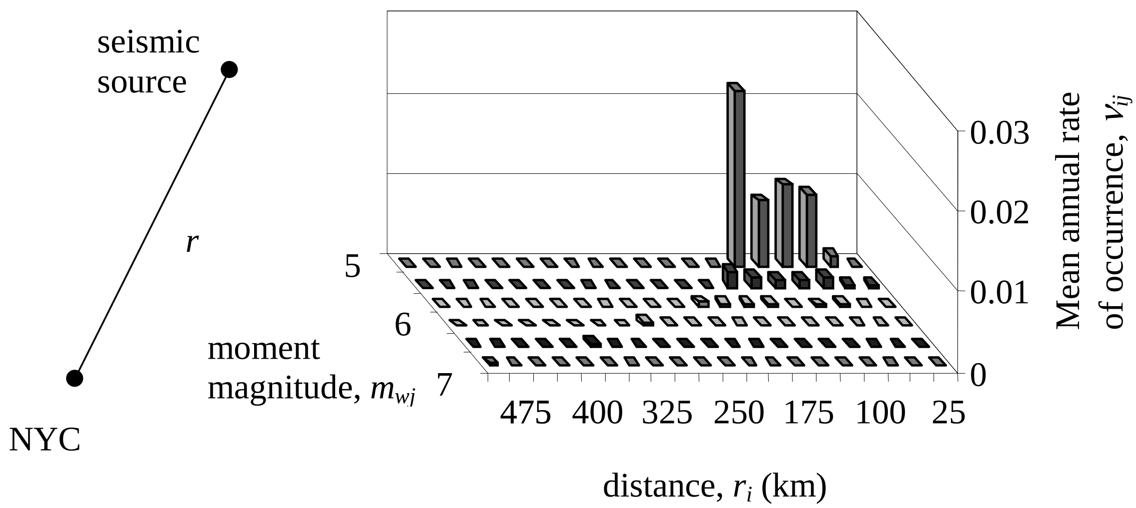

FIGURE 2-7 Seismic activity matrix of New York City.

during t, their temporal and spatial distribution, along with moment magnitude, and site-to-source distance.

Total number of earthquakes, $N(t)$, is assumed to have a Poisson distribution with annual mean rate ν,

$$\nu = \sum_{ij} \nu_{ij}. \tag{2-9}$$

Given the number of earthquake occurrences in t, assume that they are independent and uniformly distributed over the time t. Hence, the time of occurrence of each earthquake is simply a realization of a uniform distribution in $[0, t]$. The probability of each earthquake to have a moment magnitude in the range j coming from source in the ring i is as follow

$$P(m_{wj}, r_i) = \frac{\nu_{ij}}{\nu}. \tag{2-10}$$

2.3 Ground Motion Model

Seismic ground acceleration at a site can be modelled using a Gaussian process $G(t)$ with a spectral density $s_{GG}(\omega, r)$ as follow

$$s_{GG}(\omega, r) = \frac{|f_a(\omega, r)|^2}{2\pi t_w}, \tag{2-11}$$

where t_w is the duration of the strong ground motion (Halldorsson *et al.*, 2002), r is the site-to-source distance, $|f_a(\omega, r)|$ is the Fourier amplitude spectrum of the strong ground motion at the site (Halldorsson *et al.*, 2004), given by

$$|f_a(f, r)| = c \cdot q(f) \cdot d(f, r) \cdot p(f) \cdot z(f) \cdot i(f), \tag{2-12}$$

in which $f = \omega/2\pi$ is frequency in Hertz, c is a scaling factor, $q(f)$ is the acceleration source spectrum, $d(f,r)$ is the attenuation function, $p(f)$ is the high frequency cut-off filter, $z(f)$ is the function to define local soil effects, and $i(f)$ is the function used to get the desired output (acceleration, velocity, or displacement site spectrum). The acceleration source spectrum $q(f)$ is given by specific barrier model (Papageorgiou and Aki, 1983a),(Papageorgiou and Aki, 1983b),(Papageorgiou, 1988), and expressed as

$$q(f) = (2\pi)^2 \sqrt{n_s \left[1 + (n_s - 1)\left(\frac{\sin(\pi f t_f)}{\pi f t_f}\right)^2\right]} f^2 \tilde{m}_{0_i}(f), \tag{2-13}$$

where t_f is the duration of faulting event, n_s is the number of subevents, each having a seismic moment m_{0_i} and corner frequency f_2. The source spectrum of one individual subevent is given as

$$f^2 \tilde{m}_{0_i}(f) = \frac{m_{0_i} f_2^2}{1 + \left(\frac{f_2}{f}\right)^2}. \tag{2-14}$$

According to specific barrier model, fault surface is assumed to consist of circular cracks which represent areas of localized slip. Strong ground motion is the result of the cumulative contribution of localized cracks distributed on the fault plane, which rupture randomly and independently as the rupture front propagates during faulting. Rupture front is the instantaneous boundary between the slipping and locked parts of a fault during an earthquake.

2.4 Ground Motion Generation

Samples of seismic ground acceleration can be generated either for a single site or for multiple sites. Generation of samples of seismic ground acceleration for a single site will be presented first, followed by the generation of samples of seismic ground acceleration for multiple sites.

2.4.1 Ground Motion Generation for a Single Site

Seismic ground motion at a site is modeled by a Gaussian process $G(t)$ having a spectral density $s_{GG}(\omega, r)$ as described in previous section [Refer to Section 2.3]. The algorithm for generating samples of acceleration time histories is as follows:

1. **Calculate spectral density function** $s_{GG}(\omega, r)$
   Given moment magnitude m_w, site-to-source distance r, and soil type based on National Earthquake Hazard Reduction Program (NEHRP) classification [Refer to Table 2-3], obtain the spectral density function $s_{GG}(\omega, r)$.

   Figure 2-8 gives examples of spectral densities for a site experiencing 6.5 moment magnitude earthquake located at a distance of 105 km away from the seismic source for different soil types.

2. **Generate samples of stationary Gaussian process** $G(t)$
   A stationary Gaussian process $G(t)$ with a one-sided power spectral density of

TABLE 2-3 NEHRP Soil Classification.

Soil Type	Description	Mean Shear Wave Velocity to 30 m
A	Hard rock	> 1500 m/s
B	Firm to hard rock	760 - 1500 m/s
C	Dense soil, soft rock	360 - 760 m/s
D	Stiff soil	180 - 360 m/s
E	Soft clays	< 180 m/s
F	Special study soils	

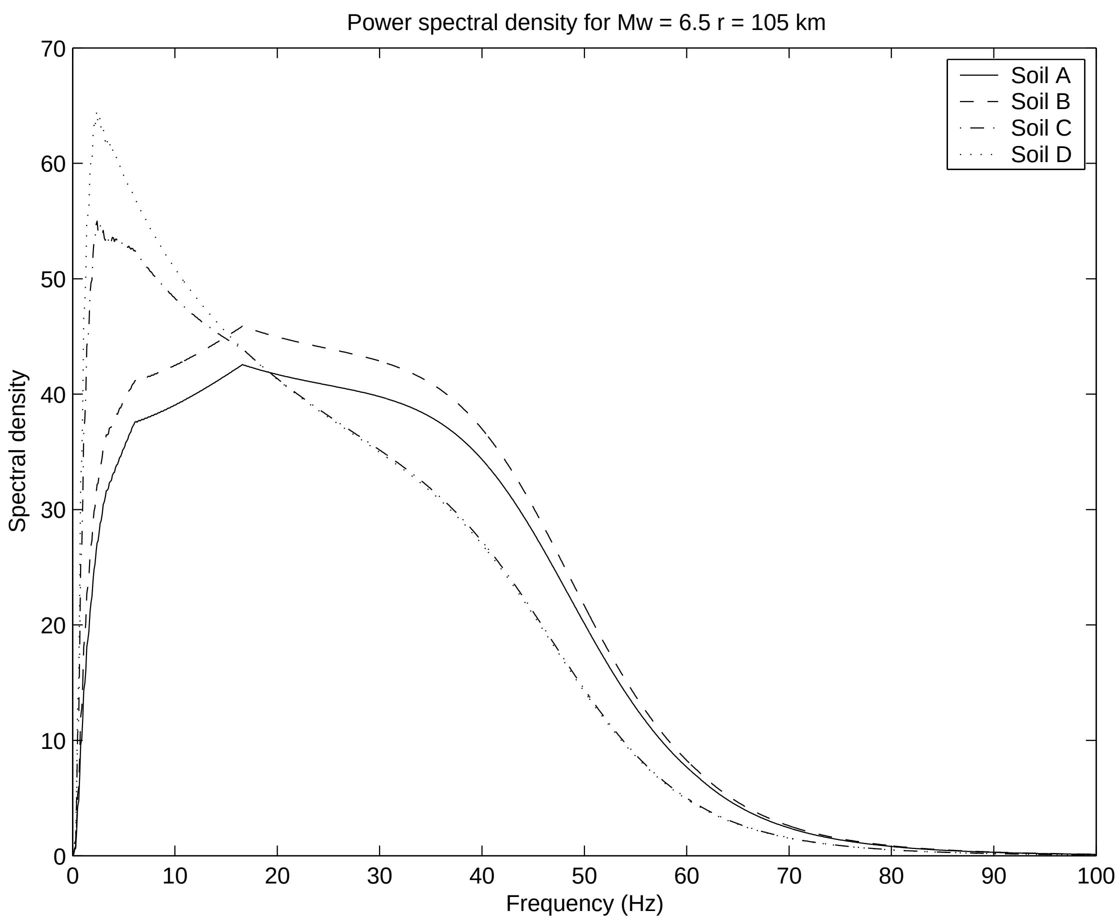

FIGURE 2-8 Power spectral densities for $m_w = 6.5$ and $r = 105$km.

$s_{GG}(\omega, r)$ has the spectral representation of

$$G(t) = \int_0^\infty \left[\cos(\omega t) dX(\omega) + \sin(\omega t) dY(\omega)\right], \tag{2-15}$$

where $X(\omega)$ and $Y(\omega)$ are processes with zero mean and orthogonal increments with increment variances $E\left[dX^2(\omega)\right] = E\left[dY^2(\omega)\right] = s_{GG}(\omega, r)d\omega$ (Soong and Grigoriu, 1992),(Grigoriu, 1995),(Grigoriu, 2002).

Since Equation (2-15) involves an uncountable set of random variables in the processes $X(\omega)$ and $Y(\omega)$, it is impossible to generate samples of $G(t)$. Instead of generating $G(t)$, an approximation of order n of $G(t)$ is used, which is expressed as

$$G_n(t) = \sum_{k=1}^{n} \sigma_k \left[A_k \cos(\omega_k t) + B_k \sin(\omega_k t)\right], \tag{2-16}$$

where $\omega_k, k = 1, \ldots, n$ are the midpoint frequencies of the partition of frequency band $[0, \omega^*]$, ω^* is the cut-off frequency, A_k and $B_k, k = 1, \ldots, n$ are Gaussian random variables with zero mean and unit variance. See Figure 2-9 for the description of σ_k (Soong and Grigoriu, 1992). The one-sided power spectral density of $G_n(t)$ is $\tilde{s}_{GG}(\omega, r)$, which equals $s_{GG}(\omega, r)$ for $0 \leq \omega \leq \omega^*$ and zero everywhere else.

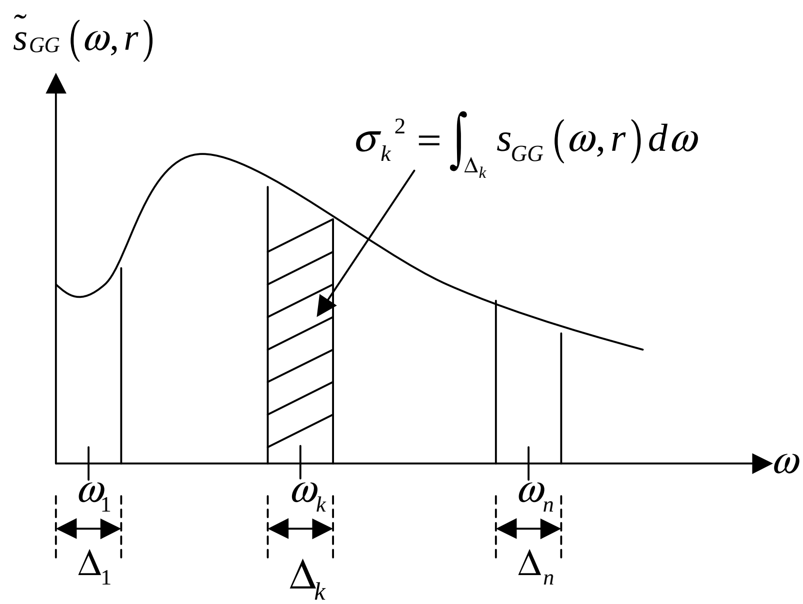

FIGURE 2-9 One sided power spectral density of $G_n(t)$.

3. **Compute samples of non-stationary Gaussian $A(t)$**
   Realistic ground acceleration samples $A(t)$ can be produced by multiplying $G_n(t)$with an envelope function $w(t)$ to introduce non-stationarity (Halldorsson *et al.*, 2004),

$$A(t) = w(t)G_n(t), \tag{2-17}$$

where

$$w(t) = at^b e^{-dt}, \text{ where } t \geq 0, \tag{2-18}$$

in which t is time, and a, b, and d are constants define as follow (Boore, 1983):

$$
\begin{aligned}
b &= \frac{-\varepsilon \ln \eta}{1+\varepsilon\,(\ln \varepsilon - 1)}, \\
d &= \frac{b}{\varepsilon t_w}, \\
a &= \left(\frac{e^1}{\varepsilon t_w}\right)^b \text{ or } a = \left[\frac{(2d)^{2b+1}}{\Gamma(2b+1)}\right]^{1/2},
\end{aligned}
$$

where t_w is the duration of the motion and Γ is the gamma function. Figure 2-10 shows a sample of acceleration time history $A(t)$, which is obtained by multiplying a Gaussian time history $G_n(t)$ with envelope function $w(t)$.

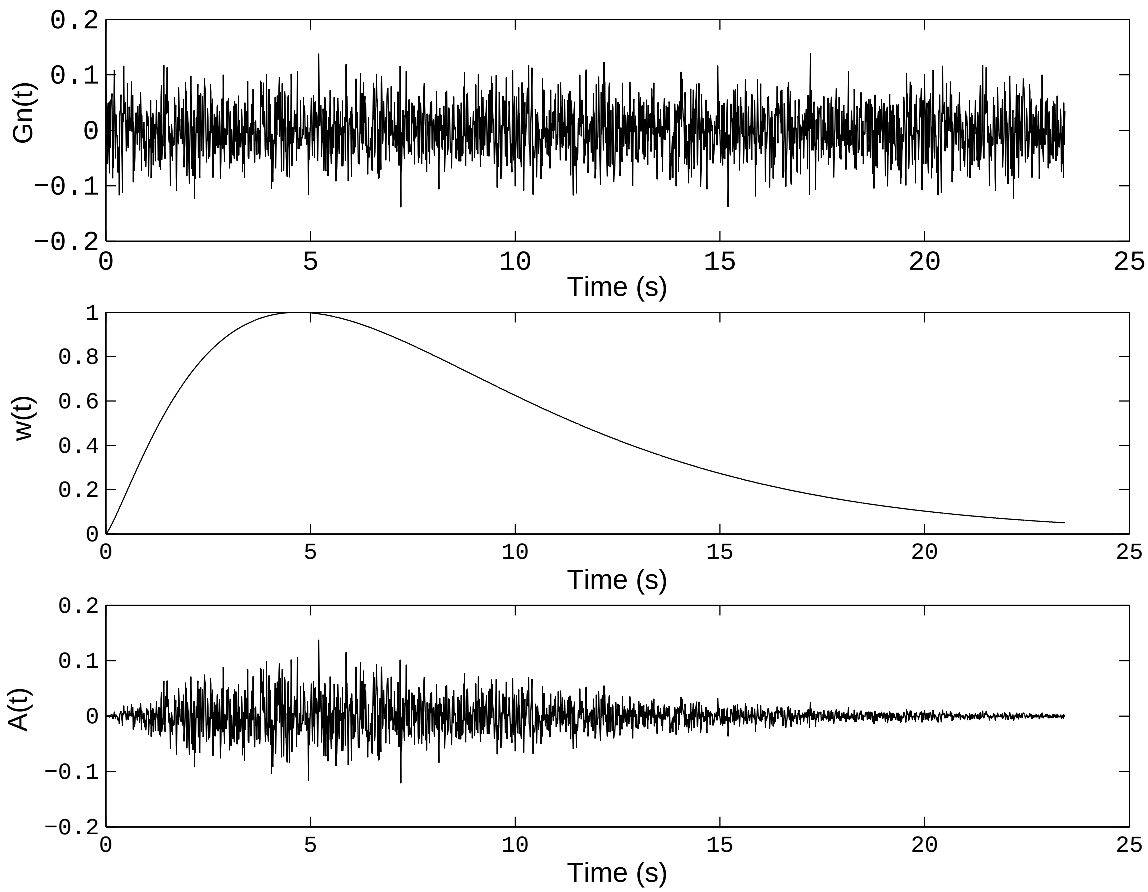

FIGURE 2-10 A sample of acceleration time history $A(t)$.

2.4.2 Ground Motion Generation for Multiple Sites

A model to generate seismic ground motion for n spatially distributed sites is developed (Kafali and Grigoriu, 2003). Let

$$\mathbf{X}(t) = (X_1(t), X_2(t), \ldots, X_n(t)), t \in [t_1, t_2]$$

be the seismic ground accelerations at n spatially distributed sites. It is assumed that $\mathbf{X}$ is a non-stationary Gaussian vector process, and the components of $\mathbf{X}(t)$ are defined by

$$X_i(t) = w_i(t)G_i(t), \ i = 1, \ldots, n$$

where $w_i(t)$ is an envelope function to account for non-stationarity, and $\mathbf{G}(t) = (G_1(t), G_2(t), \ldots, G_n(t))$ is a stationary Gaussian vector process with zero mean and unit variance. The spectral density of the underlying Gaussian process, $G_i(t)$ is given by specific barrier model (Papageorgiou and Aki, 1983a),(Papageorgiou and Aki, 1983b),(Papageorgiou, 1988).

The spectral densities of the vector process $\mathbf{G}(t)$ are

$$s_{ij}(\omega, r) = \gamma\left(\vec{\xi}_{ij}, \omega\right)\sqrt{s_{ii}(\omega, r)s_{jj}(\omega, r)} \tag{2-19}$$

where $i, j = 1, \ldots, n$, s_{ii} and s_{jj} are spectral density function at a site as given by Equation 2-11, $\vec{\xi}_{ij}$ is the separation vector between sites i and j [Refer to Figure 2-11].

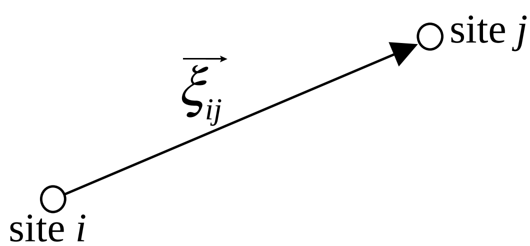

FIGURE 2-11 Separation vector between sites i and j, $\vec{\xi}_{ij}$.

$$\gamma\left(\vec{\xi}_{ij}, \omega\right) = \rho\left(\vec{\xi}_{ij}, \omega\right) e^{-i\omega d} \tag{2-20}$$

is a coherence function based on Harichandran and Vanmarcke's model (Harichandran and Vanmarcke, 1986), which depends on

$$d = \frac{\vec{V} \cdot \vec{\xi}_{ij}}{|\vec{V}|^2} \tag{2-21}$$

$$\begin{aligned}\rho\left(\vec{\xi}_{ij}, \omega\right) &= A \exp\left(\frac{-2|\vec{\xi}_{ij}|(1 - A + \alpha A)}{\alpha\theta(\omega)}\right) \\ &\quad + (1 - A)\exp\left(\frac{-2|\vec{\xi}_{ij}|(1 - A + \alpha A)}{\theta(\omega)}\right)\end{aligned} \tag{2-22}$$

$$\theta(\omega) \;=\; k\left(1+\left(\frac{|\omega|}{2\pi f_0}\right)^b\right)^{-1/2} \tag{2-23}$$

where $\vec{V}$ is the apparent wave propagation velocity vector whose direction coincides with the direction of the site from the source, and A, α, k, k, f_0, b are site specific parameters.

The coherence function describes a homogeneous, non-isotropic, space-time random field since $\rho\left(\vec{\xi}_{ij}, \omega\right)$ depends on the separation distance only, and not on the actual location.

As in the case for generating samples of seismic ground acceleration at one site, generation of samples of $\mathbf{X}(t)$ for a spatially distributed sites also involves three steps:

1. **Calculate spectral density function**
   For each site i, given the moment magnitude m_w, the site to source distance r_i, and the soil properties, calculate the spectral density function $s_{ii}(\omega, r_i)$ using Equation (2-11) .

2. **Generate samples of $\mathbf{G}(t)$**
   Let
   $$\mathbf{G}_q(t) = \sum_{r=1}^{q}\left(\mathbf{A}_r\cos(\omega_r t) + \mathbf{B}_r\sin(\omega_r t)\right) \tag{2-24}$$
   be the approximation of order q of the absolute acceleration process $\mathbf{G}(t)$,where $\omega_r = (r-1/2)\Delta\omega$ for $r = 1, \ldots, q$, in which $\Delta\omega = \omega^*/b$, ω^* is a cut-off frequency defined such that $\int_{-\infty}^{\infty} s_{kk}d\omega \simeq \int_{-\omega^*}^{\omega^*} s_{kk}d\omega$, $\forall k$, and $\mathbf{A}_r, \mathbf{B}_r$ are zero mean Gaussian vectors with the covariances,
   $$EA_{r,k}A_{p,l} \;=\; EB_{r,k}B_{p,l} = \delta_{rp}\int_{\alpha_{r-1}}^{\alpha_r} g_{kl}(\omega)d\omega \simeq \delta_{rp}g_{kl}(\omega_r)\Delta\omega \tag{2-25}$$
   $$EA_{r,k}B_{p,l} \;=\; -EB_{r,k}A_{p,l} = \delta_{rp}\int_{\alpha_{r-1}}^{\alpha_r} h_{kl}(\omega)d\omega \simeq \delta_{rp}h_{kl}(\omega_r)\Delta\omega \tag{2-26}$$
   where $g_{kl}(\omega) = s_{kl}(\omega) + s_{kl}(-\omega)$, $h_{kl}(\omega) = -i\left(s_{G_kG_l}(\omega) - s_{G_kG_l}(-\omega)\right)$, in which $k, l = 1, \ldots, n$, and $r, p = 1, \ldots, q$, $s_{kl}(\omega)$'s are the cross spectral density functions and E denotes the expectation operator (Grigoriu, 1995),(Grigoriu, 2002).

3. **Compute samples of non-stationary Gaussian $\mathbf{X}(t)$**
   To account for non-stationarity, multiply each $G_i(t)$ with an envelope function $w_i(t)$ as described in Section 2.4 for ground motion model at a site.
   Seismic ground accelerations are generated at points selected at 25 m in both directions in a 500 x 500 m^2 area characterized by NEHRP type-D soil. The samples correspond to an earthquake with moment magnitude 6.5 and site-to-source distance of 50 km. Figures 2-12 and 2-13 show samples of stationary and non-stationary Gaussian seismic ground accelerations at times 2 and 10 respectively. Figure 2-14 show the stationary and non-stationary Gaussian seismic ground acceleration time histories at the reference area.

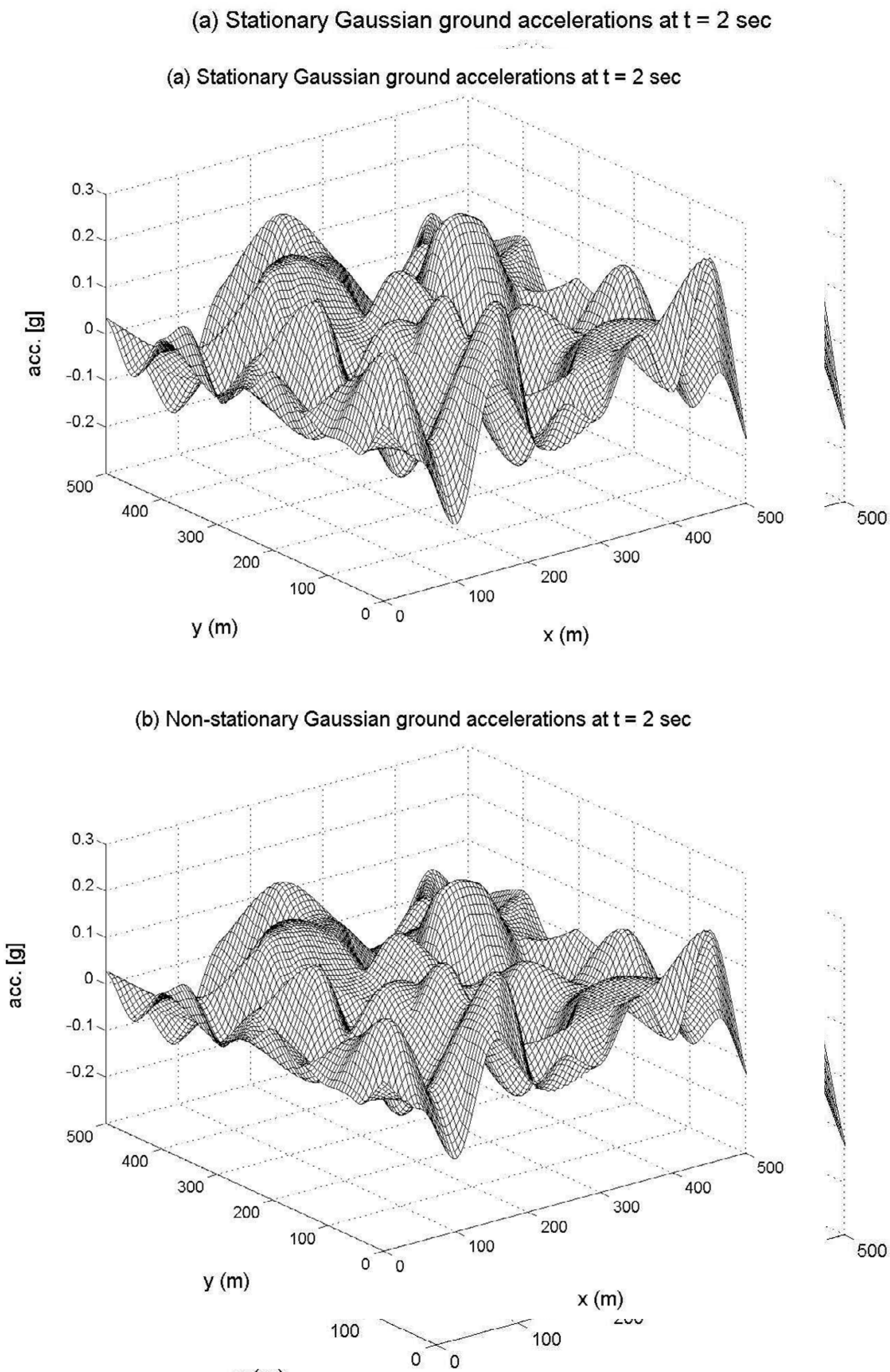

FIGURE 2-12 Stationary and non-stationary Gaussian seismic ground accelerations at t=2sec.

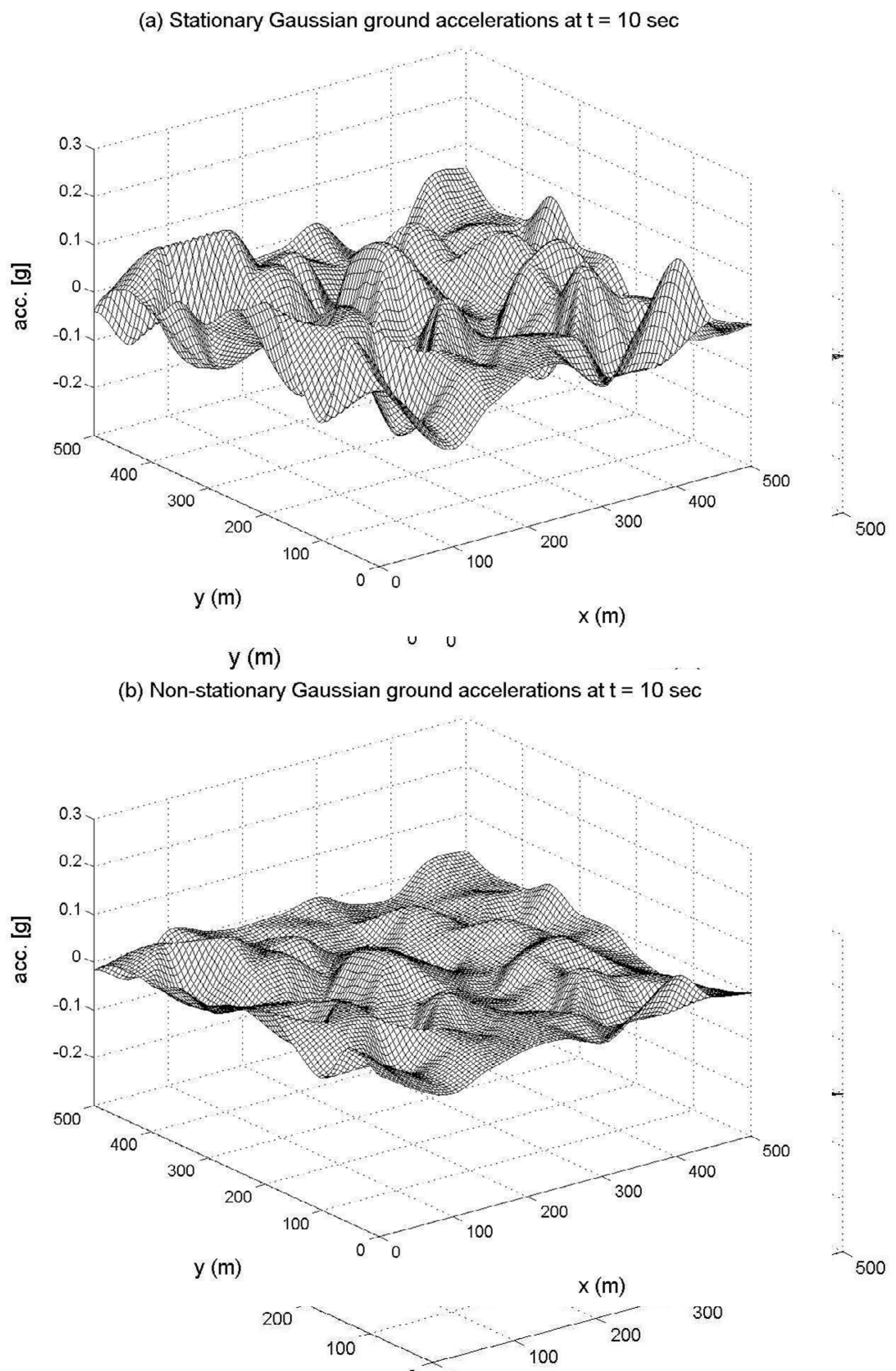

FIGURE 2-13 Stationary and non-stationary Gaussian seismic ground accelerations at t=10sec.

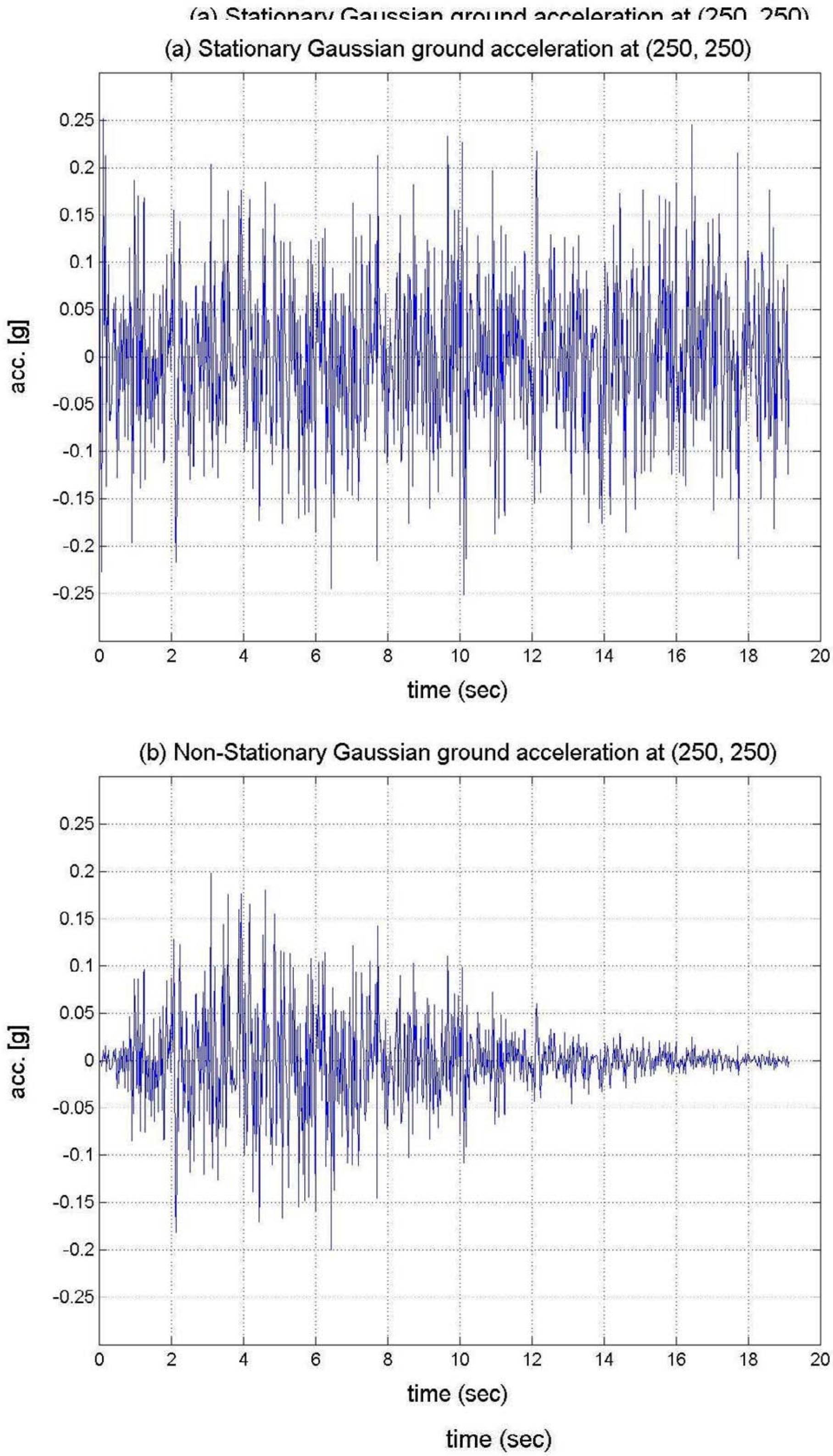

FIGURE 2-14 Stationary and non-stationary Gaussian seismic ground acceleration histories at (250,250).

SECTION 3
PIPE RESPONSE SUBJECT TO SEISMIC HAZARDS

Pipelines utilized in water supply systems typically range from 4 inches in diameter, which connects to consumers, up to 12 feet in diameter, which convey water from sources to treatment plants and from treatment plants to system nodes.

The most important pipelines in a water supply system are transmission and trunk pipelines, typically to 6 feet in diameter, with major conduits from 6 feet to 12 feet in diameter. They convey water from source collection areas to treatment plants, and from treatment plants to system nodes for distribution in smaller pipelines to individual customers (O'Rourke *et al.*, 2004).

During an earthquake, pipelines can be affected by permanent ground deformation (PGD) and transient ground deformation (TGD) (O'Rourke, 1998). Principal forms of PGD include fault displacement, landslides, seismic settlement and lateral spreading due to soil liquefaction (O'Rourke and Liu, 1999).

In the following sections, the TGD and PGD hazards will be discussed, along with the response of pipelines subjected to these hazards.

3.1 Seismic Wave Hazard

Seismic waves can be modeled as a travelling ground wave that retains its sinusoidal shape as it crosses a pipeline. Seismic waves at a site can be characterized by its peak ground velocity v_p and the apparent wave propagation velocity c (O'Rourke *et al.*, 1985).

3.2 Pipelines Response to Seismic Waves

Pipelines can have straight sections, bends, and/or tees. This research mainly deals with pipelines with straight sections, which are grouped into two broad categories, continuous pipelines and jointed pipelines.

3.2.1 Continuous Pipelines

Assuming that pipelines are rigidly attached to the surrounding soils, then the maximum pipelines axial strain ϵ_{pm} will equal the maximum ground strain ϵ_{gm} (O'Rourke *et al.*, 1985),(O'Rourke, 1996),(O'Rourke, 1998)

$$\epsilon_{pm} = \epsilon_{gm} = \frac{v_p \sin(\Omega)\cos(\Omega)}{c}, \tag{3-1}$$

where v_p is the peak ground velocity, Ω is the angle between propagation direction of the seismic wave and pipeline, and c is the apparent wave propagation velocity [Refer to Figure 3-1]. For shallow buried structures, such as pipelines, the dominating waves are S-waves with apparent wave propagation velocities in the range of 2 to 4 km/s (Hashash *et al.*, 2001).

The maximum axial force in a pipeline is

$$F_m = \epsilon_{pm} E A, \tag{3-2}$$

where E is the elastic modulus of the pipeline material and A is the cross sectional area of the pipeline. Bending strains in pipelines are often neglected in calculation, since they are usually considerably much smaller compared to axial strains (O'Rourke *et al.*, 1985).

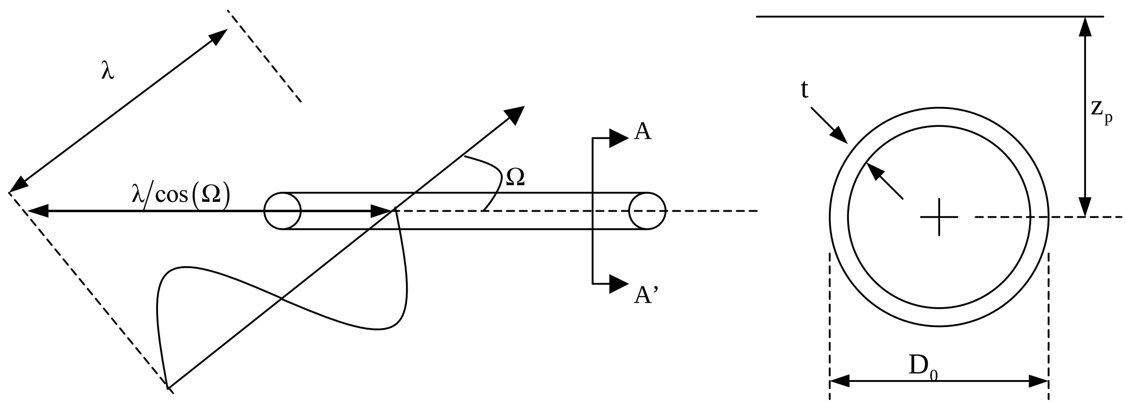

(a) wave orientation

(b) cross section A-A'

FIGURE 3-1 Seismic wave intersection with buried pipeline.

Equation (3-1) overestimates maximum pipe strain since slippage can occur at pipe-soil interface, which leads to maximum pipe strain less than maximum ground strain. Due to soil and pipeline interaction, frictional force per unit length f is conveyed to the pipe,

$$f = \frac{1}{2}(1 + k_0)\pi D_o \gamma z_p \tan\delta, \tag{3-3}$$

where k_0 is the coefficient of lateral earth pressure at rest, a value of $k_0 = 1$ is recommended (O'Rourke *et al.*, 1985),(O'Rourke, 1996), D_o is the outer diameter of the pipeline, γ is the unit weight of the soil, z_p is the depth from soil surface to the centerline of the pipe, and δ is the interface friction angle between pipe and soil. Some typical values of δ are given in Table 3-1 (O'Rourke, 1996).

The maximum pipe force F_m developed by shear transfer between soil and pipeline is

$$F_m = \frac{f\lambda}{4\cos\Omega}, \tag{3-4}$$

where $\lambda = cT_p$ is the predominant wave length and T_p is the predominant period of the transient displacement wave. The predominant period is the period of vibration corresponding to the maximum value of the Fourier amplitude spectrum (Kramer, 1996). Maximum pipe force F_m is as given in Equation (3-4) and bounded in the upper limit by Equation(3-2).

$$F_m = \frac{f\lambda}{4\cos\Omega} \leq \epsilon_{pm} E A \tag{3-5}$$

TABLE 3-1 Pipeline interface angles of friction for contact with granular soil.

Pipeline interface material	Ratio of interface to soil angle of friction, δ/ϕ, or δ-value for design
Rusted and pitted steel, partially cemented and bonded to adjacent soil; rough concrete and cement coating	1.0
Soft coatings and wrappings, such as coal tar enamels, hot or cold applied mastics, and coal tar epoxies	$\delta = 30^o$
Rough steel, some oxidation and rusting of surface with minor pitting; smooth, finished concrete surface	0.7-0.9
Resin epoxy coating (assumes some aging and softening) Polyolefin or polyethylene coating	0.6-0.8 0.6-0.7
"Frictionless" wrap, employing geogrid on polyethylene, polyolefin, or epoxy coating	$\delta = 10^o - 15^o$

3.2.2 Jointed Pipelines

Pipelines typically consist of segments made up of concrete, steel, or other materials. Jointed concrete cylinder pipelines (JCCP) is chosen to represent jointed pipeline analysis.

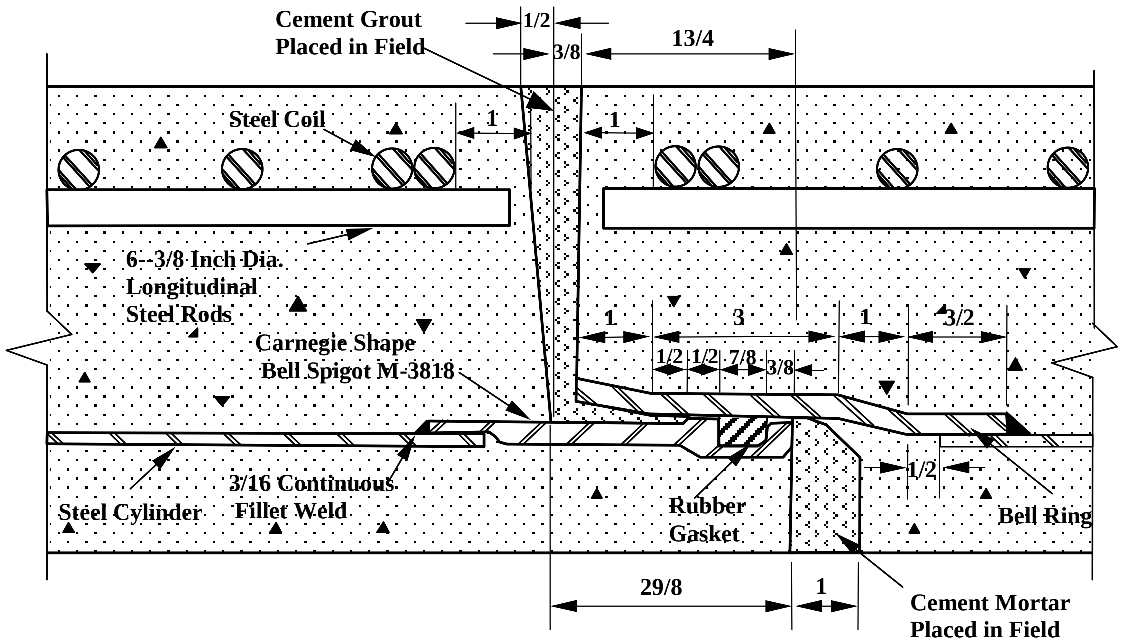

Figure Cross-Section for JCCP (unit: inch)

FIGURE 3-2 Cross section for JCCP.

JCCP represents pipelines composed of reinforced concrete and steel cylinders that are coupled with mortared, rubber-gasket bell-and-spigot joints [see Figure 3-2]. JCCP designs and methods of construction rely on a rubber-gasket bell-and-spigot connection. The rubber-gasket is around 18 to 20 mm wide when compressed to form a water tight seal. Cement mortar is poured in the field to further seal the joint. The axial tensile capacity of the joint depends on the tensile strength of the poured mortal connection and the pullout resistance of the gasket (O'Rourke *et al.*, 2004).

The pull out capacity of the joint in terms of axial slip to cause leakage depends on how much movement can occur before the rubber-gasket loses its compressive seal. Typical slip capacity is around 25 mm (O'Rourke *et al.*, 2004).

In the field, it is common for joints to be cracked and separated due to installation and subsequent ground movement loads. This condition typically leads to a pipeline that is fully flexible, which satisfies

$$\frac{f}{EA} > \frac{\pi R}{2}, \tag{3-6}$$

where f is the frictional force per unit length, E is the elastic modulus of the pipe material, A is the pipe cross sectional area, R is the ratio of v_p/c to the rise distance $\lambda/4$, where v_p is the peak ground velocity, c is the apparent wave propagation velocity, and λ is the wave length. A relatively rigid pipeline is one which $f/(EA) < 2R/\pi$.

Assuming that joints on either side of a cracked joint have full mortar connectivity to mobilize the tensile capacity across the joint and that pipeline is fully flexible, the pipe strain ϵ_p will equal the ground strain ϵ_g everywhere the pipeline is continuous. At the cracked joint, the pipeline cannot sustain strain, therefore ϵ_p is 0. As seismic wave passes across the cracked joint, strain in the continuous pipeline on each side of the joint will accumulate linearly at a slope of f/EA until ϵ_p equals ϵ_g, after which pipe and ground strain are equal.

The shaded area in Figure 3-3(a) represents the integration of the differential strain between pipeline and ground, which equals the relative joint displacement δ_j that occurs as axial slip, and can be approximated by the triangular area as shown in 3-3(b) (O'Rourke *et al.*, 2004).

$$\delta_j = \left[\frac{v_p}{c}\right]^2 \frac{EA}{f} \tag{3-7}$$

3.3 PGD Hazard

PGD hazards such as landslides and liquefaction-induced lateral spreading and seismic settlement are characterized by the amount, geometry, and spatial extent of the PGD zone. While fault displacement PGD hazard is characterized by the horizontal and vertical offset and pipe-fault crossing angle (O'Rourke and Liu, 1999).

3.3.1 Landslides

Landslides are mass movements of the ground which may be triggered by ground shaking (O'Rourke and Liu, 1999). Based on effects of landslides to pipelines, landslides can be classified into three types (Meyersohn, 1991): (1) Type I includes rock fall and rock topple, which can cause damage to above-ground pipelines by direct impact, but has almost no effect on buried pipelines, (2) Type II includes earth flow and debris flow, in which transported material behaves like a viscous fluid, and (3) Type III includes earth slump and earth slide, in which the earth moves, more or less as a block. These usually occur along natural slopes, river channels, and embankments. Buried pipelines are most affected by type III landslides.

Jibson and Keefer (Jibson and Keefer, 1993) produced an analytical estimation of expected amount of landslide movement. By searching for critical failure surface, which is the slip surface, for a given factor of safety FS, critical acceleration a_c is obtained by

$$a_c = g(FS - 1)\sin\alpha, \tag{3-8}$$

where g is the acceleration of gravity and α is the inclined angle of the slope.

Using 11 strong-motion records with critical acceleration in the range between 0.02 and 0.4 g, Jibson and Keefer estimated the displacement of the landslides D_N by regression,

$$D_N = 1.460 \log I_a - 6.642 a_c + 1.546, \tag{3-9}$$

where D_N is the displacement of the landslides in centimeters and I_a is the Arias intensity in g defined as

$$I_a = \frac{\pi}{2g} \int [a(t)]^2 \, dt, \tag{3-10}$$

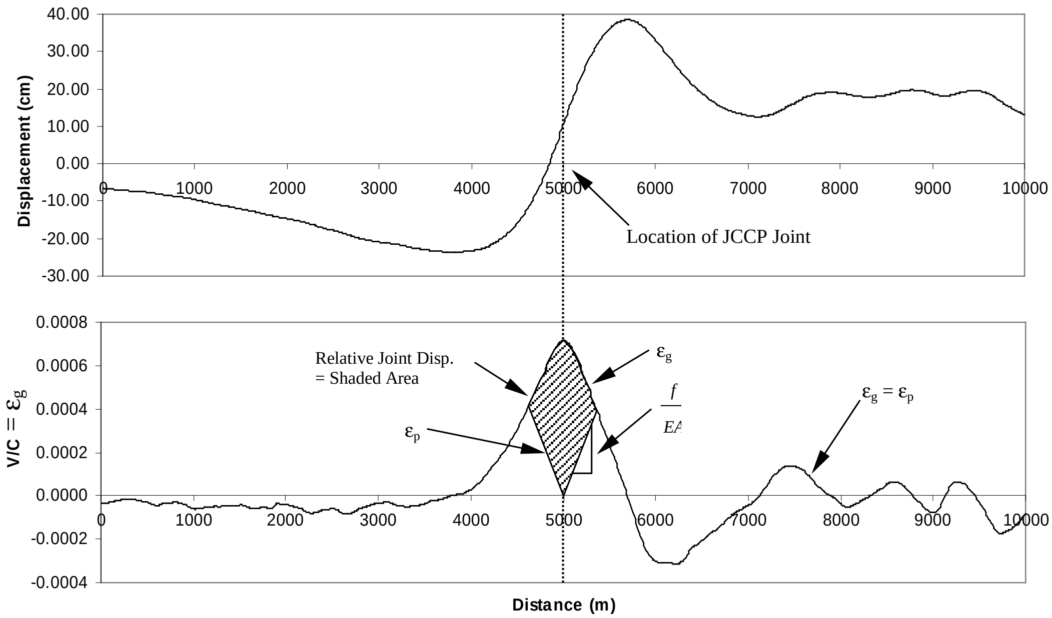

(a) Seismic displacement and velocity interaction with pipeline.

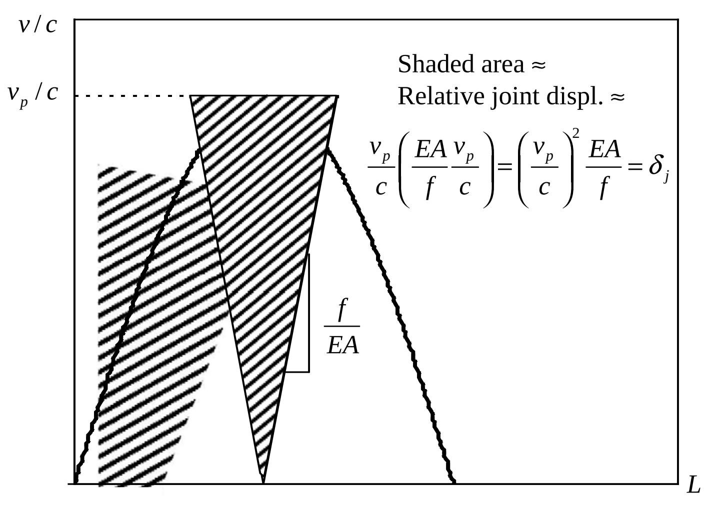

(b) Simplified model for seismic wave interaction with pipeline.

FIGURE 3-3 Seismic wave interaction with pipeline.

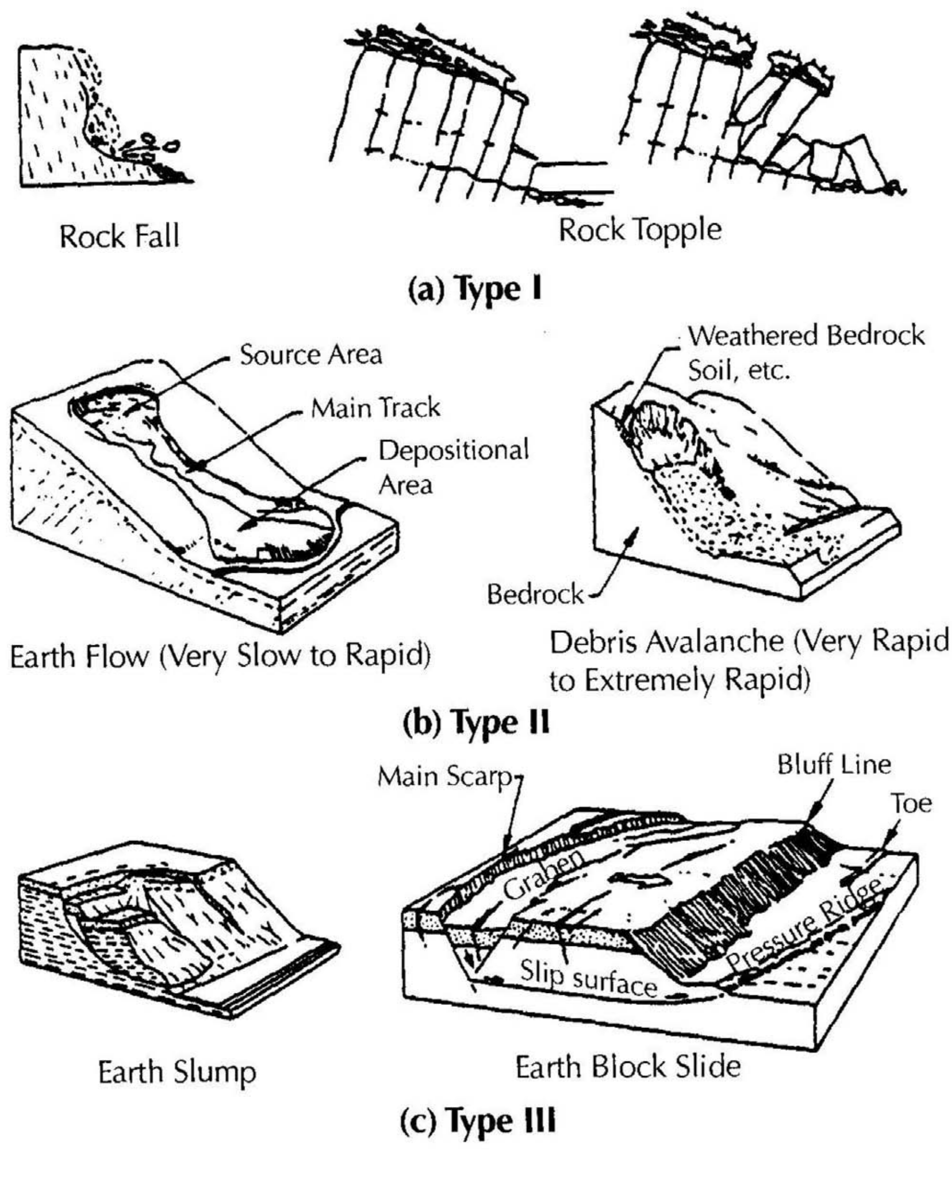

FIGURE 3-4 Types of landslides according to Meyersohn, 1991.

where $a(t)$ is the ground acceleration time history. Arias intensity can also be approximated (Wilson and Keefer, 1983) simply as a function of earthquake magnitude m_w and site-to-source distance r in kilometers by

$$\log I_a = m_w - 2\log r - 4.1. \tag{3-11}$$

3.3.2 Lateral Spreadings

Lateral spreading occurs when a loose saturated sandy soil deposit is liquefied due to ground shaking, causing soil to loose its shear strength and leads to the flow or lateral movement of liquefied soil (O'Rourke and Liu, 1999).

Lateral spreading can cause two types of pipeline response: (1) when top surface of the liquefied layer is at ground surface, pipeline is subject to horizontal force due to liquefied soil flow over and around the pipeline, as well as uplift or buoyancy force, (2) when top surface of the liquefied layer is below the pipeline (i.e. pipeline is contained in a non-liquefied soil layer which rides over the liquefied layer), pipeline is subject to horizontal forces due to non-liquefied soil-structure interaction (O'Rourke and Liu, 1999).

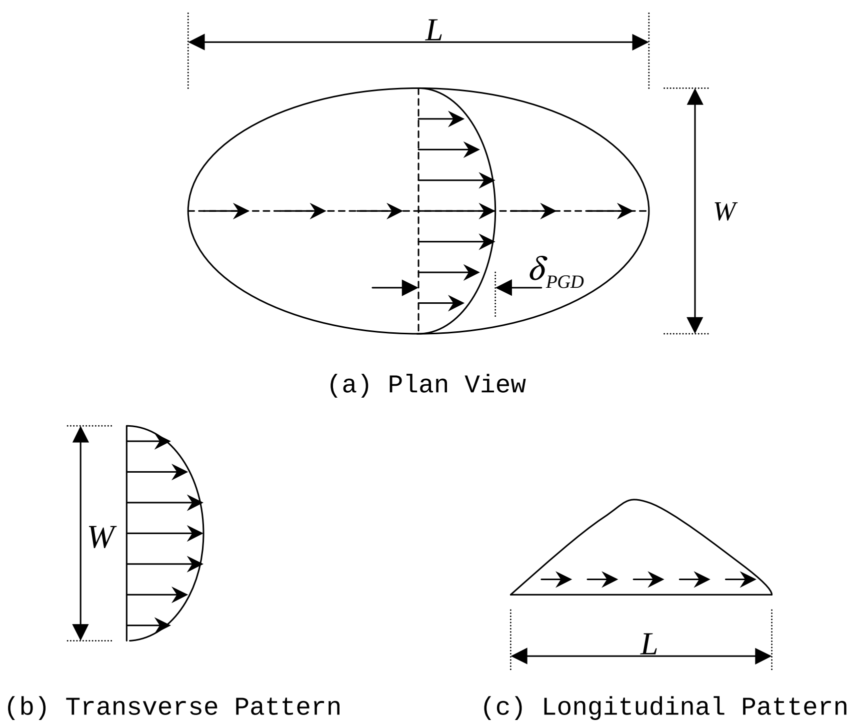

FIGURE 3-5 Characteristics of a lateral spread.

There are four geometric characteristics of a lateral spread influencing pipeline response in a horizontal plane: amount of PGD movement δ_{PGD}, transverse width of the PGD zone W, longitudinal length of the PGD zone L, and pattern or distribution of ground movement across and along the zone [Refer to Figure 3-5].

Bartlett and Youd (Barlett and Youd, 1992) developed two empirical relations for the expected amount of PGD due to liquefaction. The two empirical equations include the effects of shaking at the site, soil properties and site topography. The first is for lateral spreads occurring at sites with gentle slopes,

$$\begin{aligned}\log(\delta_{PGD}+0.01) = & -15.787 + 1.178m_w - 0.927\log r - 0.013r \\ & +0.429\log S + 0.348\log T_{15} \\ & +4.527\log(100 - F_{15}) - 0.922D_{50_{15}},\end{aligned} \tag{3-12}$$

and the second is for lateral spreads occurring at sites with steep slopes (i.e. at free faces),

$$\begin{aligned}\log(\delta_{PGD}+0.01) = & -15.787 + 1.178m_w - 0.927\log r - 0.013r \\ & +0.429\log Y + 0.348\log T_{15} \\ & +4.527\log(100 - F_{15}) - 0.922D_{50_{15}},\end{aligned} \tag{3-13}$$

where δ_{PGD}(m) is the permanent horizontal displacement of ground, m_w is the moment magnitude of the earthquake, r(km) is the site-to-source distance, S(%) is the ground slopes as shown in Figure 3-6a, Y(%) is the free face ratio as shown in Figure 3-6b, F_{15}(%) is the average fines content in T_{15}, $D_{50_{15}}$ (mm) is the mean grain size in T_{15}, and T_{15}(m) is the thickness of saturated cohesionless soils with a corrected Standard Penetration Test (SPT) value less than 15.

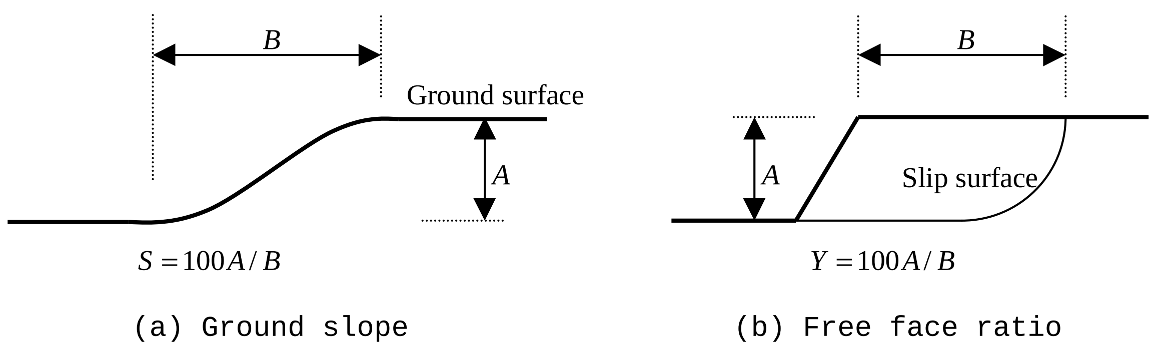

FIGURE 3-6 Elevation view showing ground slope and free face ratio.

SPT test involves driving a standard cylindrical sampler into the bottom of a borehole. The total blows required from a hammer, over the interval 150 to 450 mm are summed to give the blow count N, in blows per foot. The N-value is used as a basis for foundation design and as the primary index of liquefaction resistance (University of British Columbia, 2004).

3.3.3 Seismic Settlements

Seismic settlement can be caused by densification of dry sand, consolidation of clay or consolidation of liquefied soil (O'Rourke and Liu, 1999).

Tokimatsu and Seed (Tokimatsu and Seed, 1987) developed an analytical procedure to evaluate ground settlement for saturated sands after liquefactions without lateral spread movement, expressed as

$$\delta_{PGD} = \sum (\varepsilon_v)_i h_i, \text{ for } i = 1, 2, \ldots, n, \tag{3-14}$$

where ε_v is the volumetric strain for a saturated sandy soil layer, h is the layer thickness, and n is the number of sand layers with different SPT N-values.

The volumetric strain in each layer depends on the SPT N-value and the cyclic stress ratio as shown in Figure 3-7, where $(N_1)_{60}$ is the corrected SPT N-value. The cyclic stress ratio can be computed by

$$\frac{\tau_{ave}}{\sigma_0'} = 0.65 \frac{a_{max}}{g} \frac{\sigma_0}{\sigma_0'} r_d, \tag{3-15}$$

in which a_{max} is the maximum acceleration at the ground surface, σ_0 and σ_0' is the total overburden pressure and the initial effective overburden pressure on the sand layer under consideration and r_d is the stress reduction factor varying from a value of 1 at the ground surface to a value of 0.9 at a depth of about 10 m.

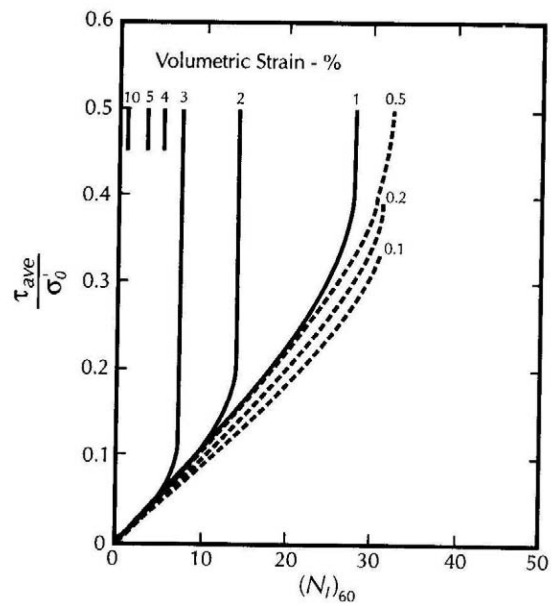

FIGURE 3-7 Relation between cyclic stress ratio $(N_1)_{60}$ and volumetric strain for saturated sands.

Another empirical method has been proposed by Takada and Tanabe (Takada *et al.*, 1987) for liquefaction-induced settlement at embankments and plain level sites based on 404 observations during five Japanese earthquakes. The formulation for embankments is

$$\delta_{PGD} = 0.11 H_1 H_2 a_{max}/N + 20, \tag{3-16}$$

and for plain level sites is

$$\delta_{PGD} = 0.3 H_1 a_{max}/N + 2, \tag{3-17}$$

where δ_{PGD} is the settlement in centimeters, H_1 is the thickness of saturated sand layers in meters, H_2 is the height of the embankment in meters, N is the SPT N-value in sand layer, and a_{max} is the ground acceleration in cm/sec^2.

In general, Takada and Tanabe's model is simpler than Seed et al.'s model, but it is also less accurate (O'Rourke and Liu, 1999).

3.3.4 Fault Displacements

Fault displacement or surface faulting is the deformation associated with the relative displacement of adjacent parts of the earth's crust (Committee on Gas and Liquid Fuel Lifelines, 1984). This displacement can occur suddenly during an earthquake or accumulate gradually over a long period of time.

Faults can be categorized into four types based on the direction of the movement or slip: strike-slip, normal, thrust, and oblique fault [see Figure 3-8]. Oblique fault is a combination of strike-slip and normal or thrust fault.

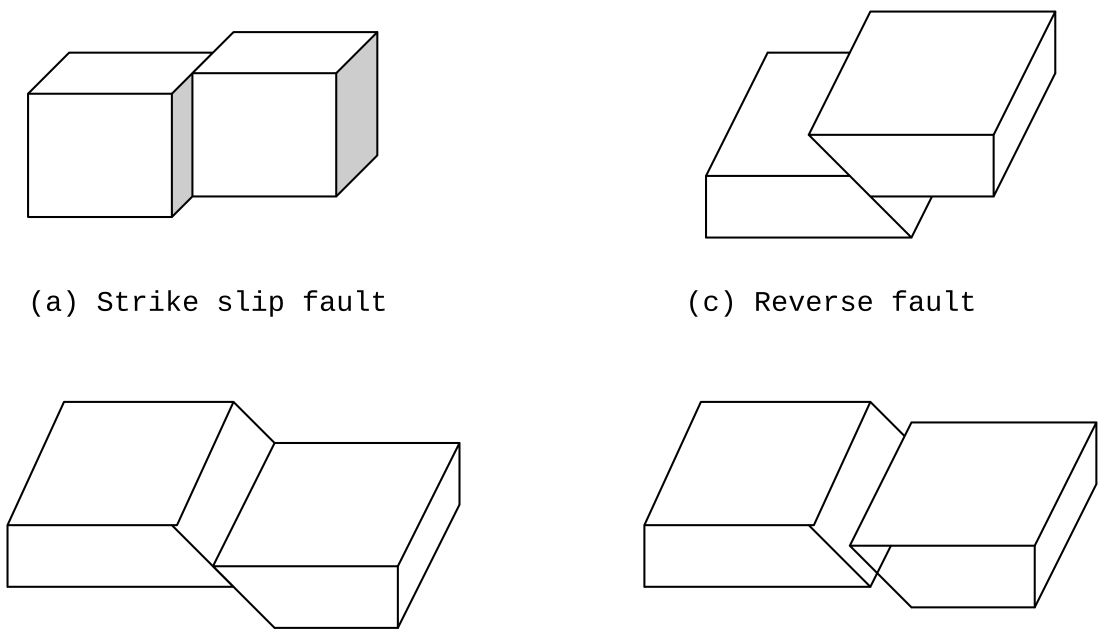

(a) Strike slip fault (c) Reverse fault

(b) Normal fault (d) Oblique fault

FIGURE 3-8 Fault types.

The predominant motion of a strike-slip fault is horizontal motion. Pipe subjects to this motion will deform primarily in tension or compression depending on the fault crossing angle β.

For normal and reverse faults, the predominant ground motion is vertical. A normal fault is defined for the condition in which the overhanging side of the fault moves downwards, and will cause tensile deformation. A reverse fault is resulted when the overhanging side of the fault moves upwards, and will cause compressive deformation (O'Rourke and Liu, 1999).

Amount of fault displacement can be determined using empirical relationships, derived from worldwide data of 421 historical earthquakes, proposed by Wells and Coppersmith (Wells and Coppersmith, 1994) as follows:

$$\log \delta_f = -6.32 + 0.90 m_w \text{ for strike-slip faults,} \tag{3-18}$$

$$\log \delta_f = -4.45 + 0.63 m_w \text{ for normal faults,} \tag{3-19}$$

$$\log \delta_f = -0.74 + 0.08 m_w \text{ for reverse faults, and} \tag{3-20}$$

$$\log \delta_f = -4.80 + 0.69 m_w \text{ for all faults,} \tag{3-21}$$

where δ_f is the amount of fault displacement in meters, and m_w is the moment magnitude.

3.4 Pipelines Response to Permanent Ground Deformations

PGD can be decomposed into two components, longitudinal and transverse components. The soil movement of longitudinal components of PGD is parallel to the pipe axis, while the soil movement of transverse components of PGD is perpendicular to the pipe axis (O'Rourke and Liu, 1999). The following sections will first describe response of pipelines subject to longitudinal and transverse components of PGD, followed with response of pipelines subject to fault displacements.

3.4.1 Pipelines Response to Longitudinal PGD

Pipelines subject to longitudinal PGD can fail at welded joints, local buckling and wrinkling in a compressive zone, tensile rupture in a tension zone, or beam buckling for shallow buried pipes (O'Rourke and Liu, 1999).

Two models of buried pipe response to longitudinal PGD are available: (1) linear elastic model, where pipe is assume to be linear elastic, and is appropriate for pipe with slip joints, (2) inelastic model, where pipe is assume to follow Ramberg-Osgood model (Ramberg and Osgood, 1943), and is appropriate for pipe with arc welded butt joints (O'Rourke and Liu, 1999).

3.4.1.1 Elastic Model

Five idealized patterns of ground deformation due to longitudinal PGD are presented by M.O'Rourke and Nordberg, the block pattern, ramp pattern, ridge pattern, ramp-block pattern, and asymmetric ridge pattern shown in Figure 3-9 (O'Rourke and Nordberg, 1992).

The block pattern is the most conservative pattern since it results in the largest strain in an elastic pipe (O'Rourke and Liu, 1999). The pipe strain due to block pattern is given by

$$\epsilon_p = \begin{cases} \frac{\alpha L}{2L_{em}} & L < 4L_{em} \\ \frac{\alpha L}{\sqrt{LL_{em}}} & L > 4L_{em} \end{cases} \tag{3-22}$$

where

$$L_{em} = \frac{\alpha EA}{f}, \tag{3-23}$$

in which α is as shown in Figure 3-9, L is the length of the PGD zone as shown in Figure 3-5, L_{em} is the length over which the frictional force per unit length f must act to induce a pipe strain equal to the equivalent ground strain.

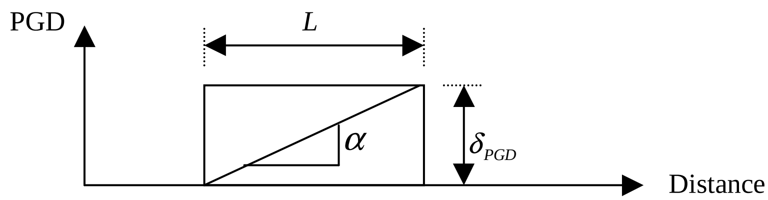

(a) Block pattern

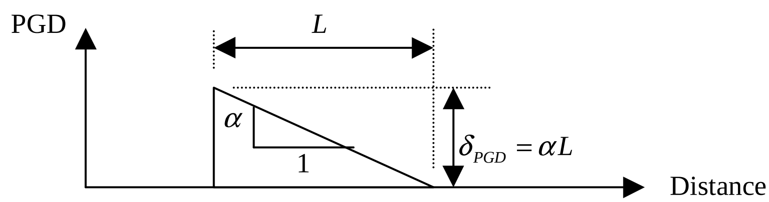

(b) Ramp pattern

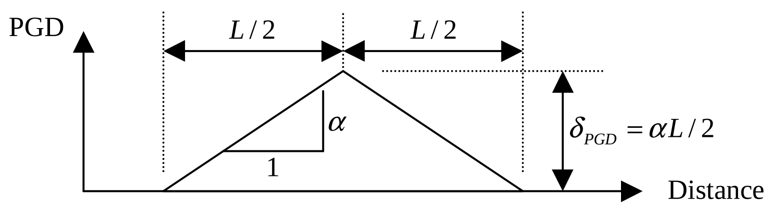

(c) Ridge pattern

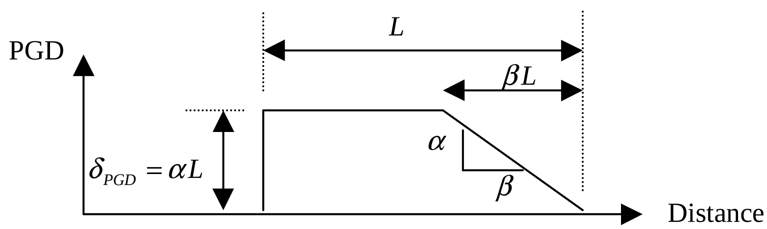

(d) Ramp-block pattern

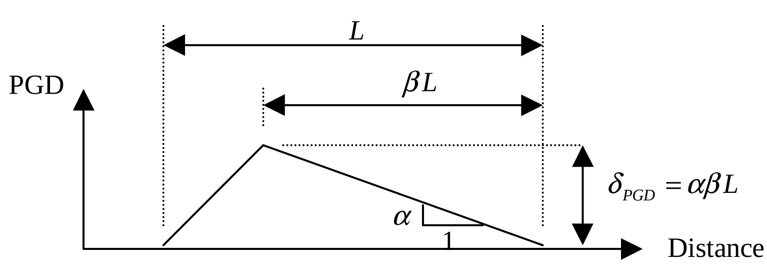

(e) Asymmetric ridge pattern

FIGURE 3-9 Five idealized patterns of ground deformation due to longitudinal PGD.

The model has been validated against the performance of pipelines that have relatively low strength of slip joints and unshielded arc welded joints during the 1994 Northridge earthquake (O'Rourke and Liu, 1999).

3.4.1.2 Inelastic Model

M.O'Rourke et al. use a Ramberg-Osgood model to calculate pipe strain and deformation for inelastic pipe, such as pipes with arc-weld joints (O'Rourke and Liu, 1999),(O'Rourke *et al.*, 1995).

Ramberg-Osgood model (Ramberg and Osgood, 1943) is expressed as

$$\epsilon = \frac{\sigma}{E}\left[1 + \frac{n}{(r+1)}\left(\frac{\sigma}{\sigma_y}\right)^r\right]. \tag{3-24}$$

Some of Ramberg-Osgood parameters for the more commonly used pipe materials are given in Table 3-2 (O'Rourke and Liu, 1999).

TABLE 3-2 Ramberg-Osgood parameters for mild steel and X-grade steel.

	Grade-B	X-42	X-52	X-60	X-70
σ_y (MPa)	227	310	358	413	517
n	10	15	9	10	5.5
r	100	32	10	12	16.6

Assuming that the pattern of ground deformation is the block pattern corresponding to a soil mass having a length L, using Ramberg-Osgood model, thepipe strain ϵ_p and pipe displacement δ_p is expressed as follows

$$\epsilon_p(x) = \frac{\beta_p x}{E}\left[1 + \frac{n}{1+r}\left(\frac{\beta_p x}{\sigma_y}\right)^r\right], \tag{3-25}$$

and

$$\delta_p(x) = \frac{\beta_p x^2}{E}\left[1 + \left(\frac{2}{2+r}\right)\left(\frac{n}{1+r}\right)\left(\frac{\beta_p x}{\sigma_y}\right)^r\right], \tag{3-26}$$

where n and r are Ramberg-Osgood parameters (Ramberg and Osgood, 1943), E is the modulus of elasticity, σ_y is the effective yield stress, β_p is the pipe burial parameter (lb/in^3), defined as

$$\beta_p = \frac{\tan(\delta)\gamma z_p}{t} \tag{3-27}$$

for granular material, where δ is the interface friction angle between pipe and soil, γ is the soil unit weight, z_p is the depth to pipe centerline, and t is the pipe wall thickness.

For a given critical strain ϵ_{cr} or critical pipe displacement δ_{cr}, we can solve for the critical length of PGD zone $x = L_{cr}$ using Equations (3-25) and/or (3-26).

This model has been used to successfully predict the behavior of two X-52 grade steel pipelines with arc welded joints subject to the longitudinal PGD at Balboa Blvd. during the 1994 Northridge earthquake (O'Rourke and Liu, 1999), (O'Rourke *et al.*, 1995).

3.4.2 Pipelines Response to Transverse PGD

Pipelines subject to transverse PGD will stretch and bend in attempt to accommodate the transverse ground displacement. Failure mode of the pipes depends on the relative amount of axial tension and flexural strain. When the axial tension is low, pipe can buckle in compression due to excessive bending. When the axial tension is high, pipe can rupture in tension due to combined effects of axial tension and bending (O'Rourke and Liu, 1999).

Response of pipe subject to transverse PGD is a function of the amount of PGD δ_{PGD}, width of PGD zone W, and the pattern of ground deformation. There are two possible patterns for transverse PGD, spatially distributed and localized abrupt as seen in Figure 3-10 (O'Rourke and Liu, 1999).

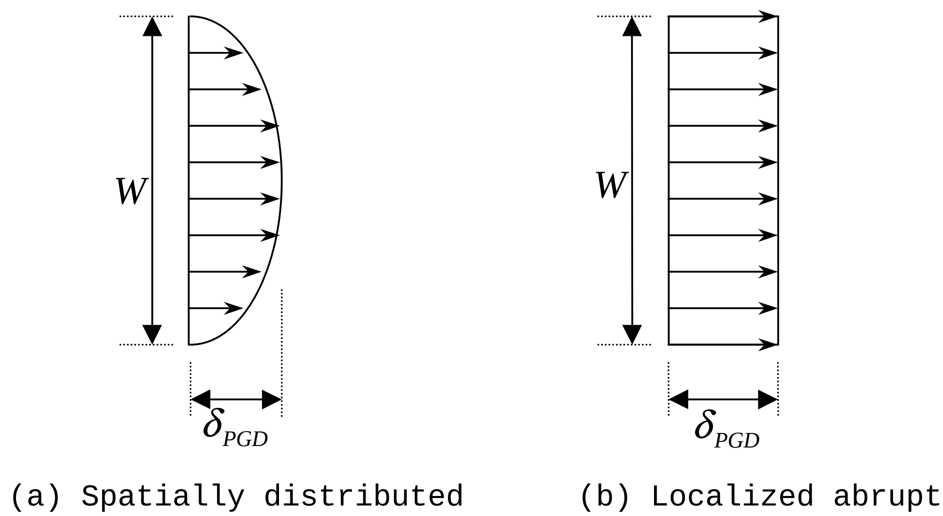

FIGURE 3-10 Patterns of transverse PGD.

When a pipe is buried directly in liquefied soil, another type of transverse PGD occurs. Pipe subjects to this type of transverse PGD will experience horizontal force due to lateral spreading and uplift due to buoyancy (O'Rourke and Liu, 1999).

Several models of spatially distributed transverse PGD is available: (1) T.D. O'Rourke's model (O'Rourke, 1988), (2) Suzuki and Kobayashi et al. model (Suzuki *et al.*, 1988),(Kobayashi *et al.*, 1989), and (3) M.O'Rourke's model (O'Rourke, 1989).

T.D.O'Rourke (O'Rourke, 1988) approximates soil deformation using a beta probability density function

$$y(x) = \delta_{PGD} \left(\frac{s}{s_m} \right)^{r'-1} \left(\frac{1-s}{1-s_m} \right)^{\tau - r' - 1}, 0 < s < 1, \tag{3-28}$$

where s is the distance between the two margins of the PGD zone normalized by the width

W, s_m is the normalized distance from the margin of the PGD zone to the location of the peak transverse ground displacement δ_{PGD}, and r' and τ are parameters for distribution. T.D.O'Rourke uses values of $s_m = 0.5, r' = 2.5$, and $\tau = 5.0$.

Suzuki et al. (Suzuki *et al.*, 1988) and Kobayashi et al. (Kobayashi *et al.*, 1989) use a cosine function raised to a power n to approximate the soil deformation as follow

$$y(x) = \delta_{PGD} \left(\cos \left(\frac{\pi x}{W} \right) \right)^n , \tag{3-29}$$

where x is a non-normalized distance measured from the center of PGD zone. They use value of $n = 0.2$, 1.0, 2.0 and 5.0 in their analysis.

M.O'Rourke (O'Rourke, 1989) use the following function to approximate soil deformation

$$y(x) = \frac{\delta_{PGD}}{2} \left(1 - \cos \left(\frac{2\pi x}{W} \right) \right) , \tag{3-30}$$

where x is again the non-normalized distance measured from the center of PGD zone. This function gives the same shape of soil deformation as the Suzuki and Kobayashi et al. function for $n = 2$ (O'Rourke and Liu, 1999).

Two types of pipe response is possible depend on whether the pipe is located in a non-liquefied soil or a liquefied soil. Following is some brief description of pipe response for each condition.

3.4.2.1 Pipe Surrounded by a Non-Liquefied Soil

When pipeline is located above the ground water level and the top surface of the liquefied soil layer, the force-deformation relations at the soil-pipeline interface correspond to a pipe in a non-liquefied soil which overrides a liquefied soil layer (O'Rourke and Liu, 1999).

M.O'Rourke (O'Rourke, 1989) developed a simple analytical model for pipeline response to spatially distributed transverse PGD. Two types of response are considered, depending on the width of the PGD zone. For a wide PGD zone, pipe is relatively flexible and its lateral displacement is assumed to closely match the soil, pipe strain is assumed to be mainly due to ground curvature. For a narrow PGD zone, pipe is relatively stiff and its lateral displacement is substantially less than that of the soil, pipe strain is assumed to be due to loading at soil-pipe interface.

For the wide PGD zone or flexible pipe case, the maximum bending strain ϵ_b in pipe is

$$\epsilon_b = \pm \frac{\pi^2 \delta_{PGD} D_o}{W^2} , \tag{3-31}$$

where δ_{PGD} is amount of ground displacement due to transverse PGD, D_o is the pipe outer diameter, and W is the width of PGD zone. The average axial tensile strain ϵ_a is approximated by

$$\epsilon_a = \left(\frac{\pi}{2} \right)^2 \left(\frac{\delta_{PGD}}{W} \right)^2 , \tag{3-32}$$

For the narrow PGD zone or stiff pipe case, the axial tension due to arc-length effects is small and neglected (O'Rourke and Liu, 1999). The maximum strain in the pipe is from bending, which is given by

$$\epsilon_b = \pm \frac{p_u W^2}{3\pi E t D_o^2}, \tag{3-33}$$

where p_u is maximum lateral force per unit length at the soil-pipe interface, p_u for granular soil is given by

$$p_u = \gamma z_p N_{qh} D_o, \tag{3-34}$$

in which γ is the soil unit weight, N_{qh} is the horizontal bearing capacity factors. Values of N_{qh} for sand is given in Figure 3-11 (Trautmann and O'Rourke, 1983).

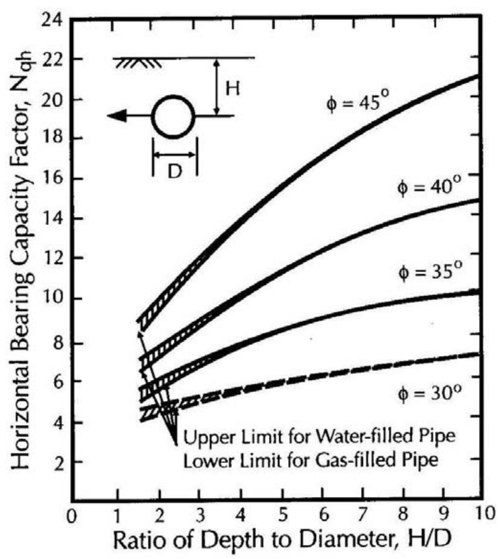

FIGURE 3-11 Horizontal bearing capacity N_{qh} for sand vs. depth to diameter ratio.

Liu and M.O'Rourke (Liu and O'Rourke, 1997b) updated the analytical method for pipeline response to transverse PGD based on their work with a finite element model. They found that pipe strain is an increasing function of ground displacement for ground displacement less than a certain value δ_{cr}, and pipe strain does not change much thereafter.

For narrow width of PGD zone, the critical ground deformation and pipe behavior are controlled by bending, with the same mechanism as the model proposed by M.O'Rourke for the stiff pipe case (O'Rourke, 1989). The critical ground deformation is given by

$$\delta_{cr-b} = \frac{5 p_u W^4}{384 E I}. \tag{3-35}$$

For wide width of PGD zone, pipe behaves like a flexible cable with a negligible flexural stiffness. Critical displacement is controlled primarily by the axial force. The relation between tensile force T and ground displacement δ_{PGD} is

$$T = \pi D_o t \sigma = \frac{p_u W^2}{16 \delta_{PGD}}, \tag{3-36}$$

where σ is the axial stress in the pipe and is assumed to be constant within the PGD zone.

At the margin of PGD zone, pipe tends to move inward due to axial force T. Assuming constant frictional force per unit length f beyond the margin, the pipe inward movement at each margin is

$$\Delta_{inward} = \frac{\pi D_o t \sigma^2}{2Ef}. \tag{3-37}$$

The total axial elongation of pipe within the PGD zone is approximated by the average axial strain given in Equation (3-32) due to arc-length effect times the width W, which is due to stretching within the zone ($\sigma W/E$) and inward movement at the margins. That is

$$\frac{\pi^2 \delta_{PGD}^2}{4W} = \frac{\sigma W}{E} + 2\frac{\pi D_o t \sigma^2}{2Ef}. \tag{3-38}$$

The critical ground deformation δ_{cr-a} and the corresponding axial pipe stress σ can be obtained by solving simultaneously for Equations (3-36) and (3-38).

For any arbitrary width of PGD zone, resistance is provided by both flexural and axial effects. Assuming that these two components act in parallel,

$$\delta_{cr} = \frac{1}{\frac{1}{\delta_{cr-b}} + \frac{1}{\delta_{cr-a}}}. \tag{3-39}$$

The maximum strain in a pipe ϵ_p due to the combined effects of axial and flexural is given by

$$\epsilon_p = \begin{cases} \frac{\pi \delta_{PGD}}{2}\sqrt{\frac{f}{AEW}} \pm \frac{\pi^2 \delta_{PGD} D_o}{W^2} & \delta_{PGD} \le \delta_{cr} \\ \frac{\pi \delta_{cr}}{2}\sqrt{\frac{f}{AEW}} \pm \frac{\pi^2 \delta_{cr} D_o}{W^2} & \delta_{PGD} > \delta_{cr} \end{cases} \tag{3-40}$$

where A is the pipe cross sectional area.

3.4.2.2 Pipe Located in a Liquefied Soil

Pipes located in liquefied soil can deform laterally following the flow of liquefied soil down a gentle slope, and/or can move upward due to buoyancy (O'Rourke and Liu, 1999).

Suzuki et al. (Suzuki *et al.*, 1988) analyze the pipe response surrounded by liquefied soil subject to spatially distributed transverse PGD. The presence of liquefied soil was modeled by assuming that the lateral soil coefficient for a pipe surrounded by liquefied soil K_1 is some fraction of the corresponding value of the non-liquefied soil K_2. They found that the pipe strain for $\delta_{PGD} \ge 1.5$ m is proportional to the soil coefficient reduction factor K_1/K_2.

According to Takada et al. (Takada *et al.*, 1987), equivalent soil spring coefficient for liquefied soil ranges from 1/1000 to 1/3000 of that for non-liquefied soil. Other scholars suggest that the ratio is 1/100 to 1/500 (O'Rourke and Liu, 1999). Therefore, pipe surrounded by liquefied soil is very unlikely to be damaged by spatially disturbed transverse PGD.

Hou et al. (Hou *et al.*, 1990) analyze pipe strain due to buoyancy effects. The uplifting force per unit length P_{uplift} acting on a pipe within a liquefied zone can be expressed as

$$P_{uplift} = \frac{1}{4}\pi D_o^2 (\gamma - \gamma_{contents}) - \pi D_o t \gamma_{pipe}, \tag{3-41}$$

where D_o is the pipe outer diameter, γ is the unit weight of soil, $\gamma_{content}$ is the unit weight of the pipe content, for example water and gas, t is the pipe wall thickness, and γ_{pipe} is the unit weight of pipe material. Note that the uplifting force will decrease when a portion of the pipe is at the ground surface (O'Rourke and Liu, 1999).

The maximum pipe strain is a function of the liquefied zone length W, and occurs at a certain width of liquefied zone W_{cr} which can be expressed as

$$W_{cr} = \left(\frac{3\pi^3 EtH_c D_o^3}{p_u} \right)^{1/4}, \tag{3-42}$$

where E is pipe elastic modulus, H_c is the depth from the soil surface to the top of the pipe, and p_u is the lateral force per unit length at the soil-pipe interface given by Equation (3-34).

The uplifting force per unit length P_{uplift} is around 10% of lateral pipe-soil interaction for a pipe surrounded by non-liquefied soil, therefore it is very unlikely for a pipe to be damaged due to buoyancy, although it may uplift out of ground when the width of the liquefied zone W is large (O'Rourke and Liu, 1999).

If the large uplift displacement is not desirable, following equation can be used to determine the relation between maximum uplift displacement and the spacing of pipe restraints

$$\delta_{max}^3 + \frac{16I}{A}\delta_{max} - \frac{16p_u W_s^4}{AE\pi^5} = 0, \tag{3-43}$$

where I is the moment of inertia of the pipe, A is the pipe cross-sectional area, and W_s is the spacing of the pipe restraints to prevent pipe vertical displacement greater than δ_{max}.

3.4.3 Pipelines Response to Fault Displacements

The response of pipelines subject to fault displacement can be categorized into two cases (O'Rourke and Liu, 1999): (1) pipes are deformed due to bending and axial tensile force, typically caused by normal fault or strike-slip fault with fault crossing angle less than 90 degree, the failure mode is tensile rupture since the fault offset results primarily in tensile strain, and (2) pipes are deformed due to bending and axial compressive force, typically caused by reverse fault or strike-slip fault with fault crossing angle more than 90 degree, the failure mode is buckling since the fault offset results primarily in compressive strain.

Several methods are available to analyze pipelines response subject to fault displacement: (1) analytical methods such as Newmark-Hall procedure (Newmark and Hall, 1975) and Kennedy, et.al procedure (Kennedy *et al.*, 1977), and (2) using finite element analysis. Only analytical methods will be discussed.

3.4.3.1 Newmark-Hall Procedure

A model, such as shown in Figure 3-12 is considered. In this model, pipe deforms with amount of δ_f equals to the total fault movement due to a right lateral strike-slip fault with a fault crossing angle β. For β less than 90 degree, strike-slip fault will primarily cause a tensile strain in the pipe.

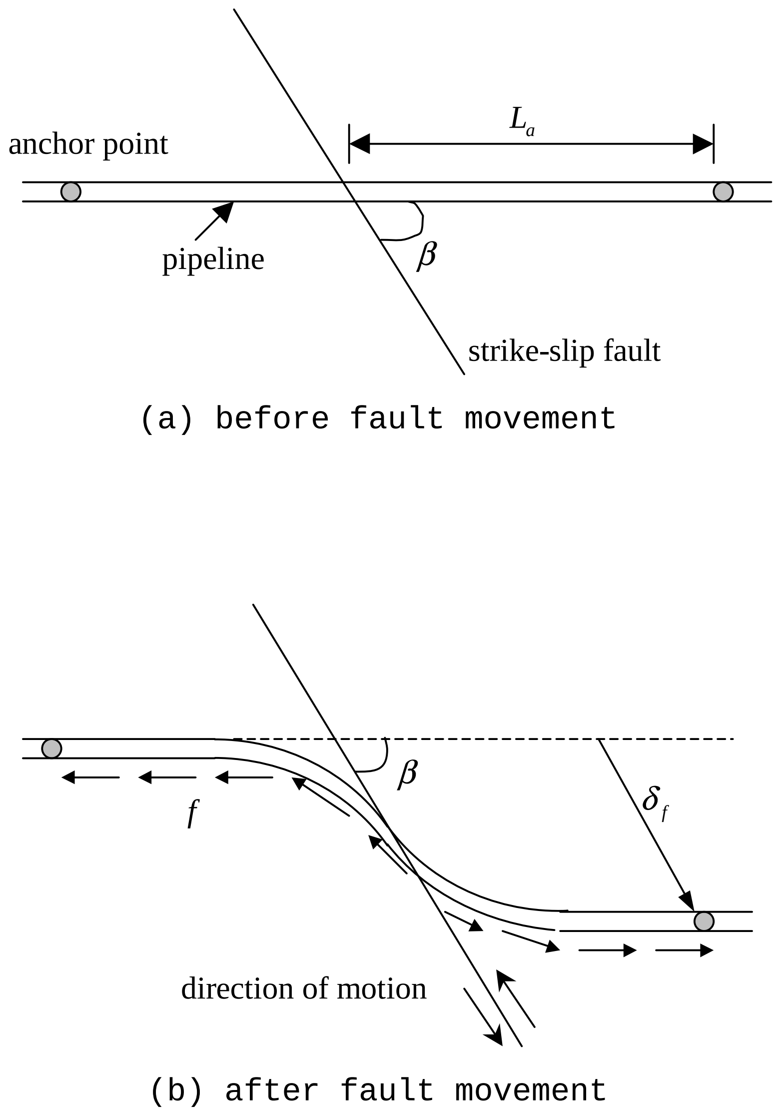

FIGURE 3-12 Newmark-Hall model of pipe response due to fault displacement.

Newmark-Hall model assumes that pipeline is firmly attached to soil at the two anchor points located at L_a away from the fault trace. Anchor points can be bends, tie-ins, or other features which develop substantial resistance to axial movement. Alternatively when no constraints are located near the fault trench, an effective anchor length can be used, beyond which there is no axial stress induced in the pipeline due to the fault movement (O'Rourke *et al.*, 1985). The model neglects the bending stiffness of the pipe and the lateral interactions at the pipe-soil interface (O'Rourke and Liu, 1999).

Total elongation of the pipe due to the fault displacement δ_f is the sum of the axial component of the fault movement $\delta_f \cos\beta$ and the arc-length effects caused by the lateral component of the fault movement $\delta_f \sin\beta$ (O'Rourke and Liu, 1999).

The average strain $\bar{\epsilon}$ resulted from the fault movement is

$$\bar{\epsilon} = \frac{\Delta L}{2L_a} \cong \frac{\delta_f}{2L_a}\cos\beta + \frac{1}{2}\left(\frac{\delta_f}{2L_a}\sin\beta\right)^2. \tag{3-44}$$

When no physical constraints are located near the fault trench, L_a can be approximated as follows

$$L_a = L_e + L_p, \tag{3-45}$$

$$L_e = \frac{E\epsilon_y \pi D_o t}{f}, \tag{3-46}$$

$$L_p = \frac{E_p\left(\epsilon_p - \epsilon_y\right)\pi D_o t}{f}, \tag{3-47}$$

where L_e is the length of pipe over which elastic strain develops, L_p is the length of pipe over which plastic strain develops, ϵ_y is the material yield strain, E_p is the modulus after yield, and ϵ_p is the plastic tensile strain of the pipe (O'Rourke and Liu, 1999).

To accommodate the resulted average strain $\bar{\epsilon}$, pipe must also elongate with the amount ΔL, which can be expressed as follows (Fau, 1976)

$$\Delta L = 2\epsilon_y\left[B_M L_a - \frac{hL_a^2}{2} - C\left[\frac{(B_M - hL_a)^{r+2}}{h(r+2)}\right] + C\frac{B_M^{r+2}}{h(r+2)}\right], \tag{3-48}$$

where

$$B_M = \frac{\sigma_m}{\sigma_y},$$

$$h = \frac{f}{A\sigma_y},$$

$$C = \frac{n}{r+1},$$

in which σ_m is the maximum stress resulted in the pipe, and n and r are the Ramberg-Osgood parameters (Ramberg and Osgood, 1943). Maximum strain in the pipe ϵ_m can be calculated with Ramberg-Osgood equation once the maximum stress σ_m is known.

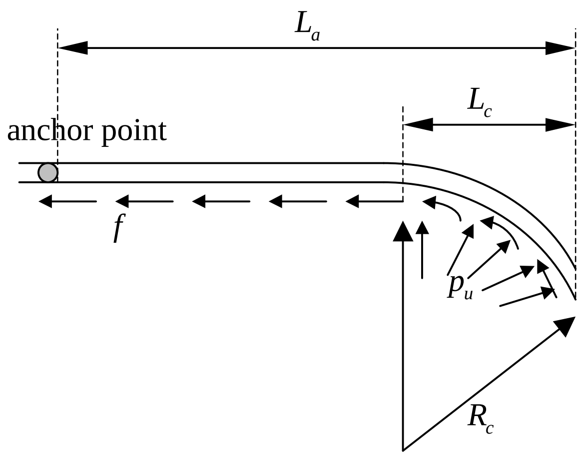

FIGURE 3-13 Kennedy, et al. model of pipe response due to fault displacement.

3.4.3.2 Kennedy, et al. Procedure

Kennedy, et al. extend the Newmark-Hall procedure by incorporating some improvements in the methodology for evaluating the maximum axial strain in the pipe. Effects of lateral interaction, which was omitted in the Newmark-Hall procedure, is incorporated in the analysis, and the influence of large axial strains on bending stiffness of the pipe is considered (Kennedy *et al.*, 1977),(O'Rourke and Liu, 1999).

Bending strain occurs in the curved region of the pipe with an assumed constant curvature $1/R_c$. Total strain resulted in the pipe $\bar{\epsilon}$ due to the fault movement is the sum of axial strain ϵ_a and bending strain ϵ_b (Kennedy *et al.*, 1977),(O'Rourke *et al.*, 1985),(O'Rourke and Liu, 1999). Bending strain ϵ_b is given as

$$\epsilon_b = \frac{D_o}{2R_c}, \tag{3-49}$$

where

$$R_c = \frac{\sigma_m \pi D_o t}{p_u}, \tag{3-50}$$

in which σ_m is the maximum stress seen in the pipe, for granular soils, $p_u = \gamma z_p N_{qh} D_o$ is the lateral soil-pipe interaction force per unit length, and N_{qh} is the horizontal bearing capacity factors.

Total elongation in the pipe ΔL resulted from the strain $\bar{\epsilon}$ is expressed as

$$\Delta L = \delta_f \cos\beta + \frac{(\delta_f \sin\beta)^2}{3L_c}, \tag{3-51}$$

where L_c is the horizontal projection length of the laterally deformed pipe and is given as

$$L_c = \sqrt{R_c \delta_f \sin\beta}. \tag{3-52}$$

To accommodate the resulted elongation ΔL resulting from strain $\bar{\epsilon}$, the pipe must also deform with the amount of ΔL_p which should equal ΔL (Fau, 1976).

$$\Delta L_p = \Delta L_s + \Delta L_c, \tag{3-53}$$

where

$$\Delta L_c = 2\epsilon_y \left\{ L_c \left[\frac{B_M + B_s}{2} \right] + \frac{C}{h_c (r+2)} \left[(B_M)^{r+2} - (B_s)^{r+2} \right] \right\}, \tag{3-54}$$

$$\Delta L_s = 2\epsilon_y \left\{ L_s \left[\frac{B_s + B_L}{2} \right] + \frac{C}{h_s (r+2)} \left[(B_s)^{r+2} - (B_L)^{r+2} \right] \right\}, \tag{3-55}$$

and

$$\begin{aligned} L_s &= L_a - L_c, \\ B_s &= B_M - h_c L_c, \\ B_L &= B_s - h_s L_s, \\ h_c &= \frac{f_c}{A\sigma_y}, \\ h_s &= \frac{f}{A\sigma_y}, \end{aligned}$$

where L_s is the straight portion of the pipe, and the ratio of f_c to f ranges from 2.4 for z_p/D_o equals 1 to 3.3 for z_p/D_o equals 3 (Kennedy *et al.*, 1977).

The maximum stress in the pipe σ_m can be determined from Equations 3-51 and 3-53. As in Newmark-Hall procedure, maximum pipe strain ϵ_m can be obtained from the Ramberg-Osgood model as given in Equation 3-24.

3.5 Summary of Equations

Equations for calculating pipe responses subject to various seismic hazards are summarized in Figures 3-14 and 3-15. Figures 3-14 shows the equations used for calculating pipe responses subject to seismic waves and PGD hazards. Figure 3-15 shows the equations used for calculating pipe responses subject to fault displacement hazard.

Summary of equations used to calculate pipe responses subject to seismic hazards

I. Seismic wave analysis:

1. Continuous pipelines

$$F_m = \frac{f\lambda}{4\cos(\Omega)} \le \varepsilon_{gm} EA$$

$$f = \frac{1}{2}(k_0+1)\pi D_o \gamma z_p \tan(\delta), \quad \lambda = cT_p$$

$$\varepsilon_{gm} = \frac{v_p}{c}\sin(\Omega)\cos(\Omega)$$

2. Jointed pipelines

$$\delta_j = \left[\frac{v_p}{c}\right]^2 \frac{EA}{f}$$

II. Permanent Ground Deformation (PGD) hazard analysis:

(landslides, lateral spreads and seismic settlements induced by liquefactions)

1. Longitudinal component

$$\varepsilon_p = \begin{cases} \dfrac{\alpha L}{2L_{em}} & \text{, for } L < 4L_{em} \\ \dfrac{\alpha L}{\sqrt{L L_{em}}} & \text{, for } L > 4L_{em} \end{cases} \qquad L_{em} = \frac{\alpha EA}{f}, \quad \alpha = \frac{\delta_{PGD}}{L}$$

2. Transverse component

$$\varepsilon_p = \begin{cases} \dfrac{\pi\delta_{PGD}}{2}\sqrt{\dfrac{f}{AEW}} \pm \dfrac{\pi^2\delta_{PGD}D_o}{W^2} & \text{, for } \delta_{PGD} < \delta_{cr} \\ \dfrac{\pi\delta_{cr}}{2}\sqrt{\dfrac{f}{AEW}} \pm \dfrac{\pi^2\delta_{cr}D_o}{W^2} & \text{, for } \delta_{PGD} < \delta_{cr} \end{cases}$$

$$\delta_{cr} = \frac{1}{\dfrac{1}{\delta_{cr\text{-}b}} + \dfrac{1}{\delta_{cr\text{-}a}}}, \quad \delta_{cr\text{-}b} = \frac{5p_u W^4}{384EI}, \quad p_u = \gamma z_p N_{qh} D_o$$

Solve simultaneously (1) and (2) for $\delta_{cr\text{-}a}$ and σ_a:

$$(1)\ \pi D_o t\sigma_a = \frac{p_u W^2}{16\delta_{cr\text{-}a}}, \quad (2)\ \frac{\pi^2\delta_{cr\text{-}a}^2}{4W} = \frac{\sigma_a W}{E} + \frac{\pi D_o t\sigma_a^2}{Ef}$$

F_m = maximum pipe force
f = frictional force per unit length
λ = wave length
Ω = angle between pipe and wave
ε_{gm} = maximum ground strain
E = Young's modulus
A = pipe cross sectional area
k_0 = coefficient of lateral earth pressure at rest
D_o = pipe outer diameter
γ = soil unit weight
z_p = depth to pipe centerline
δ = interface friction angle between pipe and soil
c = apparent wave propagation velocity
T_p = predominant period of transient displacement wave
v_p = peak ground velocity
δ_j = relative joint displacement
ε_p = pipe strain
L = length of PGD zone
δ_{PGD} = amount of PGD
W = width of PGD zone
δ_{cr} = critical amount of PGD
$\delta_{cr\text{-}b} = \delta_{cr}$ due to bending
$\delta_{cr\text{-}a} = \delta_{cr}$ due to axial stress
p_u = maximum lateral force per unit length at pipe-soil interface
I = moment of inertia
t = pipe wall thickness

FIGURE 3-14 Equations for pipe responses subject to seismic waves and PGD hazards.

Summary of equations used to calculate pipe responses subject to seismic hazards

III. Fault displacement hazard analysis:

1. Newmark-Hall method

Calculate σ_m so that (1) matches (2)

$$(1)\ \Delta L = \delta_f \cos(\beta) + \frac{\delta_f^2 \sin^2(\beta)}{4L_a}$$

$$(2)\ \Delta L = 2\,\varepsilon_y \left[B_M L_a - \frac{hL_a^2}{2} - C\left[\frac{(B_M - hL_a)^{r+2}}{h(r+2)}\right] + C\frac{B_M^{r+2}}{h(r+2)} \right]$$

where: $B_M = \frac{\sigma_m}{\sigma_y},\ h = \frac{f}{A\sigma_y},\ C = \frac{n}{r+1}$ then, $\varepsilon_m = \frac{\sigma_m}{E}\left[1 + C(B_M)^r\right]$

2. Kennedy et al. Method

Calculate σ_m so that (1) matches (2)

$$(1)\ \Delta L = \delta_f \cos(\beta) + \frac{\delta_f^2 \sin^2(\beta)}{3L_c}$$

$$(2)\ \Delta L = \Delta L_s + \Delta L_c$$

where: $L_c = \sqrt{R_c \delta_f \sin(\beta)}\ ,\ R_c = \frac{\sigma_m \pi D_o t}{p_u}$

$$\Delta L_c = 2\,\varepsilon_y \left\{ L_c\left[\frac{B_M + B_s}{2}\right] + \frac{C}{h_c(r+2)}\left[B_M^{r+2} - B_s^{r+2}\right] \right\}$$

$$\Delta L_s = 2\,\varepsilon_y \left\{ L_s\left[\frac{B_s + B_L}{2}\right] + \frac{C}{h_s(r+2)}\left[B_s^{r+2} - B_L^{r+2}\right] \right\}$$

$$L_s = L_a - L_c,\ \ B_s = B_m - h_c L_c,\ \ B_L = B_s - h_s L_s,\ \ h_s = h,\ \ h_c = \frac{f_c}{A\sigma_y}$$

Ratio of $f_c : f = 2.4$ for $z_p/D_o = 1$ upto 3.3 for $z_p/D_o = 3$

then, $\varepsilon_m = \frac{\sigma_m}{E}\left[1 + C(B_M)^r\right]$

N_{qh} = soil horizontal bearing capacity factor	β = angle between pipe and fault
σ_a = pipe axial stress	L_a = anchor length
σ_m = maximum pipe stress	ε_y = pipe yield strain
ΔL = pipe elongation	n,r = Ramberg-Osgood coefficients
δ_f = amount of fault displacement	R_c = radius of curvature for curved portion

δ

FIGURE 3-15 Equations for pipe responses subject to fault displacement hazard.

SECTION 4
FRAGILITY ANALYSIS OF PIPELINES

The variation of the conditional probability of failure or damage for a system/system component with some earthquake parameters is called fragility. Fragility curves provide the probability of exceeding different levels of damage or limit states as a function of peak ground acceleration (PGA) or other ground motion intensity measures (Grigoriu and Mostafa, 2002a).

Fragility curves can be produced analytically or empirically. Analytical fragility curves are generated from the results of simulations of the system subject to either historical or artificial ground motion records. The challenge in producing analytical fragility curves lies in the difficulties to generate ground motion histories that are consistent with the site and relating the results of simulation to predefined limit and/or damage states. Empirical fragility curves can be based from experimental results or real data collected from historical earthquakes. Scarcity in available data is the main challenge for this method.

Most commonly used seismic intensities against which fragility curves are plotted includes PGA, spectral acceleration (Sa), spectral velocity (Sv), and Modified Mercali Intensity (MMI). However, it has been shown that it is not adequate to characterize ground motion with only one parameter (Sewell, 1989).

Grigoriu and Mostafa (Grigoriu and Mostafa, 2002a) proposed the use of fragility surface, which has similar concept as fragility curves. Instead of using one parameter to characterize the ground motion, fragility surfaces provides the failure probability of a system as a function of moment magnitude m_w and site-to-source distance r. Fragility surface corresponds to the ith limit state is the conditional probability that the damage index DI exceeds a critical value DI_i given the seismic occurrence with moment magnitude m_w and site-to-source distance r.

$$F_i(x, y) = P\left[DI > DI_i | m_w, r\right]. \tag{4-1}$$

Figure 4-1 shows the typical configuration of fragility curves, the ground motion parameters are the combination of moment magnitude and site-to-source distance (m_w, r), and three different damage indexes DI_1, DI_2, DI_3 are plotted.

Fragility analysis of pipelines subject to transient ground deformation (TGD) hazard (i.e. seismic waves), permanent ground deformation (PGD) hazard including landslides, lateral spread and seismic settlement induced by liquefaction, and fault displacement hazard are performed and described in the following sections.

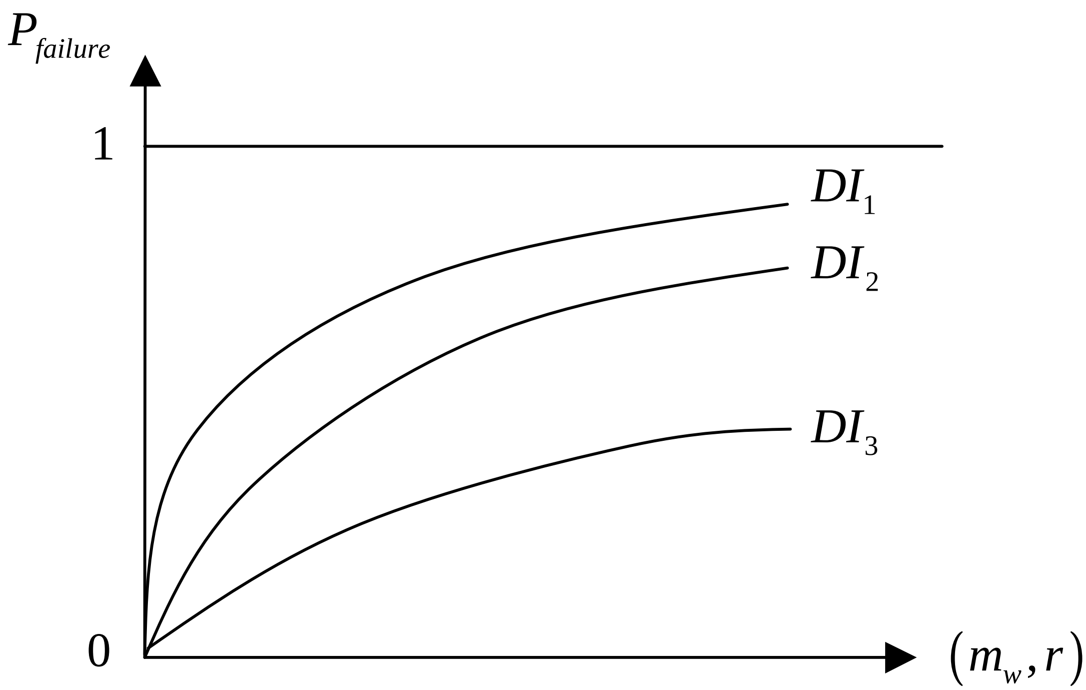

FIGURE 4-1 Typical configuration of fragility curves.

4.1 Fragility of Continuous Pipelines Subject to Seismic Waves

The response of pipelines subject to seismic wave hazard is discussed in Chapter 3, Section 3.2. Furthermore, the behavior of continuous pipelines subjected to seismic waves is examined in Section 3.2.1.

4.1.1 Limit State

It is assumed that a continuous pipelines fails when the pipeline strain ϵ_p caused by the seismic event with moment magnitude m_w and site-to-source distance r exceeds a specified limit strain limit ϵ_{limit}. The corresponding fragility surface is given by the conditional probability

$$P_f(m_w, r) = P\left[\epsilon_p > \epsilon_{limit} | m_w, r\right]. \tag{4-2}$$

4.1.2 Fragility Analysis

Three types of input parameters are needed to perform fragility analysis of continuous pipelines subject to seismic wave hazard: (1) seismic inputs, (2) pipeline and soil properties, and (3) limit state.

Seismic inputs include moment magnitude m_w and site-to-source distance r. Using these parameters, seismic ground motion histories can be generated as described in Chapter 2 Section 2.4.1.

Required pipeline inputs are: outer diameter D_o, pipe wall thickness t, depth from soil surface to centerline of the pipe z_p, elastic modulus of pipe material E, interface friction angle between pipe and soil δ, and the angle between pipeline and seismic wave Ω.

Soil parameters needed are: its unit weight γ, apparent wave propagation velocity c, and coefficient of lateral earth pressure at rest k_0, also the soil type as specified by the NEHRP as shown in Table 2-3. The soil type may modify the seismic input and thus the generation of seismic ground motion.

Maximum force F_m in the pipeline can be determined using Equation (3-5). Maximum pipe strain is calculated by realizing that strain is equal to force divided by stiffness and cross sectional area (i.e.$\epsilon_p = F_m/(EA)$). Performing the analysis with different moment magnitudes m_{w_i}, $i = 1, \ldots, p$, and site-to-source distances r_j, $j = 1, \ldots, q$), with n samples for each (m_{w_i}, r_j) pair, a fragility surface can be produced for the specified limit strain ϵ_{limit}. The procedure can be summarized with the flowchart given in Figure 4-2.

Fragility surfaces are obtained for a pipe with 12 inches diameter and 0.5 inches wall thickness with 48 inches of depth to its centerline. The pipe is made of steel with elastic modulus of 29000 ksi. It is assumed that the angle between pipeline and seismic wave is 45 degree, and the specified limit strain is 0.005%. Figure 4-3 shows fragility surfaces of the pipe for various soil types based on NEHRP classification. The fragility surfaces are calculated for moment magnitude m_w from 4.0 to 8.0 with an increment of 0.5, site-to-source distance r from 50 km to 250 km with an increment of 50 km, and 250 samples for each (m_w, r) pair.

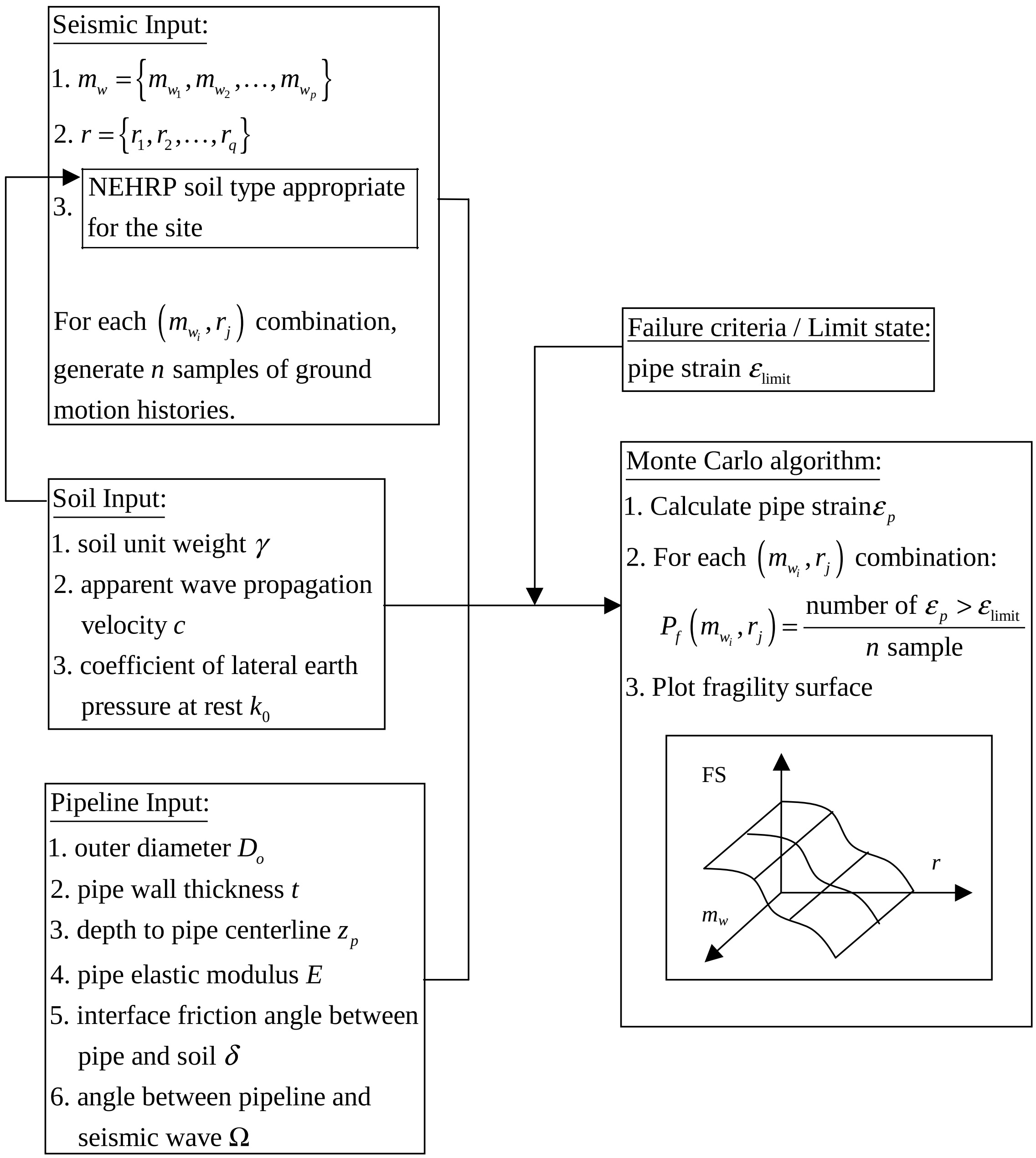

FIGURE 4-2 Fragility analysis of continuous pipelines subject to seismic wave hazard.

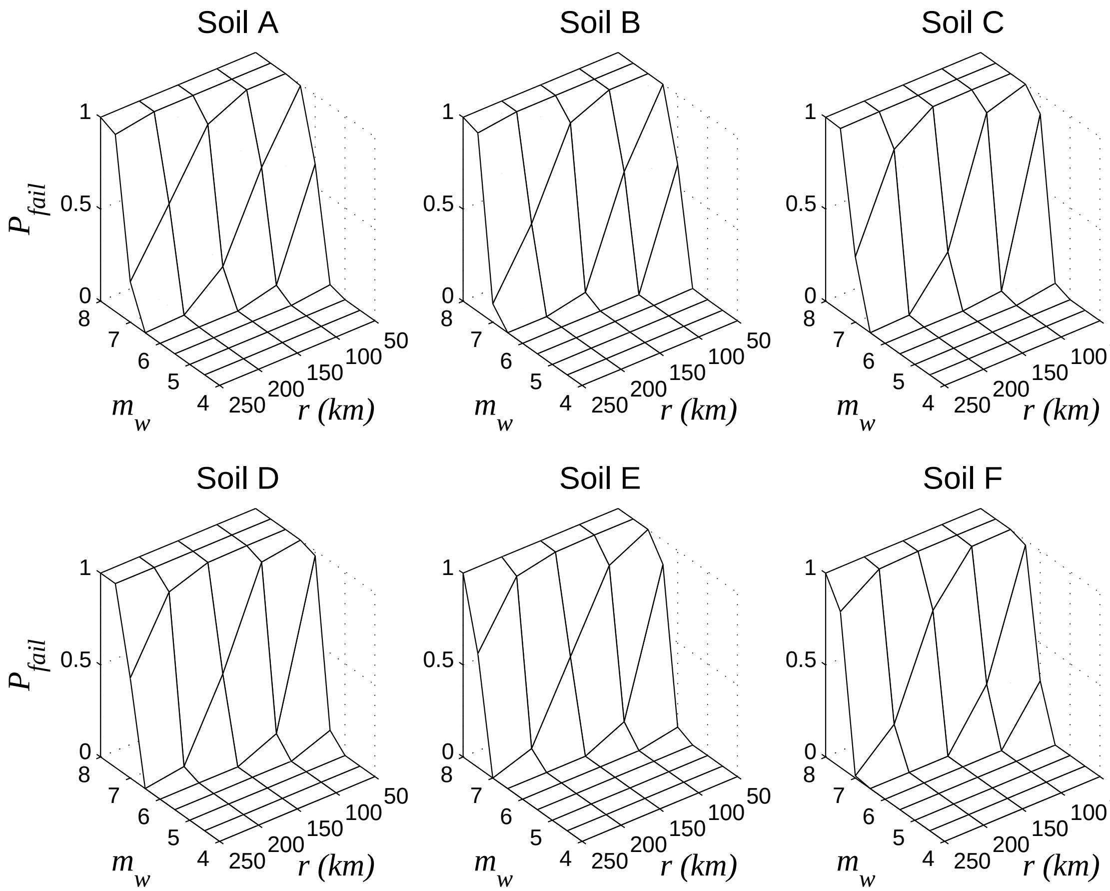

FIGURE 4-3 Fragility surfaces of a continuous pipe for various soil types.

4.2 Fragility of Jointed Pipelines Subject to Seismic Waves

The response of pipelines subject to seismic wave hazard is discussed in Chapter 3, Section 3.2. Furthermore, the behavior of jointed pipelines (represented with the jointed concrete cylinder pipeline, or JCCP) subjected to seismic waves is examined in Section 3.2.2.

4.2.1 Limit State

It is assumed that a jointed pipeline fails when the relative joint displacement δ_j caused by a seismic event with moment magnitude m_w and site-to-source distance r exceeds the specified slip capacity δ_j. As discussed in Section 3.2.2, the typical range of slip capacity falls in between 15 mm to 60 mm, with an average of 25 mm. The corresponding fragility surface is given by the conditional probability

$$P_f(m_w, r) = P\left[\delta_j > \delta_{limit} | m_w, r\right]. \tag{4-3}$$

4.2.2 Fragility Analysis

Fragility analysis of jointed pipelines is very similar to that for continuous pipelines. The same inputs (seismic inputs, pipeline and soil inputs, and limit state) are used to calculate the relative joint displacement δ_j using Equation (3-7).

Failure probability is determined by comparing value of joint displacement δ_j to the specified slip capacity δ_{limit}. The procedure is summarized in Figure 4-4.

Fragility surfaces are obtained for a pipe with 24 inches diameter and 0.5 inches wall thickness with 48 inches of depth to its centerline. The pipe is made of steel with elastic modulus of 29000 ksi. It is assumed that the angle between pipeline and seismic wave is 15 degree, and the specified slip capacity is 0.25 inches. Figure 4-5 shows fragility surfaces of the pipe for various soil types. The fragility surfaces are calculated for moment magnitude m_w from 4.0 to 8.0 with an increment of 0.5, site-to-source distance r from 50 km to 250 km with an increment of 50 km, and 250 samples for each (m_w, r) pair.

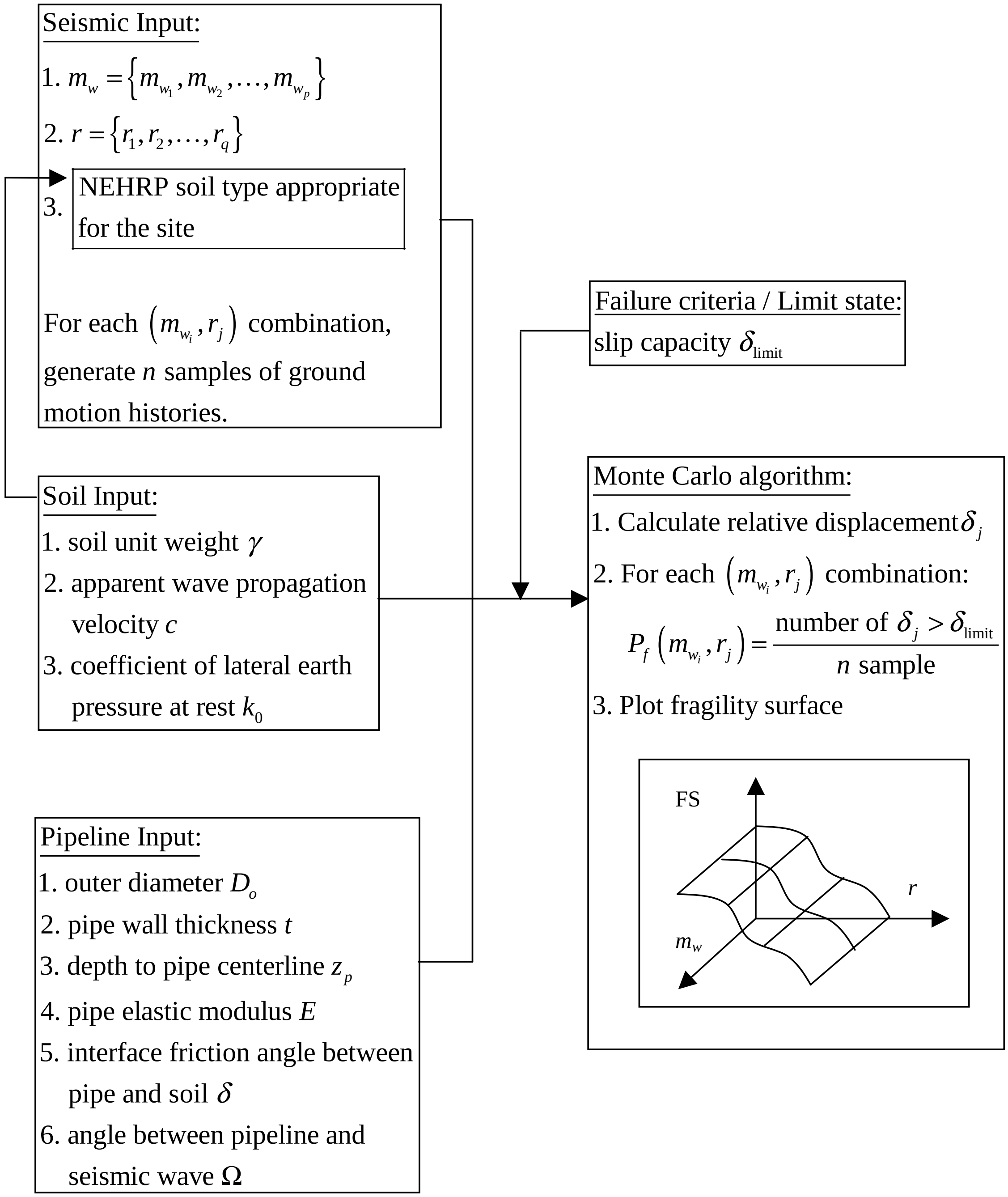

FIGURE 4-4 Fragility analysis of jointed pipelines subject to seismic wave hazard.

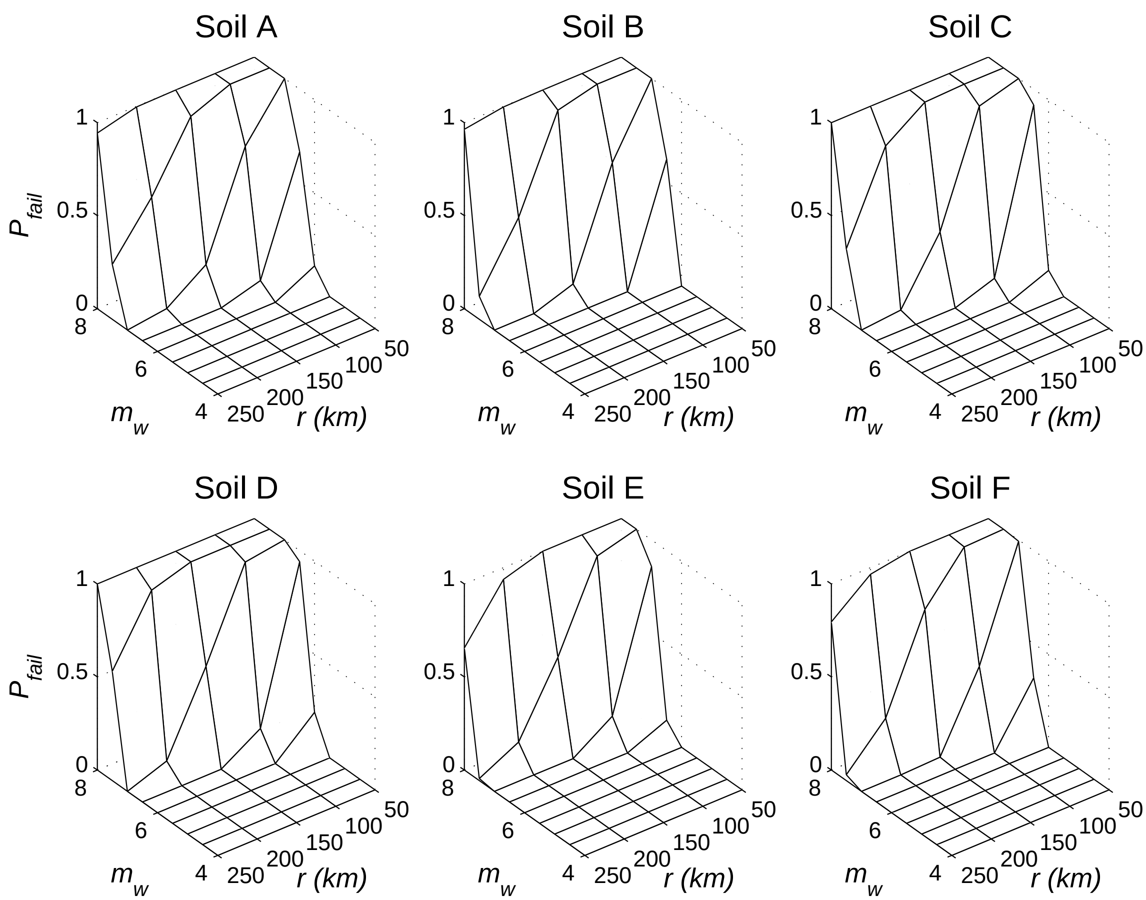

FIGURE 4-5 Fragility surfaces of a JCCP for various soil types.

4.3 Fragility of Pipelines Subject to Landslides, Lateral Spreads, or Seismic Settlements

Fragility analysis of pipes subject to landslides, lateral spreads and seismic settlements induced by liquefaction follows the same logic. The three types of PGD hazard result in an amount of PGD movement δ_{PGD} which can be decomposed into longitudinal and transverse components. The difference among the three types of hazard lies on the calculation to obtain δ_{PGD}.

The amount of δ_{PGD} can be obtained using Equation (3-9) by Jibson and Keefer (Jibson and Keefer, 1993) for landslides, Equations (3-12) and (3-13) proposed by Bartlett and Youd (Barlett and Youd, 1992) for lateral spreads induced by liquefaction, and Equations (3-16) and (3-17) proposed by Takada and Tanabe (Takada *et al.*, 1987) for seismic settlement induced by liquefaction. If the angle of inclination ψ between pipeline axis and δ_{PGD} is known, then δ_{PGD} can be decomposed into its longitudinal component and transverse component, in which the longitudinal component acts parallel to the pipe axis and transverse component perpendicular to the pipe axis.

4.3.1 Limit State

The amount of PGD movement δ_{PGD} will induce a certain amount of strain in a pipe ϵ_p. Therefore, the appropriate limit state for fragility analysis of pipes subject to landslides, lateral spreads and seismic settlement induced by liquefactions is a specified amount of limit strain ϵ_{limit}.

A continuous pipeline subject to some amount of PGD movement δ_{PGD} resulted from a source with moment magnitude m_w and site-to-source distance r is said to be in failure when the pipe strain ϵ_p is greater than the specified limit strain ϵ_{limit}.

$$P_f(m_w, r) = P\left[\epsilon_p > \epsilon_{limit} | m_w, r\right] \tag{4-4}$$

4.3.2 Fragility Analysis

The input for fragility analysis of pipelines subjected to PGD consists of: (1) inputs for calculation of δ_{PGD}, (2) pipe and soil properties, and (3) limit state.

Inputs for calculation of δ_{PGD} differ for different types of PGD hazard. The differences are as follow:

Information needed for the calculation of amount of PGD δ_{PGD} due to landslides are moment magnitude m_w, site-to-source distance r in kilometers, slope of landslide (i.e. possible failure surface if landslide occurs) α, and a factor of safety corresponds to the critical failure surface FS. The amount of PGD δ_{PGD} caused by landslides can then be obtained with Equation (3-9).

Information required for the calculation of amount of PGD δ_{PGD} for lateral spreads induced by liquefactions are moment magnitude m_w, site-to-source distance r in kilometers, A and B (i.e. the depth and length of the critical failure surface)as described in Figure 3-6 found in Section 3.3.2, the thickness of saturated cohesionless soils with a corrected SPT N-value less than 15 T_{15} in meters, average of fines contents in T_{15}, F_{15} in %, and the mean grain size in T_{15}, $D50_{15}$ in millimeters. For a gentle sloping site, amount of PGD δ_{PGD} caused by lateral spreads can be calculated using Equation (3-12), while for a free face site, δ_{PGD} can be obtained with Equation (3-13).

Information neccesary for the calculation of amount of PGD δ_{PGD} for seismic settlements induced by liquefactions include the thickness of saturated sand layer H_1 in meters, the height of embankment (for pipes located at embankments) H_2 in meters, the SPT N-value in the sandy layer N, and the maximum ground acceleration a_{max} in cm/sec^2. Amount of PGD δ_{PGD} caused by seismic settlements can be calculated with Equation (3-17).

The various inputs for calculating δ_{PGD} for all three types of PGD hazard are summarized in Figure 4-6. For convenience, we will termed the various inputs for calculating δ_{PGD} as seismic input. If the angle ψ between the direction of PGD movement and the pipe axis is known, δ_{PGD} can be decomposed into its longitudinal and transverse components.

Assuming that all pipes are linear elastic, pipe strain ϵ_p resulted from the longitudinal component of δ_{PGD} can be calculated using Equation (3-22) if the following parameters are known: length of the PGD zone L, the length over which the frictional force per unit length f must act to induce a pipe strain equal to the equivalent ground strain L_{em}, pipe outer diameter D_o, pipe wall thickness t, elastic modulus of pipe material E, depth to pipe centerline z_p, interface friction angle between pipe and soil δ, soil unit weight γ, and coefficient of lateral earth pressure at rest k_0. The assumption is conservative since elastic model assumes that pipe fails in the elastic region (O'Rourke and Liu, 1999).

Effect of transverse component of PGD on pipes considered is the spatially distributed pattern on pipes located in a non-liquefied soil. This effect is the most damaging among the types of transverse PGD (O'Rourke and Liu, 1999), and therefore is conservative. Pipe strain ϵ_p can be obtained with Equation (3-40) once the following parameters are known: the width of PGD zone W, pipe outer diameter D_o, pipe wall thickness t, elastic modulus of pipe material E, depth to pipe centerline z_p, soil unit weight γ, coefficient of lateral earth pressure at rest k_0, and soil horizontal bearing capacity factor N_{qh}.

Failure probability is determined by comparing the values of pipe strain ϵ_p to the specified limit strain ϵ_{limit}. If ϵ_p is greater than ϵ_{limit}, then the pipe fails. As described previously, a fragility surface for a pipeline subject to PGD hazard can be obtained for a specified limit state ϵ_{limit}. The procedure can be summarized with the flowchart given in Figure 4-7.

Fragility surfaces have been obtained for a pipe experiencing a lateral spread hazard induced by liquefaction. The pipe has a 12 inch diameter and 1/2 inch thickness, located at a depth of 48 inch from the surface to its centerline. It is a steel pipe with elastic modulus of 29000 ksi, with interface friction angle between pipe and soil of 30 degree, the soil has a unit weight of 120 pcf with coefficient of lateral earth pressure at rest assumed to be 1.0 and horizontal bearing capacity factor of 4. The PGD zone has a length of 500 km and width of 100 km. The site is a gentle slope with $A = 50$ m, and $B = 150$ m. The thickness of saturated cohesionless soils is 10 m, the average fines contents is 30%, and the mean grain size is 0.35 mm.

The calculated fragility surfaces are shown in Figure 4-8. Fragility surfaces for longitudinal and lateral components are obtained by assuming that all components of the calculated δ_{PGD} is longitudinal and lateral component respectively. The fragility surfaces are calculated for moment magnitude m_w from 4.0 to 8.0 with an increment of 0.5, site-to-source distance r from 50 km to 250 km with an increment of 50 km, with 100 samples for each (m_w, r) pair.

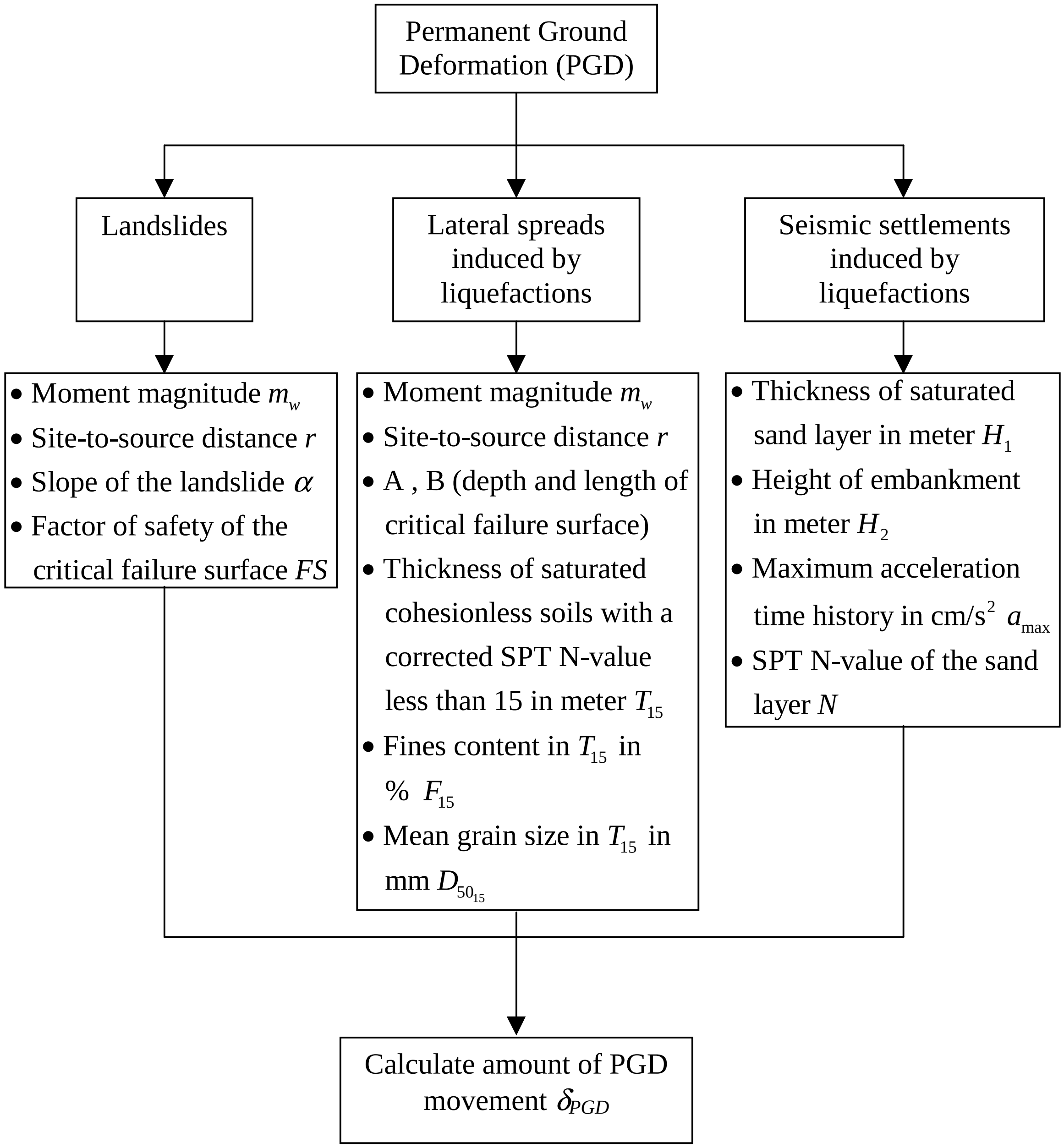

FIGURE 4-6 Seismic input of PGD required to calculate amount of PGD movement δ_{PGD}.

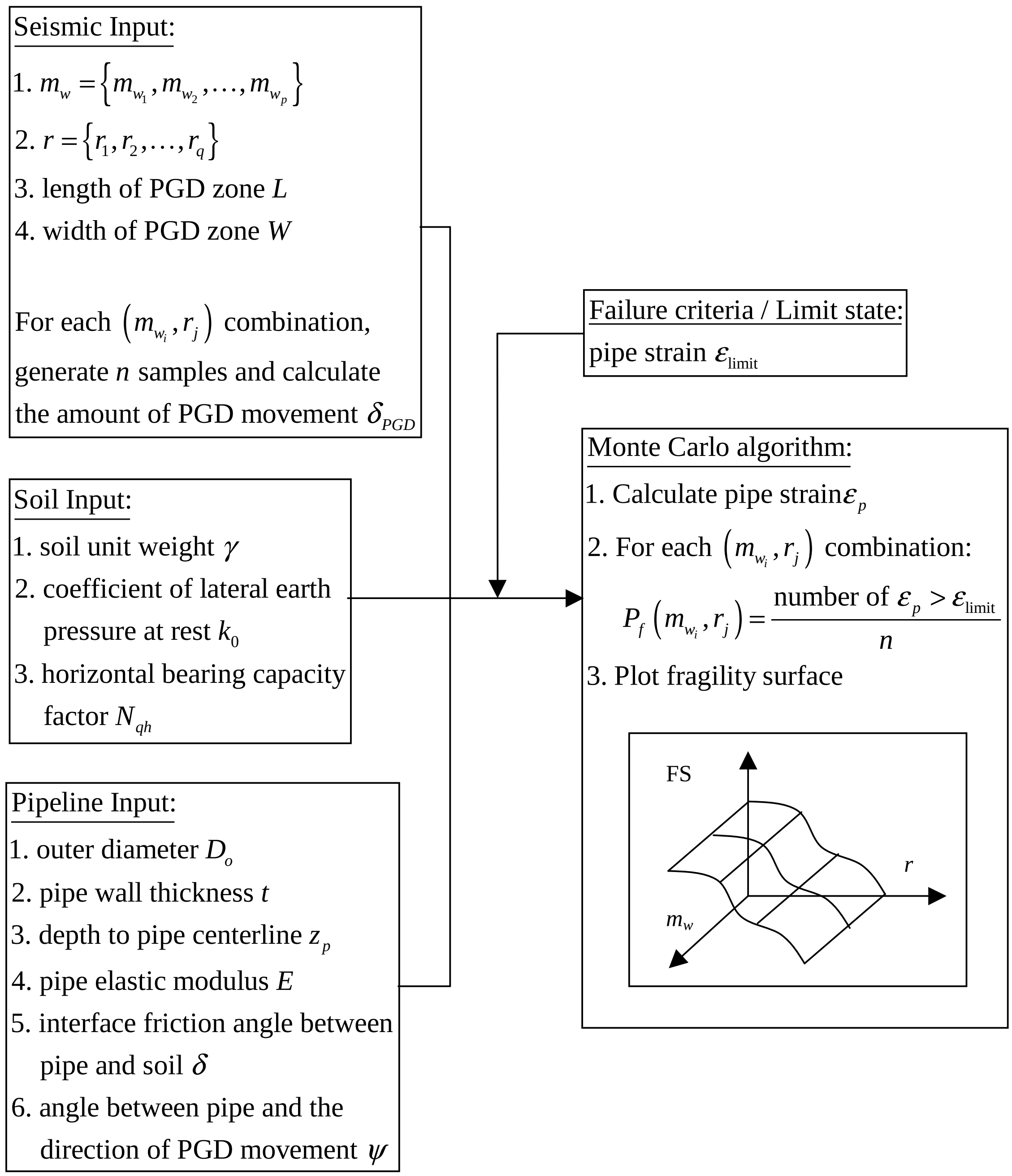

FIGURE 4-7 Fragility analysis of pipelines subject to landslides, lateral spreads and seismic settlements induced by liquefactions.

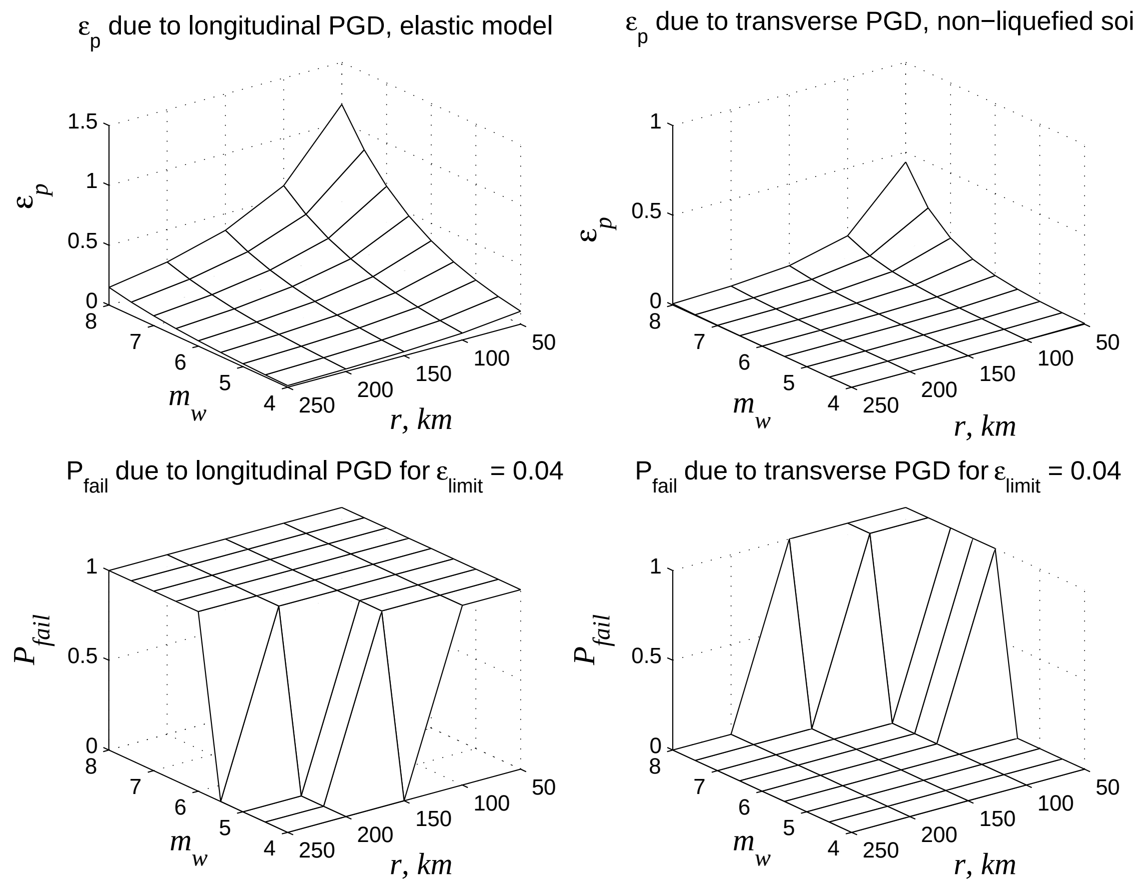

FIGURE 4-8 Fragility surfaces of a pipe subject to lateral spreads.

Fragility surfaces are also obtained for the same pipe subject to seismic settlement hazard induced by liquefaction. The PGD zone is again has a length of 500 km and width of 100 km. The pipe is located at embankment having a height of 10 m. The thickness of the saturated soil is 5 m, and the number of SPT N-value is 30 counts. Again, the fragility surfaces for longitudinal and lateral components are obtained by assuming that all components of the calculated δ_{PGD} is longitudinal and lateral component respectively.

The calculated fragility surfaces are shown in Figure 4-9. As for the case of lateral spread, the fragility surfaces are calculated for moment magnitude m_w from 4.0 to 8.0 with an increment of 0.5, site-to-source distance r from 50 km to 250 km with an increment of 50 km, with 100 samples for each (m_w, r) pair.

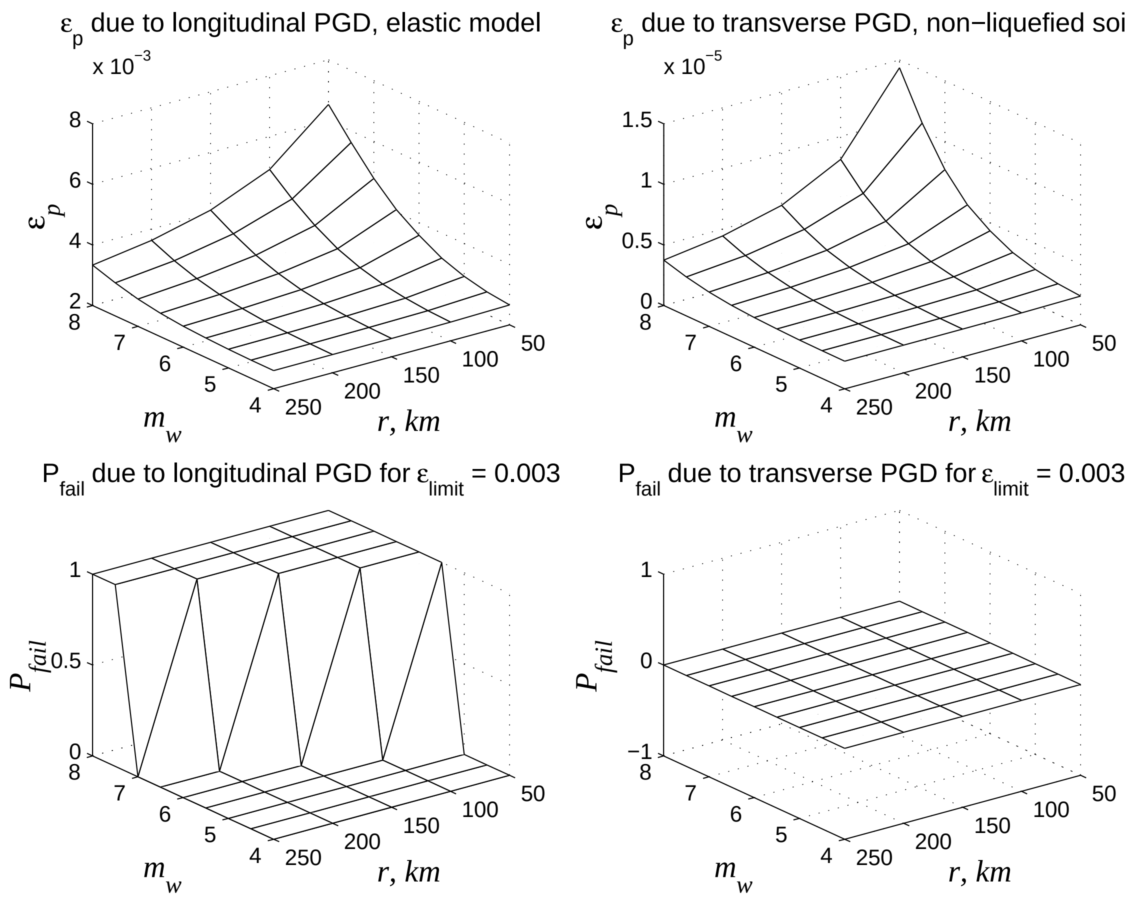

FIGURE 4-9 Fragility surfaces of a pipe subject to seismic settlement.

4.4 Fragility of Pipelines Subject to Fault Displacements

Response of pipelines subject to fault displacement has been described in Chapter 3, Section 3.4.3. Two analytical methods are available: Newmark-Hall procedure and Kennedy, et al. procedure.

4.4.1 Limit State

Parameter chosen to define the damage state is the limiting pipe strain ϵ_{limit}. Pipeline subjects to fault displacement under a moment magnitude m_w is said to be in failure when the resulting maximum pipe strain ϵ_m is greater than the limiting pipe strain ϵ_{limit}.

$$P_f(m_w) = P\left(\epsilon_m > \epsilon_{limit} | m_w\right) \tag{4-5}$$

4.4.2 Fragility Analysis for Newmark-Hall Model

The input for fragility analysis of pipelines subject to fault displacement hazard using Newmark-Hall procedure consists of: (1) seismic input, (2) pipeline and soil properties, and (3) limit state.

The parameter needed for seismic input is the moment magnitude m_w, which can be used to calculate the peak ground displacement using either Equation (3-18), (3-19), (3-20), or (3-21) depending on the types of fault considered.

Pipeline input includes the pipe outer diameter D_o, pipe wall thickness t, depth to the pipe centerline z_p, interface friction angle between soil and pipe δ, pipe material yield stress σ_y and elastic modulus E, Ramberg-Osgood parameters n and r defining material stress-strain curve, anchor length of the pipe L_a, and the fault crossing angle β.

Soil properties required are the unit weight γ and coefficient of lateral earth pressure at rest k_0.

Following procedure described in Chapter 3, Section 3.4.3, calculate the maximum pipe strain ϵ_m using Equations (3-44) and (3-48). Failure is defined when maximum strain ϵ_m is greater than the specified limiting pipe strain ϵ_{lim}.

The procedure for calculating fragility surface for pipelines subject to fault displacement using Newmark-Hall method is summarized in the flowchart given in Figure 4-10.

4.4.3 Fragility Analysis for Kennedy, et al. Model

All inputs for performing fragility analysis of pipelines subject to fault displacement using Kennedy, et al. procedure are the same as the inputs using Newmark-Hall procedure, with an additional input of the horizontal bearing capacity factor N_{qh} into the soil inputs.

Using the methodology described in Chapter 3, Section 3.4.3, calculate the maximum pipe strain ϵ_m using Equations (3-51) and (3-53), and compared with the specified limiting strain

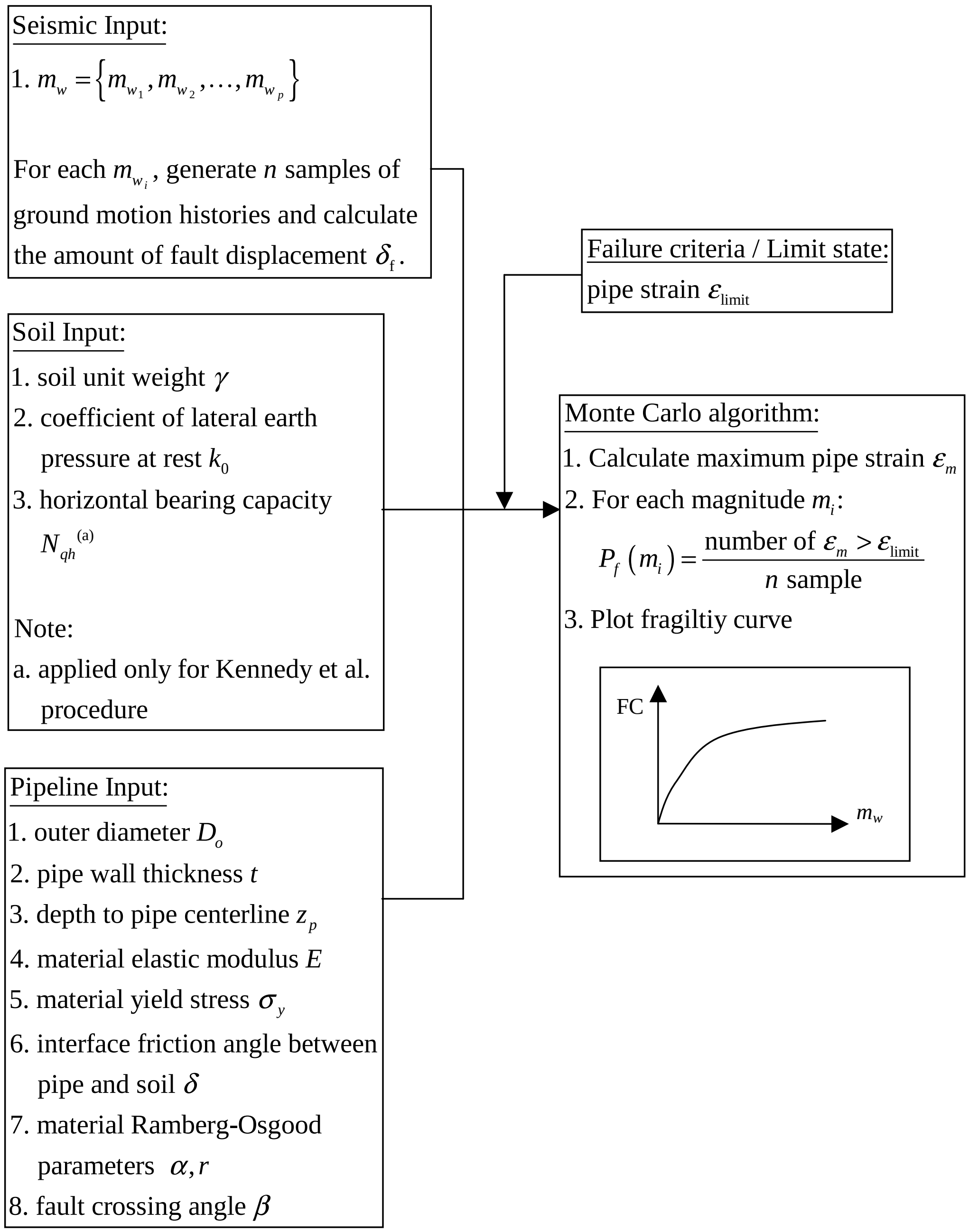

FIGURE 4-10 Fragility analysis of pipelines subject to fault displacement hazard using Newmark-Hall or Kennedy et al. procedure.

ϵ_{lim}. Failure is defined when maximum strain ϵ_m is greater than the limiting strain ϵ_{lim}. Fragility surfaces can be obtained using the flowchart given in Figure 4-10.

A comparison between fragilities obtained by Newmark-Hall procedure and Kennedy et al. procedure is shown in Figure 4-11. The fragilities are calculated for a pipe with 12 inches diameter and 0.5 inches wall thickness, buried at a depth of 48 inches to its centerline and has an anchor length of 100 ft. The pipeline is made of steel with a yield stress of 60 ksi and initial elastic modulus of 29000 ksi. The stress-strain curve is defined by Ramberg-Osgood parameters $n = 10$ and $r = 12$. The soil has a unit weight of 110 pcf with interface of friction angle between soil and pipe of 30 degree. For Kennedy et al. procedure, the soil horizontal bearing capacity factor is assumed to be 5. The fault crossing angle is assumed to be 30 degree and the specified limit strain is 0.1%. The fragility curves are calculated for moment magnitude m_w from 4.0 to 8.0 with 0.5 increment, with 100 samples for each moment magnitude. Since amount of fault displacement δ_f depends only on moment magnitude, failure probability is presented as a function of moment magnitude m_w only, thus the results are plotted as fragility curves.

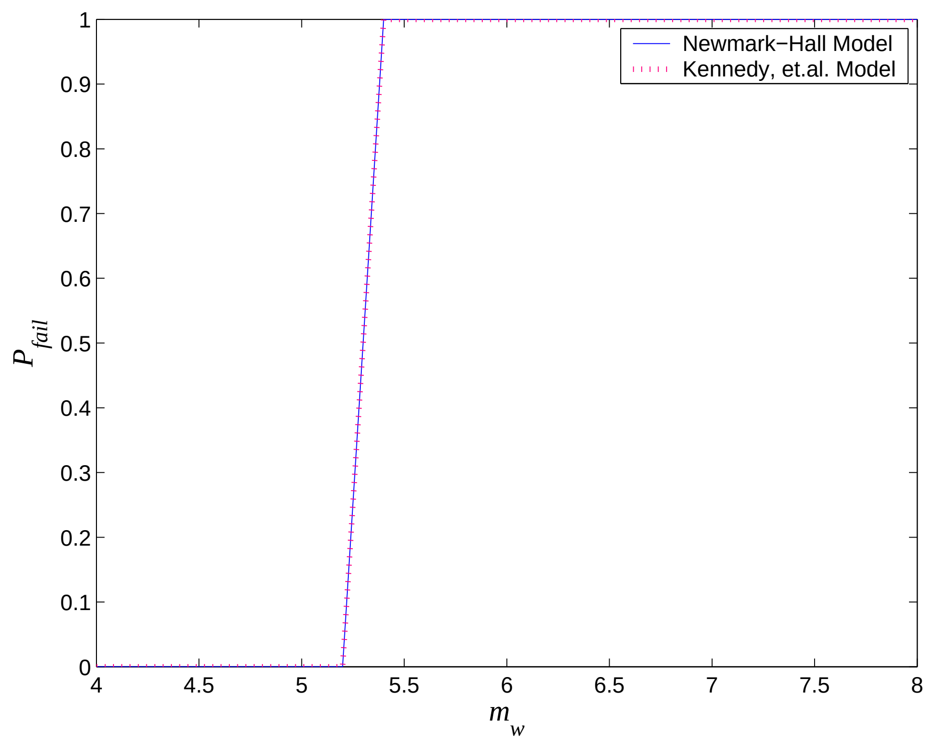

FIGURE 4-11 Comparison of fragilities of a pipe between Newmark-Hall and Kennedy et al. procedure.

SECTION 5
FRAGILITY INFORMATION ON SOME COMPONENTS OF WATER SUPPLY SYSTEMS

The seismic performance of a water supply system depends on the performance of its components, for example, water tanks, tunnels, hydrants, valves, pumps, and pumping stations.

The American Lifelines Alliance (ALA) (American Lifelines Alliance, 2001a),(American Lifelines Alliance, 2001b) provides a comprehensive fragility formulations for some of the components of water supply systems, including the fragility formulations for buried pipelines, water tanks, water tunnels, and water canals.

Following sections provide the fragility information for water tanks, water tunnels (American Lifelines Alliance, 2001a),(American Lifelines Alliance, 2001b), and various components of groundwater systems (Ballantyne, 2000).

5.1 Fragility Information for Water Tanks

Typical failure modes in steel tanks (American Lifelines Alliance, 2001a) are shell buckling mode (sometimes termed as elephant foot), roof damage, anchorage failure, failures of the tank support system, tank support system, foundation, hydrodynamic pressure, connecting pipe, and failure of manhole.

Historical seismic performance of tanks (damage data) have been published by various researchers. ALA provides the compilation of these damage data and is reproduced here in Table 5-1 (American Lifelines Alliance, 2001a).

The seismic performances of tanks are categorized into five damage states as seen in Table 5-2. The various damage states are in accordance with damage states defined by HAZUS (HAZUS, 1997), where damage state 1 (DS1) indicates no damage, damage state 2 (DS2) slight damage, damage state 3 (DS3) moderate damage, damage state 4 (DS4) extensive damage, and damage state 5 (DS5) indicates total failure or collapse of the system.

Damage state 2 includes roof damage, anchor bolt damage, and overflow pipe damage. These type of damages need minor repair and tanks remain in service after earthquake. Damage state 3 includes elephant foot buckling with no leak. This damage requires major repair but tank remains in service after earthquake. Damage state 4 includes inlet pipe leaks, wall uplift with leaks, elephant foot buckling with leaks, and hoop overstress. These damages need major repairs and tanks will be out of service after earthquake (American Lifelines Alliance, 2001a).

Fragility curves used by ALA is a measure of the probability that a certain damage state will be achieved or exceeded as a function of PGA. The mathematical expression of the fragility is given as

$$P[DS|x] = \Phi\left[\frac{1}{\beta}\ln\frac{x}{A}\right], \tag{5-1}$$

where $P[DS|x]$ is the probability of being in or exceeding damage state DS given a PGA of x, A is the median value of PGA for which the tank reaches the threshold for damage state DS (i.e. the PGA value when 50% of probability value is reached for being in or exceeding

TABLE 5-1 Historical tank damaged data provided by ALA.

Event	No. of tanks	PGA range (g)	Average PGA (g)
1933 Long Beach	49	0.17	0.17
1952 Kern Country	24	0.19	0.19
1964 Alaska	39	0.20 - 0.30	0.22
1971 San Fernando	27	0.20 - 1.20	0.51
1979 Imperial Valley	24	0.24 - 0.49	0.24
1983 Coalinga	48	0.20 - 0.62	0.49
1984 Morgan Hill	12	0.25 - 0.50	0.30
1989 Loma Prieta	141	0.11 - 0.54	0.16
1991 Costa Rica	38	0.35	0.35
1992 Landers	33	0.10 - 0.56	0.30
1994 Northridge	70	0.30 - 1.00	0.63
Others	27	0.17 - 0.50	0.34

TABLE 5-2 Tank damage states based on historical data of damaged tanks as provided by ALA.

PGA (g)	All Tanks	Damage State 1	Damage State 2	Damage State 3	Damage State 4	Damage State 5
0.1	4	4	0	0	0	0
0.16	263	196	42	13	8	4
0.26	62	31	17	10	4	0
0.36	53	22	19	8	3	1
0.47	47	32	11	3	1	0
0.56	53	26	15	7	3	2
0.67	25	9	5	5	3	3
0.87	14	10	0	1	3	0
1.18	10	1	3	0	0	6
Total	531	331	112	47	25	16[1]

1. Most of the collapsed tanks were made of riveted steel. Application of Damage State 5 for welded steel tanks should be used with caution.

damage state DS) [Refer to Figure 5-1], β is the standard deviation of the natural logarithm of PGA for damage state DS, and Φ is the standard normal cumulative distribution function (American Lifelines Alliance, 2001a),(O'Rourke and So, 1999).

Table 5-3 provides the fragility curves for tanks as a function of fill level, and Table 5-4 provides the fragility curves for tanks as a function of fill level and anchorage (American Lifelines Alliance, 2001a).

TABLE 5-3 Fragility curves of tanks as a function of fill level.

DS	A	β	A	β	A	β	A	β	A	β
DS $\geq$ 2	0.38	0.80	0.56	0.80	0.18	0.80	0.22	0.80	0.13	0.07
DS $\geq$ 3	0.86	0.80	>2.00	0.40	0.73	0.80	0.70	0.80	0.67	0.80
DS $\geq$ 4	1.18	0.61			1.14	0.80	1.09	0.80	1.01	0.80
DS = 5	1.16	0.07			1.16	0.40	1.16	0.41	1.15	0.10
	All Tanks N=531		Fill < 50% N=95		Fill $\geq$ 50% N=251		Fill $\geq$ 60% N=209		Fill $\geq$ 90% N=120	

TABLE 5-4 Fragility curves of tanks as a function of fill level and anchorage.

DS	A	β	A	β	A	β	A	β	A	β
DS $\geq$ 2	0.18	0.80	0.17	0.80	0.15	0.12	0.30	0.60	0.15	0.70
DS $\geq$ 3	0.73	0.80	2.36	0.80	0.62	0.80	0.70	0.60	0.35	0.75
DS $\geq$ 4	1.14	0.80	3.72	0.80	1.06	0.80	1.23	0.65	0.68	0.75
DS = 5	1.16	0.80	4.26	0.80	1.13	0.10	1.60	0.60	0.95	0.70
	Fill $\geq$ 50% All tanks N=251		Fill $\geq$ 50% Anchored tanks N=46		Fill $\geq$ 50% Unanchored tanks N=205[1]		Near full Anchored tanks HAZUS		Near full Unanchored tanks HAZUS	

1. The low β values reflect the sample set. However, $\beta = 0.80$ is recommended for use for all damage states for regional loss estimates for unanchored steel tanks with fill $\geq$ 50% unless otherwise justified.

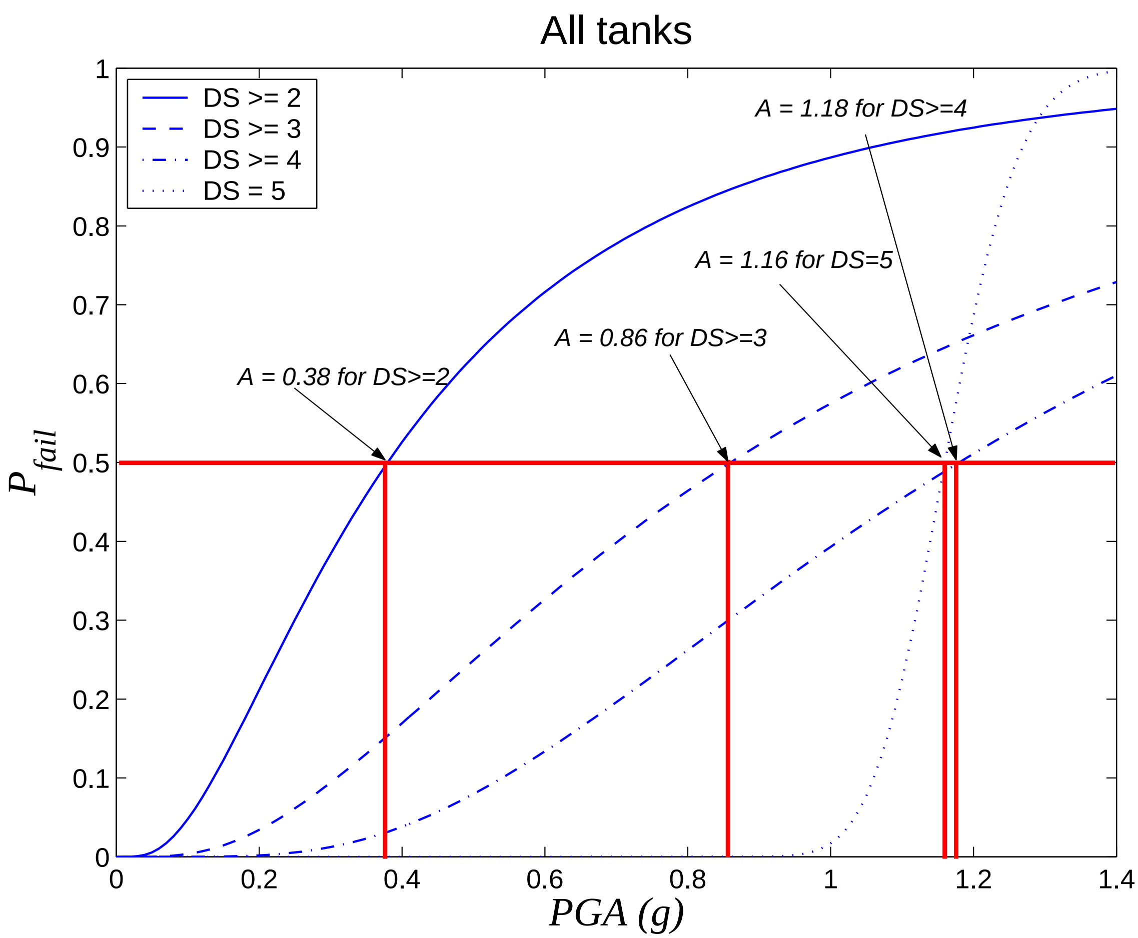

FIGURE 5-1 The median values, As, for all tanks as a function of fill level.

Fragility curves for tanks as a function of fill level are shown in Figure 5-2 for: (1) all tanks, (2) fill level $\geq$ 50%, (3) fill level $\geq$ 60%, and (4) fill level $\geq$ 70%.

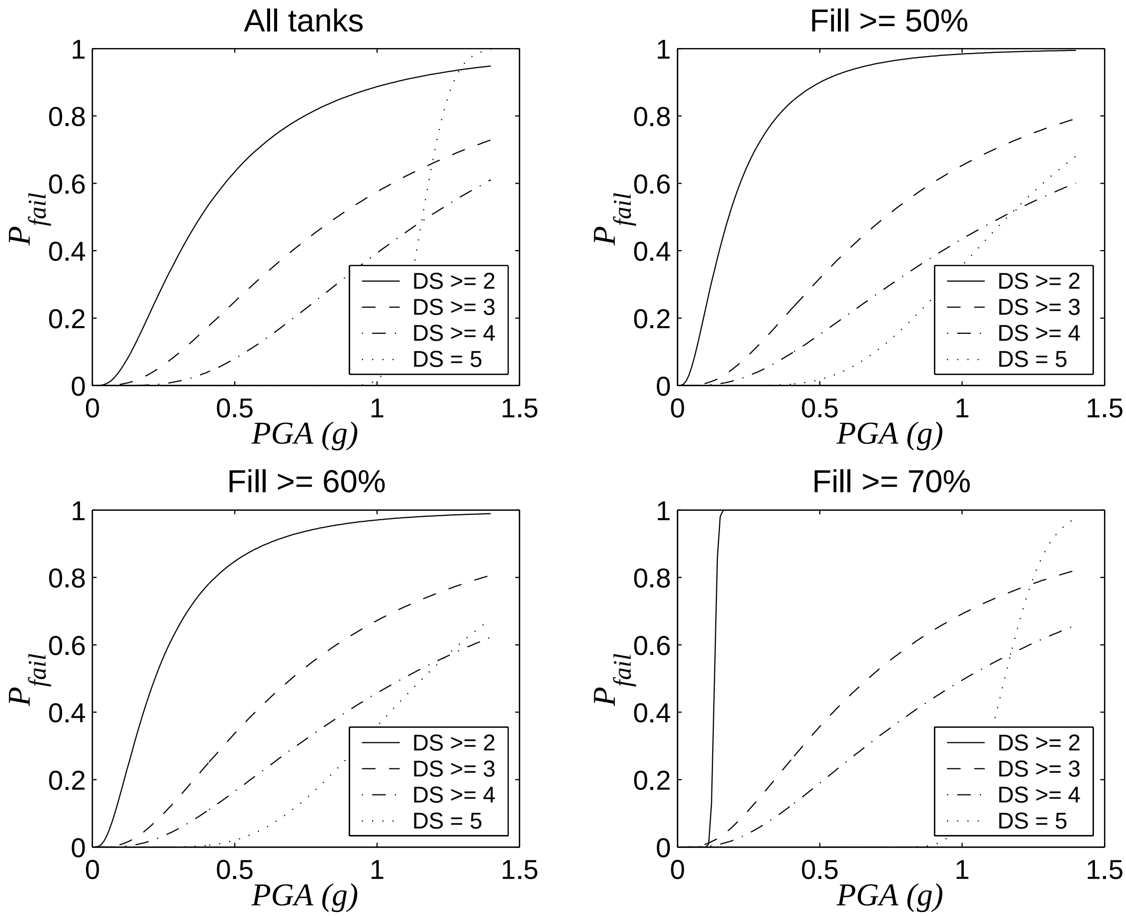

FIGURE 5-2 Fragility curves for tanks as a function of fill level.

Fragility curves for tanks as a function of both fill level and anchorage are shown in Figure 5-3 for: (1) fill level $\geq 50\%$ and anchored, (2) fill level $\geq 50\%$ and unanchored, (3) near full and anchored, and (4) near full and unanchored.

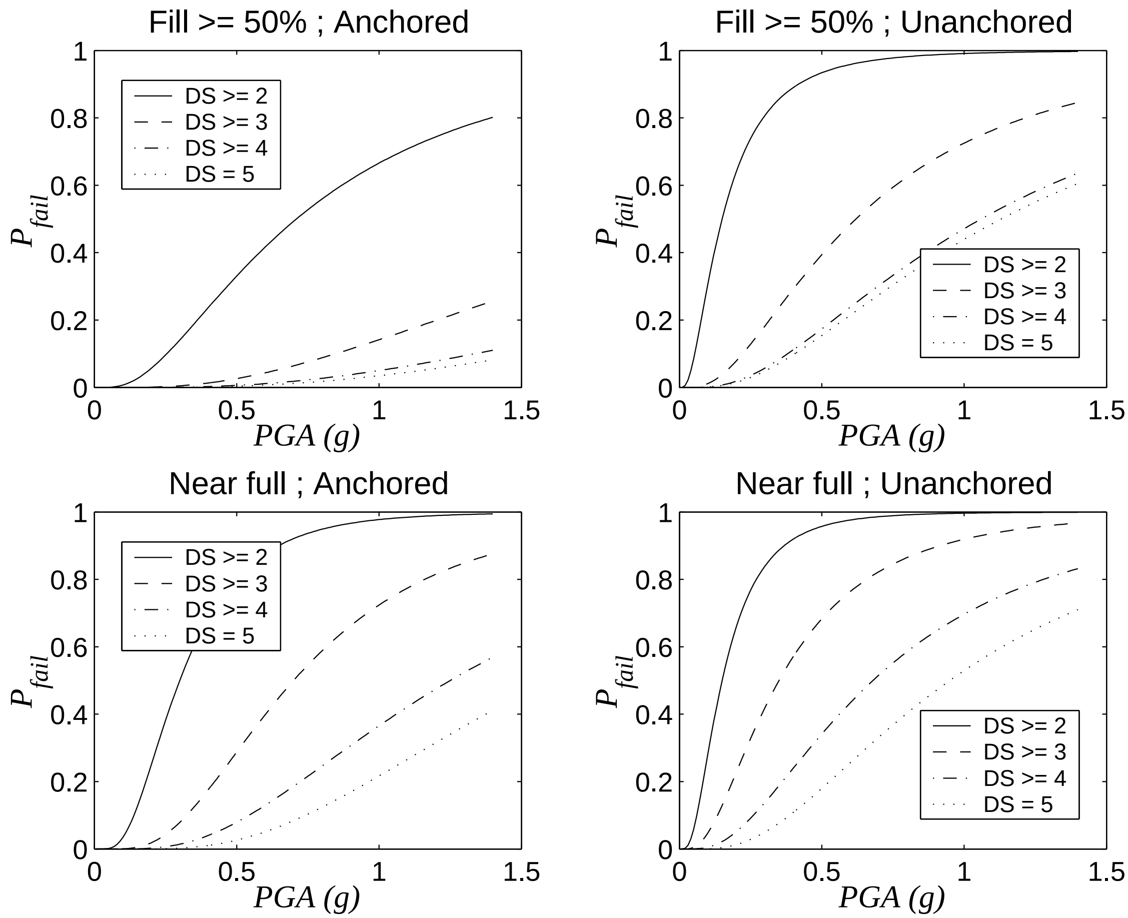

FIGURE 5-3 Fragility curves for tanks as a function of fill level and anchorage.

5.2 Fragility Information for Water Tunnels

Database of 217 bored tunnels that have experienced strong ground motions in prior earthquakes have been compiled by ALA (American Lifelines Alliance, 2001a),(American Lifelines Alliance, 2001b). The tabulated data of the tunnels are reproduced here in Table 5-5.

TABLE 5-5 Tunnel database for fragility analysis provided by ALA.

PGA (g)	All Tanks	Damage State 1	Damage State 2	Damage State 3	Damage State 4
0.07	30	30	0	0	0
0.14	19	18	1	0	0
0.25	22	19	2	0	1
0.37	15	14	0	0	1
0.45	44	36	6	2	0
0.57	66	44	12	9	1
0.67	19	3	7	8	1
0.73	2	0	0	2	0
Total	217	164	28	21	4

Ground motion induces stress in the liner system of tunnels. If sufficient level of ground motion occurs, liner can cracked, and some part of the liner can collapse into the tunnel. For unlined tunnels, ground motion can cause failure to the native materials.

Small damage in water liner may gives an increase of head loss over time, and small cracks allow water from the tunnel to enter the native material behind the liner, which can lead to erosion and more damage to the liner (American Lifelines Alliance, 2001a).

Large cracks in liners can cause partial blockage of water flow, or carry debris in the water flow that will decrease the water quality of downstream or even cause damages to in-line equipments such as pumps (American Lifelines Alliance, 2001a).

Table 5-6 gives the parameters A and β that describe the fragility curves as a function of liner system (American Lifelines Alliance, 2001a).

Figure 5-4 shows fragility curves for: (1) all tunnels, (2) unlined tunnels, (3) timber, masonry, and brick tunnels, and (4) unreinforced concrete tunnels.

TABLE 5-6 Fragility curves of tunnels as a function of liner system.

DS	A	β	A	β	A	β	A	β	A	β
DS $\geq$ 2	0.60	0.11	0.33	0.21	0.43	0.03	0.61	0.10	0.61	0.27
DS $\geq$ 3	0.65	0.12	0.55	0.39	0.57	0.01	0.67	0.11	0.82	0.34
DS = 4										
	All N=217		Unlined N=28		Timber, Masonry, Brick N=14		Unreinforced Concrete N=125		Reinforced Concrete, Steel N=38	

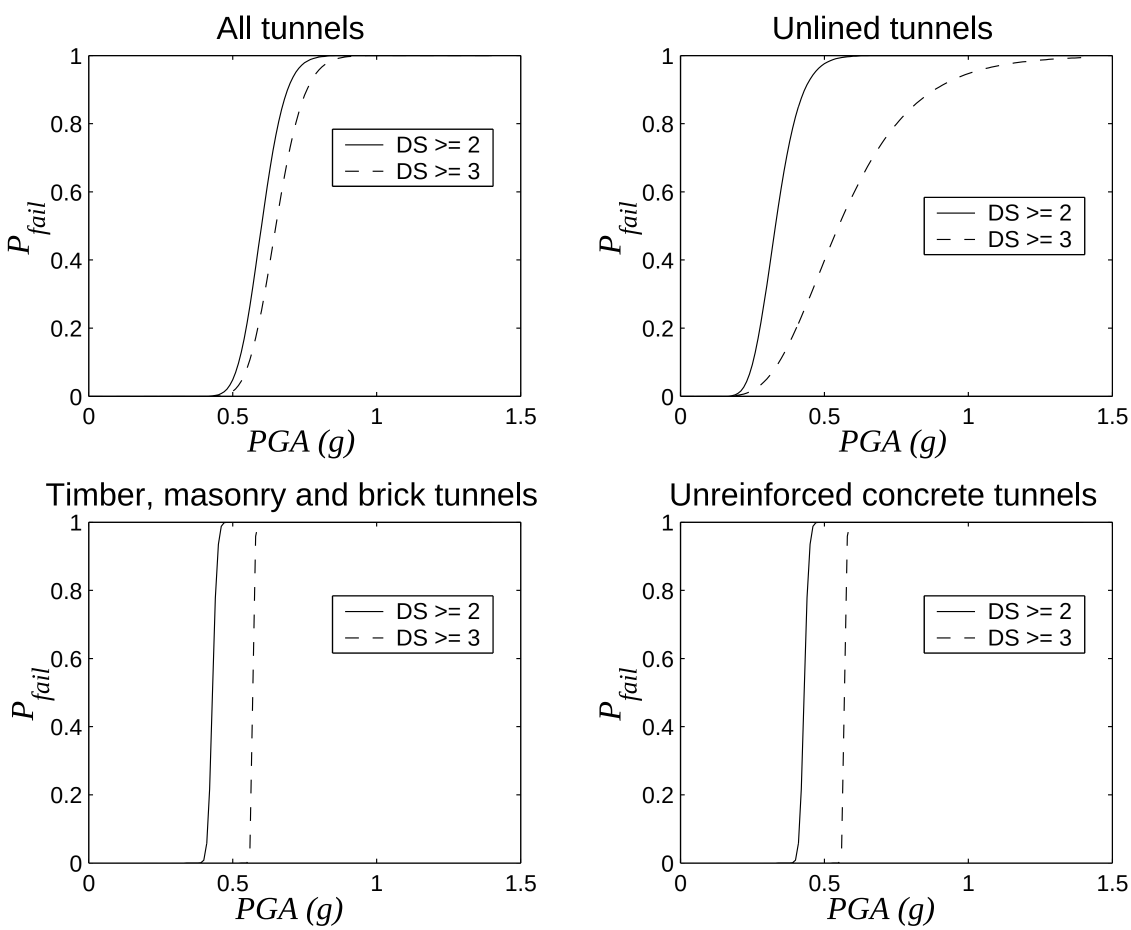

FIGURE 5-4 Fragility curves for all tunnels, unlined tunnels, timber, masonry, and brick tunnels, and unreinforced concrete tunnels.

5.3 Fragility Information for Other Components

Ballantyne (Ballantyne, 2000) presented reliability curves for some of the components of groundwater system. Fragility curves can be obtained from the reliability curves since fragility is one minus reliability. Only one damage state is attached to each curves, which is assumed to be associated with the probability of the components being out of service.

Components included in the reliability curves are wells, substations, pump buildings, control equipments, reservoirs, control buildings, and main pumps. Table 5-7 gives the reliability of the components at different values of PGA. Figure 5-5 shows the reliability curves of the components reproduced from the original source (Ballantyne, 2000), and also the respective fragility curves.

TABLE 5-7 Reliability information for various components of groundwater systems.

PGA	Reliability						
	Well	Substation	Pump Building	Control Equipment	Reservoir	Control Building	Main Pump
0.0	1.000	1.000	1.000	1.000	1.000	1.000	1.000
0.1	1.000	1.000	1.000	1.000	0.967	0.964	0.864
0.2	1.000	1.000	0.983	0.971	0.700	0.673	0.425
0.3	0.942	0.938	0.933	0.855	0.386	0.300	0.154
0.4	0.836	0.800	0.783	0.682	0.200	0.100	0.064
0.5	0.700	0.655	0.591	0.500	0.100	0.045	0.027
0.6	0.565	0.500	0.417	0.364	0.055	0.009	0.009
0.7	0.450	0.386	0.270	0.256	0.027	0.000	0.000
0.8	0.341	0.283	0.175	0.175	0.018	0.000	0.000
0.9	0.257	0.209	0.108	0.125	0.009	0.000	0.000
1.0	0.192	0.158	0.073	0.086	0.000	0.000	0.000

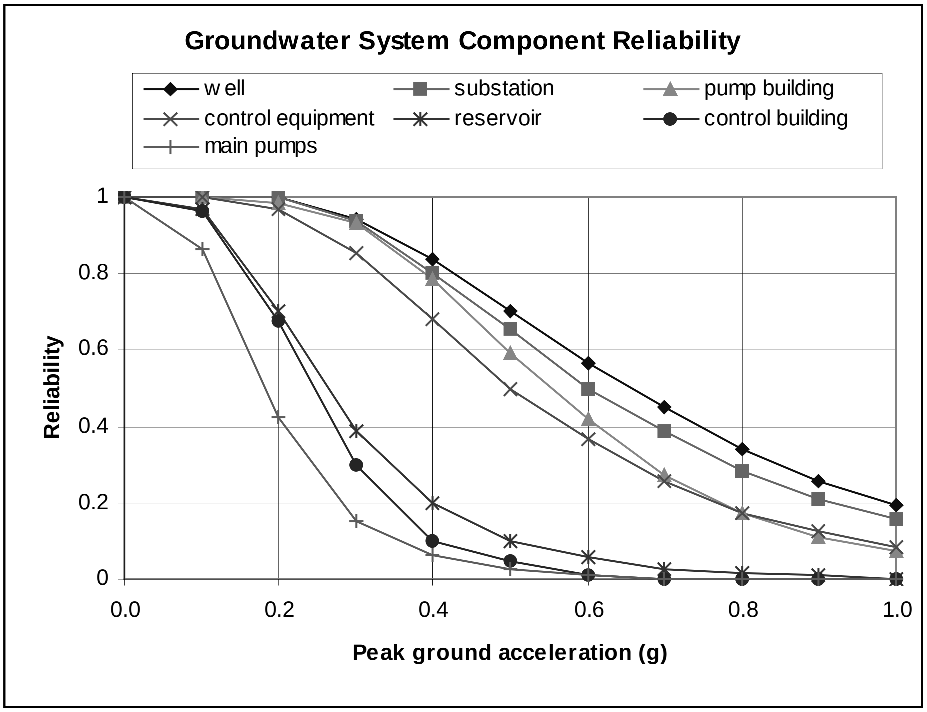

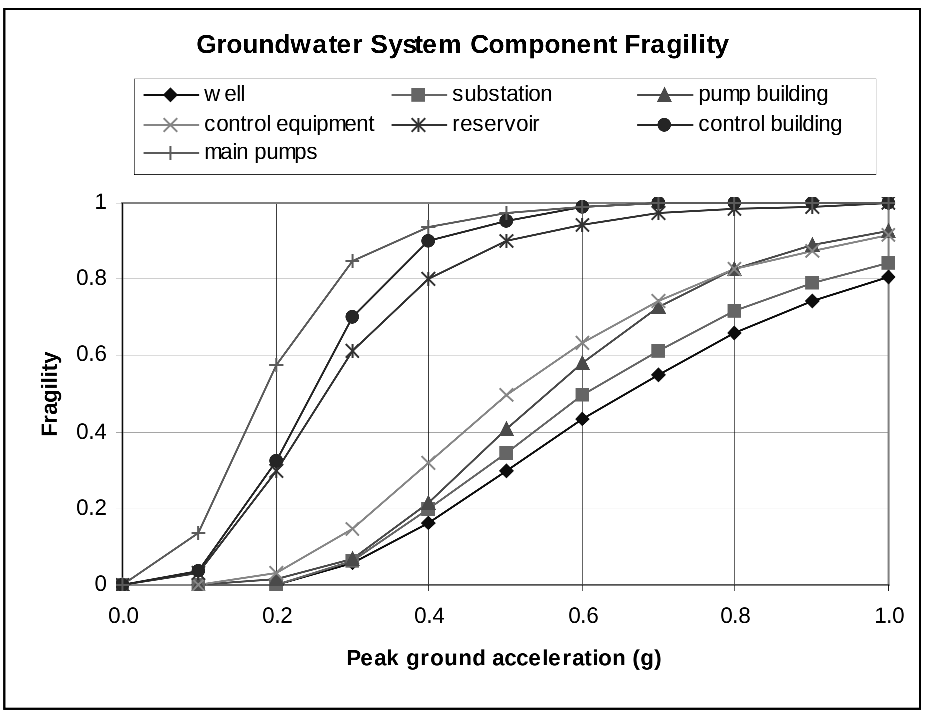

FIGURE 5-5 Reliability and fragility curves for groundwater system component.

SECTION 6
FRAGILITY ANALYSIS OF WATER SUPPLY SYSTEMS

Fragility analysis can be used to assess seismic performance of water supply systems. A methodology is developed for fragility analysis of water supply systems [Refer to Figure 6-1].

Parameters to perform fragility analysis of a water supply system include: (1) the moment magnitude of the earthquake, (2) site-to-source distances from the source to each component, (3) soil properties at each location of the components, (4) the fragility information for each component of the water supply system, and (5) a performance criteria for the water supply system.

The methodology developed for fragility analysis of water supply systems follows three steps:

Step 1: *Generate a system damage state*
The analysis is initiated by shaking the water supply system with a seismic ground motion having a moment magnitude m^* to obtain the peak ground acceleration (PGA) values at each location of the components. The next step is to toss a coin, which has a uniform distribution $U(0,1)$, for each component of the water supply system. The coin tossing exercise will determine the damage state of each component based on the outcome of the coin toss and the fragility information of the component.

Step 2: *Hydraulic analysis of a damaged system generated in step 1*
Measure the performance of the damaged water supply system by running a hydraulic analysis. Failure probability of the water supply system under the seismic occurrence with moment magnitude m^* can be approximated by repeating the analysis for n times. For each analysis, check the satisfaction of the system performance against a specified criteria or limit state, for example, pressure at a certain demand node or flow at a certain pipe.

Step 3: *Develop system fragilities*
Failure of the system corresponds to the situation in which the specified performance criteria is violated. Failure probability for m^* is approximately the number of failure divided by n run of analysis. Repeat the process with various moment magnitude m_w values to obtain a fragility curve.

6.1 Locating the source and the components

Relative to the distance between a seismic source and a water supply system, different approaches are needed. If the distance between a seismic source and a water supply system is such that the distances among the components of the water supply system are much smaller than the distance from the seismic source to the water supply system as a group, then the seismic source can be modelled as a point source with moment magnitude m_w and a site-to-source distance r from the seismic source to the water supply system. Note that with this configuration, it is possible to present the seismic performance of the water supply system with fragility surfaces (i.e. plotting failure probability of the system as a function of moment magnitude m_w and site-to-source distance r).

If the seismic source is located relatively near the water supply system such that the distance

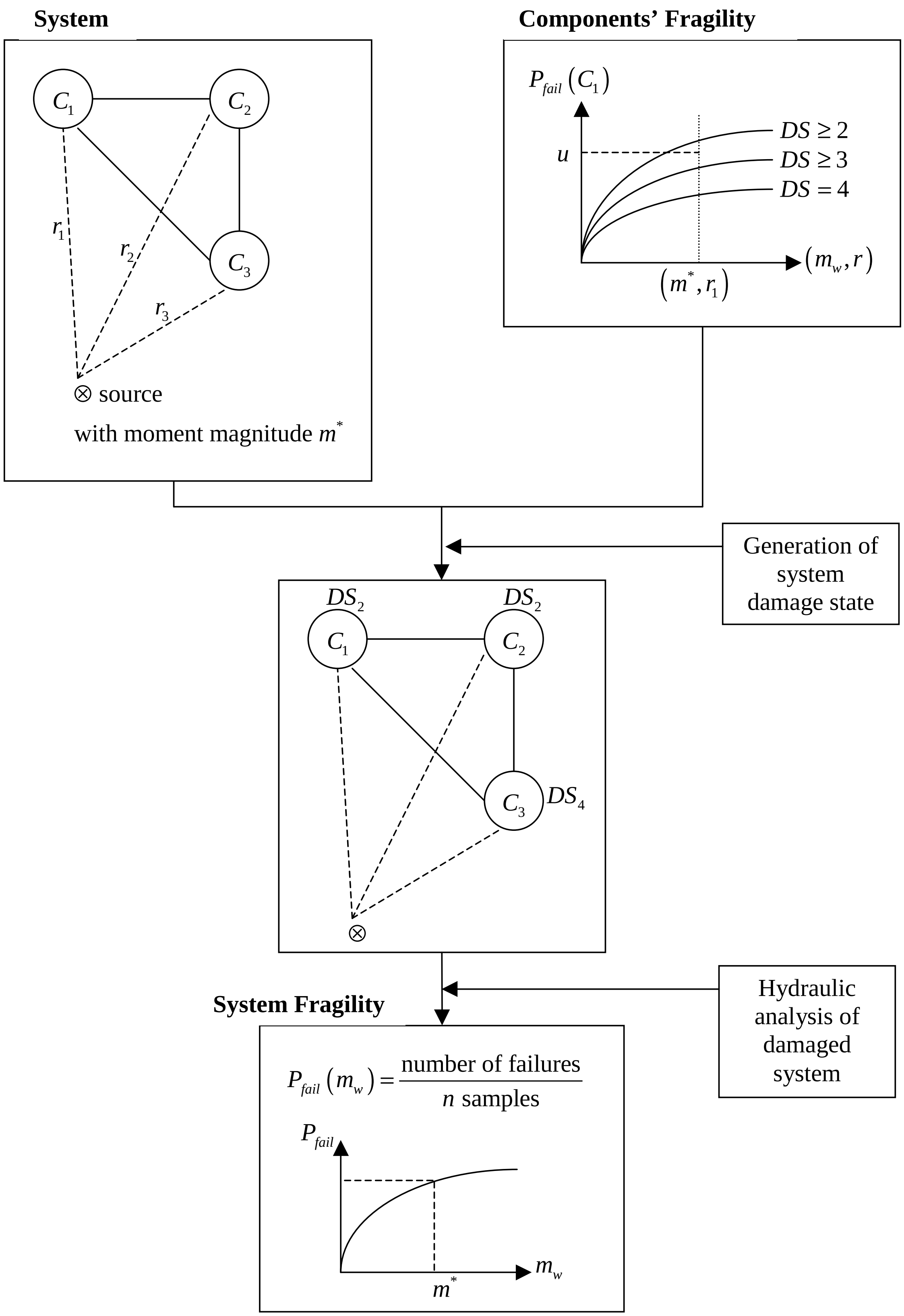

FIGURE 6-1 Methodology of fragility analysis of water supply systems.

from the source to the system is approximately in the same order of magnitude compared to the distances among the components of the water supply system, then it is most likely that the source must be modelled as a plane source (i.e. fault), and a more rigorous approach is needed to calculate the site-to-source distance from the seismic source to each individual components of the system. Seismic performance of water supply systems with this configuration can only be presented in the form of fragility curves, since it will be difficult to pick a value of site-to-source distance r that is representative of the distance from the seismic source to the closely located water supply systems.

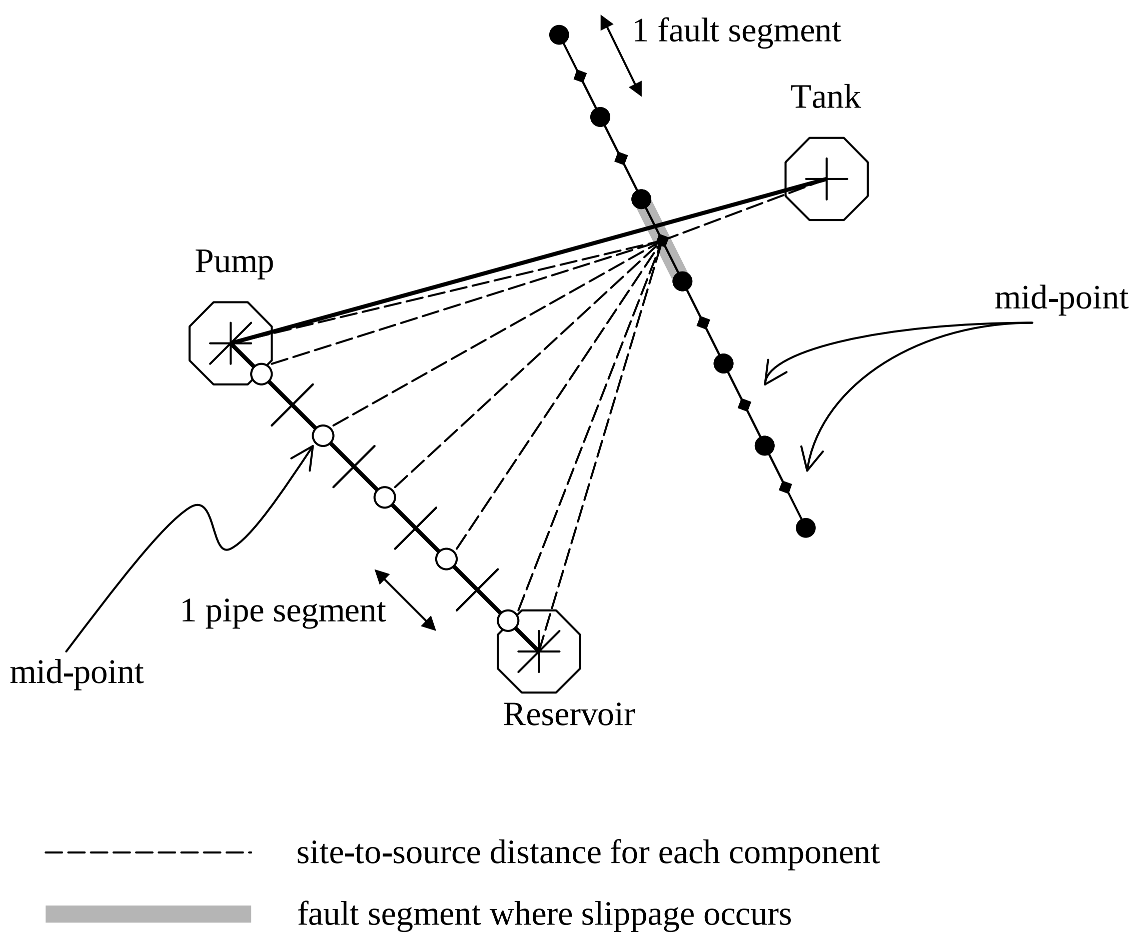

FIGURE 6-2 Locating seismic source and components and measuring site-to-source distance of each component.

A plane seismic source located near the proximity of a water supply system is assumed to consist of equal length segments, and the occurrence of slippage that trigger an earthquake can happen at any segment along the plane source with equal probability. The segment where slippage occurs is modelled as a point source located at its midpoint with a moment magnitude m_w.

Components of a water supply system can either be model as a point component or a segmented component. Components such as pumps and water tanks are modelled as a point, while pipes and tunnels are assumed to be composed of equal length segments with each segment modelled as a point.

The segmented components model is not applicable when a pipe crosses a fault segment that triggers an earthquake. For this scenario, the entire length of the pipe is considered as one component, since the models utilized to determine pipes response subject to fault displacement (i.e. the Newmark and Hall model, and Kennedy et. al. model) measure the strains ϵ_p only at the location where the pipe crosses the fault [Refer to Chapter 3, Section 3.4.3].

Using the above procedure to locate a seismic source and components of a water supply system, site-to-source distance between the source and each component can easily be obtained as summarized in Figure 6-2.

6.2 Uniformity of Fragility Information

Fragility information of each component can either be calculated analytically or obtained from literatures, such as described previously for pipes in Chapter 4 or for other components of water supply systems in Chapter 5. Two forms of fragility information have been presented, fragility surface and fragility curve. Fragility surface gives the failure probability of a component as a function of earthquake moment magnitude m_w and site-to-source distance r, while fragility curve gives the failure probability of a component as a function of peak ground acceleration (PGA), or other ground motion parameters. For uniformity, fragility surface will be converted into fragility curve with the following procedure:

For a given moment magnitude m_w, site-to-source distance r and soil properties at a site, we can generate n samples of acceleration time histories using Monte Carlo simulation. For each sample, obtain the value of peak ground acceleration along with the performance of the component (i.e. success or fail). Combine all the results into a matrix $\mathbf{M}$ having the following format,

$$\mathbf{M} = [\{m_w\}\,\{r\}\,\{PGA\}\,\{performance\}]$$

where $\{m_w\}$ is a vector of moment magnitudes, $\{r\}$ is a vector of site-to-source distances, $\{PGA\}$ is a vector of peak ground accelerations, and $\{performance\}$ is a vector of performance which can have values of either 1 if the component fails for that particular run or 0 if the component satisfies the requirement for that particular run. For example,

$$\mathbf{M} = \begin{bmatrix} 4 & 50 & 0.05 & 0 \\ \vdots & \vdots & \vdots & \vdots \\ 4 & 100 & 0.03 & 0 \\ \vdots & \vdots & \vdots & \vdots \\ 8 & 250 & 0.54 & 1 \\ \vdots & \vdots & \vdots & \vdots \end{bmatrix}$$

for the range of moment magnitudes m_w between 4 and 8, range of site-to-source distances r between 50 km and 250 km, and n samples for each (m_w, r) combination.

With the matrix $\mathbf{M}$, a fragility surface can be obtained from the information given in $\{m_w\}$, $\{r\}$, and $\{performance\}$. The failure probability for a given moment magnitude m_w and site-to-source distance r is approximately the sum of number of failure (i.e. summing vector $\{performance\}$) divided by number of samples n.

From matrix **M**, failure probability of a component can also be presented in the form of fragility curve by using $\{PGA\}$ and $\{performance\}$. This can be done by sorting matrix **M** so that the values of PGA in $\{PGA\}$ are in ascending order. Then, create a histogram of the sorted $\{PGA\}$ to discretize PGA into bins. In each PGA bin, approximate the failure probability by summing the number of failure (i.e. summing sorted vector $\{performance\}$) divided by number of samples in the bin.

6.3 Hydraulic Analysis

Hydraulic analysis is performed by using a computer program EPANET (Rossman, 2000), developed by National Risk Management Research Laboratory, and is available for free download at the U.S. Environmental Protection Agency (EPA) website http://www.epa.gov/ORD/NRMRL/wswrd/epanet.html. EPANET can perform extended period simulation of hydraulic and water quality behavior within pressurized pipe networks. The underlying analytical computations is based on fundamentals of fluid mechanics.

Some of the basic principals in fluid mechanics are continuity, conservation of energy, and momentum principal (Jeppson, 1976).

6.3.1 Continuity

Continuity principal states that the mass flow into a junction must equal the mass flow out of the junction (Jeppson, 1976). This principal is expressed mathematically as follow,

$$\Sigma Q_i = 0, \tag{6-1}$$

where Q_i is the flow in pipe i, for $i = 1, 2, \ldots$. Figure 6-3 shows an example of continuity principal applied at a junction in pipelines.

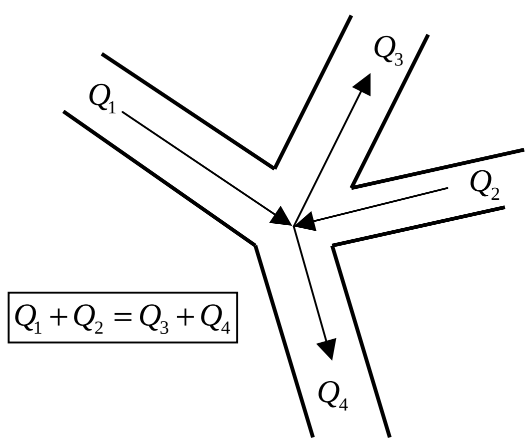

FIGURE 6-3 Continuity principal shown for a junction in pipelines.

6.3.2 Conservation of Energy

Flowing water carries three forms of energy (Jeppson, 1976): (1) potential energy due to its elevation, (2) potential energy due to the presence of pressure, and (3) kinetic energy from the motion of water flowing.

The total energy per unit mass E/M can be expressed in the form

$$E/M = gz + p/\rho + V^2/2, \tag{6-2}$$

where gz is the energy per unit mass due to elevation, p/ρ is the energy per unit mass due to pressure, and $V^2/2$ is the energy per unit mass from kinetic. g is the acceleration of gravity, z is the vertical distance above some datum, p is the water pressure, ρ is the water density, and V is the velocity of flowing water.

When some external machines exist, such as turbines or pumps, in a water network, these machines supply energy per unit mass of E_m. There are also some energy loss E_l when a body of water flows from one position to another position due to friction.

Conservation of energy between two points within a flow, such as illustrated with Figure 6-4], is given as

$$gz_1 + \frac{p_1}{\rho} + \frac{V_1^2}{2} + E_m = gz_2 + \frac{p_2}{\rho} + \frac{V_2^2}{2} + E_l. \tag{6-3}$$

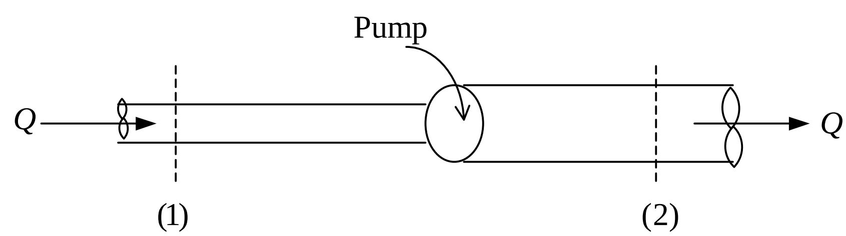

FIGURE 6-4 Conservation of energy between two points within a flow.

Principal of conservation of energy in fluid mechanics is typically represented as energy per unit weight (Jeppson, 1976), better known as the Bernoulli equation,

$$z_1 + \frac{p_1}{\gamma} + \frac{V_1^2}{2g} + h_m = z_2 + \frac{p_2}{\gamma} + \frac{V_2^2}{2g} + h_l, \tag{6-4}$$

where each term represents energy per unit weight with dimension length L and is typically denoted as head. z is simply denoted as head, the sum $z+p/\gamma$ is the piezometric or hydraulic head, $z+p/\gamma+V^2/2g$ is the total head, h_m is mechanical head that is supplied by machines such as turbines and pumps, and h_l is the head loss resulted from frictions.

There are two types of head loss, frictional head loss h_f and minor loss h_L. Frictional head loss results from friction in a flowing body of water. Minor head loss comes from the devices in pipelines such as bends, elbows, and valves that alter the flow pattern in the pipe and causing additional energy loss.

Three most widely used methods for calculating frictional head loss are: (1) Darcy-Weisbach equation, (2) Hazen-Williams equation, and (3) Mannings equation.

The Darcy-Weisbach equation (Jeppson, 1976) is

$$h_f = f\frac{L}{D}\frac{V^2}{2g}, \tag{6-5}$$

where f is a dimensionless friction factor, L is the length of the pipe, D is the pipe diameter, V is the average flow velocity and g is the acceleration of gravity.

Formulation for friction factor f is different for different type of flow. A summary of the formulations is given in Table 6-1 for laminar flow, hydraulically smooth or turbulent smooth flow, transition between hydraulically smooth and wholly rough flow, and hydraulically rough or turbulent rough flow (Jeppson, 1976).

TABLE 6-1 Summary of friction factor formulation for Darcy-Weisbach equation.

Flow type	Formulation calculating f	Range of application
Laminar	$f = 64/Re$	$Re < 2100$
Hydraulically smooth or turbulent smooth	$f = 0.316/Re^{0.25}$	$4000 < Re < 10^5$
	$\frac{1}{\sqrt{f}} = 2\log_{10}\left(Re\sqrt{f}\right) - 0.8$	$Re > 4000$
Transition between hydraulically smooth and wholly smoth	$\frac{1}{\sqrt{f}} = 2\log_{10}\left(\frac{e/D}{3.7} + \frac{2.52}{Re\sqrt{f}}\right) = \ldots$ $\ldots 1.14 - 2\log_{10}\left(\frac{e}{D} + \frac{9.35}{Re\sqrt{f}}\right)$	$Re > 4000$
Hydraulically rough and turbulent rough	$\frac{1}{\sqrt{f}} = 1.14 - 2\log_{10}(e/D) = \ldots$ $\ldots 1.14 + 2\log_{10}(D/e)$	$Re > 4000$

$Re = VD/\nu$ is Reynolds number, in which ν is the fluid kinematic viscosity, and e/D is the relative roughness (Jeppson, 1976). Values of e for some commonly used pipe material is given in Table 6-2.

The Hazen-William equation (Jeppson, 1976) is

$$h_f = \frac{4.73L}{C_{HW}^{1.852}D^{4.87}}Q^{1.852} \tag{6-6}$$

where D and L is the diameter and length of pipe respectively in feet. C_{HW} is the Hazen-William roughness coefficient, which is given in Table 6-3 (Jeppson, 1976). Hazen-William equation is an empirical formulation, and is more commonly used than Darcy-Weisbach equation.

Another empirical equation is the Manning equation (Jeppson, 1976), which is used for flow analysis in open channels. The Manning equation is

$$h_f = \frac{4.637n^2L}{D^{5.333}}Q^2 \tag{6-7}$$

TABLE 6-2 Values of equivalent roughness e for some commonly used pipes.

Material	e (inches)	e (cm)
Riveted steel	0.04 to 0.4	0.09 to 0.9
Concrete	0.01 to 0.1	0.02 to 0.2
Wood stove	0.007 to 0.04	0.02 to 0.09
Cast iron	0.0102	0.026
Galvanized iron	0.006	0.015
Asphalted cast iron	0.0048	0.012
Commercial steel or wrought iron	0.0018	0.046
PVC	0.000084	0.00021
Drawn tubing	0.00006	0.00015

TABLE 6-3 Hazen-Williams coefficient C_{HW} and Manning coefficient n for some common pipe materials.

Pipe material	C_{HW}	n
PVC	150	0.008
Very smooth pipe	140	0.011
New cast iron or welded steel	130	0.014
Wood, concrete	120	0.016
Clay, new riveted steel	110	0.017
Old cast iron, brick	100	0.020
Badly corroded cast iron or steel	80	0.035

in which D and L is the pipe diameter and length respectively in feet, and n is Manning coefficient as given in Table 6-3.

Minor head losses are caused by the added turbulence occurring at bends or fittings. For a long pipeline, these losses are negligible (Jeppson, 1976). Minor loss is expressed as

$$h_L = K_L \frac{V^2}{2g} \tag{6-8}$$

where K_L is a minor loss coefficient. Values of K_L for some typical types of fittings and valves are given in Table 6-4 (Jeppson, 1976).

TABLE 6-4 Minor loss coefficient K_L for valves and other pipe fittings.

Fittings	Minor loss coefficient K_L
Global valve, fully open	10
Angle valve, fully open	5
Gate valve, fully open	0.19
Gate valve, 3/4 open	1
Gate valve, 1/2 open	5.6
Ball check valve, fully open	70
Foot valve, fully open,	15
Swing check valve, fully open	2.3
Close return bend	2.2
Tee, through side outlet	1.8
Standard short radius elbow	0.9
Medium sweep elbow	0.8
Long sweep elbow	0.6
45^o elbow	0.4

6.3.3 Momentum Principal

Equation for momentum principal (Jeppson, 1976) is

$$\vec{F} = \rho Q \left(\vec{V}_2 - \vec{V}_1\right) \tag{6-9}$$

in which $\vec{F}$ is the resultant force acting on the fluid in a control volume being analyzed, and $\vec{V}_1$ and $\vec{V}_2$ are the average velocities entering and leaving the control volume respectively.

The momentum principal does not play an important role for flow analysis of water supply system.

6.4 Application: Numerical Example

To better understand the proposed methodology for fragility analysis of water supply systems, two numerical examples are presented as follows:

6.4.1 Example 1

Consider a water supply system that consists of one reservoir, one pump, one tank, and several pipes. Layout of the system is shown in Figure 6-5. The characteristics of each node in the system is shown in Table 6-5, and pipe properties are listed in Table 6-6. The pump can deliver 150 ft of head at a flow of 600 gpm. The tank has a 60 ft diameter, with a maximum level of 20 ft.

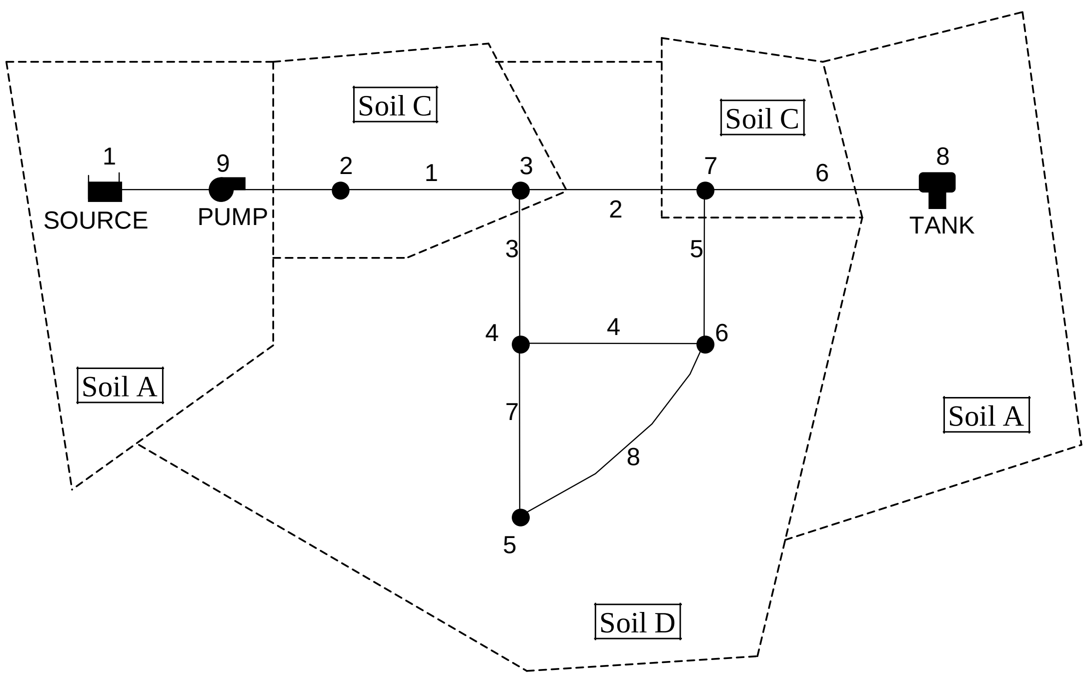

FIGURE 6-5 Example of a water supply system.

Using EPANET, the heads and pressures at each node along with the flows in each link can be obtained. These results are shown in Table 6-7.

Consider the case where a seismic source is located at far enough away from the water supply system such that the distance from the source to the water supply system is much greater compared to the distances among the components of the water supply system. Consider also that the seismic source is located at an angle of 45-degree with respect to the reservoir (i.e. node 1) and the distances between the source and the reservoir considered are r = 50 km, 100 km, 150 km, and 200 km. Fragility surfaces are to be obtained for the water supply system subjected to earthquakes with moment magnitude m_w = 4.0 to 8.0 with 0.5 increment. The layout can be seen in Figure 6-6.

TABLE 6-5 Node properties of the example system.

Node	Elevation (ft)	Demand (gpm)
1	700	0
2	700	0
3	710	150
4	700	150
5	650	200
6	700	150
7	700	0
8	830	0

TABLE 6-6 Pipe properties of the example system.

Pipe	Length (ft)	Diameter (inch)	C_{HW}
1	3000	14	100
2	5000	12	100
3	5000	8	100
4	5000	8	100
5	5000	8	100
6	7000	10	100
7	5000	6	100
8	7000	6	100

TABLE 6-7 Original states of the nodes and links of the example network.

Node ID	Head (ft)	Pressure (psi)	Link ID	Flow (gpm)
Junc 2	852.56	66.10	Pipe 1	584.43
Junc 3	850.40	60.84	Pipe 2	179.34
Junc 4	838.58	60.05	Pipe 3	255.09
Junc 5	828.63	77.40	Pipe 4	3.95
Junc 6	838.58	60.05	Pipe 5	244.91
Junc 7	849.55	64.80	Pipe 6	65.57
			Pipe 7	109.04
			Pipe 8	90.96

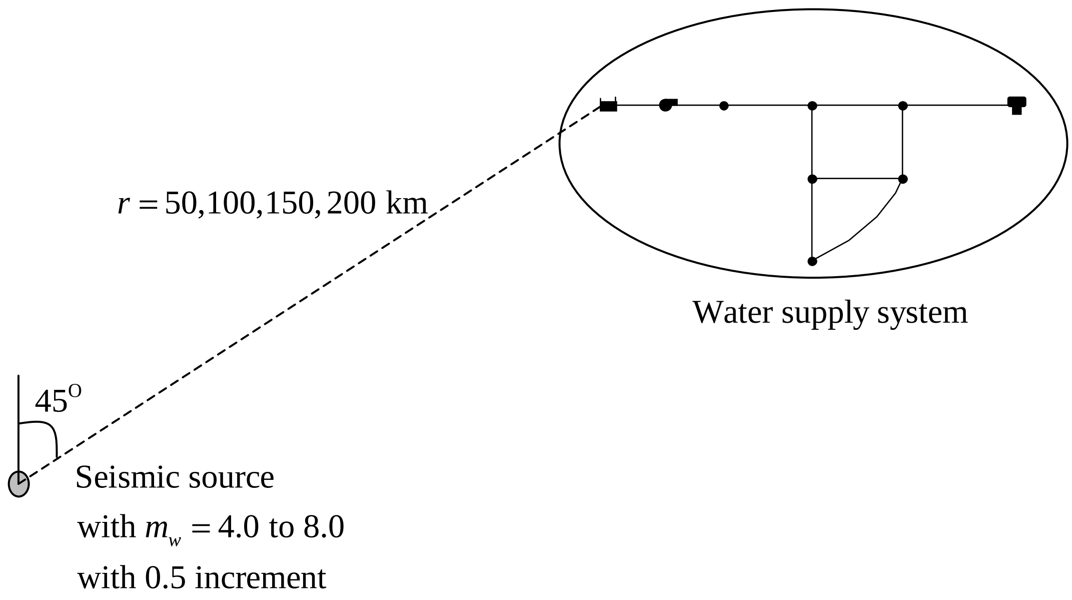

FIGURE 6-6 Location of the seismic source with respect to the example network.

The sequence of fragility analysis is as follow:

Step 1: *Generate system damage state*

For each moment magnitude and site-to-source distance pair (m_w, r), 50 samples of spatially correlated seismic ground acceleration is generated for the water supply system [Methodology as described in Chapter 2, Section 2.4.2].

For each sample, obtain the damage state of each component by coin tossing exercise, and the fragility information of the component. The fragility information of the individual component can be obtained either analytically for pipes, with methodology as described in Chapter 4, or from published fragility information, as presented in Chapter 5.

Step 2: *Hydraulic analysis of damaged system generated in step 1*

A hydraulic analysis is then performed on the damaged system by assuming that the pump, water tank, and reservoir follow the criteria given in Table 6-8.

Assume that pipes have two damage states, DS1(no damage) and DS5(damage). Pipes in DS1 operate normally, while pipes in DS5 will have leakages modelled as emitters with an assumed emitter coefficient of 5. Note that a sprinkler typically has an emitter coefficient of 0.5 (Rossman, 2000). Flow rate through an emitter is given with the following expression

$$q = Cp^{\gamma} \tag{6-10}$$

where q is flow rate, p is pressure, C is discharge coefficient, and γ is pressure exponent (Rossman, 2000). Emitters in EPANET are specified with emitter coefficients, which is C^{γ}.

Step 3: *Develop system fragilities*

TABLE 6-8 Capacity of pump, water tank, and reservoir for the sample water supply system at various damage states.

Damage State	Pump Flow (gpm)	Pump Head (ft)	Tank Level (ft)	Reservoir Elevation (ft)
1	600	150	20	700
2	550	150	16	675
3	500	150	12	650
4	450	150	8	625
5	400	150	4	600

From the hydraulic analysis, the heads and pressures at each node along with the flows in each link can be obtained for the damaged system. Following are several postulated options/examples of limit states criteria for the water supply system:

1. Option 1
   Assuming that the critical node is Junction 3 with an initial pressure of 60.84 psi, and the critical link is Pipe 1 with an initial flow of 584.43 gpm. The system can fall into four different damage states according to the following rules established in Table 6-9. Water supply system in DS1 has a slight damage, DS2 has a moderate damage, DS3 has a severe damage, and DS4 represents a total collapse.
   Using this option, fragility surfaces are obtained for the system under DS1, DS2,

TABLE 6-9 Damage states of the water supply system for option 1.

	Junc 3 $\geq$ 50 psi	Junc 3 $<$ 50 psi
Pipe 1 $\geq$ 450 gpm	DS1	DS3
Pipe 1 $<$ 450 gpm	DS2	DS4

   DS3, and DS4 as shown in Figure 6-7.

2. Option 2
   Assuming that the critical node is Junction 7 with an initial pressure of 64.80 psi, and the critical link is Pipe 6 with an initial flow of 65.57 gpm. The system can fall into four different damage states according to the following rules established in Table 6-10.
   Using this option, fragility surfaces are obtained for the system under DS1, DS2, DS3, and DS4 as shown in Figure 6-8.

3. Option 3
   Consider for the loss of pressure at junction 2 to junction 7. Assume that 5% or less in pressure loss puts the junction into DS1, loss of pressure in between 5 to 15% puts the junction into DS2, and pressure loss of more than 15% puts the junction into DS3. Assuming that option 4 categorizes the water supply system into four damage states

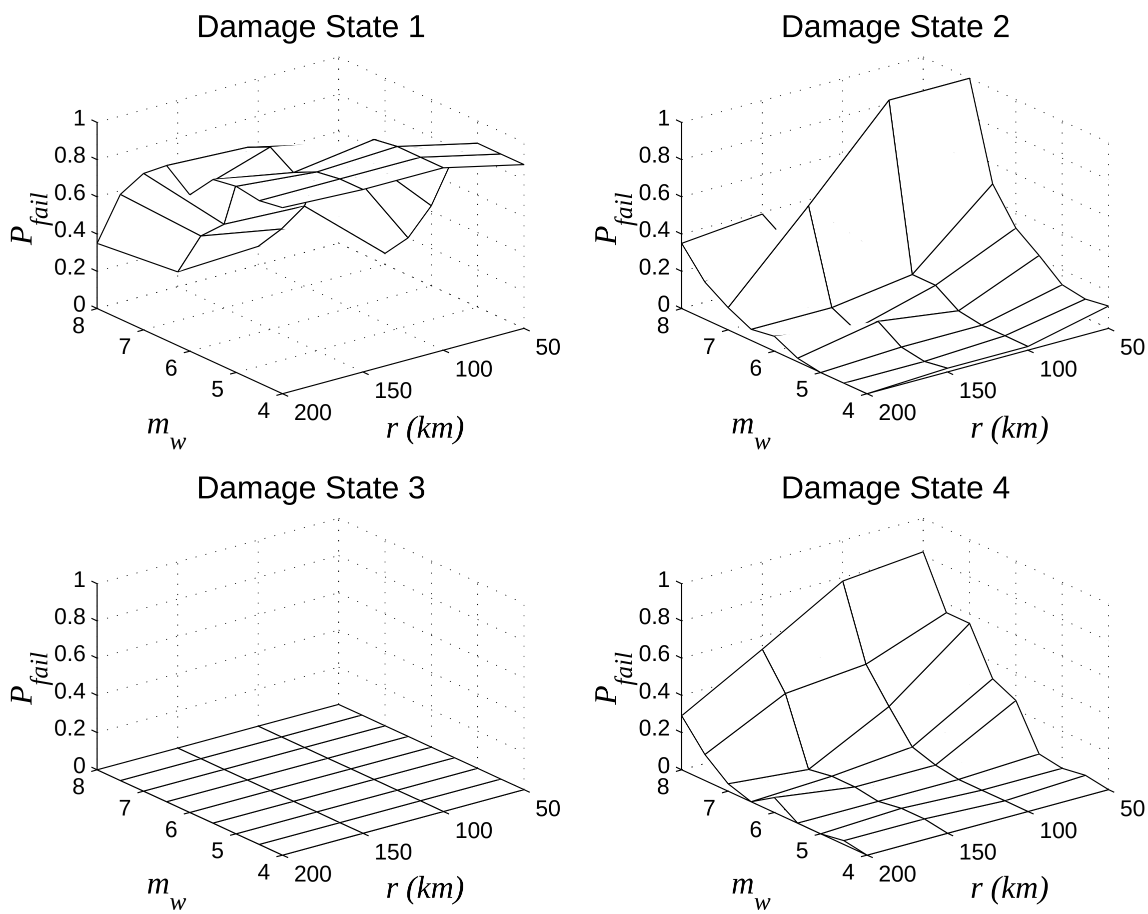

FIGURE 6-7 Fragility surfaces of the sample network for damage states prescribed in option 1 or Table 6-9.

TABLE 6-10 Damage states of the water supply system for option 2.

	Junc 7 $\geq$ 50 psi	Junc 7 $<$ 50 psi
Pipe 6 $\geq$ 50 gpm	DS1	DS3
Pipe 6 $<$ 50 gpm	DS2	DS4

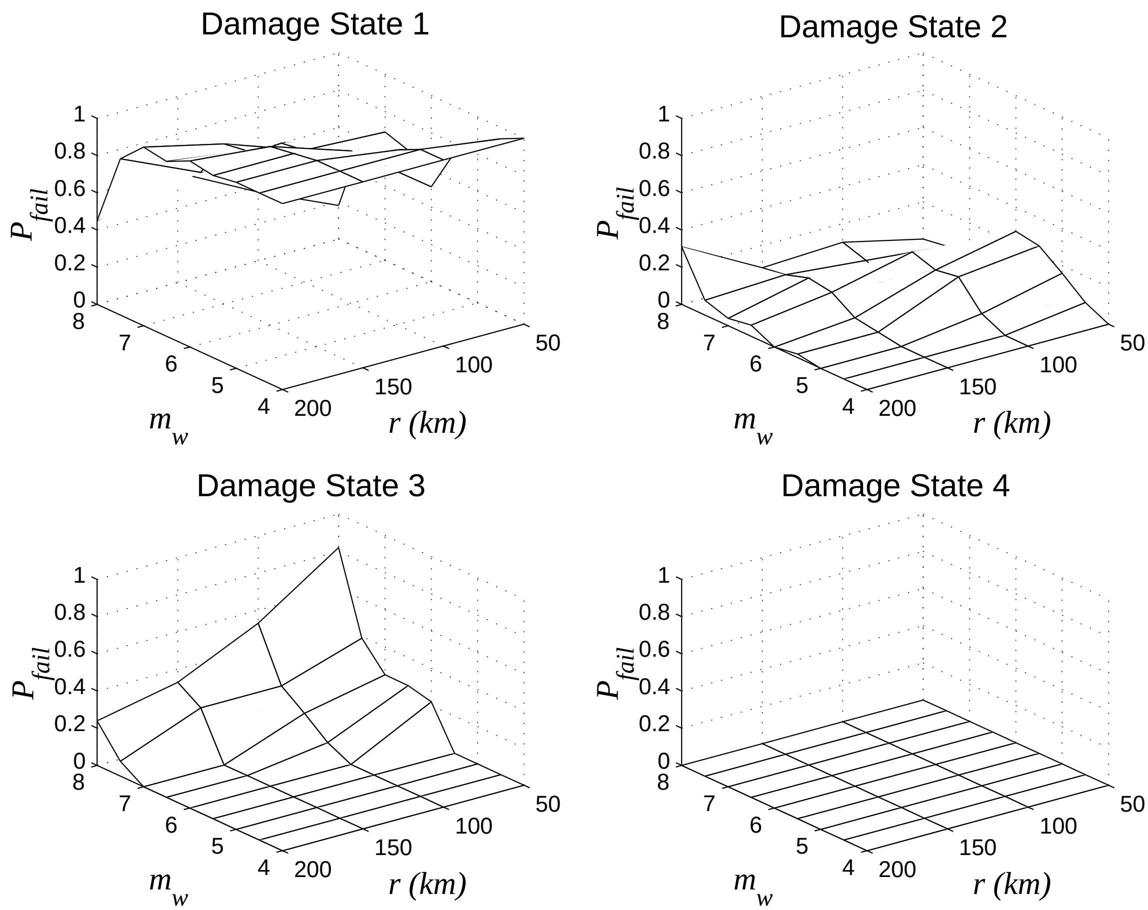

FIGURE 6-8 Fragility surfaces of the sample network for damage states prescribed in option 2 or Table 6-10.

TABLE 6-11 Damage states of the water supply system for option 3.

No. of junctions with DS1	System DS
5 - 6	1
3 - 4	2
1 - 2	3
0	4

based following the criteria given in Table 6-11. Using this option, fragility surfaces are obtained for the system under DS1, DS2, DS3, and DS4 as shown in Figure 6-9.

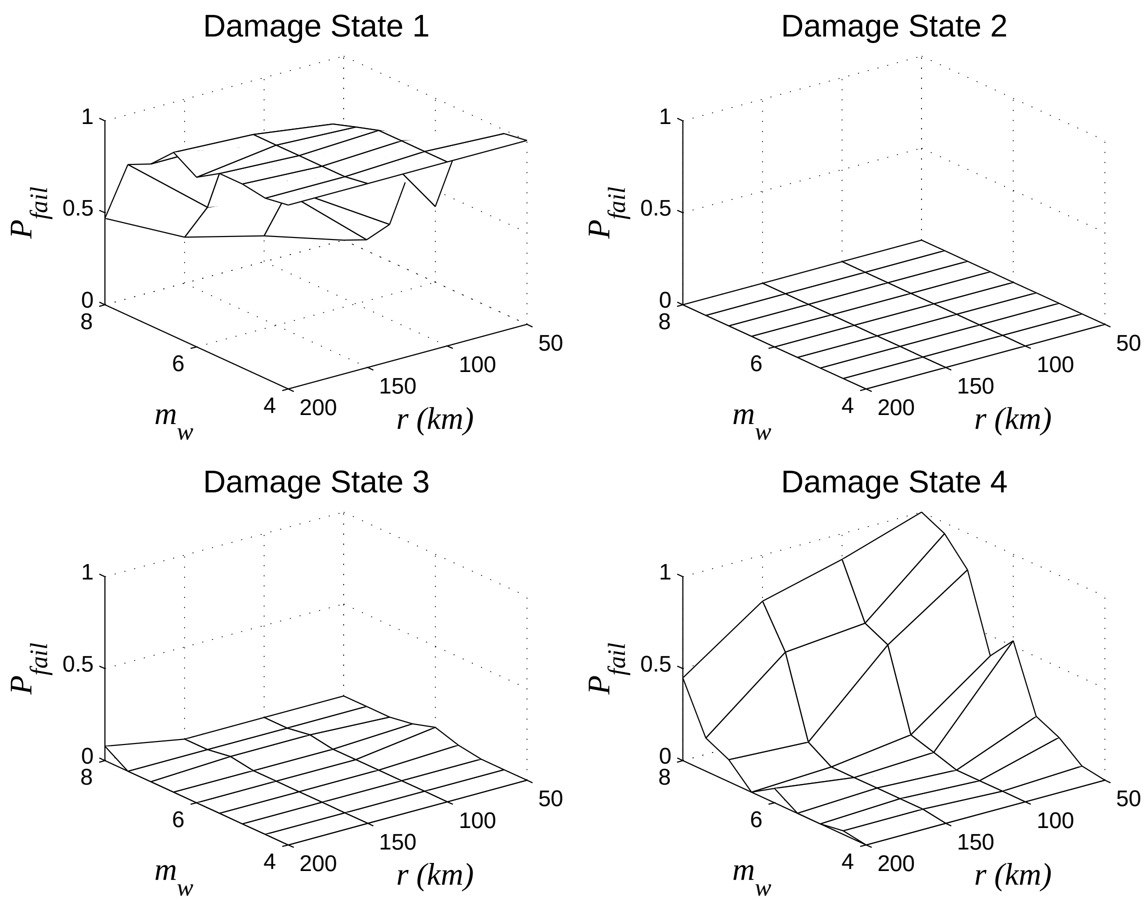

FIGURE 6-9 Fragility surfaces of the sample network for damage states prescribed in option 3 or Table 6-11.

4. Option 4
   Similar to option 3, consider for the loss of pressure at junction 2 to junction 7. Assume that 5% or less in pressure loss puts the junction into DS1, loss of pressure in between 5 to 15% puts the junction into DS2, and pressure loss of more than 15% puts the junction into DS3.
   Assuming that option 4 categorizes the water supply system into four damage states based following the criteria given in Table 6-12. Using this option, fragility surfaces are obtained for the system under DS1, DS2, DS3, and DS4 as shown in Figure 6-10.

Options 1 and 2 are chosen since the junctions and pipes for each respective options seems to be the critical junctions and/or pipes of the example system. Pressure supplies at junctions 4, 5 and 6 depend on either junction 3 supplied by pipe 1 (i.e. option 1), or junction 7 supplied by pipe 6 (i.e. option 2). Looking at the fragility curves obtained for option 1 and option 2, it can be inferred that the combination of junction 3 and pipe 1 (i.e. option 1) is more critical compared to the combination of junction 7 and pipe 6 (i.e. option 2).

TABLE 6-12 Damage states of the water supply system for option 4.

Sum of the damage states of junction 2 to 7	System DS
6 - 9	1
10 - 12	2
13 - 15	3
16 - 18	4

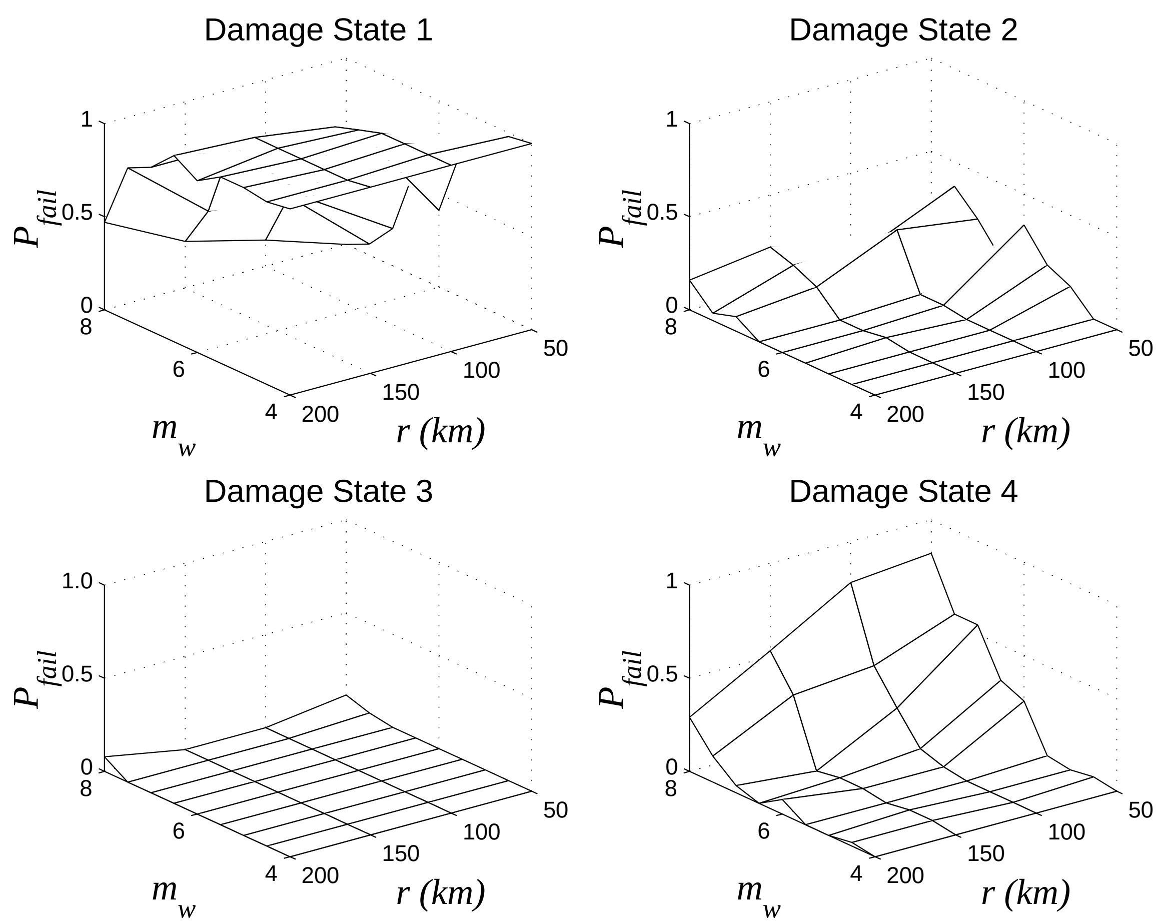

FIGURE 6-10 Fragility surfaces of the sample network for damage states prescribed in option 3 or Table 6-12.

Options 3 and 4 measure the overall pressure satisfaction at each demand node (i.e. junctions 2 to 7). Both options yield very similar fragility surfaces although different failure criteria are specified for each option.

6.4.2 Example 2

Suppose that we take the pump out from the sample water supply system and replace it with a 14 inch diameter pipe with a length of 1000 feet and coefficient of Hazen William C_{HW} of 100 as shown in Figure 6-11.

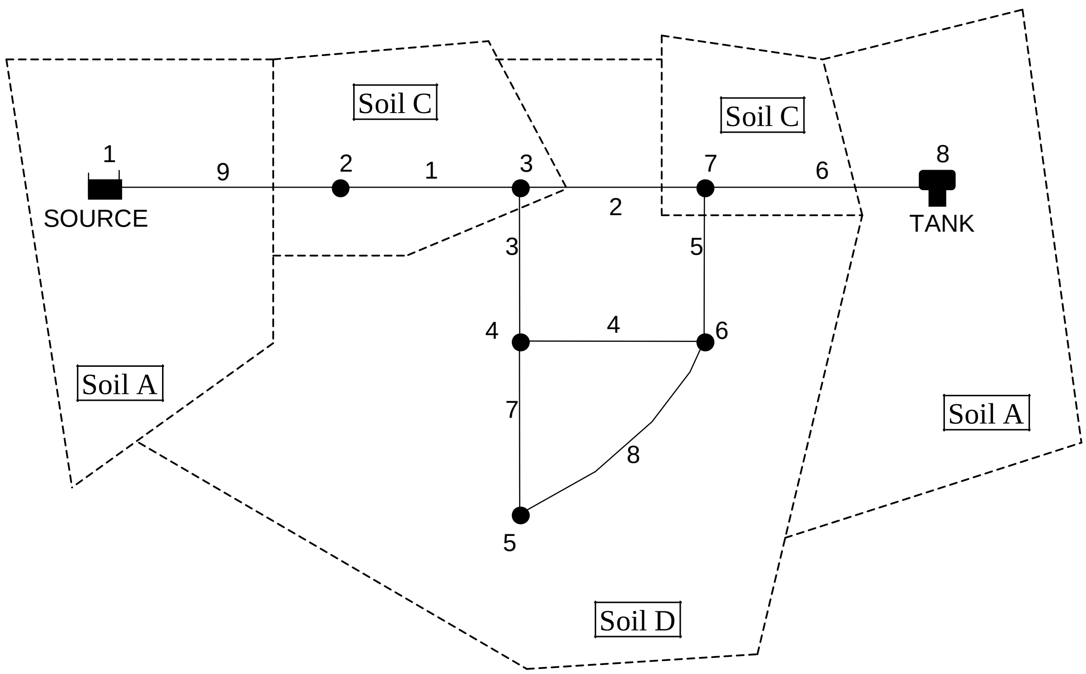

FIGURE 6-11 Example of a water supply system (modified).

Properties of the other pipes, from pipe 1 to pipe 8, are the same as for the previous example [Refer to Table 6-6]. The nodes have properties as shown in Table 6-13.

For this modified system, the initial system performance (i.e. under no damage condition) can be obtained from EPANET and is given in Table 6-14.

The modified system is still to be considered for seismic sources located at an angle of 45-degree with respect to the reservoir (i.e. node 1) with moment magnitude $m_w = 4.0$ to 8.0 with 0.5 increment and site-to-source distance $r = 50$ km to 200 km with 50 km increment, similar to previous example.

To obtain fragility surfaces for the modified system, again use the same procedure as for the first example, as follows:

Step 1: *Generate system damage state*

TABLE 6-13 Node properties of the example system (modified).

Node	Elevation (ft)	Demand (gpm)
1	1000	0
2	850	0
3	800	150
4	700	150
5	650	200
6	850	150
7	850	0
8	1100	0

TABLE 6-14 Original states of the nodes and links of the example network (modified).

Node ID	Head (ft)	Pressure (psi)	Link ID	Flow (gpm)
Junc 2	1000.68	65.29	Pipe 1	567.78
Junc 3	1002.73	87.84	Pipe 2	881.32
Junc 4	997.54	128.92	Pipe 3	163.54
Junc 5	988.36	146.61	Pipe 4	90.84
Junc 6	999.28	64.68	Pipe 5	336.46
Junc 7	1019.03	73.23	Pipe 6	1217.78
			Pipe 7	104.38
			Pipe 8	95.62
			Pipe 9	567.78

For each moment magnitude and site-to-source distance pair (m_w, r), 50 samples of spatially correlated seismic ground acceleration is generated. For each sample, damage state of each component is determined.

Step 2: *Hydraulic analysis of damaged system generated in step 1*

A hydraulic analysis is then performed on the damaged system. The capacity of components at different damage states are given in Table 6-15.

TABLE 6-15 Capacity of water tank, reservoir and pipelines for the modified water supply system at different damage states.

Damage State	Tank Level (ft)	Reservoir Elevation (ft)	Pipe Emitter Coefficient
1	20	1000	0
2	16	975	5
3	12	950	–
4	8	925	–
5	4	900	–

Step 3: *Develop system fragilities*

From the hydraulic analysis, the heads and pressures at each node along with the flows in each link can be obtained for the damaged system. Only one specified limit states (i.e. option) will be considered for the modified system.

Consider for the loss of pressure at junction 2 to junction 7. Assume that 5% or less in pressure loss puts the junction into DS1, loss of pressure in between 5 to 15% puts the junction into DS2, and pressure loss of more than 15% puts the junction into DS3.

Assuming that the modified system damage states are specified in Table 6-16.

TABLE 6-16 Damage states of the modified water supply system.

No. of junctions with DS1	System DS
5 - 6	1
3 - 4	2
1 - 2	3
0	4

Using this option, fragility surfaces are obtained for the modified system under DS1, DS2, DS3, and DS4 as shown in Figure 6-12.

More options can be specified by users either at individual component level or the system

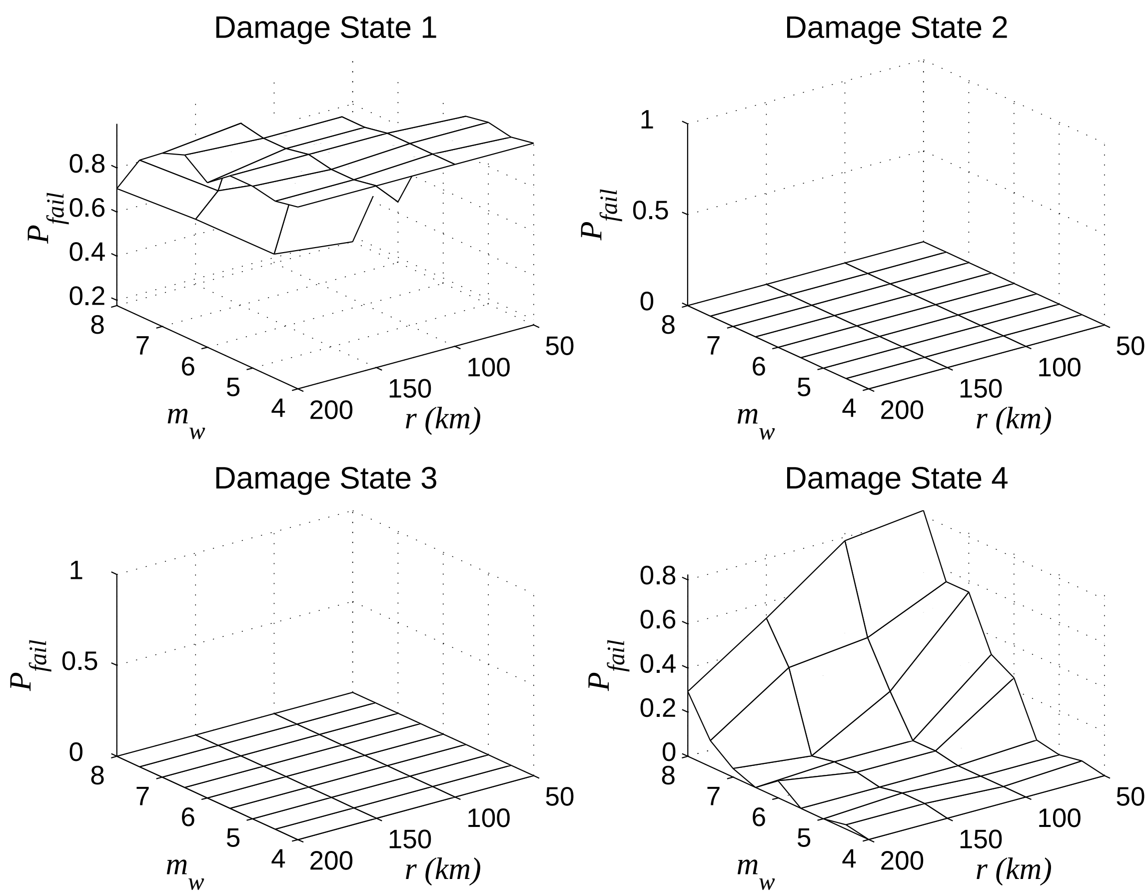

FIGURE 6-12 Fragility surfaces of the modified sample network for damage states prescribed Table 6-16.

level to better analyze the seismic performance of the system.

6.5 Life Cycle Damage Estimation

Assuming that the water supply system is located at a site with a seismic activity matrix or mean annual rate of seismic occurrence ν_{ij}. A life cycle damage estimation of a water supply system can be performed for a given fragility surface and seismic activity matrix of the site. The procedure for life cycle damage estimation is as follow [Refer to Figure 6-13]:

For a given lifespan of a water supply system t and the seismic activity matrix at the site ν_{ij}, samples of seismic hazard in $[0, t]$ can be produced. For each seismic event i with moment magnitude and site-to-source distance (m_{wi}, r_i), the damage state of the system can be obtained from the fragility surface of the water supply system. Repeating this for each event i, the damage sequence of the water supply system can be obtained.

The damage sequence gives an estimation of the system damages during its lifespan t. Since each damage state DS_i is associated with a cost C_i, estimation of total cost C_T of the system due to seismic hazard can be estimated, which is simply the sum of all cost as follow:

$$C_T = \sum_i C_i, \tag{6-11}$$

for $i = 1, 2, \ldots, n$, and n is the number of seismic event during time period t.

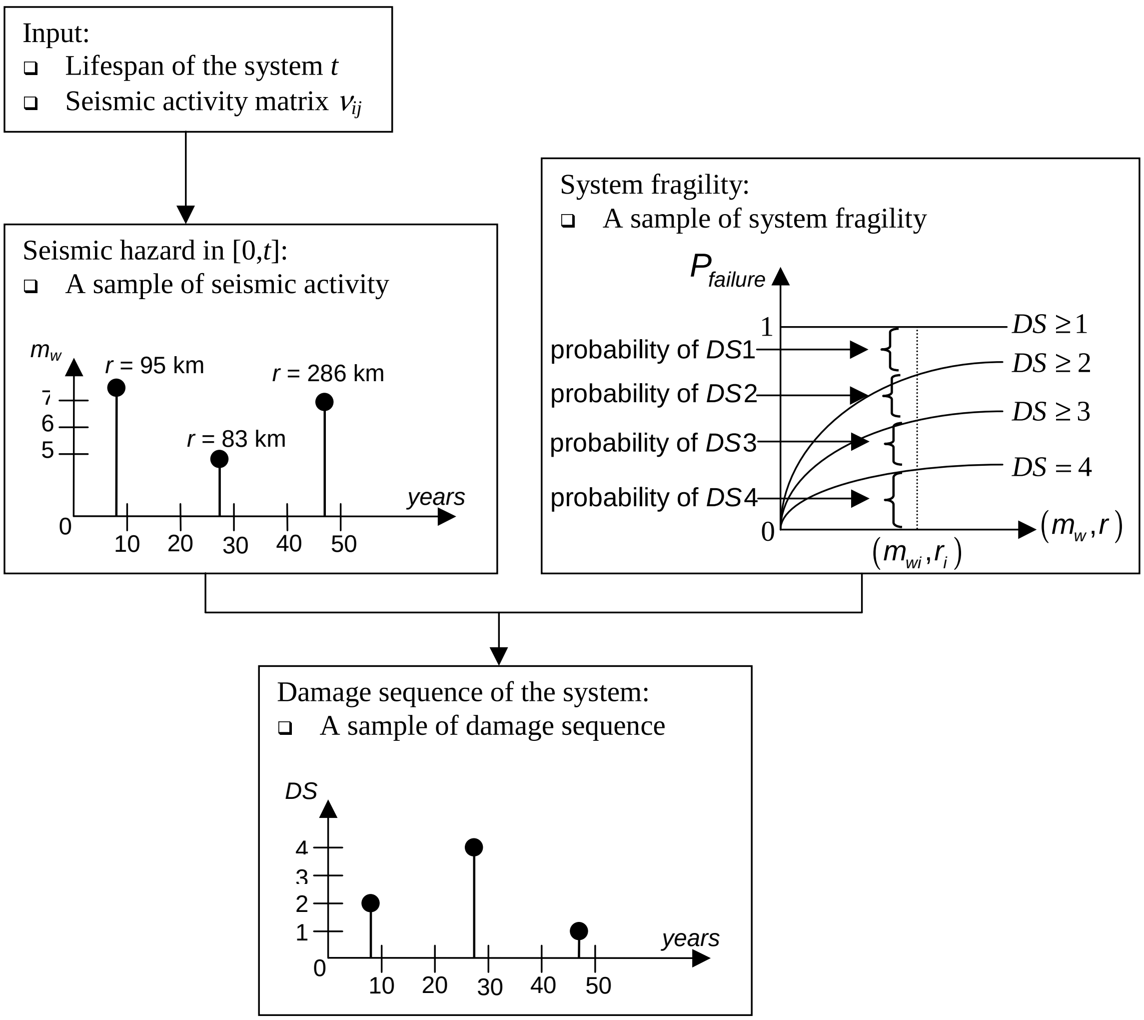

FIGURE 6-13 Life cycle damage estimation of a system.

SECTION 7
SUMMARY AND CONCLUSION

Seismic hazard models have been developed for generating random samples of seismic activity at a single site and multiple sites. A ground motion model (i.e. specific barrier model by Papageorgiou (Papageorgiou and Aki, 1983a),(Papageorgiou and Aki, 1983b),(Papageorgiou, 1988)) and Monte Carlo simulation are used to produce seismic ground acceleration records at a site. A coherence model proposed by Harichandran and Vanmarcke (Harichandran and Vanmarcke, 1986) is used in conjunction with the ground motion model and Monte Carlo simulation to produce seismic ground acceleration for multiple sites. The coherence model captures the coherency of motions experienced at different sites originating from a same seismic source.

Permanent ground deformation (PGD) hazards can cause a certain amount of ground displacement. The amount of ground displacement can be obtained by empirical models, such as: (1) Jibson and Keefer's model (Jibson and Keefer, 1993) for landslides, (2) Bartlett and Youd's model (Barlett and Youd, 1992) for lateral spreads, and (3) Takada and Tanabe's model (Takada *et al.*, 1987) for seismic settlements. The ground displacement can be decomposed into its longitudinal and transverse components. The effect of each component on pipelines can be calculated with models proposed by O'Rourke (O'Rourke and Liu, 1999),(O'Rourke and Nordberg, 1992),(O'Rourke, 1989).

Ground movement caused by fault displacements can be approximated with near-fault ground motion model proposed by Mavroeidis and Papageorgiou (Mavroeidis and Papageorgiou, 2003). The effects of the ground movement on pipelines can be analyzed either by employing Newmark-Hall model (Newmark and Hall, 1975) or Kennedy, et.al. model (Kennedy *et al.*, 1977).

Several methodologies for obtaining pipeline's fragility are developed, which includes : (1) fragility analysis of continuous and jointed pipelines subject to seismic waves, (2) fragility analysis of pipelines subject to PGD hazards, and (3) fragility analysis of pipelines subject to fault displacements.

Fragility information of some components of water supply system have been obtained from published works, which includes fragility information of : (1) water tanks, tunnels, and canals from the American Lifelines Alliance (American Lifelines Alliance, 2001a), and (2) wells, substations, pump buildings, control equipments, reservoirs, control buildings, and main pumps from Ballantyne (Ballantyne, 2000).

An algorithm for obtaining fragility surfaces of an arbitrary water supply system has been developed. The algorithm consists of three steps: (1) generate a system damage state, (2) hydraulic analysis of a damaged system generated in step 1, and (3) develop system fragilities. These steps are illustrated with numerical examples.

A procedure for estimating the life cycle system damage is discussed. This procedure yields the damage sequence of the system during its lifespan. Each damage is associated with a cost, thus the total cost due to seismic hazard of the system during its lifespan can be determined.

REFERENCES

(1976), "West Coast Mid-Continent Pipeline Project: Parametric Evaluation of Fault Movement Capacity of Buried Oil Pipeline", Tech. Rep. HN 5113.7R Task 3008, Holmes & Narver, Inc.

American Lifelines Alliance (2001a), "Seismic Fragility Formulations for Water Systems: Part I-Guideline", Tech. rep., URL: http://www.americanlifelinesalliance.org.

American Lifelines Alliance (2001b), "Seismic Fragility Formulations for Water Systems: Part II-Appendices", Tech. rep. URL: http://www.americanlifelinesalliance.org.

Atkinson, G. and D. Boore (1995), "Ground-Motion Relations for Eastern North America", Bulletin of the Seismological Society of America, vol. 85, pp. 17–30.

Ballantyne, D. (2000), "Case Study of Portland's Water System", Presented at Oregon Center for Advanced Technology Education Earthquake in the Civil Engineering Lecture Series.

Barlett, S. F. and T. L. Youd (1992), "Empirical Analysis of Horizontal Ground Displacement Generated by Liquefaction-induced Lateral Spreads", Tech. Rep. NCEER-92-0021, Multidisciplinary Center for Earthquake Engineering Research, Buffalo, New York.

Boore, D. (1983), "Stochastic Simulation of High-Frequency Ground Motions Based on Seismological Models of the Radiated Spectra", Bulletin of the Seismological Society of America, vol. 73, pp. 1865–1894.

Committee on Gas and Liquid Fuel Lifelines (1984), "Guidelines for the Seismic Design of Oil and Gas Pipeline Systems", ASCE.

Frankel, A., C. Mueller, T. Barnhard, D. Perkins, E. Leyendecker, N. Dickman, S. Hanson and M. Hopper (1996), "National Seismic Hazard Maps", Tech. rep., U.S. Geological Survey.

Grigoriu, M. (1995), "Applied Non-Gaussian Process: Examples, Theory, Simulation, Linear Random Vibration, and MATLAB Solutions", Prentice Hall, Englewood Cliffs, NJ.

Grigoriu, M. (2002), "Stochastic Calculus: Applications in Science and Engineering", Birkhäuser, Boston, MA.

Grigoriu, M. and E. Mostafa (2002a), "Fragility Surfaces as a Measure of Seismic Performance", in The 7th U.S. National Conference on Earthquake Engineering, Boston.

Grigoriu, M. and E. Mostafa (2002b), "A Methodology for Optimizing Retrofitting Techniques", in The 7th U.S. National Conference on Earthquake Engineering, Boston.

Halldorsson, B., G. Dong and A. Papageorgiou (2004), "Strong Ground Motion Simulation for Eastern North America Code User Manual", URL: http://civil.eng.buffalo.edu/engseislab.

Halldorsson, B., D. G. and P. A. S. (2002), "Earthquake Motion Input and its Dissemination via the Internet", Journal of Engineering and Engineering Vibration, vol. 1(1), pp. 20–26.

Harichandran, R. S. and E. H. Vanmarcke (1986), "Stochastic Variation of Earthquake Ground Motion in Space and Time", Journal of Engineering Mechanics, vol. 112, pp. 154–175.

Hashash, Y. M. A., J. J. Hook, B. Schmidt and J. I. C. Yao (2001), "Seismic Design and Analysis of Underground Structures", Tunnelling and Underground Space Technology, pp. 247–293.

HAZUS (1997), "Earthquake Loss Estimation Methodology", National Institute of Building Sciences, prepared by Risk Management Solutions, Menlo Park, CA.

Hou, A., J. Cai and X. Liu (1990), "Response Calculation of Oil Pipeline Subjected to Permanent Ground Movement Induced by Soil Liquefaction", in Proceedings of the China-Japan Symposium on Lifeline Earthquake Engineering, Beijing, China.

Jeppson, R. W. (1976), "Analysis of Flow in Pipe Networks", Butterworth Publishers, Boston.

Jibson, R. W. and D. K. Keefer (1993), "Analysis of the Seismic Origin of Landslides: Examples from the New Madrid Seismic Zone", Geological Society of America Bulletin, vol. 105, pp. 521–536.

Kafali, C. and M. Grigoriu (2003), "Non-Gaussian Model for Spatially Coherent Seismic Grount Motions", in Proceedings of the 9th International Conference on Applications of Statistics and Probability in Civil Engineering, San Francisco, CA.

Kennedy, R. P., A. W. Chow and R. A. Williamson (1977), "Fault Movement Effects on Buried Oil Pipeline", Journal of the Transportation Engineering Division, ASCE, vol. 103, pp. 617–633.

Kobayashi, T., H. Nakane, N. Suzuki and M. Ishikawa (1989), "Parametric Study on Flexibility of Buried Pipeline Subject to Large Ground Displacement", in Proceedings of the Second U.S.-Japan Workshop on Liquefaction, Large Ground Deformation and Their Effects on Lifeline Facilities, Technical Report NCEER-89-0032, Multidisciplinary Center for Earthquake Engineering Research, Buffalo, New York.

Kramer, S. L. (1996), "Geotechnical Earthquake Engineering", Prentice Hall, 76 pp.

Liu, X. J. and M. J. O'Rourke (1997b), "Behavior of Continuous Pipeline Subject to Transverse PGD", Journal of Earthquake Engineering and Structural Dynamics, vol. 26, pp. 998–1003.

Mavroeidis, G. P. and A. S. Papageorgiou (2003), "A Mathematical Representation of Near-Fault Ground Motions", Bulletin of the Seismological Society of America, vol. 93, pp. 1099–1131.

Meyersohn, W. (1991), "Analytical and Design Considerations for the Seismic Response of Buried Pipelines", Ph.D. thesis, Cornell University.

Newmark, N. M. and W. J. Hall (1975), "Pipeline Design to Resist Large Fault Displacement", in Proceedings of the 1975 U.S. National Conference on Earthquake Engineering, Ann Arbor, Michigan.

O'Rourke, M. J. (1989), "Approximate Analysis Procedures for Permanent Ground Deformation Effects on Buried Pipelines", in Proceedings of the Second U.S.-Japan Workshop on Liquefaction, Large Ground Deformation and Their Effects on Lifeline Facilities, Technical Report NCEER-89-0032, Multidisciplinary Center for Earthquake Engineering Research, Buffalo, New York.

O'Rourke, M. J. and X. Liu (1999), "Response of Buried Pipelines Subject to Earthquake Effects", Multidisciplinary Center for Earthquake Engineering Research.

O'Rourke, M. J., X. J. Liu and R. Flores-Berrones (1995), "Steel Pipe Wrinkling Due to Longitudinal Permanent Ground Deformation", Journal of Transportation Engineering, vol. 121.

O'Rourke, M. J. and G. Nordberg (1992), "Analysis Procedures for Buried Pipelines Subject to Permanent Ground Deformation", in Tenth World Conference on Earthquake Engineering, vol. 9, Madrid, Spain.

O'Rourke, M. J. and P. So (1999), "Seismic Behavior of On-Grade Steel Tanks, Fragility Curves", in Optimizing Post-Earthquake Lifeline System Reliability, Proceedings of the 5th U.S. Conference on Lifeline Earthquake Engineering (Edited by W. M. Elliot and P. McDonough).

O'Rourke, T., Y. Wang, P. Shi and S. Jones (2004), "Seismic Wave Effects on Water Trunk and Transmission Lines", in 11th International Conference on Soil Dynamics and Earthquake Engineering, 3rh International Conference on Earthquake Geotechnical Engineering.

O'Rourke, T. D. (1988), "Critical Aspects of Soil-Pipeline Interaction for Large Ground Deformation", in Proceedings of the First Japan-U.S. Workshop on Liquefaction, Large Ground Deformation and Their Effects on Lifeline Facilities, Tokyo, Japan.

O'Rourke, T. D. (1996), "Lessons Learned for Lifeline Engineering from Major Urban Earthquakes", in Eleventh World Conference on Earthquake Engineering.

O'Rourke, T. D. (1998), "An Overview of Geotechnical and Lifeline Earthquake Engineering", in Geotechnical Special Publication No. 75, ASCE, Reston, VA. Proceedings of Geotechnical Earthquake Engineering and Soil Dynamics Conference, vol. 2, Seattle, WA.

O'Rourke, T. D., M. D. Grigoriu and M. M. Khater (1985), "Seismic Response of Buried Pipelines", Pressure Vessel and Piping Technology: A Decade of Progress.

Papageorgiou, A. S. (1988), "On Two Characteristic Frequencies of Acceleration Spectra: Patch Corner Frequency and f_{max}", Bulletin of the Seismological Society of America, vol. 78, pp. 509–528.

Papageorgiou, A. S. and K. Aki (1983a), "A Specific Barrier Model for the Quantitative Description of Inhomogeneous Faulting and the Prediction of Strong Ground Motion. Part I: Description of the Model", Bulletin of the Seismological Society of America, vol. 73, pp. 693–722.

Papageorgiou, A. S. and K. Aki (1983b), "A Specific Barrier Model for the Quantitative Description of Inhomogeneous Faulting and the Prediction of Strong Ground Motion. Part II: Application of the Model", Bulletin of the Seismological Society of America, vol. 73, pp. 953–978.

Ramberg, W. and W. Osgood (1943), "Description of Stress-Strain Curves by Three Parameters", Technical Note 902, National Advisory Committee for Aeronautics.

Rossman, L. A. (2000), "EPANET 2 Users Manual", Tech. Rep. EPA/600/R-00/057, Water Supply and Water Resources Division, National Risk Management Research Laboratory, Cincinnati, OH 45268.

Sewell, R. T. (1989), "Damage Effectiveness of Earthquake Ground Motion: Characterizations Based on the Performance of Structures and Equipment", Ph.D. thesis, Stanford University, Stanford, CA.

Soong, T. T. and M. Grigoriu (1992), “Random Vibration of Mechanical and Structural Systems”, Prentice Hall, Englewood Cliffs, NJ.

Suzuki, N., O. Arata and I. Suzuki (1988), “Subject to Liquefaction-Induced Permanent Ground Displacement”, in Proceedings of the First Japan-U.S. Workshop on Liquefaction, Large Ground Deformation and Their Effects on Lifeline Facilities, Tokyo, Japan.

Takada, S., K. Tanabe, K. Yamajyo and S. Katagiri (1987), “Liquefaction Analysis for Buried Pipelines”, in Proceedings of the Third International Conference on Soil Dynamics and Earthquake Engineering.

Tokimatsu, K. and H. B. Seed (1987), “Evaluation of Settlements in Sands Due to Earthquake Shaking”, Journal of Geotechnical Engineering, ASCE, vol. 113, pp. 861–878.

Trautmann, C. H. and T. D. O’Rourke (1983), “Load-Displacement Characteristics of a Buried Pipe Affected by Permanent Earthquake Ground Movements”, Earthquake Behavior and Safety of Oil and Gas Storage Facilities, Buried Pipelines and Equipments, pp. 254–262.

University of British Columbia (2004), “Energy Measurement in the Standard Penetration Test (SPT)”, URL: http://www.civil.ubc.ca/research/geotech/sptenergy/sptenergy.htm.

Wells, D. L. and K. J. Coppersmith (1994), “New Empirical Relationships among Magnitude, Rupture Length, Rupture Width, Rupture Area, and Surface Displacement”, Bulletin of the Seismological Society of America, vol. 84, pp. 974–1002.

Wilson, R. C. and D. K. Keefer (1983), “Dynamic Analysis of a Slope Failure from the 6 August 1979 Coyote Lake, California Earthquake”, Bulletin of the Seismological Society of America, vol. 73, pp. 863–877.

MCEER Technical Reports

MCEER publishes technical reports on a variety of subjects written by authors funded through MCEER. These reports are available from both MCEER Publications and the National Technical Information Service (NTIS). Requests for reports should be directed to MCEER Publications, MCEER, University at Buffalo, State University of New York, Red Jacket Quadrangle, Buffalo, New York 14261. Reports can also be requested through NTIS, 5285 Port Royal Road, Springfield, Virginia 22161. NTIS accession numbers are shown in parenthesis, if available.

NCEER-87-0001 "First-Year Program in Research, Education and Technology Transfer," 3/5/87, (PB88-134275, A04, MF-A01).

NCEER-87-0002 "Experimental Evaluation of Instantaneous Optimal Algorithms for Structural Control," by R.C. Lin, T.T. Soong and A.M. Reinhorn, 4/20/87, (PB88-134341, A04, MF-A01).

NCEER-87-0003 "Experimentation Using the Earthquake Simulation Facilities at University at Buffalo," by A.M. Reinhorn and R.L. Ketter, to be published.

NCEER-87-0004 "The System Characteristics and Performance of a Shaking Table," by J.S. Hwang, K.C. Chang and G.C. Lee, 6/1/87, (PB88-134259, A03, MF-A01). This report is available only through NTIS (see address given above).

NCEER-87-0005 "A Finite Element Formulation for Nonlinear Viscoplastic Material Using a Q Model," by O. Gyebi and G. Dasgupta, 11/2/87, (PB88-213764, A08, MF-A01).

NCEER-87-0006 "Symbolic Manipulation Program (SMP) - Algebraic Codes for Two and Three Dimensional Finite Element Formulations," by X. Lee and G. Dasgupta, 11/9/87, (PB88-218522, A05, MF-A01).

NCEER-87-0007 "Instantaneous Optimal Control Laws for Tall Buildings Under Seismic Excitations," by J.N. Yang, A. Akbarpour and P. Ghaemmaghami, 6/10/87, (PB88-134333, A06, MF-A01). This report is only available through NTIS (see address given above).

NCEER-87-0008 "IDARC: Inelastic Damage Analysis of Reinforced Concrete Frame - Shear-Wall Structures," by Y.J. Park, A.M. Reinhorn and S.K. Kunnath, 7/20/87, (PB88-134325, A09, MF-A01). This report is only available through NTIS (see address given above).

NCEER-87-0009 "Liquefaction Potential for New York State: A Preliminary Report on Sites in Manhattan and Buffalo," by M. Budhu, V. Vijayakumar, R.F. Giese and L. Baumgras, 8/31/87, (PB88-163704, A03, MF-A01). This report is available only through NTIS (see address given above).

NCEER-87-0010 "Vertical and Torsional Vibration of Foundations in Inhomogeneous Media," by A.S. Veletsos and K.W. Dotson, 6/1/87, (PB88-134291, A03, MF-A01). This report is only available through NTIS (see address given above).

NCEER-87-0011 "Seismic Probabilistic Risk Assessment and Seismic Margins Studies for Nuclear Power Plants," by Howard H.M. Hwang, 6/15/87, (PB88-134267, A03, MF-A01). This report is only available through NTIS (see address given above).

NCEER-87-0012 "Parametric Studies of Frequency Response of Secondary Systems Under Ground-Acceleration Excitations," by Y. Yong and Y.K. Lin, 6/10/87, (PB88-134309, A03, MF-A01). This report is only available through NTIS (see address given above).

NCEER-87-0013 "Frequency Response of Secondary Systems Under Seismic Excitation," by J.A. HoLung, J. Cai and Y.K. Lin, 7/31/87, (PB88-134317, A05, MF-A01). This report is only available through NTIS (see address given above).

NCEER-87-0014 "Modelling Earthquake Ground Motions in Seismically Active Regions Using Parametric Time Series Methods," by G.W. Ellis and A.S. Cakmak, 8/25/87, (PB88-134283, A08, MF-A01). This report is only available through NTIS (see address given above).

NCEER-87-0015 "Detection and Assessment of Seismic Structural Damage," by E. DiPasquale and A.S. Cakmak, 8/25/87, (PB88-163712, A05, MF-A01). This report is only available through NTIS (see address given above).

NCEER-87-0016 "Pipeline Experiment at Parkfield, California," by J. Isenberg and E. Richardson, 9/15/87, (PB88-163720, A03, MF-A01). This report is available only through NTIS (see address given above).

NCEER-87-0017 "Digital Simulation of Seismic Ground Motion," by M. Shinozuka, G. Deodatis and T. Harada, 8/31/87, (PB88-155197, A04, MF-A01). This report is available only through NTIS (see address given above).

NCEER-87-0018 "Practical Considerations for Structural Control: System Uncertainty, System Time Delay and Truncation of Small Control Forces," J.N. Yang and A. Akbarpour, 8/10/87, (PB88-163738, A08, MF-A01). This report is only available through NTIS (see address given above).

NCEER-87-0019 "Modal Analysis of Nonclassically Damped Structural Systems Using Canonical Transformation," by J.N. Yang, S. Sarkani and F.X. Long, 9/27/87, (PB88-187851, A04, MF-A01).

NCEER-87-0020 "A Nonstationary Solution in Random Vibration Theory," by J.R. Red-Horse and P.D. Spanos, 11/3/87, (PB88-163746, A03, MF-A01).

NCEER-87-0021 "Horizontal Impedances for Radially Inhomogeneous Viscoelastic Soil Layers," by A.S. Veletsos and K.W. Dotson, 10/15/87, (PB88-150859, A04, MF-A01).

NCEER-87-0022 "Seismic Damage Assessment of Reinforced Concrete Members," by Y.S. Chung, C. Meyer and M. Shinozuka, 10/9/87, (PB88-150867, A05, MF-A01). This report is available only through NTIS (see address given above).

NCEER-87-0023 "Active Structural Control in Civil Engineering," by T.T. Soong, 11/11/87, (PB88-187778, A03, MF-A01).

NCEER-87-0024 "Vertical and Torsional Impedances for Radially Inhomogeneous Viscoelastic Soil Layers," by K.W. Dotson and A.S. Veletsos, 12/87, (PB88-187786, A03, MF-A01).

NCEER-87-0025 "Proceedings from the Symposium on Seismic Hazards, Ground Motions, Soil-Liquefaction and Engineering Practice in Eastern North America," October 20-22, 1987, edited by K.H. Jacob, 12/87, (PB88-188115, A23, MF-A01). This report is available only through NTIS (see address given above).

NCEER-87-0026 "Report on the Whittier-Narrows, California, Earthquake of October 1, 1987," by J. Pantelic and A. Reinhorn, 11/87, (PB88-187752, A03, MF-A01). This report is available only through NTIS (see address given above).

NCEER-87-0027 "Design of a Modular Program for Transient Nonlinear Analysis of Large 3-D Building Structures," by S. Srivastav and J.F. Abel, 12/30/87, (PB88-187950, A05, MF-A01). This report is only available through NTIS (see address given above).

NCEER-87-0028 "Second-Year Program in Research, Education and Technology Transfer," 3/8/88, (PB88-219480, A04, MF-A01).

NCEER-88-0001 "Workshop on Seismic Computer Analysis and Design of Buildings With Interactive Graphics," by W. McGuire, J.F. Abel and C.H. Conley, 1/18/88, (PB88-187760, A03, MF-A01). This report is only available through NTIS (see address given above).

NCEER-88-0002 "Optimal Control of Nonlinear Flexible Structures," by J.N. Yang, F.X. Long and D. Wong, 1/22/88, (PB88-213772, A06, MF-A01).

NCEER-88-0003 "Substructuring Techniques in the Time Domain for Primary-Secondary Structural Systems," by G.D. Manolis and G. Juhn, 2/10/88, (PB88-213780, A04, MF-A01).

NCEER-88-0004 "Iterative Seismic Analysis of Primary-Secondary Systems," by A. Singhal, L.D. Lutes and P.D. Spanos, 2/23/88, (PB88-213798, A04, MF-A01).

NCEER-88-0005 "Stochastic Finite Element Expansion for Random Media," by P.D. Spanos and R. Ghanem, 3/14/88, (PB88-213806, A03, MF-A01).

NCEER-88-0006 "Combining Structural Optimization and Structural Control," by F.Y. Cheng and C.P. Pantelides, 1/10/88, (PB88-213814, A05, MF-A01).

NCEER-88-0007 "Seismic Performance Assessment of Code-Designed Structures," by H.H-M. Hwang, J-W. Jaw and H-J. Shau, 3/20/88, (PB88-219423, A04, MF-A01). This report is only available through NTIS (see address given above).

NCEER-88-0008 "Reliability Analysis of Code-Designed Structures Under Natural Hazards," by H.H-M. Hwang, H. Ushiba and M. Shinozuka, 2/29/88, (PB88-229471, A07, MF-A01). This report is only available through NTIS (see address given above).

NCEER-88-0009 "Seismic Fragility Analysis of Shear Wall Structures," by J-W Jaw and H.H-M. Hwang, 4/30/88, (PB89-102867, A04, MF-A01).

NCEER-88-0010 "Base Isolation of a Multi-Story Building Under a Harmonic Ground Motion - A Comparison of Performances of Various Systems," by F-G Fan, G. Ahmadi and I.G. Tadjbakhsh, 5/18/88, (PB89-122238, A06, MF-A01). This report is only available through NTIS (see address given above).

NCEER-88-0011 "Seismic Floor Response Spectra for a Combined System by Green's Functions," by F.M. Lavelle, L.A. Bergman and P.D. Spanos, 5/1/88, (PB89-102875, A03, MF-A01).

NCEER-88-0012 "A New Solution Technique for Randomly Excited Hysteretic Structures," by G.Q. Cai and Y.K. Lin, 5/16/88, (PB89-102883, A03, MF-A01).

NCEER-88-0013 "A Study of Radiation Damping and Soil-Structure Interaction Effects in the Centrifuge," by K. Weissman, supervised by J.H. Prevost, 5/24/88, (PB89-144703, A06, MF-A01).

NCEER-88-0014 "Parameter Identification and Implementation of a Kinematic Plasticity Model for Frictional Soils," by J.H. Prevost and D.V. Griffiths, to be published.

NCEER-88-0015 "Two- and Three- Dimensional Dynamic Finite Element Analyses of the Long Valley Dam," by D.V. Griffiths and J.H. Prevost, 6/17/88, (PB89-144711, A04, MF-A01).

NCEER-88-0016 "Damage Assessment of Reinforced Concrete Structures in Eastern United States," by A.M. Reinhorn, M.J. Seidel, S.K. Kunnath and Y.J. Park, 6/15/88, (PB89-122220, A04, MF-A01). This report is only available through NTIS (see address given above).

NCEER-88-0017 "Dynamic Compliance of Vertically Loaded Strip Foundations in Multilayered Viscoelastic Soils," by S. Ahmad and A.S.M. Israil, 6/17/88, (PB89-102891, A04, MF-A01).

NCEER-88-0018 "An Experimental Study of Seismic Structural Response With Added Viscoelastic Dampers," by R.C. Lin, Z. Liang, T.T. Soong and R.H. Zhang, 6/30/88, (PB89-122212, A05, MF-A01). This report is available only through NTIS (see address given above).

NCEER-88-0019 "Experimental Investigation of Primary - Secondary System Interaction," by G.D. Manolis, G. Juhn and A.M. Reinhorn, 5/27/88, (PB89-122204, A04, MF-A01).

NCEER-88-0020 "A Response Spectrum Approach For Analysis of Nonclassically Damped Structures," by J.N. Yang, S. Sarkani and F.X. Long, 4/22/88, (PB89-102909, A04, MF-A01).

NCEER-88-0021 "Seismic Interaction of Structures and Soils: Stochastic Approach," by A.S. Veletsos and A.M. Prasad, 7/21/88, (PB89-122196, A04, MF-A01). This report is only available through NTIS (see address given above).

NCEER-88-0022 "Identification of the Serviceability Limit State and Detection of Seismic Structural Damage," by E. DiPasquale and A.S. Cakmak, 6/15/88, (PB89-122188, A05, MF-A01). This report is available only through NTIS (see address given above).

NCEER-88-0023 "Multi-Hazard Risk Analysis: Case of a Simple Offshore Structure," by B.K. Bhartia and E.H. Vanmarcke, 7/21/88, (PB89-145213, A05, MF-A01).

NCEER-88-0024 "Automated Seismic Design of Reinforced Concrete Buildings," by Y.S. Chung, C. Meyer and M. Shinozuka, 7/5/88, (PB89-122170, A06, MF-A01). This report is available only through NTIS (see address given above).

NCEER-88-0025 "Experimental Study of Active Control of MDOF Structures Under Seismic Excitations," by L.L. Chung, R.C. Lin, T.T. Soong and A.M. Reinhorn, 7/10/88, (PB89-122600, A04, MF-A01).

NCEER-88-0026 "Earthquake Simulation Tests of a Low-Rise Metal Structure," by J.S. Hwang, K.C. Chang, G.C. Lee and R.L. Ketter, 8/1/88, (PB89-102917, A04, MF-A01).

NCEER-88-0027 "Systems Study of Urban Response and Reconstruction Due to Catastrophic Earthquakes," by F. Kozin and H.K. Zhou, 9/22/88, (PB90-162348, A04, MF-A01).

NCEER-88-0028 "Seismic Fragility Analysis of Plane Frame Structures," by H.H-M. Hwang and Y.K. Low, 7/31/88, (PB89-131445, A06, MF-A01).

NCEER-88-0029 "Response Analysis of Stochastic Structures," by A. Kardara, C. Bucher and M. Shinozuka, 9/22/88, (PB89-174429, A04, MF-A01).

NCEER-88-0030 "Nonnormal Accelerations Due to Yielding in a Primary Structure," by D.C.K. Chen and L.D. Lutes, 9/19/88, (PB89-131437, A04, MF-A01).

NCEER-88-0031 "Design Approaches for Soil-Structure Interaction," by A.S. Veletsos, A.M. Prasad and Y. Tang, 12/30/88, (PB89-174437, A03, MF-A01). This report is available only through NTIS (see address given above).

NCEER-88-0032 "A Re-evaluation of Design Spectra for Seismic Damage Control," by C.J. Turkstra and A.G. Tallin, 11/7/88, (PB89-145221, A05, MF-A01).

NCEER-88-0033 "The Behavior and Design of Noncontact Lap Splices Subjected to Repeated Inelastic Tensile Loading," by V.E. Sagan, P. Gergely and R.N. White, 12/8/88, (PB89-163737, A08, MF-A01).

NCEER-88-0034 "Seismic Response of Pile Foundations," by S.M. Mamoon, P.K. Banerjee and S. Ahmad, 11/1/88, (PB89-145239, A04, MF-A01).

NCEER-88-0035 "Modeling of R/C Building Structures With Flexible Floor Diaphragms (IDARC2)," by A.M. Reinhorn, S.K. Kunnath and N. Panahshahi, 9/7/88, (PB89-207153, A07, MF-A01).

NCEER-88-0036 "Solution of the Dam-Reservoir Interaction Problem Using a Combination of FEM, BEM with Particular Integrals, Modal Analysis, and Substructuring," by C-S. Tsai, G.C. Lee and R.L. Ketter, 12/31/88, (PB89-207146, A04, MF-A01).

NCEER-88-0037 "Optimal Placement of Actuators for Structural Control," by F.Y. Cheng and C.P. Pantelides, 8/15/88, (PB89-162846, A05, MF-A01).

NCEER-88-0038 "Teflon Bearings in Aseismic Base Isolation: Experimental Studies and Mathematical Modeling," by A. Mokha, M.C. Constantinou and A.M. Reinhorn, 12/5/88, (PB89-218457, A10, MF-A01). This report is available only through NTIS (see address given above).

NCEER-88-0039 "Seismic Behavior of Flat Slab High-Rise Buildings in the New York City Area," by P. Weidlinger and M. Ettouney, 10/15/88, (PB90-145681, A04, MF-A01).

NCEER-88-0040 "Evaluation of the Earthquake Resistance of Existing Buildings in New York City," by P. Weidlinger and M. Ettouney, 10/15/88, to be published.

NCEER-88-0041 "Small-Scale Modeling Techniques for Reinforced Concrete Structures Subjected to Seismic Loads," by W. Kim, A. El-Attar and R.N. White, 11/22/88, (PB89-189625, A05, MF-A01).

NCEER-88-0042 "Modeling Strong Ground Motion from Multiple Event Earthquakes," by G.W. Ellis and A.S. Cakmak, 10/15/88, (PB89-174445, A03, MF-A01).

NCEER-88-0043 "Nonstationary Models of Seismic Ground Acceleration," by M. Grigoriu, S.E. Ruiz and E. Rosenblueth, 7/15/88, (PB89-189617, A04, MF-A01).

NCEER-88-0044 "SARCF User's Guide: Seismic Analysis of Reinforced Concrete Frames," by Y.S. Chung, C. Meyer and M. Shinozuka, 11/9/88, (PB89-174452, A08, MF-A01).

NCEER-88-0045 "First Expert Panel Meeting on Disaster Research and Planning," edited by J. Pantelic and J. Stoyle, 9/15/88, (PB89-174460, A05, MF-A01).

NCEER-88-0046 "Preliminary Studies of the Effect of Degrading Infill Walls on the Nonlinear Seismic Response of Steel Frames," by C.Z. Chrysostomou, P. Gergely and J.F. Abel, 12/19/88, (PB89-208383, A05, MF-A01).

NCEER-88-0047 "Reinforced Concrete Frame Component Testing Facility - Design, Construction, Instrumentation and Operation," by S.P. Pessiki, C. Conley, T. Bond, P. Gergely and R.N. White, 12/16/88, (PB89-174478, A04, MF-A01).

NCEER-89-0001 "Effects of Protective Cushion and Soil Compliancy on the Response of Equipment Within a Seismically Excited Building," by J.A. HoLung, 2/16/89, (PB89-207179, A04, MF-A01).

NCEER-89-0002 "Statistical Evaluation of Response Modification Factors for Reinforced Concrete Structures," by H.H-M. Hwang and J-W. Jaw, 2/17/89, (PB89-207187, A05, MF-A01).

NCEER-89-0003 "Hysteretic Columns Under Random Excitation," by G-Q. Cai and Y.K. Lin, 1/9/89, (PB89-196513, A03, MF-A01).

NCEER-89-0004 "Experimental Study of `Elephant Foot Bulge' Instability of Thin-Walled Metal Tanks," by Z-H. Jia and R.L. Ketter, 2/22/89, (PB89-207195, A03, MF-A01).

NCEER-89-0005 "Experiment on Performance of Buried Pipelines Across San Andreas Fault," by J. Isenberg, E. Richardson and T.D. O'Rourke, 3/10/89, (PB89-218440, A04, MF-A01). This report is available only through NTIS (see address given above).

NCEER-89-0006 "A Knowledge-Based Approach to Structural Design of Earthquake-Resistant Buildings," by M. Subramani, P. Gergely, C.H. Conley, J.F. Abel and A.H. Zaghw, 1/15/89, (PB89-218465, A06, MF-A01).

NCEER-89-0007 "Liquefaction Hazards and Their Effects on Buried Pipelines," by T.D. O'Rourke and P.A. Lane, 2/1/89, (PB89-218481, A09, MF-A01).

NCEER-89-0008 "Fundamentals of System Identification in Structural Dynamics," by H. Imai, C-B. Yun, O. Maruyama and M. Shinozuka, 1/26/89, (PB89-207211, A04, MF-A01).

NCEER-89-0009 "Effects of the 1985 Michoacan Earthquake on Water Systems and Other Buried Lifelines in Mexico," by A.G. Ayala and M.J. O'Rourke, 3/8/89, (PB89-207229, A06, MF-A01).

NCEER-89-R010 "NCEER Bibliography of Earthquake Education Materials," by K.E.K. Ross, Second Revision, 9/1/89, (PB90-125352, A05, MF-A01). This report is replaced by NCEER-92-0018.

NCEER-89-0011 "Inelastic Three-Dimensional Response Analysis of Reinforced Concrete Building Structures (IDARC-3D), Part I - Modeling," by S.K. Kunnath and A.M. Reinhorn, 4/17/89, (PB90-114612, A07, MF-A01). This report is available only through NTIS (see address given above).

NCEER-89-0012 "Recommended Modifications to ATC-14," by C.D. Poland and J.O. Malley, 4/12/89, (PB90-108648, A15, MF-A01).

NCEER-89-0013 "Repair and Strengthening of Beam-to-Column Connections Subjected to Earthquake Loading," by M. Corazao and A.J. Durrani, 2/28/89, (PB90-109885, A06, MF-A01).

NCEER-89-0014 "Program EXKAL2 for Identification of Structural Dynamic Systems," by O. Maruyama, C-B. Yun, M. Hoshiya and M. Shinozuka, 5/19/89, (PB90-109877, A09, MF-A01).

NCEER-89-0015 "Response of Frames With Bolted Semi-Rigid Connections, Part I - Experimental Study and Analytical Predictions," by P.J. DiCorso, A.M. Reinhorn, J.R. Dickerson, J.B. Radziminski and W.L. Harper, 6/1/89, to be published.

NCEER-89-0016 "ARMA Monte Carlo Simulation in Probabilistic Structural Analysis," by P.D. Spanos and M.P. Mignolet, 7/10/89, (PB90-109893, A03, MF-A01).

NCEER-89-P017 "Preliminary Proceedings from the Conference on Disaster Preparedness - The Place of Earthquake Education in Our Schools," Edited by K.E.K. Ross, 6/23/89, (PB90-108606, A03, MF-A01).

NCEER-89-0017 "Proceedings from the Conference on Disaster Preparedness - The Place of Earthquake Education in Our Schools," Edited by K.E.K. Ross, 12/31/89, (PB90-207895, A012, MF-A02). This report is available only through NTIS (see address given above).

NCEER-89-0018 "Multidimensional Models of Hysteretic Material Behavior for Vibration Analysis of Shape Memory Energy Absorbing Devices, by E.J. Graesser and F.A. Cozzarelli, 6/7/89, (PB90-164146, A04, MF-A01).

NCEER-89-0019 "Nonlinear Dynamic Analysis of Three-Dimensional Base Isolated Structures (3D-BASIS)," by S. Nagarajaiah, A.M. Reinhorn and M.C. Constantinou, 8/3/89, (PB90-161936, A06, MF-A01). This report has been replaced by NCEER-93-0011.

NCEER-89-0020 "Structural Control Considering Time-Rate of Control Forces and Control Rate Constraints," by F.Y. Cheng and C.P. Pantelides, 8/3/89, (PB90-120445, A04, MF-A01).

NCEER-89-0021 "Subsurface Conditions of Memphis and Shelby County," by K.W. Ng, T-S. Chang and H-H.M. Hwang, 7/26/89, (PB90-120437, A03, MF-A01).

NCEER-89-0022 "Seismic Wave Propagation Effects on Straight Jointed Buried Pipelines," by K. Elhmadi and M.J. O'Rourke, 8/24/89, (PB90-162322, A10, MF-A02).

NCEER-89-0023 "Workshop on Serviceability Analysis of Water Delivery Systems," edited by M. Grigoriu, 3/6/89, (PB90-127424, A03, MF-A01).

NCEER-89-0024 "Shaking Table Study of a 1/5 Scale Steel Frame Composed of Tapered Members," by K.C. Chang, J.S. Hwang and G.C. Lee, 9/18/89, (PB90-160169, A04, MF-A01).

NCEER-89-0025 "DYNA1D: A Computer Program for Nonlinear Seismic Site Response Analysis - Technical Documentation," by Jean H. Prevost, 9/14/89, (PB90-161944, A07, MF-A01). This report is available only through NTIS (see address given above).

NCEER-89-0026 "1:4 Scale Model Studies of Active Tendon Systems and Active Mass Dampers for Aseismic Protection," by A.M. Reinhorn, T.T. Soong, R.C. Lin, Y.P. Yang, Y. Fukao, H. Abe and M. Nakai, 9/15/89, (PB90-173246, A10, MF-A02). This report is available only through NTIS (see address given above).

NCEER-89-0027 "Scattering of Waves by Inclusions in a Nonhomogeneous Elastic Half Space Solved by Boundary Element Methods," by P.K. Hadley, A. Askar and A.S. Cakmak, 6/15/89, (PB90-145699, A07, MF-A01).

NCEER-89-0028 "Statistical Evaluation of Deflection Amplification Factors for Reinforced Concrete Structures," by H.H.M. Hwang, J-W. Jaw and A.L. Ch'ng, 8/31/89, (PB90-164633, A05, MF-A01).

NCEER-89-0029 "Bedrock Accelerations in Memphis Area Due to Large New Madrid Earthquakes," by H.H.M. Hwang, C.H.S. Chen and G. Yu, 11/7/89, (PB90-162330, A04, MF-A01).

NCEER-89-0030 "Seismic Behavior and Response Sensitivity of Secondary Structural Systems," by Y.Q. Chen and T.T. Soong, 10/23/89, (PB90-164658, A08, MF-A01).

NCEER-89-0031 "Random Vibration and Reliability Analysis of Primary-Secondary Structural Systems," by Y. Ibrahim, M. Grigoriu and T.T. Soong, 11/10/89, (PB90-161951, A04, MF-A01).

NCEER-89-0032 "Proceedings from the Second U.S. - Japan Workshop on Liquefaction, Large Ground Deformation and Their Effects on Lifelines, September 26-29, 1989," Edited by T.D. O'Rourke and M. Hamada, 12/1/89, (PB90-209388, A22, MF-A03).

NCEER-89-0033 "Deterministic Model for Seismic Damage Evaluation of Reinforced Concrete Structures," by J.M. Bracci, A.M. Reinhorn, J.B. Mander and S.K. Kunnath, 9/27/89, (PB91-108803, A06, MF-A01).

NCEER-89-0034 "On the Relation Between Local and Global Damage Indices," by E. DiPasquale and A.S. Cakmak, 8/15/89, (PB90-173865, A05, MF-A01).

NCEER-89-0035 "Cyclic Undrained Behavior of Nonplastic and Low Plasticity Silts," by A.J. Walker and H.E. Stewart, 7/26/89, (PB90-183518, A10, MF-A01).

NCEER-89-0036 "Liquefaction Potential of Surficial Deposits in the City of Buffalo, New York," by M. Budhu, R. Giese and L. Baumgrass, 1/17/89, (PB90-208455, A04, MF-A01).

NCEER-89-0037 "A Deterministic Assessment of Effects of Ground Motion Incoherence," by A.S. Veletsos and Y. Tang, 7/15/89, (PB90-164294, A03, MF-A01).

NCEER-89-0038 "Workshop on Ground Motion Parameters for Seismic Hazard Mapping," July 17-18, 1989, edited by R.V. Whitman, 12/1/89, (PB90-173923, A04, MF-A01).

NCEER-89-0039 "Seismic Effects on Elevated Transit Lines of the New York City Transit Authority," by C.J. Costantino, C.A. Miller and E. Heymsfield, 12/26/89, (PB90-207887, A06, MF-A01).

NCEER-89-0040 "Centrifugal Modeling of Dynamic Soil-Structure Interaction," by K. Weissman, Supervised by J.H. Prevost, 5/10/89, (PB90-207879, A07, MF-A01).

NCEER-89-0041 "Linearized Identification of Buildings With Cores for Seismic Vulnerability Assessment," by I-K. Ho and A.E. Aktan, 11/1/89, (PB90-251943, A07, MF-A01).

NCEER-90-0001 "Geotechnical and Lifeline Aspects of the October 17, 1989 Loma Prieta Earthquake in San Francisco," by T.D. O'Rourke, H.E. Stewart, F.T. Blackburn and T.S. Dickerman, 1/90, (PB90-208596, A05, MF-A01).

NCEER-90-0002 "Nonnormal Secondary Response Due to Yielding in a Primary Structure," by D.C.K. Chen and L.D. Lutes, 2/28/90, (PB90-251976, A07, MF-A01).

NCEER-90-0003 "Earthquake Education Materials for Grades K-12," by K.E.K. Ross, 4/16/90, (PB91-251984, A05, MF-A05). This report has been replaced by NCEER-92-0018.

NCEER-90-0004 "Catalog of Strong Motion Stations in Eastern North America," by R.W. Busby, 4/3/90, (PB90-251984, A05, MF-A01).

NCEER-90-0005 "NCEER Strong-Motion Data Base: A User Manual for the GeoBase Release (Version 1.0 for the Sun3)," by P. Friberg and K. Jacob, 3/31/90 (PB90-258062, A04, MF-A01).

NCEER-90-0006 "Seismic Hazard Along a Crude Oil Pipeline in the Event of an 1811-1812 Type New Madrid Earthquake," by H.H.M. Hwang and C-H.S. Chen, 4/16/90, (PB90-258054, A04, MF-A01).

NCEER-90-0007 "Site-Specific Response Spectra for Memphis Sheahan Pumping Station," by H.H.M. Hwang and C.S. Lee, 5/15/90, (PB91-108811, A05, MF-A01).

NCEER-90-0008 "Pilot Study on Seismic Vulnerability of Crude Oil Transmission Systems," by T. Ariman, R. Dobry, M. Grigoriu, F. Kozin, M. O'Rourke, T. O'Rourke and M. Shinozuka, 5/25/90, (PB91-108837, A06, MF-A01).

NCEER-90-0009 "A Program to Generate Site Dependent Time Histories: EQGEN," by G.W. Ellis, M. Srinivasan and A.S. Cakmak, 1/30/90, (PB91-108829, A04, MF-A01).

NCEER-90-0010 "Active Isolation for Seismic Protection of Operating Rooms," by M.E. Talbott, Supervised by M. Shinozuka, 6/8/9, (PB91-110205, A05, MF-A01).

NCEER-90-0011 "Program LINEARID for Identification of Linear Structural Dynamic Systems," by C-B. Yun and M. Shinozuka, 6/25/90, (PB91-110312, A08, MF-A01).

NCEER-90-0012 "Two-Dimensional Two-Phase Elasto-Plastic Seismic Response of Earth Dams," by A.N. Yiagos, Supervised by J.H. Prevost, 6/20/90, (PB91-110197, A13, MF-A02).

NCEER-90-0013 "Secondary Systems in Base-Isolated Structures: Experimental Investigation, Stochastic Response and Stochastic Sensitivity," by G.D. Manolis, G. Juhn, M.C. Constantinou and A.M. Reinhorn, 7/1/90, (PB91-110320, A08, MF-A01).

NCEER-90-0014 "Seismic Behavior of Lightly-Reinforced Concrete Column and Beam-Column Joint Details," by S.P. Pessiki, C.H. Conley, P. Gergely and R.N. White, 8/22/90, (PB91-108795, A11, MF-A02).

NCEER-90-0015 "Two Hybrid Control Systems for Building Structures Under Strong Earthquakes," by J.N. Yang and A. Danielians, 6/29/90, (PB91-125393, A04, MF-A01).

NCEER-90-0016 "Instantaneous Optimal Control with Acceleration and Velocity Feedback," by J.N. Yang and Z. Li, 6/29/90, (PB91-125401, A03, MF-A01).

NCEER-90-0017 "Reconnaissance Report on the Northern Iran Earthquake of June 21, 1990," by M. Mehrain, 10/4/90, (PB91-125377, A03, MF-A01).

NCEER-90-0018 "Evaluation of Liquefaction Potential in Memphis and Shelby County," by T.S. Chang, P.S. Tang, C.S. Lee and H. Hwang, 8/10/90, (PB91-125427, A09, MF-A01).

NCEER-90-0019 "Experimental and Analytical Study of a Combined Sliding Disc Bearing and Helical Steel Spring Isolation System," by M.C. Constantinou, A.S. Mokha and A.M. Reinhorn, 10/4/90, (PB91-125385, A06, MF-A01). This report is available only through NTIS (see address given above).

NCEER-90-0020 "Experimental Study and Analytical Prediction of Earthquake Response of a Sliding Isolation System with a Spherical Surface," by A.S. Mokha, M.C. Constantinou and A.M. Reinhorn, 10/11/90, (PB91-125419, A05, MF-A01).

NCEER-90-0021 "Dynamic Interaction Factors for Floating Pile Groups," by G. Gazetas, K. Fan, A. Kaynia and E. Kausel, 9/10/90, (PB91-170381, A05, MF-A01).

NCEER-90-0022 "Evaluation of Seismic Damage Indices for Reinforced Concrete Structures," by S. Rodriguez-Gomez and A.S. Cakmak, 9/30/90, PB91-171322, A06, MF-A01).

NCEER-90-0023 "Study of Site Response at a Selected Memphis Site," by H. Desai, S. Ahmad, E.S. Gazetas and M.R. Oh, 10/11/90, (PB91-196857, A03, MF-A01).

NCEER-90-0024 "A User's Guide to Strongmo: Version 1.0 of NCEER's Strong-Motion Data Access Tool for PCs and Terminals," by P.A. Friberg and C.A.T. Susch, 11/15/90, (PB91-171272, A03, MF-A01).

NCEER-90-0025 "A Three-Dimensional Analytical Study of Spatial Variability of Seismic Ground Motions," by L-L. Hong and A.H.-S. Ang, 10/30/90, (PB91-170399, A09, MF-A01).

NCEER-90-0026 "MUMOID User's Guide - A Program for the Identification of Modal Parameters," by S. Rodriguez-Gomez and E. DiPasquale, 9/30/90, (PB91-171298, A04, MF-A01).

NCEER-90-0027 "SARCF-II User's Guide - Seismic Analysis of Reinforced Concrete Frames," by S. Rodriguez-Gomez, Y.S. Chung and C. Meyer, 9/30/90, (PB91-171280, A05, MF-A01).

NCEER-90-0028 "Viscous Dampers: Testing, Modeling and Application in Vibration and Seismic Isolation," by N. Makris and M.C. Constantinou, 12/20/90 (PB91-190561, A06, MF-A01).

NCEER-90-0029 "Soil Effects on Earthquake Ground Motions in the Memphis Area," by H. Hwang, C.S. Lee, K.W. Ng and T.S. Chang, 8/2/90, (PB91-190751, A05, MF-A01).

NCEER-91-0001 "Proceedings from the Third Japan-U.S. Workshop on Earthquake Resistant Design of Lifeline Facilities and Countermeasures for Soil Liquefaction, December 17-19, 1990," edited by T.D. O'Rourke and M. Hamada, 2/1/91, (PB91-179259, A99, MF-A04).

NCEER-91-0002 "Physical Space Solutions of Non-Proportionally Damped Systems," by M. Tong, Z. Liang and G.C. Lee, 1/15/91, (PB91-179242, A04, MF-A01).

NCEER-91-0003 "Seismic Response of Single Piles and Pile Groups," by K. Fan and G. Gazetas, 1/10/91, (PB92-174994, A04, MF-A01).

NCEER-91-0004 "Damping of Structures: Part 1 - Theory of Complex Damping," by Z. Liang and G. Lee, 10/10/91, (PB92-197235, A12, MF-A03).

NCEER-91-0005 "3D-BASIS - Nonlinear Dynamic Analysis of Three Dimensional Base Isolated Structures: Part II," by S. Nagarajaiah, A.M. Reinhorn and M.C. Constantinou, 2/28/91, (PB91-190553, A07, MF-A01). This report has been replaced by NCEER-93-0011.

NCEER-91-0006 "A Multidimensional Hysteretic Model for Plasticity Deforming Metals in Energy Absorbing Devices," by E.J. Graesser and F.A. Cozzarelli, 4/9/91, (PB92-108364, A04, MF-A01).

NCEER-91-0007 "A Framework for Customizable Knowledge-Based Expert Systems with an Application to a KBES for Evaluating the Seismic Resistance of Existing Buildings," by E.G. Ibarra-Anaya and S.J. Fenves, 4/9/91, (PB91-210930, A08, MF-A01).

NCEER-91-0008 "Nonlinear Analysis of Steel Frames with Semi-Rigid Connections Using the Capacity Spectrum Method," by G.G. Deierlein, S-H. Hsieh, Y-J. Shen and J.F. Abel, 7/2/91, (PB92-113828, A05, MF-A01).

NCEER-91-0009 "Earthquake Education Materials for Grades K-12," by K.E.K. Ross, 4/30/91, (PB91-212142, A06, MF-A01). This report has been replaced by NCEER-92-0018.

NCEER-91-0010 "Phase Wave Velocities and Displacement Phase Differences in a Harmonically Oscillating Pile," by N. Makris and G. Gazetas, 7/8/91, (PB92-108356, A04, MF-A01).

NCEER-91-0011 "Dynamic Characteristics of a Full-Size Five-Story Steel Structure and a 2/5 Scale Model," by K.C. Chang, G.C. Yao, G.C. Lee, D.S. Hao and Y.C. Yeh," 7/2/91, (PB93-116648, A06, MF-A02).

NCEER-91-0012 "Seismic Response of a 2/5 Scale Steel Structure with Added Viscoelastic Dampers," by K.C. Chang, T.T. Soong, S-T. Oh and M.L. Lai, 5/17/91, (PB92-110816, A05, MF-A01).

NCEER-91-0013 "Earthquake Response of Retaining Walls; Full-Scale Testing and Computational Modeling," by S. Alampalli and A-W.M. Elgamal, 6/20/91, to be published.

NCEER-91-0014 "3D-BASIS-M: Nonlinear Dynamic Analysis of Multiple Building Base Isolated Structures," by P.C. Tsopelas, S. Nagarajaiah, M.C. Constantinou and A.M. Reinhorn, 5/28/91, (PB92-113885, A09, MF-A02).

NCEER-91-0015 "Evaluation of SEAOC Design Requirements for Sliding Isolated Structures," by D. Theodossiou and M.C. Constantinou, 6/10/91, (PB92-114602, A11, MF-A03).

NCEER-91-0016 "Closed-Loop Modal Testing of a 27-Story Reinforced Concrete Flat Plate-Core Building," by H.R. Somaprasad, T. Toksoy, H. Yoshiyuki and A.E. Aktan, 7/15/91, (PB92-129980, A07, MF-A02).

NCEER-91-0017 "Shake Table Test of a 1/6 Scale Two-Story Lightly Reinforced Concrete Building," by A.G. El-Attar, R.N. White and P. Gergely, 2/28/91, (PB92-222447, A06, MF-A02).

NCEER-91-0018 "Shake Table Test of a 1/8 Scale Three-Story Lightly Reinforced Concrete Building," by A.G. El-Attar, R.N. White and P. Gergely, 2/28/91, (PB93-116630, A08, MF-A02).

NCEER-91-0019 "Transfer Functions for Rigid Rectangular Foundations," by A.S. Veletsos, A.M. Prasad and W.H. Wu, 7/31/91, to be published.

NCEER-91-0020 "Hybrid Control of Seismic-Excited Nonlinear and Inelastic Structural Systems," by J.N. Yang, Z. Li and A. Danielians, 8/1/91, (PB92-143171, A06, MF-A02).

NCEER-91-0021 "The NCEER-91 Earthquake Catalog: Improved Intensity-Based Magnitudes and Recurrence Relations for U.S. Earthquakes East of New Madrid," by L. Seeber and J.G. Armbruster, 8/28/91, (PB92-176742, A06, MF-A02).

NCEER-91-0022 "Proceedings from the Implementation of Earthquake Planning and Education in Schools: The Need for Change - The Roles of the Changemakers," by K.E.K. Ross and F. Winslow, 7/23/91, (PB92-129998, A12, MF-A03).

NCEER-91-0023 "A Study of Reliability-Based Criteria for Seismic Design of Reinforced Concrete Frame Buildings," by H.H.M. Hwang and H-M. Hsu, 8/10/91, (PB92-140235, A09, MF-A02).

NCEER-91-0024 "Experimental Verification of a Number of Structural System Identification Algorithms," by R.G. Ghanem, H. Gavin and M. Shinozuka, 9/18/91, (PB92-176577, A18, MF-A04).

NCEER-91-0025 "Probabilistic Evaluation of Liquefaction Potential," by H.H.M. Hwang and C.S. Lee," 11/25/91, (PB92-143429, A05, MF-A01).

NCEER-91-0026 "Instantaneous Optimal Control for Linear, Nonlinear and Hysteretic Structures - Stable Controllers," by J.N. Yang and Z. Li, 11/15/91, (PB92-163807, A04, MF-A01).

NCEER-91-0027 "Experimental and Theoretical Study of a Sliding Isolation System for Bridges," by M.C. Constantinou, A. Kartoum, A.M. Reinhorn and P. Bradford, 11/15/91, (PB92-176973, A10, MF-A03).

NCEER-92-0001 "Case Studies of Liquefaction and Lifeline Performance During Past Earthquakes, Volume 1: Japanese Case Studies," Edited by M. Hamada and T. O'Rourke, 2/17/92, (PB92-197243, A18, MF-A04).

NCEER-92-0002 "Case Studies of Liquefaction and Lifeline Performance During Past Earthquakes, Volume 2: United States Case Studies," Edited by T. O'Rourke and M. Hamada, 2/17/92, (PB92-197250, A20, MF-A04).

NCEER-92-0003 "Issues in Earthquake Education," Edited by K. Ross, 2/3/92, (PB92-222389, A07, MF-A02).

NCEER-92-0004 "Proceedings from the First U.S. - Japan Workshop on Earthquake Protective Systems for Bridges," Edited by I.G. Buckle, 2/4/92, (PB94-142239, A99, MF-A06).

NCEER-92-0005 "Seismic Ground Motion from a Haskell-Type Source in a Multiple-Layered Half-Space," A.P. Theoharis, G. Deodatis and M. Shinozuka, 1/2/92, to be published.

NCEER-92-0006 "Proceedings from the Site Effects Workshop," Edited by R. Whitman, 2/29/92, (PB92-197201, A04, MF-A01).

NCEER-92-0007 "Engineering Evaluation of Permanent Ground Deformations Due to Seismically-Induced Liquefaction," by M.H. Baziar, R. Dobry and A-W.M. Elgamal, 3/24/92, (PB92-222421, A13, MF-A03).

NCEER-92-0008 "A Procedure for the Seismic Evaluation of Buildings in the Central and Eastern United States," by C.D. Poland and J.O. Malley, 4/2/92, (PB92-222439, A20, MF-A04).

NCEER-92-0009 "Experimental and Analytical Study of a Hybrid Isolation System Using Friction Controllable Sliding Bearings," by M.Q. Feng, S. Fujii and M. Shinozuka, 5/15/92, (PB93-150282, A06, MF-A02).

NCEER-92-0010 "Seismic Resistance of Slab-Column Connections in Existing Non-Ductile Flat-Plate Buildings," by A.J. Durrani and Y. Du, 5/18/92, (PB93-116812, A06, MF-A02).

NCEER-92-0011 "The Hysteretic and Dynamic Behavior of Brick Masonry Walls Upgraded by Ferrocement Coatings Under Cyclic Loading and Strong Simulated Ground Motion," by H. Lee and S.P. Prawel, 5/11/92, to be published.

NCEER-92-0012 "Study of Wire Rope Systems for Seismic Protection of Equipment in Buildings," by G.F. Demetriades, M.C. Constantinou and A.M. Reinhorn, 5/20/92, (PB93-116655, A08, MF-A02).

NCEER-92-0013 "Shape Memory Structural Dampers: Material Properties, Design and Seismic Testing," by P.R. Witting and F.A. Cozzarelli, 5/26/92, (PB93-116663, A05, MF-A01).

NCEER-92-0014 "Longitudinal Permanent Ground Deformation Effects on Buried Continuous Pipelines," by M.J. O'Rourke, and C. Nordberg, 6/15/92, (PB93-116671, A08, MF-A02).

NCEER-92-0015 "A Simulation Method for Stationary Gaussian Random Functions Based on the Sampling Theorem," by M. Grigoriu and S. Balopoulou, 6/11/92, (PB93-127496, A05, MF-A01).

NCEER-92-0016 "Gravity-Load-Designed Reinforced Concrete Buildings: Seismic Evaluation of Existing Construction and Detailing Strategies for Improved Seismic Resistance," by G.W. Hoffmann, S.K. Kunnath, A.M. Reinhorn and J.B. Mander, 7/15/92, (PB94-142007, A08, MF-A02).

NCEER-92-0017 "Observations on Water System and Pipeline Performance in the Limón Area of Costa Rica Due to the April 22, 1991 Earthquake," by M. O'Rourke and D. Ballantyne, 6/30/92, (PB93-126811, A06, MF-A02).

NCEER-92-0018 "Fourth Edition of Earthquake Education Materials for Grades K-12," Edited by K.E.K. Ross, 8/10/92, (PB93-114023, A07, MF-A02).

NCEER-92-0019 "Proceedings from the Fourth Japan-U.S. Workshop on Earthquake Resistant Design of Lifeline Facilities and Countermeasures for Soil Liquefaction," Edited by M. Hamada and T.D. O'Rourke, 8/12/92, (PB93-163939, A99, MF-E11).

NCEER-92-0020 "Active Bracing System: A Full Scale Implementation of Active Control," by A.M. Reinhorn, T.T. Soong, R.C. Lin, M.A. Riley, Y.P. Wang, S. Aizawa and M. Higashino, 8/14/92, (PB93-127512, A06, MF-A02).

NCEER-92-0021 "Empirical Analysis of Horizontal Ground Displacement Generated by Liquefaction-Induced Lateral Spreads," by S.F. Bartlett and T.L. Youd, 8/17/92, (PB93-188241, A06, MF-A02).

NCEER-92-0022 "IDARC Version 3.0: Inelastic Damage Analysis of Reinforced Concrete Structures," by S.K. Kunnath, A.M. Reinhorn and R.F. Lobo, 8/31/92, (PB93-227502, A07, MF-A02).

NCEER-92-0023 "A Semi-Empirical Analysis of Strong-Motion Peaks in Terms of Seismic Source, Propagation Path and Local Site Conditions, by M. Kamiyama, M.J. O'Rourke and R. Flores-Berrones, 9/9/92, (PB93-150266, A08, MF-A02).

NCEER-92-0024 "Seismic Behavior of Reinforced Concrete Frame Structures with Nonductile Details, Part I: Summary of Experimental Findings of Full Scale Beam-Column Joint Tests," by A. Beres, R.N. White and P. Gergely, 9/30/92, (PB93-227783, A05, MF-A01).

NCEER-92-0025 "Experimental Results of Repaired and Retrofitted Beam-Column Joint Tests in Lightly Reinforced Concrete Frame Buildings," by A. Beres, S. El-Borgi, R.N. White and P. Gergely, 10/29/92, (PB93-227791, A05, MF-A01).

NCEER-92-0026 "A Generalization of Optimal Control Theory: Linear and Nonlinear Structures," by J.N. Yang, Z. Li and S. Vongchavalitkul, 11/2/92, (PB93-188621, A05, MF-A01).

NCEER-92-0027 "Seismic Resistance of Reinforced Concrete Frame Structures Designed Only for Gravity Loads: Part I - Design and Properties of a One-Third Scale Model Structure," by J.M. Bracci, A.M. Reinhorn and J.B. Mander, 12/1/92, (PB94-104502, A08, MF-A02).

NCEER-92-0028 "Seismic Resistance of Reinforced Concrete Frame Structures Designed Only for Gravity Loads: Part II - Experimental Performance of Subassemblages," by L.E. Aycardi, J.B. Mander and A.M. Reinhorn, 12/1/92, (PB94-104510, A08, MF-A02).

NCEER-92-0029 "Seismic Resistance of Reinforced Concrete Frame Structures Designed Only for Gravity Loads: Part III - Experimental Performance and Analytical Study of a Structural Model," by J.M. Bracci, A.M. Reinhorn and J.B. Mander, 12/1/92, (PB93-227528, A09, MF-A01).

NCEER-92-0030 "Evaluation of Seismic Retrofit of Reinforced Concrete Frame Structures: Part I - Experimental Performance of Retrofitted Subassemblages," by D. Choudhuri, J.B. Mander and A.M. Reinhorn, 12/8/92, (PB93-198307, A07, MF-A02).

NCEER-92-0031 "Evaluation of Seismic Retrofit of Reinforced Concrete Frame Structures: Part II - Experimental Performance and Analytical Study of a Retrofitted Structural Model," by J.M. Bracci, A.M. Reinhorn and J.B. Mander, 12/8/92, (PB93-198315, A09, MF-A03).

NCEER-92-0032 "Experimental and Analytical Investigation of Seismic Response of Structures with Supplemental Fluid Viscous Dampers," by M.C. Constantinou and M.D. Symans, 12/21/92, (PB93-191435, A10, MF-A03). This report is available only through NTIS (see address given above).

NCEER-92-0033 "Reconnaissance Report on the Cairo, Egypt Earthquake of October 12, 1992," by M. Khater, 12/23/92, (PB93-188621, A03, MF-A01).

NCEER-92-0034 "Low-Level Dynamic Characteristics of Four Tall Flat-Plate Buildings in New York City," by H. Gavin, S. Yuan, J. Grossman, E. Pekelis and K. Jacob, 12/28/92, (PB93-188217, A07, MF-A02).

NCEER-93-0001 "An Experimental Study on the Seismic Performance of Brick-Infilled Steel Frames With and Without Retrofit," by J.B. Mander, B. Nair, K. Wojtkowski and J. Ma, 1/29/93, (PB93-227510, A07, MF-A02).

NCEER-93-0002 "Social Accounting for Disaster Preparedness and Recovery Planning," by S. Cole, E. Pantoja and V. Razak, 2/22/93, (PB94-142114, A12, MF-A03).

NCEER-93-0003 "Assessment of 1991 NEHRP Provisions for Nonstructural Components and Recommended Revisions," by T.T. Soong, G. Chen, Z. Wu, R-H. Zhang and M. Grigoriu, 3/1/93, (PB93-188639, A06, MF-A02).

NCEER-93-0004 "Evaluation of Static and Response Spectrum Analysis Procedures of SEAOC/UBC for Seismic Isolated Structures," by C.W. Winters and M.C. Constantinou, 3/23/93, (PB93-198299, A10, MF-A03).

NCEER-93-0005 "Earthquakes in the Northeast - Are We Ignoring the Hazard? A Workshop on Earthquake Science and Safety for Educators," edited by K.E.K. Ross, 4/2/93, (PB94-103066, A09, MF-A02).

NCEER-93-0006 "Inelastic Response of Reinforced Concrete Structures with Viscoelastic Braces," by R.F. Lobo, J.M. Bracci, K.L. Shen, A.M. Reinhorn and T.T. Soong, 4/5/93, (PB93-227486, A05, MF-A02).

NCEER-93-0007 "Seismic Testing of Installation Methods for Computers and Data Processing Equipment," by K. Kosar, T.T. Soong, K.L. Shen, J.A. HoLung and Y.K. Lin, 4/12/93, (PB93-198299, A07, MF-A02).

NCEER-93-0008 "Retrofit of Reinforced Concrete Frames Using Added Dampers," by A. Reinhorn, M. Constantinou and C. Li, to be published.

NCEER-93-0009 "Seismic Behavior and Design Guidelines for Steel Frame Structures with Added Viscoelastic Dampers," by K.C. Chang, M.L. Lai, T.T. Soong, D.S. Hao and Y.C. Yeh, 5/1/93, (PB94-141959, A07, MF-A02).

NCEER-93-0010 "Seismic Performance of Shear-Critical Reinforced Concrete Bridge Piers," by J.B. Mander, S.M. Waheed, M.T.A. Chaudhary and S.S. Chen, 5/12/93, (PB93-227494, A08, MF-A02).

NCEER-93-0011 "3D-BASIS-TABS: Computer Program for Nonlinear Dynamic Analysis of Three Dimensional Base Isolated Structures," by S. Nagarajaiah, C. Li, A.M. Reinhorn and M.C. Constantinou, 8/2/93, (PB94-141819, A09, MF-A02).

NCEER-93-0012 "Effects of Hydrocarbon Spills from an Oil Pipeline Break on Ground Water," by O.J. Helweg and H.H.M. Hwang, 8/3/93, (PB94-141942, A06, MF-A02).

NCEER-93-0013 "Simplified Procedures for Seismic Design of Nonstructural Components and Assessment of Current Code Provisions," by M.P. Singh, L.E. Suarez, E.E. Matheu and G.O. Maldonado, 8/4/93, (PB94-141827, A09, MF-A02).

NCEER-93-0014 "An Energy Approach to Seismic Analysis and Design of Secondary Systems," by G. Chen and T.T. Soong, 8/6/93, (PB94-142767, A11, MF-A03).

NCEER-93-0015 "Proceedings from School Sites: Becoming Prepared for Earthquakes - Commemorating the Third Anniversary of the Loma Prieta Earthquake," Edited by F.E. Winslow and K.E.K. Ross, 8/16/93, (PB94-154275, A16, MF-A02).

NCEER-93-0016 "Reconnaissance Report of Damage to Historic Monuments in Cairo, Egypt Following the October 12, 1992 Dahshur Earthquake," by D. Sykora, D. Look, G. Croci, E. Karaesmen and E. Karaesmen, 8/19/93, (PB94-142221, A08, MF-A02).

NCEER-93-0017 "The Island of Guam Earthquake of August 8, 1993," by S.W. Swan and S.K. Harris, 9/30/93, (PB94-141843, A04, MF-A01).

NCEER-93-0018 "Engineering Aspects of the October 12, 1992 Egyptian Earthquake," by A.W. Elgamal, M. Amer, K. Adalier and A. Abul-Fadl, 10/7/93, (PB94-141983, A05, MF-A01).

NCEER-93-0019 "Development of an Earthquake Motion Simulator and its Application in Dynamic Centrifuge Testing," by I. Krstelj, Supervised by J.H. Prevost, 10/23/93, (PB94-181773, A-10, MF-A03).

NCEER-93-0020 "NCEER-Taisei Corporation Research Program on Sliding Seismic Isolation Systems for Bridges: Experimental and Analytical Study of a Friction Pendulum System (FPS)," by M.C. Constantinou, P. Tsopelas, Y-S. Kim and S. Okamoto, 11/1/93, (PB94-142775, A08, MF-A02).

NCEER-93-0021 "Finite Element Modeling of Elastomeric Seismic Isolation Bearings," by L.J. Billings, Supervised by R. Shepherd, 11/8/93, to be published.

NCEER-93-0022 "Seismic Vulnerability of Equipment in Critical Facilities: Life-Safety and Operational Consequences," by K. Porter, G.S. Johnson, M.M. Zadeh, C. Scawthorn and S. Eder, 11/24/93, (PB94-181765, A16, MF-A03).

NCEER-93-0023 "Hokkaido Nansei-oki, Japan Earthquake of July 12, 1993, by P.I. Yanev and C.R. Scawthorn, 12/23/93, (PB94-181500, A07, MF-A01).

NCEER-94-0001 "An Evaluation of Seismic Serviceability of Water Supply Networks with Application to the San Francisco Auxiliary Water Supply System," by I. Markov, Supervised by M. Grigoriu and T. O'Rourke, 1/21/94, (PB94-204013, A07, MF-A02).

NCEER-94-0002 "NCEER-Taisei Corporation Research Program on Sliding Seismic Isolation Systems for Bridges: Experimental and Analytical Study of Systems Consisting of Sliding Bearings, Rubber Restoring Force Devices and Fluid Dampers," Volumes I and II, by P. Tsopelas, S. Okamoto, M.C. Constantinou, D. Ozaki and S. Fujii, 2/4/94, (PB94-181740, A09, MF-A02 and PB94-181757, A12, MF-A03).

NCEER-94-0003 "A Markov Model for Local and Global Damage Indices in Seismic Analysis," by S. Rahman and M. Grigoriu, 2/18/94, (PB94-206000, A12, MF-A03).

NCEER-94-0004 "Proceedings from the NCEER Workshop on Seismic Response of Masonry Infills," edited by D.P. Abrams, 3/1/94, (PB94-180783, A07, MF-A02).

NCEER-94-0005 "The Northridge, California Earthquake of January 17, 1994: General Reconnaissance Report," edited by J.D. Goltz, 3/11/94, (PB94-193943, A10, MF-A03).

NCEER-94-0006 "Seismic Energy Based Fatigue Damage Analysis of Bridge Columns: Part I - Evaluation of Seismic Capacity," by G.A. Chang and J.B. Mander, 3/14/94, (PB94-219185, A11, MF-A03).

NCEER-94-0007 "Seismic Isolation of Multi-Story Frame Structures Using Spherical Sliding Isolation Systems," by T.M. Al-Hussaini, V.A. Zayas and M.C. Constantinou, 3/17/94, (PB94-193745, A09, MF-A02).

NCEER-94-0008 "The Northridge, California Earthquake of January 17, 1994: Performance of Highway Bridges," edited by I.G. Buckle, 3/24/94, (PB94-193851, A06, MF-A02).

NCEER-94-0009 "Proceedings of the Third U.S.-Japan Workshop on Earthquake Protective Systems for Bridges," edited by I.G. Buckle and I. Friedland, 3/31/94, (PB94-195815, A99, MF-A06).

NCEER-94-0010 "3D-BASIS-ME: Computer Program for Nonlinear Dynamic Analysis of Seismically Isolated Single and Multiple Structures and Liquid Storage Tanks," by P.C. Tsopelas, M.C. Constantinou and A.M. Reinhorn, 4/12/94, (PB94-204922, A09, MF-A02).

NCEER-94-0011 "The Northridge, California Earthquake of January 17, 1994: Performance of Gas Transmission Pipelines," by T.D. O'Rourke and M.C. Palmer, 5/16/94, (PB94-204989, A05, MF-A01).

NCEER-94-0012 "Feasibility Study of Replacement Procedures and Earthquake Performance Related to Gas Transmission Pipelines," by T.D. O'Rourke and M.C. Palmer, 5/25/94, (PB94-206638, A09, MF-A02).

NCEER-94-0013 "Seismic Energy Based Fatigue Damage Analysis of Bridge Columns: Part II - Evaluation of Seismic Demand," by G.A. Chang and J.B. Mander, 6/1/94, (PB95-18106, A08, MF-A02).

NCEER-94-0014 "NCEER-Taisei Corporation Research Program on Sliding Seismic Isolation Systems for Bridges: Experimental and Analytical Study of a System Consisting of Sliding Bearings and Fluid Restoring Force/Damping Devices," by P. Tsopelas and M.C. Constantinou, 6/13/94, (PB94-219144, A10, MF-A03).

NCEER-94-0015 "Generation of Hazard-Consistent Fragility Curves for Seismic Loss Estimation Studies," by H. Hwang and J-R. Huo, 6/14/94, (PB95-181996, A09, MF-A02).

NCEER-94-0016 "Seismic Study of Building Frames with Added Energy-Absorbing Devices," by W.S. Pong, C.S. Tsai and G.C. Lee, 6/20/94, (PB94-219136, A10, A03).

NCEER-94-0017 "Sliding Mode Control for Seismic-Excited Linear and Nonlinear Civil Engineering Structures," by J. Yang, J. Wu, A. Agrawal and Z. Li, 6/21/94, (PB95-138483, A06, MF-A02).

NCEER-94-0018 "3D-BASIS-TABS Version 2.0: Computer Program for Nonlinear Dynamic Analysis of Three Dimensional Base Isolated Structures," by A.M. Reinhorn, S. Nagarajaiah, M.C. Constantinou, P. Tsopelas and R. Li, 6/22/94, (PB95-182176, A08, MF-A02).

NCEER-94-0019 "Proceedings of the International Workshop on Civil Infrastructure Systems: Application of Intelligent Systems and Advanced Materials on Bridge Systems," Edited by G.C. Lee and K.C. Chang, 7/18/94, (PB95-252474, A20, MF-A04).

NCEER-94-0020 "Study of Seismic Isolation Systems for Computer Floors," by V. Lambrou and M.C. Constantinou, 7/19/94, (PB95-138533, A10, MF-A03).

NCEER-94-0021 "Proceedings of the U.S.-Italian Workshop on Guidelines for Seismic Evaluation and Rehabilitation of Unreinforced Masonry Buildings," Edited by D.P. Abrams and G.M. Calvi, 7/20/94, (PB95-138749, A13, MF-A03).

NCEER-94-0022 "NCEER-Taisei Corporation Research Program on Sliding Seismic Isolation Systems for Bridges: Experimental and Analytical Study of a System Consisting of Lubricated PTFE Sliding Bearings and Mild Steel Dampers," by P. Tsopelas and M.C. Constantinou, 7/22/94, (PB95-182184, A08, MF-A02).

NCEER-94-0023 “Development of Reliability-Based Design Criteria for Buildings Under Seismic Load,” by Y.K. Wen, H. Hwang and M. Shinozuka, 8/1/94, (PB95-211934, A08, MF-A02).

NCEER-94-0024 “Experimental Verification of Acceleration Feedback Control Strategies for an Active Tendon System,” by S.J. Dyke, B.F. Spencer, Jr., P. Quast, M.K. Sain, D.C. Kaspari, Jr. and T.T. Soong, 8/29/94, (PB95-212320, A05, MF-A01).

NCEER-94-0025 “Seismic Retrofitting Manual for Highway Bridges,” Edited by I.G. Buckle and I.F. Friedland, published by the Federal Highway Administration (PB95-212676, A15, MF-A03).

NCEER-94-0026 “Proceedings from the Fifth U.S.-Japan Workshop on Earthquake Resistant Design of Lifeline Facilities and Countermeasures Against Soil Liquefaction,” Edited by T.D. O’Rourke and M. Hamada, 11/7/94, (PB95-220802, A99, MF-E08).

NCEER-95-0001 "Experimental and Analytical Investigation of Seismic Retrofit of Structures with Supplemental Damping: Part 1 - Fluid Viscous Damping Devices," by A.M. Reinhorn, C. Li and M.C. Constantinou, 1/3/95, (PB95-266599, A09, MF-A02).

NCEER-95-0002 "Experimental and Analytical Study of Low-Cycle Fatigue Behavior of Semi-Rigid Top-And-Seat Angle Connections," by G. Pekcan, J.B. Mander and S.S. Chen, 1/5/95, (PB95-220042, A07, MF-A02).

NCEER-95-0003 "NCEER-ATC Joint Study on Fragility of Buildings," by T. Anagnos, C. Rojahn and A.S. Kiremidjian, 1/20/95, (PB95-220026, A06, MF-A02).

NCEER-95-0004 "Nonlinear Control Algorithms for Peak Response Reduction," by Z. Wu, T.T. Soong, V. Gattulli and R.C. Lin, 2/16/95, (PB95-220349, A05, MF-A01).

NCEER-95-0005 "Pipeline Replacement Feasibility Study: A Methodology for Minimizing Seismic and Corrosion Risks to Underground Natural Gas Pipelines," by R.T. Eguchi, H.A. Seligson and D.G. Honegger, 3/2/95, (PB95-252326, A06, MF-A02).

NCEER-95-0006 "Evaluation of Seismic Performance of an 11-Story Frame Building During the 1994 Northridge Earthquake," by F. Naeim, R. DiSulio, K. Benuska, A. Reinhorn and C. Li, to be published.

NCEER-95-0007 "Prioritization of Bridges for Seismic Retrofitting," by N. Basöz and A.S. Kiremidjian, 4/24/95, (PB95-252300, A08, MF-A02).

NCEER-95-0008 "Method for Developing Motion Damage Relationships for Reinforced Concrete Frames," by A. Singhal and A.S. Kiremidjian, 5/11/95, (PB95-266607, A06, MF-A02).

NCEER-95-0009 "Experimental and Analytical Investigation of Seismic Retrofit of Structures with Supplemental Damping: Part II - Friction Devices," by C. Li and A.M. Reinhorn, 7/6/95, (PB96-128087, A11, MF-A03).

NCEER-95-0010 "Experimental Performance and Analytical Study of a Non-Ductile Reinforced Concrete Frame Structure Retrofitted with Elastomeric Spring Dampers," by G. Pekcan, J.B. Mander and S.S. Chen, 7/14/95, (PB96-137161, A08, MF-A02).

NCEER-95-0011 "Development and Experimental Study of Semi-Active Fluid Damping Devices for Seismic Protection of Structures," by M.D. Symans and M.C. Constantinou, 8/3/95, (PB96-136940, A23, MF-A04).

NCEER-95-0012 "Real-Time Structural Parameter Modification (RSPM): Development of Innervated Structures," by Z. Liang, M. Tong and G.C. Lee, 4/11/95, (PB96-137153, A06, MF-A01).

NCEER-95-0013 "Experimental and Analytical Investigation of Seismic Retrofit of Structures with Supplemental Damping: Part III - Viscous Damping Walls," by A.M. Reinhorn and C. Li, 10/1/95, (PB96-176409, A11, MF-A03).

NCEER-95-0014 "Seismic Fragility Analysis of Equipment and Structures in a Memphis Electric Substation," by J-R. Huo and H.H.M. Hwang, 8/10/95, (PB96-128087, A09, MF-A02).

NCEER-95-0015 "The Hanshin-Awaji Earthquake of January 17, 1995: Performance of Lifelines," Edited by M. Shinozuka, 11/3/95, (PB96-176383, A15, MF-A03).

NCEER-95-0016 "Highway Culvert Performance During Earthquakes," by T.L. Youd and C.J. Beckman, available as NCEER-96-0015.

NCEER-95-0017 "The Hanshin-Awaji Earthquake of January 17, 1995: Performance of Highway Bridges," Edited by I.G. Buckle, 12/1/95, to be published.

NCEER-95-0018 "Modeling of Masonry Infill Panels for Structural Analysis," by A.M. Reinhorn, A. Madan, R.E. Valles, Y. Reichmann and J.B. Mander, 12/8/95, (PB97-110886, MF-A01, A06).

NCEER-95-0019 "Optimal Polynomial Control for Linear and Nonlinear Structures," by A.K. Agrawal and J.N. Yang, 12/11/95, (PB96-168737, A07, MF-A02).

NCEER-95-0020 "Retrofit of Non-Ductile Reinforced Concrete Frames Using Friction Dampers," by R.S. Rao, P. Gergely and R.N. White, 12/22/95, (PB97-133508, A10, MF-A02).

NCEER-95-0021 "Parametric Results for Seismic Response of Pile-Supported Bridge Bents," by G. Mylonakis, A. Nikolaou and G. Gazetas, 12/22/95, (PB97-100242, A12, MF-A03).

NCEER-95-0022 "Kinematic Bending Moments in Seismically Stressed Piles," by A. Nikolaou, G. Mylonakis and G. Gazetas, 12/23/95, (PB97-113914, MF-A03, A13).

NCEER-96-0001 "Dynamic Response of Unreinforced Masonry Buildings with Flexible Diaphragms," by A.C. Costley and D.P. Abrams," 10/10/96, (PB97-133573, MF-A03, A15).

NCEER-96-0002 "State of the Art Review: Foundations and Retaining Structures," by I. Po Lam, to be published.

NCEER-96-0003 "Ductility of Rectangular Reinforced Concrete Bridge Columns with Moderate Confinement," by N. Wehbe, M. Saiidi, D. Sanders and B. Douglas, 11/7/96, (PB97-133557, A06, MF-A02).

NCEER-96-0004 "Proceedings of the Long-Span Bridge Seismic Research Workshop," edited by I.G. Buckle and I.M. Friedland, to be published.

NCEER-96-0005 "Establish Representative Pier Types for Comprehensive Study: Eastern United States," by J. Kulicki and Z. Prucz, 5/28/96, (PB98-119217, A07, MF-A02).

NCEER-96-0006 "Establish Representative Pier Types for Comprehensive Study: Western United States," by R. Imbsen, R.A. Schamber and T.A. Osterkamp, 5/28/96, (PB98-118607, A07, MF-A02).

NCEER-96-0007 "Nonlinear Control Techniques for Dynamical Systems with Uncertain Parameters," by R.G. Ghanem and M.I. Bujakov, 5/27/96, (PB97-100259, A17, MF-A03).

NCEER-96-0008 "Seismic Evaluation of a 30-Year Old Non-Ductile Highway Bridge Pier and Its Retrofit," by J.B. Mander, B. Mahmoodzadegan, S. Bhadra and S.S. Chen, 5/31/96, (PB97-110902, MF-A03, A10).

NCEER-96-0009 "Seismic Performance of a Model Reinforced Concrete Bridge Pier Before and After Retrofit," by J.B. Mander, J.H. Kim and C.A. Ligozio, 5/31/96, (PB97-110910, MF-A02, A10).

NCEER-96-0010 "IDARC2D Version 4.0: A Computer Program for the Inelastic Damage Analysis of Buildings," by R.E. Valles, A.M. Reinhorn, S.K. Kunnath, C. Li and A. Madan, 6/3/96, (PB97-100234, A17, MF-A03).

NCEER-96-0011 "Estimation of the Economic Impact of Multiple Lifeline Disruption: Memphis Light, Gas and Water Division Case Study," by S.E. Chang, H.A. Seligson and R.T. Eguchi, 8/16/96, (PB97-133490, A11, MF-A03).

NCEER-96-0012 "Proceedings from the Sixth Japan-U.S. Workshop on Earthquake Resistant Design of Lifeline Facilities and Countermeasures Against Soil Liquefaction, Edited by M. Hamada and T. O'Rourke, 9/11/96, (PB97-133581, A99, MF-A06).

NCEER-96-0013 "Chemical Hazards, Mitigation and Preparedness in Areas of High Seismic Risk: A Methodology for Estimating the Risk of Post-Earthquake Hazardous Materials Release," by H.A. Seligson, R.T. Eguchi, K.J. Tierney and K. Richmond, 11/7/96, (PB97-133565, MF-A02, A08).

NCEER-96-0014 "Response of Steel Bridge Bearings to Reversed Cyclic Loading," by J.B. Mander, D-K. Kim, S.S. Chen and G.J. Premus, 11/13/96, (PB97-140735, A12, MF-A03).

NCEER-96-0015 "Highway Culvert Performance During Past Earthquakes," by T.L. Youd and C.J. Beckman, 11/25/96, (PB97-133532, A06, MF-A01).

NCEER-97-0001 "Evaluation, Prevention and Mitigation of Pounding Effects in Building Structures," by R.E. Valles and A.M. Reinhorn, 2/20/97, (PB97-159552, A14, MF-A03).

NCEER-97-0002 "Seismic Design Criteria for Bridges and Other Highway Structures," by C. Rojahn, R. Mayes, D.G. Anderson, J. Clark, J.H. Hom, R.V. Nutt and M.J. O'Rourke, 4/30/97, (PB97-194658, A06, MF-A03).

NCEER-97-0003 “Proceedings of the U.S.-Italian Workshop on Seismic Evaluation and Retrofit,” Edited by D.P. Abrams and G.M. Calvi, 3/19/97, (PB97-194666, A13, MF-A03).

NCEER-97-0004 "Investigation of Seismic Response of Buildings with Linear and Nonlinear Fluid Viscous Dampers," by A.A. Seleemah and M.C. Constantinou, 5/21/97, (PB98-109002, A15, MF-A03).

NCEER-97-0005 "Proceedings of the Workshop on Earthquake Engineering Frontiers in Transportation Facilities," edited by G.C. Lee and I.M. Friedland, 8/29/97, (PB98-128911, A25, MR-A04).

NCEER-97-0006 "Cumulative Seismic Damage of Reinforced Concrete Bridge Piers," by S.K. Kunnath, A. El-Bahy, A. Taylor and W. Stone, 9/2/97, (PB98-108814, A11, MF-A03).

NCEER-97-0007 "Structural Details to Accommodate Seismic Movements of Highway Bridges and Retaining Walls," by R.A. Imbsen, R.A. Schamber, E. Thorkildsen, A. Kartoum, B.T. Martin, T.N. Rosser and J.M. Kulicki, 9/3/97, (PB98-108996, A09, MF-A02).

NCEER-97-0008 "A Method for Earthquake Motion-Damage Relationships with Application to Reinforced Concrete Frames," by A. Singhal and A.S. Kiremidjian, 9/10/97, (PB98-108988, A13, MF-A03).

NCEER-97-0009 "Seismic Analysis and Design of Bridge Abutments Considering Sliding and Rotation," by K. Fishman and R. Richards, Jr., 9/15/97, (PB98-108897, A06, MF-A02).

NCEER-97-0010 "Proceedings of the FHWA/NCEER Workshop on the National Representation of Seismic Ground Motion for New and Existing Highway Facilities," edited by I.M. Friedland, M.S. Power and R.L. Mayes, 9/22/97, (PB98-128903, A21, MF-A04).

NCEER-97-0011 "Seismic Analysis for Design or Retrofit of Gravity Bridge Abutments," by K.L. Fishman, R. Richards, Jr. and R.C. Divito, 10/2/97, (PB98-128937, A08, MF-A02).

NCEER-97-0012 "Evaluation of Simplified Methods of Analysis for Yielding Structures," by P. Tsopelas, M.C. Constantinou, C.A. Kircher and A.S. Whittaker, 10/31/97, (PB98-128929, A10, MF-A03).

NCEER-97-0013 "Seismic Design of Bridge Columns Based on Control and Repairability of Damage," by C-T. Cheng and J.B. Mander, 12/8/97, (PB98-144249, A11, MF-A03).

NCEER-97-0014 "Seismic Resistance of Bridge Piers Based on Damage Avoidance Design," by J.B. Mander and C-T. Cheng, 12/10/97, (PB98-144223, A09, MF-A02).

NCEER-97-0015 “Seismic Response of Nominally Symmetric Systems with Strength Uncertainty,” by S. Balopoulou and M. Grigoriu, 12/23/97, (PB98-153422, A11, MF-A03).

NCEER-97-0016 “Evaluation of Seismic Retrofit Methods for Reinforced Concrete Bridge Columns,” by T.J. Wipf, F.W. Klaiber and F.M. Russo, 12/28/97, (PB98-144215, A12, MF-A03).

NCEER-97-0017 “Seismic Fragility of Existing Conventional Reinforced Concrete Highway Bridges,” by C.L. Mullen and A.S. Cakmak, 12/30/97, (PB98-153406, A08, MF-A02).

NCEER-97-0018 “Loss Asssessment of Memphis Buildings,” edited by D.P. Abrams and M. Shinozuka, 12/31/97, (PB98-144231, A13, MF-A03).

NCEER-97-0019 “Seismic Evaluation of Frames with Infill Walls Using Quasi-static Experiments,” by K.M. Mosalam, R.N. White and P. Gergely, 12/31/97, (PB98-153455, A07, MF-A02).

NCEER-97-0020 “Seismic Evaluation of Frames with Infill Walls Using Pseudo-dynamic Experiments,” by K.M. Mosalam, R.N. White and P. Gergely, 12/31/97, (PB98-153430, A07, MF-A02).

NCEER-97-0021 “Computational Strategies for Frames with Infill Walls: Discrete and Smeared Crack Analyses and Seismic Fragility,” by K.M. Mosalam, R.N. White and P. Gergely, 12/31/97, (PB98-153414, A10, MF-A02).

NCEER-97-0022 "Proceedings of the NCEER Workshop on Evaluation of Liquefaction Resistance of Soils," edited by T.L. Youd and I.M. Idriss, 12/31/97, (PB98-155617, A15, MF-A03).

MCEER-98-0001 "Extraction of Nonlinear Hysteretic Properties of Seismically Isolated Bridges from Quick-Release Field Tests," by Q. Chen, B.M. Douglas, E.M. Maragakis and I.G. Buckle, 5/26/98, (PB99-118838, A06, MF-A01).

MCEER-98-0002 "Methodologies for Evaluating the Importance of Highway Bridges," by A. Thomas, S. Eshenaur and J. Kulicki, 5/29/98, (PB99-118846, A10, MF-A02).

MCEER-98-0003 "Capacity Design of Bridge Piers and the Analysis of Overstrength," by J.B. Mander, A. Dutta and P. Goel, 6/1/98, (PB99-118853, A09, MF-A02).

MCEER-98-0004 "Evaluation of Bridge Damage Data from the Loma Prieta and Northridge, California Earthquakes," by N. Basoz and A. Kiremidjian, 6/2/98, (PB99-118861, A15, MF-A03).

MCEER-98-0005 "Screening Guide for Rapid Assessment of Liquefaction Hazard at Highway Bridge Sites," by T. L. Youd, 6/16/98, (PB99-118879, A06, not available on microfiche).

MCEER-98-0006 "Structural Steel and Steel/Concrete Interface Details for Bridges," by P. Ritchie, N. Kauhl and J. Kulicki, 7/13/98, (PB99-118945, A06, MF-A01).

MCEER-98-0007 "Capacity Design and Fatigue Analysis of Confined Concrete Columns," by A. Dutta and J.B. Mander, 7/14/98, (PB99-118960, A14, MF-A03).

MCEER-98-0008 "Proceedings of the Workshop on Performance Criteria for Telecommunication Services Under Earthquake Conditions," edited by A.J. Schiff, 7/15/98, (PB99-118952, A08, MF-A02).

MCEER-98-0009 "Fatigue Analysis of Unconfined Concrete Columns," by J.B. Mander, A. Dutta and J.H. Kim, 9/12/98, (PB99-123655, A10, MF-A02).

MCEER-98-0010 "Centrifuge Modeling of Cyclic Lateral Response of Pile-Cap Systems and Seat-Type Abutments in Dry Sands," by A.D. Gadre and R. Dobry, 10/2/98, (PB99-123606, A13, MF-A03).

MCEER-98-0011 "IDARC-BRIDGE: A Computational Platform for Seismic Damage Assessment of Bridge Structures," by A.M. Reinhorn, V. Simeonov, G. Mylonakis and Y. Reichman, 10/2/98, (PB99-162919, A15, MF-A03).

MCEER-98-0012 "Experimental Investigation of the Dynamic Response of Two Bridges Before and After Retrofitting with Elastomeric Bearings," by D.A. Wendichansky, S.S. Chen and J.B. Mander, 10/2/98, (PB99-162927, A15, MF-A03).

MCEER-98-0013 "Design Procedures for Hinge Restrainers and Hinge Sear Width for Multiple-Frame Bridges," by R. Des Roches and G.L. Fenves, 11/3/98, (PB99-140477, A13, MF-A03).

MCEER-98-0014 "Response Modification Factors for Seismically Isolated Bridges," by M.C. Constantinou and J.K. Quarshie, 11/3/98, (PB99-140485, A14, MF-A03).

MCEER-98-0015 "Proceedings of the U.S.-Italy Workshop on Seismic Protective Systems for Bridges," edited by I.M. Friedland and M.C. Constantinou, 11/3/98, (PB2000-101711, A22, MF-A04).

MCEER-98-0016 "Appropriate Seismic Reliability for Critical Equipment Systems: Recommendations Based on Regional Analysis of Financial and Life Loss," by K. Porter, C. Scawthorn, C. Taylor and N. Blais, 11/10/98, (PB99-157265, A08, MF-A02).

MCEER-98-0017 "Proceedings of the U.S. Japan Joint Seminar on Civil Infrastructure Systems Research," edited by M. Shinozuka and A. Rose, 11/12/98, (PB99-156713, A16, MF-A03).

MCEER-98-0018 "Modeling of Pile Footings and Drilled Shafts for Seismic Design," by I. PoLam, M. Kapuskar and D. Chaudhuri, 12/21/98, (PB99-157257, A09, MF-A02).

MCEER-99-0001 "Seismic Evaluation of a Masonry Infilled Reinforced Concrete Frame by Pseudodynamic Testing," by S.G. Buonopane and R.N. White, 2/16/99, (PB99-162851, A09, MF-A02).

MCEER-99-0002 "Response History Analysis of Structures with Seismic Isolation and Energy Dissipation Systems: Verification Examples for Program SAP2000," by J. Scheller and M.C. Constantinou, 2/22/99, (PB99-162869, A08, MF-A02).

MCEER-99-0003 "Experimental Study on the Seismic Design and Retrofit of Bridge Columns Including Axial Load Effects," by A. Dutta, T. Kokorina and J.B. Mander, 2/22/99, (PB99-162877, A09, MF-A02).

MCEER-99-0004 "Experimental Study of Bridge Elastomeric and Other Isolation and Energy Dissipation Systems with Emphasis on Uplift Prevention and High Velocity Near-source Seismic Excitation," by A. Kasalanati and M. C. Constantinou, 2/26/99, (PB99-162885, A12, MF-A03).

MCEER-99-0005 "Truss Modeling of Reinforced Concrete Shear-flexure Behavior," by J.H. Kim and J.B. Mander, 3/8/99, (PB99-163693, A12, MF-A03).

MCEER-99-0006 "Experimental Investigation and Computational Modeling of Seismic Response of a 1:4 Scale Model Steel Structure with a Load Balancing Supplemental Damping System," by G. Pekcan, J.B. Mander and S.S. Chen, 4/2/99, (PB99-162893, A11, MF-A03).

MCEER-99-0007 "Effect of Vertical Ground Motions on the Structural Response of Highway Bridges," by M.R. Button, C.J. Cronin and R.L. Mayes, 4/10/99, (PB2000-101411, A10, MF-A03).

MCEER-99-0008 "Seismic Reliability Assessment of Critical Facilities: A Handbook, Supporting Documentation, and Model Code Provisions," by G.S. Johnson, R.E. Sheppard, M.D. Quilici, S.J. Eder and C.R. Scawthorn, 4/12/99, (PB2000-101701, A18, MF-A04).

MCEER-99-0009 "Impact Assessment of Selected MCEER Highway Project Research on the Seismic Design of Highway Structures," by C. Rojahn, R. Mayes, D.G. Anderson, J.H. Clark, D'Appolonia Engineering, S. Gloyd and R.V. Nutt, 4/14/99, (PB99-162901, A10, MF-A02).

MCEER-99-0010 "Site Factors and Site Categories in Seismic Codes," by R. Dobry, R. Ramos and M.S. Power, 7/19/99, (PB2000-101705, A08, MF-A02).

MCEER-99-0011 "Restrainer Design Procedures for Multi-Span Simply-Supported Bridges," by M.J. Randall, M. Saiidi, E. Maragakis and T. Isakovic, 7/20/99, (PB2000-101702, A10, MF-A02).

MCEER-99-0012 "Property Modification Factors for Seismic Isolation Bearings," by M.C. Constantinou, P. Tsopelas, A. Kasalanati and E. Wolff, 7/20/99, (PB2000-103387, A11, MF-A03).

MCEER-99-0013 "Critical Seismic Issues for Existing Steel Bridges," by P. Ritchie, N. Kauhl and J. Kulicki, 7/20/99, (PB2000-101697, A09, MF-A02).

MCEER-99-0014 "Nonstructural Damage Database," by A. Kao, T.T. Soong and A. Vender, 7/24/99, (PB2000-101407, A06, MF-A01).

MCEER-99-0015 "Guide to Remedial Measures for Liquefaction Mitigation at Existing Highway Bridge Sites," by H.G. Cooke and J. K. Mitchell, 7/26/99, (PB2000-101703, A11, MF-A03).

MCEER-99-0016 "Proceedings of the MCEER Workshop on Ground Motion Methodologies for the Eastern United States," edited by N. Abrahamson and A. Becker, 8/11/99, (PB2000-103385, A07, MF-A02).

MCEER-99-0017 "Quindío, Colombia Earthquake of January 25, 1999: Reconnaissance Report," by A.P. Asfura and P.J. Flores, 10/4/99, (PB2000-106893, A06, MF-A01).

MCEER-99-0018 "Hysteretic Models for Cyclic Behavior of Deteriorating Inelastic Structures," by M.V. Sivaselvan and A.M. Reinhorn, 11/5/99, (PB2000-103386, A08, MF-A02).

MCEER-99-0019 "Proceedings of the 7th U.S.- Japan Workshop on Earthquake Resistant Design of Lifeline Facilities and Countermeasures Against Soil Liquefaction," edited by T.D. O'Rourke, J.P. Bardet and M. Hamada, 11/19/99, (PB2000-103354, A99, MF-A06).

MCEER-99-0020 "Development of Measurement Capability for Micro-Vibration Evaluations with Application to Chip Fabrication Facilities," by G.C. Lee, Z. Liang, J.W. Song, J.D. Shen and W.C. Liu, 12/1/99, (PB2000-105993, A08, MF-A02).

MCEER-99-0021 "Design and Retrofit Methodology for Building Structures with Supplemental Energy Dissipating Systems," by G. Pekcan, J.B. Mander and S.S. Chen, 12/31/99, (PB2000-105994, A11, MF-A03).

MCEER-00-0001 "The Marmara, Turkey Earthquake of August 17, 1999: Reconnaissance Report," edited by C. Scawthorn; with major contributions by M. Bruneau, R. Eguchi, T. Holzer, G. Johnson, J. Mander, J. Mitchell, W. Mitchell, A. Papageorgiou, C. Scaethorn, and G. Webb, 3/23/00, (PB2000-106200, A11, MF-A03).

MCEER-00-0002 "Proceedings of the MCEER Workshop for Seismic Hazard Mitigation of Health Care Facilities," edited by G.C. Lee, M. Ettouney, M. Grigoriu, J. Hauer and J. Nigg, 3/29/00, (PB2000-106892, A08, MF-A02).

MCEER-00-0003 "The Chi-Chi, Taiwan Earthquake of September 21, 1999: Reconnaissance Report," edited by G.C. Lee and C.H. Loh, with major contributions by G.C. Lee, M. Bruneau, I.G. Buckle, S.E. Chang, P.J. Flores, T.D. O'Rourke, M. Shinozuka, T.T. Soong, C-H. Loh, K-C. Chang, Z-J. Chen, J-S. Hwang, M-L. Lin, G-Y. Liu, K-C. Tsai, G.C. Yao and C-L. Yen, 4/30/00, (PB2001-100980, A10, MF-A02).

MCEER-00-0004 "Seismic Retrofit of End-Sway Frames of Steel Deck-Truss Bridges with a Supplemental Tendon System: Experimental and Analytical Investigation," by G. Pekcan, J.B. Mander and S.S. Chen, 7/1/00, (PB2001-100982, A10, MF-A02).

MCEER-00-0005 "Sliding Fragility of Unrestrained Equipment in Critical Facilities," by W.H. Chong and T.T. Soong, 7/5/00, (PB2001-100983, A08, MF-A02).

MCEER-00-0006 "Seismic Response of Reinforced Concrete Bridge Pier Walls in the Weak Direction," by N. Abo-Shadi, M. Saiidi and D. Sanders, 7/17/00, (PB2001-100981, A17, MF-A03).

MCEER-00-0007 "Low-Cycle Fatigue Behavior of Longitudinal Reinforcement in Reinforced Concrete Bridge Columns," by J. Brown and S.K. Kunnath, 7/23/00, (PB2001-104392, A08, MF-A02).

MCEER-00-0008 "Soil Structure Interaction of Bridges for Seismic Analysis," I. PoLam and H. Law, 9/25/00, (PB2001-105397, A08, MF-A02).

MCEER-00-0009 "Proceedings of the First MCEER Workshop on Mitigation of Earthquake Disaster by Advanced Technologies (MEDAT-1), edited by M. Shinozuka, D.J. Inman and T.D. O'Rourke, 11/10/00, (PB2001-105399, A14, MF-A03).

MCEER-00-0010 "Development and Evaluation of Simplified Procedures for Analysis and Design of Buildings with Passive Energy Dissipation Systems, Revision 01," by O.M. Ramirez, M.C. Constantinou, C.A. Kircher, A.S. Whittaker, M.W. Johnson, J.D. Gomez and C. Chrysostomou, 11/16/01, (PB2001-105523, A23, MF-A04).

MCEER-00-0011 "Dynamic Soil-Foundation-Structure Interaction Analyses of Large Caissons," by C-Y. Chang, C-M. Mok, Z-L. Wang, R. Settgast, F. Waggoner, M.A. Ketchum, H.M. Gonnermann and C-C. Chin, 12/30/00, (PB2001-104373, A07, MF-A02).

MCEER-00-0012 "Experimental Evaluation of Seismic Performance of Bridge Restrainers," by A.G. Vlassis, E.M. Maragakis and M. Saiid Saiidi, 12/30/00, (PB2001-104354, A09, MF-A02).

MCEER-00-0013 "Effect of Spatial Variation of Ground Motion on Highway Structures," by M. Shinozuka, V. Saxena and G. Deodatis, 12/31/00, (PB2001-108755, A13, MF-A03).

MCEER-00-0014 "A Risk-Based Methodology for Assessing the Seismic Performance of Highway Systems," by S.D. Werner, C.E. Taylor, J.E. Moore, II, J.S. Walton and S. Cho, 12/31/00, (PB2001-108756, A14, MF-A03).

MCEER-01-0001 "Experimental Investigation of P-Delta Effects to Collapse During Earthquakes," by D. Vian and M. Bruneau, 6/25/01, (PB2002-100534, A17, MF-A03).

MCEER-01-0002 "Proceedings of the Second MCEER Workshop on Mitigation of Earthquake Disaster by Advanced Technologies (MEDAT-2)," edited by M. Bruneau and D.J. Inman, 7/23/01, (PB2002-100434, A16, MF-A03).

MCEER-01-0003 "Sensitivity Analysis of Dynamic Systems Subjected to Seismic Loads," by C. Roth and M. Grigoriu, 9/18/01, (PB2003-100884, A12, MF-A03).

MCEER-01-0004 "Overcoming Obstacles to Implementing Earthquake Hazard Mitigation Policies: Stage 1 Report," by D.J. Alesch and W.J. Petak, 12/17/01, (PB2002-107949, A07, MF-A02).

MCEER-01-0005 "Updating Real-Time Earthquake Loss Estimates: Methods, Problems and Insights," by C.E. Taylor, S.E. Chang and R.T. Eguchi, 12/17/01, (PB2002-107948, A05, MF-A01).

MCEER-01-0006 "Experimental Investigation and Retrofit of Steel Pile Foundations and Pile Bents Under Cyclic Lateral Loadings," by A. Shama, J. Mander, B. Blabac and S. Chen, 12/31/01, (PB2002-107950, A13, MF-A03).

MCEER-02-0001 "Assessment of Performance of Bolu Viaduct in the 1999 Duzce Earthquake in Turkey" by P.C. Roussis, M.C. Constantinou, M. Erdik, E. Durukal and M. Dicleli, 5/8/02, (PB2003-100883, A08, MF-A02).

MCEER-02-0002 "Seismic Behavior of Rail Counterweight Systems of Elevators in Buildings," by M.P. Singh, Rildova and L.E. Suarez, 5/27/02. (PB2003-100882, A11, MF-A03).

MCEER-02-0003 "Development of Analysis and Design Procedures for Spread Footings," by G. Mylonakis, G. Gazetas, S. Nikolaou and A. Chauncey, 10/02/02, (PB2004-101636, A13, MF-A03, CD-A13).

MCEER-02-0004 "Bare-Earth Algorithms for Use with SAR and LIDAR Digital Elevation Models," by C.K. Huyck, R.T. Eguchi and B. Houshmand, 10/16/02, (PB2004-101637, A07, CD-A07).

MCEER-02-0005 "Review of Energy Dissipation of Compression Members in Concentrically Braced Frames," by K.Lee and M. Bruneau, 10/18/02, (PB2004-101638, A10, CD-A10).

MCEER-03-0001 "Experimental Investigation of Light-Gauge Steel Plate Shear Walls for the Seismic Retrofit of Buildings" by J. Berman and M. Bruneau, 5/2/03, (PB2004-101622, A10, MF-A03, CD-A10).

MCEER-03-0002 "Statistical Analysis of Fragility Curves," by M. Shinozuka, M.Q. Feng, H. Kim, T. Uzawa and T. Ueda, 6/16/03, (PB2004-101849, A09, CD-A09).

MCEER-03-0003 "Proceedings of the Eighth U.S.-Japan Workshop on Earthquake Resistant Design f Lifeline Facilities and Countermeasures Against Liquefaction," edited by M. Hamada, J.P. Bardet and T.D. O'Rourke, 6/30/03, (PB2004-104386, A99, CD-A99).

MCEER-03-0004 "Proceedings of the PRC-US Workshop on Seismic Analysis and Design of Special Bridges," edited by L.C. Fan and G.C. Lee, 7/15/03, (PB2004-104387, A14, CD-A14).

MCEER-03-0005 "Urban Disaster Recovery: A Framework and Simulation Model," by S.B. Miles and S.E. Chang, 7/25/03, (PB2004-104388, A07, CD-A07).

MCEER-03-0006 "Behavior of Underground Piping Joints Due to Static and Dynamic Loading," by R.D. Meis, M. Maragakis and R. Siddharthan, 11/17/03, (PB2005-102194, A13, MF-A03, CD-A00).

MCEER-03-0007 "Seismic Vulnerability of Timber Bridges and Timber Substructures," by A.A. Shama, J.B. Mander, I.M. Friedland and D.R. Allicock, 12/15/03.

MCEER-04-0001 "Experimental Study of Seismic Isolation Systems with Emphasis on Secondary System Response and Verification of Accuracy of Dynamic Response History Analysis Methods," by E. Wolff and M. Constantinou, 1/16/04 (PB2005-102195, A99, MF-E08, CD-A00).

MCEER-04-0002 "Tension, Compression and Cyclic Testing of Engineered Cementitious Composite Materials," by K. Kesner and S.L. Billington, 3/1/04, (PB2005-102196, A08, CD-A08).

MCEER-04-0003 "Cyclic Testing of Braces Laterally Restrained by Steel Studs to Enhance Performance During Earthquakes," by O.C. Celik, J.W. Berman and M. Bruneau, 3/16/04, (PB2005-102197, A13, MF-A03, CD-A00).

MCEER-04-0004 "Methodologies for Post Earthquake Building Damage Detection Using SAR and Optical Remote Sensing: Application to the August 17, 1999 Marmara, Turkey Earthquake," by C.K. Huyck, B.J. Adams, S. Cho, R.T. Eguchi, B. Mansouri and B. Houshmand, 6/15/04, (PB2005-104888, A10, CD-A00).

MCEER-04-0005 "Nonlinear Structural Analysis Towards Collapse Simulation: A Dynamical Systems Approach," by M.V. Sivaselvan and A.M. Reinhorn, 6/16/04, (PB2005-104889, A11, MF-A03, CD-A00).

MCEER-04-0006 "Proceedings of the Second PRC-US Workshop on Seismic Analysis and Design of Special Bridges," edited by G.C. Lee and L.C. Fan, 6/25/04, (PB2005-104890, A16, CD-A00).

MCEER-04-0007 "Seismic Vulnerability Evaluation of Axially Loaded Steel Built-up Laced Members," by K. Lee and M. Bruneau, 6/30/04, (PB2005-104891, A16, CD-A00).

MCEER-04-0008 "Evaluation of Accuracy of Simplified Methods of Analysis and Design of Buildings with Damping Systems for Near-Fault and for Soft-Soil Seismic Motions," by E.A. Pavlou and M.C. Constantinou, 8/16/04, (PB2005-104892, A08, MF-A02, CD-A00).

MCEER-04-0009 "Assessment of Geotechnical Issues in Acute Care Facilities in California," by M. Lew, T.D. O'Rourke, R. Dobry and M. Koch, 9/15/04, (PB2005-104893, A08, CD-A00).

MCEER-04-0010 "Scissor-Jack-Damper Energy Dissipation System," by A.N. Sigaher-Boyle and M.C. Constantinou, 12/1/04 (PB2005-108221).

MCEER-04-0011 "Seismic Retrofit of Bridge Steel Truss Piers Using a Controlled Rocking Approach," by M. Pollino and M. Bruneau, 12/20/04 (PB2006-105795).

MCEER-05-0001 "Experimental and Analytical Studies of Structures Seismically Isolated with an Uplift-Restraint Isolation System," by P.C. Roussis and M.C. Constantinou, 1/10/05 (PB2005-108222).

MCEER-05-0002 "A Versatile Experimentation Model for Study of Structures Near Collapse Applied to Seismic Evaluation of Irregular Structures," by D. Kusumastuti, A.M. Reinhorn and A. Rutenberg, 3/31/05 (PB2006-101523).

MCEER-05-0003 "Proceedings of the Third PRC-US Workshop on Seismic Analysis and Design of Special Bridges," edited by L.C. Fan and G.C. Lee, 4/20/05, (PB2006-105796).

MCEER-05-0004 "Approaches for the Seismic Retrofit of Braced Steel Bridge Piers and Proof-of-Concept Testing of an Eccentrically Braced Frame with Tubular Link," by J.W. Berman and M. Bruneau, 4/21/05 (PB2006-101524).

MCEER-05-0005 "Simulation of Strong Ground Motions for Seismic Fragility Evaluation of Nonstructural Components in Hospitals," by A. Wanitkorkul and A. Filiatrault, 5/26/05 (PB2006-500027).

MCEER-05-0006 "Seismic Safety in California Hospitals: Assessing an Attempt to Accelerate the Replacement or Seismic Retrofit of Older Hospital Facilities," by D.J. Alesch, L.A. Arendt and W.J. Petak, 6/6/05 (PB2006-105794).

MCEER-05-0007 "Development of Seismic Strengthening and Retrofit Strategies for Critical Facilities Using Engineered Cementitious Composite Materials," by K. Kesner and S.L. Billington, 8/29/05 (PB2006-111701).

MCEER-05-0008 "Experimental and Analytical Studies of Base Isolation Systems for Seismic Protection of Power Transformers," by N. Murota, M.Q. Feng and G-Y. Liu, 9/30/05 (PB2006-111702).

MCEER-05-0009 "3D-BASIS-ME-MB: Computer Program for Nonlinear Dynamic Analysis of Seismically Isolated Structures," by P.C. Tsopelas, P.C. Roussis, M.C. Constantinou, R. Buchanan and A.M. Reinhorn, 10/3/05 (PB2006-111703).

MCEER-05-0010 "Steel Plate Shear Walls for Seismic Design and Retrofit of Building Structures," by D. Vian and M. Bruneau, 12/15/05 (PB2006-111704).

MCEER-05-0011 "The Performance-Based Design Paradigm," by M.J. Astrella and A. Whittaker, 12/15/05 (PB2006-111705).

MCEER-06-0001 "Seismic Fragility of Suspended Ceiling Systems," H. Badillo-Almaraz, A.S. Whittaker, A.M. Reinhorn and G.P. Cimellaro, 2/4/06 (PB2006-111706).

MCEER-06-0002 "Multi-Dimensional Fragility of Structures," by G.P. Cimellaro, A.M. Reinhorn and M. Bruneau, 3/1/06 (PB2007-106974, A09, MF-A02, CD A00).

MCEER-06-0003 "Built-Up Shear Links as Energy Dissipators for Seismic Protection of Bridges," by P. Dusicka, A.M. Itani and I.G. Buckle, 3/15/06 (PB2006-111708).

MCEER-06-0004 "Analytical Investigation of the Structural Fuse Concept," by R.E. Vargas and M. Bruneau, 3/16/06 (PB2006-111709).

MCEER-06-0005 "Experimental Investigation of the Structural Fuse Concept," by R.E. Vargas and M. Bruneau, 3/17/06 (PB2006-111710).

MCEER-06-0006 "Further Development of Tubular Eccentrically Braced Frame Links for the Seismic Retrofit of Braced Steel Truss Bridge Piers," by J.W. Berman and M. Bruneau, 3/27/06 (PB2007-105147).

MCEER-06-0007 "REDARS Validation Report," by S. Cho, C.K. Huyck, S. Ghosh and R.T. Eguchi, 8/8/06 (PB2007-106983).

MCEER-06-0008 "Review of Current NDE Technologies for Post-Earthquake Assessment of Retrofitted Bridge Columns," by J.W. Song, Z. Liang and G.C. Lee, 8/21/06 06 (PB2007-106984).

MCEER-06-0009 "Liquefaction Remediation in Silty Soils Using Dynamic Compaction and Stone Columns," by S. Thevanayagam, G.R. Martin, R. Nashed, T. Shenthan, T. Kanagalingam and N. Ecemis, 8/28/06 06 (PB2007-106985).

MCEER-06-0010 "Conceptual Design and Experimental Investigation of Polymer Matrix Composite Infill Panels for Seismic Retrofitting," by W. Jung, M. Chiewanichakorn and A.J. Aref, 9/21/06 (PB2007-106986).

MCEER-06-0011 "A Study of the Coupled Horizontal-Vertical Behavior of Elastomeric and Lead-Rubber Seismic Isolation Bearings," by G.P. Warn and A.S. Whittaker, 9/22/06 (PB2007-108679).

MCEER-06-0012 "Proceedings of the Fourth PRC-US Workshop on Seismic Analysis and Design of Special Bridges: Advancing Bridge Technologies in Research, Design, Construction and Preservation," Edited by L.C. Fan, G.C. Lee and L. Ziang, 10/12/06 (PB2007-109042).

MCEER-06-0013 "Cyclic Response and Low Cycle Fatigue Characteristics of Plate Steels," by P. Dusicka, A.M. Itani and I.G. Buckle, 11/1/06 06 (PB2007-106987).

MCEER-06-0014 "Proceedings of the Second US-Taiwan Bridge Engineering Workshop," edited by W.P. Yen, J. Shen, J-Y. Chen and M. Wang, 11/15/06 (PB2008-500041).

MCEER-06-0015 "User Manual and Technical Documentation for the REDARS^{TM} Import Wizard," by S. Cho, S. Ghosh, C.K. Huyck and S.D. Werner, 11/30/06 (PB2007-114766).

MCEER-06-0016 "Hazard Mitigation Strategy and Monitoring Technologies for Urban and Infrastructure Public Buildings: Proceedings of the China-US Workshops," edited by X.Y. Zhou, A.L. Zhang, G.C. Lee and M. Tong, 12/12/06 (PB2008-500018).

MCEER-07-0001 "Static and Kinetic Coefficients of Friction for Rigid Blocks," by C. Kafali, S. Fathali, M. Grigoriu and A.S. Whittaker, 3/20/07 (PB2007-114767).

MCEER-07-0002 "Hazard Mitigation Investment Decision Making: Organizational Response to Legislative Mandate," by L.A. Arendt, D.J. Alesch and W.J. Petak, 4/9/07 (PB2007-114768).

MCEER-07-0003 "Seismic Behavior of Bidirectional-Resistant Ductile End Diaphragms with Unbonded Braces in Straight or Skewed Steel Bridges," by O. Celik and M. Bruneau, 4/11/07 (PB2008-105141).

MCEER-07-0004 "Modeling Pile Behavior in Large Pile Groups Under Lateral Loading," by A.M. Dodds and G.R. Martin, 4/16/07(PB2008-105142).

MCEER-07-0005 "Experimental Investigation of Blast Performance of Seismically Resistant Concrete-Filled Steel Tube Bridge Piers," by S. Fujikura, M. Bruneau and D. Lopez-Garcia, 4/20/07 (PB2008-105143).

MCEER-07-0006 "Seismic Analysis of Conventional and Isolated Liquefied Natural Gas Tanks Using Mechanical Analogs," by I.P. Christovasilis and A.S. Whittaker, 5/1/07.

MCEER-07-0007 "Experimental Seismic Performance Evaluation of Isolation/Restraint Systems for Mechanical Equipment – Part 1: Heavy Equipment Study," by S. Fathali and A. Filiatrault, 6/6/07 (PB2008-105144).

MCEER-07-0008 "Seismic Vulnerability of Timber Bridges and Timber Substructures," by A.A. Sharma, J.B. Mander, I.M. Friedland and D.R. Allicock, 6/7/07 (PB2008-105145).

MCEER-07-0009 "Experimental and Analytical Study of the XY-Friction Pendulum (XY-FP) Bearing for Bridge Applications," by C.C. Marin-Artieda, A.S. Whittaker and M.C. Constantinou, 6/7/07 (PB2008-105191).

MCEER-07-0010 "Proceedings of the PRC-US Earthquake Engineering Forum for Young Researchers," Edited by G.C. Lee and X.Z. Qi, 6/8/07.

MCEER-07-0011 "Design Recommendations for Perforated Steel Plate Shear Walls," by R. Purba and M. Bruneau, 6/18/07, (PB2008-105192).

MCEER-07-0012 "Performance of Seismic Isolation Hardware Under Service and Seismic Loading," by M.C. Constantinou, A.S. Whittaker, Y. Kalpakidis, D.M. Fenz and G.P. Warn, 8/27/07, (PB2008-105193).

MCEER-07-0013 "Experimental Evaluation of the Seismic Performance of Hospital Piping Subassemblies," by E.R. Goodwin, E. Maragakis and A.M. Itani, 9/4/07, (PB2008-105194).

MCEER-07-0014 "A Simulation Model of Urban Disaster Recovery and Resilience: Implementation for the 1994 Northridge Earthquake," by S. Miles and S.E. Chang, 9/7/07, (PB2008-106426).

MCEER-07-0015 "Statistical and Mechanistic Fragility Analysis of Concrete Bridges," by M. Shinozuka, S. Banerjee and S-H. Kim, 9/10/07, (PB2008-106427).

MCEER-07-0016 "Three-Dimensional Modeling of Inelastic Buckling in Frame Structures," by M. Schachter and AM. Reinhorn, 9/13/07, (PB2008-108125).

MCEER-07-0017 "Modeling of Seismic Wave Scattering on Pile Groups and Caissons," by I. Po Lam, H. Law and C.T. Yang, 9/17/07 (PB2008-108150).

MCEER-07-0018 "Bridge Foundations: Modeling Large Pile Groups and Caissons for Seismic Design," by I. Po Lam, H. Law and G.R. Martin (Coordinating Author), 12/1/07 (PB2008-111190).

MCEER-07-0019 "Principles and Performance of Roller Seismic Isolation Bearings for Highway Bridges," by G.C. Lee, Y.C. Ou, Z. Liang, T.C. Niu and J. Song, 12/10/07.

MCEER-07-0020 "Centrifuge Modeling of Permeability and Pinning Reinforcement Effects on Pile Response to Lateral Spreading," by L.L Gonzalez-Lagos, T. Abdoun and R. Dobry, 12/10/07 (PB2008-111191).

MCEER-07-0021 "Damage to the Highway System from the Pisco, Perú Earthquake of August 15, 2007," by J.S. O'Connor, L. Mesa and M. Nykamp, 12/10/07, (PB2008-108126).

MCEER-07-0022 "Experimental Seismic Performance Evaluation of Isolation/Restraint Systems for Mechanical Equipment – Part 2: Light Equipment Study," by S. Fathali and A. Filiatrault, 12/13/07 (PB2008-111192).

MCEER-07-0023 "Fragility Considerations in Highway Bridge Design," by M. Shinozuka, S. Banerjee and S.H. Kim, 12/14/07 (PB2008-111193).

MCEER-07-0024 "Performance Estimates for Seismically Isolated Bridges," by G.P. Warn and A.S. Whittaker, 12/30/07.

MCEER-08-0001 "Seismic Performance of Steel Girder Bridge Superstructures with Conventional Cross Frames," by L.P. Carden, A.M. Itani and I.G. Buckle, 1/7/08.

MCEER-08-0002 "Seismic Performance of Steel Girder Bridge Superstructures with Ductile End Cross Frames with Seismic Isolators," by L.P. Carden, A.M. Itani and I.G. Buckle, 1/7/08.

MCEER-08-0003 "Analytical and Experimental Investigation of a Controlled Rocking Approach for Seismic Protection of Bridge Steel Truss Piers," by M. Pollino and M. Bruneau, 1/21/08.

MCEER-08-0004 "Linking Lifeline Infrastructure Performance and Community Disaster Resilience: Models and Multi-Stakeholder Processes," by S.E. Chang, C. Pasion, K. Tatebe and R. Ahmad, 3/3/08.

MCEER-08-0005 "Modal Analysis of Generally Damped Linear Structures Subjected to Seismic Excitations," by J. Song, Y-L. Chu, Z. Liang and G.C. Lee, 3/4/08.

MCEER-08-0006 "System Performance Under Multi-Hazard Environments," by C. Kafali and M. Grigoriu, 3/4/08.

MCEER-08-0007 "Mechanical Behavior of Multi-Spherical Sliding Bearings," by D.M. Fenz and M.C. Constantinou, 3/6/08.

MCEER-08-0008 "Post-Earthquake Restoration of the Los Angeles Water Supply System," by T.H.P. Tabucchi and R.A. Davidson, 3/7/08.

MCEER-08-0009 "Fragility Analysis of Water Supply Systems," by A. Jacobson and M. Grigoriu, 3/10/08.

MCEER

EARTHQUAKE ENGINEERING TO EXTREME EVENTS

University at Buffalo, The State University of New York
Red Jacket Quadrangle ▪ Buffalo, New York 14261
Phone: (716) 645-3391 ▪ Fax: (716) 645-3399
E-mail: *mceer@buffalo.edu* ▪ WWW Site *http://mceer.buffalo.edu*

University at Buffalo *The State University of New York*

ISSN 1520-295X